Title
Development of Genetically Targeted Voltage Sensitive Dyes

Author
Liu, Pei

Publication Date
2019

Peer reviewed|Thesis/dissertation

Development of Genetically Targeted Voltage Sensitive Dyes

By
Pei Liu

A Dissertation submitted in partial satisfaction of the
requirements for the degree of
Doctor of Philosophy
In
Chemistry
In the
Graduate Division
of the
University of California, Berkeley

Committee in charge:

Professor Evan W. Miller, Chair
Professor Christopher J. Chang
Professor Hillel Adesnik

Summer 2019

Development of Genetically Targeted Voltage Sensitive Dyes

By Pei Liu

Abstract

Development of Genetically Targeted Voltage Sensitive Dyes

By

Pei Liu

Doctor of Philosophy in Chemistry
University of California, Berkeley
Professor Evan W. Miller, Chair

Comprehensively mapping and recording the electrical inputs and outputs of multiple neurons simultaneously with cellular spatial resolution and millisecond time resolution remains an outstanding challenge in the field of neurobiology. Development of fluorescence indicators for direct visualization of membrane potential changes offers a powerful method for probing voltage dynamics in neurons with unprecedented spatial and temporal resolution. Despite the promise of voltage imaging, key challenges of speed, sensitivity, brightness, and localization remain. The Miller lab has developed a new class of small molecules dyes, VoltageFluors (VF), that rely on photoinduced electron transfer (PeT) and display voltage-sensitive fluorescence due to modulation of the rate of PeT within the VF scaffold by the transmembrane electric field. This approach allows for fast, sensitive and non-invasive recording of neuronal activity in cultured mammalian neurons and in ex vivo tissue slices in single trials. One major limitation of small-molecule dye imaging is the inability to target the dye to specific cells of interest, which significantly erodes signal to noise and cellular resolution. To solve this problem, we have worked to combine VF dyes with a genetically encoded component to enable high-contrast imaging in defined neurons. We first attempted a fluorogenic approach, in which the parent VF dye is chemically modified to be minimally fluorescent and non-voltage-sensitive and must be enzymatically activated prior to imaging. We designed a couple of dyes which can only be activated by a cell-surface pig liver esterase (PLE) and observed enhanced contrast in both HEK cells and cultured neurons with good sensitivity. We have also shown that our genetically targeted voltage dyes outperform purely genetically encoded voltage indicators. In addition, we are exploring other enzyme/substrate pair for fluorogenic activation purpose. The second approach is covalent labeling of voltage sensitive dye to cells of interest using a cell-surface HaloTag enzyme. We have successfully demonstrated selective membrane staining in mouse brain slices and live animal using this strategy. Current efforts focus on applying this method for targeted voltage imaging in live animals to probe specific neuroscience questions.

Dedicated to my family

Table of contents

Acknowledgements

First of all, I would like to say a big thank you to my advisor Professor Evan Miller for his continuous support and guidance throughout my PhD studies. Evan is not only a great scientist but also a wonderful mentor. I can't say enough to appreciate all the help from Evan. He encouraged me to step out of my comfort zone and is always so supportive of me learning new techniques and experiments. His confidence in me really pushed me forward. It's my greatest pleasure to join the lab and work for him. I look forward to the lab retreat at Hawaii ☺

In the Miller lab where a group of amazing scientists gather, I have truly enjoyed working and having fun with everyone. Before I started graduate school, my friend warned me that the peer pressure would burn one out but the Miller lab is simply amazing that everyone is super friendly and helpful. In particular, I would like to my classmates Gloria Ortiz, Julia Lazarri-Dean, Steven Boggess and Jenna Franke. I could still remember the first (and I think the only?) photo that all five of us took together during first year. Now, I have become the oldest graduate student in the lab (not Vince any more) and Jenna has just left and I will leave after this thesis and everyone else has already made plans for the next step. Time really flies! I would miss the days discussing baking with Julia (or rather how I'm obsessed with Julia's brownies and how I simply don't get baking); the days gossiping with Gloria in the dark room and with Steven in the TC room; the days hearing Jenna's laughter and how proud she is about BODIPYs (they are really awesome dyes!). I'm glad that we have worked together over the past years and finally made it through! I would also like to thank Vincent Grenier, who synthesized a lot of dyes I used in my projects and taught me patching, UV/Vis and fluorescence spectroscopy as well as HPLC, which I have again forgotten the procedures. Parker Deal, who I collaborated with on the RhoVR-HaloTag project. He is a great chemist and researcher and I really enjoy talking with him about science and games (e.g. Hearthstone, Stardew Valley, etc). Ali Walker, our 'neuron queen', who is our go-to person for neuroscience. I really appreciate the opportunity she provided to allow me, a rotation student back then, to learn neuron prep. I think that's when I started to develop an interest in working with animals and eventually move towards in vivo research towards the end of graduate years and future post-doc career. Rishi Kulkarni, who taught me slice imaging on confocal and synthesis briefly, which I failed terribly. Ben and Monica, who take over neuron prep and are doing such a wonderful job. I've learned about the hotdog eating competition, a balanced lunch and a lot other fun stuff from Ben. Monica is just super considerate and sweet, who shared me her hand cream, snacks and even brought a can of Izze all the way from home simply because I mentioned that I hadn't tried the new flavor. Molly, who is just hilarious and her cheerful spirits bring much joy to the lab. Pavel, with whom I complained about GOT last season from first to final episode and I also learned the 'shenanigans' reaction from him. Brittany, who is both funny and cool and a super fast learner on slicing. Xinqi, another hardcore Grey's Anatomy fan and a brilliant chemist. Anneliese, Josh, Marisol, Susanna, Kayli, the younger graduate students, whose addition to the lab brings more fun. I would also like to thank the undergraduates that worked with me, Vikram Muller and Hannah Thorner, who were able to work independently on not only cloning but also imaging and data analysis. Both of them contributed significantly to the projects I have worked on throughout the years.

I would also like to thank a couple of labs and professors that have helped and trained me in one way or another. The Adesnik lab, who helped with our slice and live animal experiments. Everyone in the lab is just friendly and constantly offers help and guidance. In particular, I would like to thank Professor Hillel Adesnik, who serves on my qual and thesis committee and offers me the opportunity to learn new techniques in this lab. I'm also grateful to Hillel for taking time to teach me slicing and patching. Kiarash, who maintained the animals, did so many IUEs for us (with such high success rate) and taught me slicing and perfusion. I could not have done any of the slice work without him. Savitha, who provided many plasmids and taught me slice patching. Alan and Silvio, who taught me slicing and helped me get familiar with the lab in general. Julia, who taught me neonatal viral injection. The C. Chang lab, who helped with our neuron prep significantly at the beginning and where I did my rotation on synthesis. Professor Chris Chang, who serves on my qual and thesis committee and our academic grandfather! The M. Chang lab, where I borrowed many enzymes and used their incubator and centrifuge too many times. The Hammond lab, where I used the plate reader and had so many snacks in the group room. The Hamsters are all amazing! The Xu lab, where I did my rotation on super-resolution imaging (I love the images!) and Professor Ke Xu who served on my qual committee. The Bateup lab, in particular Dan, who helped me on the virus injection and slice imaging. The Weinstein lab, our collaborator at Tel Aviv University, who gives me the opportunity to work on the BODIPY uncaging project as a rotation student.

I would like to thank my friends who have accompanied me over the past five years. Thanks to Ze and Bo, my former roommates and all the board games we played together. Thanks to Sasilada, Zhennan, Ruoxing, Jing, Zhe, Xingyu, Fangying and my other friends at Berkeley. Thanks to my friends at the Bay Area, Xin, Ce, Qian, Liang, Rongfeng, Guanhong, Guofeng with whom weekends and holidays are always full of fun and excitement. Thanks to my A*STAR friends, Zhewang, Yao, Yuxin, Han Teng, Hengjiang, Yuan, Tong, Kang Yong, some of whom I've known for close to a decade through this scholarship and I can't believe we are all finishing soon! Thanks to my A*STAR mentor, Dr. Song-Gil Lee, who has taught and helped me so much. Thanks to my friends back at Singapore, Shuting, Weilu, Yin, Jinyu, Dan, Qing, Cidong, Feng, Lingying, Miao, Ying, Haoyang, Peipei, Yanjun, Yi, Yue, Yiru, Xintong, who always make me feel at home every time I go back. Some of them have already left or will leave Singapore in a couple of years later, but I'm sure our friendship will last wherever we go. Thanks to Wei, Yue, Yucheng, Zisang, Jiayi, Qingyuan and a lot others whom I may not have seen for a long time but we are always excited every time we reunite. Thanks to my new friends at GRC who made the conference so fun.

Last but not least, I would like to thank my family. I have been attending schools overseas since 15 years old and I'm barely home over the years. But my parents have been so supportive and always have my back. I would not have been here to complete my PhD without the countless opportunities they fought so hard to offer me. My parents-in-law and the entire family who have been so caring and loving. My husband (still sounds a bit weird), Yichi, who understands me and loves me wholeheartedly. I can't wait to join him at Stanford soon (after a few weeks of break)!

Chapter 1:

Genetic Targeting of Small Molecule Fluorescent Sensors for Studying Membrane Potential

Membrane potential (V_m) arises from an unequal distribution of multiple ions across the lipid bilayer. Movement of these ions, depending on ion species and types of channels or transporters, establishes changes in the electrochemical gradient that play a critical role in multitude of biological pathways and physiological processes. In non-excitable cells, changes in membrane potential have been noted to impact cell division, proliferation and migration and are especially implicated in cancer cell biology.[1-3] Meanwhile, excitable cells such as neurons employ rapid changes in V_m or depolarization and hyperpolarization to transmit signals, creating intriguing communication networks in complex biological settings. Relentless efforts have been dedicated to understand the voltage dynamics in neuronal activity and connectivity to elucidate how the brain functions, a longstanding challenge in the field of neurobiology.

The traditional method or gold standard to quantify V_m is patch-clamp electrophysiology in which a glass electrode makes contact with a chosen cell for direct measurement. Despite the high temporal resolution, this technique is destructive and suffers from low throughput and poor spatial resolution. Fluorescence-based optical sensors have emerged as attractive tools to visualize voltage changes in a non-invasive and high throughput manner.[4-6] Advances in microscopy permit tracking fluorescence fluctuations in hundreds of cells simultaneously with desirable temporal and spatial resolution, which is particularly meaningful to dissect convoluted neural signaling pathways.

Genetically encoded voltage indicators (GEVIs) are purely protein-based sensors that can be divided into three classes (Figure 1-1). The first and earliest class of GEVIs relies on coupling a fluorescent protein with the voltage sensitive domains from ion channels or voltage-sensitive phosphatases (VSP) (Figure 1-1a). Representative tools that have been shown to work in vivo include ArcLight which combines a single FP with voltage-sensitive domain from *Ciona intestinalis* VSP (CiVSD)[7-8] as well as ASAP that uses CiVSD and circularly permutated GFP[9-11]. The second class involves the engineering of microbial rhodopsins to exhibit fluorescence fluctuations upon membrane potential changes (Figure 1-1b). One of the first designed sensors in this class is Arch[12-14] and shortly after, QuasAr (Quality superior to Arch)[15-16] were developed with enhanced properties. To overcome the low brightness of opsin-based sensors, a third class of GEVIs combing opsin with a bright fluorescent protein becomes prominent (Figure 1-1c). The FRET efficiency between the opsin and FP depends on the electric field change across the membrane. Examples in this class include a mNeon-based reporter Ace2N-mNeon[17] and a mRuby3-based reporter VARNAM[18], which both report neuronal activity with much improved signal. In the past decades, researchers have endeavored to improve the brightness, sensitivity, kinetics and membrane trafficking of GEVIs, but none is perfect or convenient enough for widespread in vivo applications in neuroscience.

Organic molecules have long been synthesized for fluorescence detection of bioactive analytes and the synthesis of small molecule voltage sensitive dyes (VSD) precedes the development of GEVIs.[4-5] Traditional VSDs fall into two categories: fast, electrochromic dyes to report neuronal action potentials but with low sensitivity[19-20], and slow dyes such as oxonols[21-22] and merocyanine 540[23-24] that shows large fractional change but perturbs membrane capacitance and do not suffice to measure fast spiking events (Figure 1-2). The Miller lab has designed a novel small molecule scaffold for monitoring voltage changes with high speed, sensitivity and brightness. This new class of

sensors, VoltageFluors or VF dyes, consist of a fluorescence dye fused with a lipophilic and electron-rich molecular wire that allows VF dyes to localize to plasma membrane for voltage sensing (Figure 1-3a).[25-26] Modulated by the transmembrane electric field, the rate of photo-induced electron transfer (PeT) from the electron-rich donor moiety affects the extent of fluorescence quenching on the dye head (Figure 1-3b). Depolarization slows down the PeT process and attenuates the quenching effect, thus fluorescence increase is expected. The mechanism of VF dyes to detect voltage changes relies on movement of electrons occurring on a nanosecond scale, which is fast enough to record millisecond-scale action potentials. In addition to the superior speed, the chemical structures can be readily modified to achieve variations in the color, sensitivity, photo-stability and other photo-physical properties to create a wide range of sensors for different applications.[27-31]

The first generation dye VF2.1.Cl is built upon a dichlorofluorescein sensor with a 27% ΔF/F per 100 mV change and its voltage sensing ability is demonstrated in cultured neurons and in ex vivo leech preparations.[25] We have later synthesized a far-red, silicon-rhodamine based sensor BeRST 1[28] and a tetramethyalrhodamine-based sensor RhoVR 1[27], which both record spontaneous spiking events in cultured hippocampal neurons with favorable sensitivity and signal-to-noise ratio. Furthermore, due to the spectral separation, both can be used simultaneously with GFP-based tools such as GCaMP6 to assess calcium and voltage fluctuations at the same time. Besides expanding the palette, we have also modified the position[27,32] or composition[29] of the molecular wire that significantly enhances sensitivity or reduces photo-toxicity of VF dyes to investigate various biological questions.

As chemically synthesized sensors lack the specificity provided by GEVIs, increasing attention has been attracted to combine synthetic sensors with a genetic component, a hybrid approach marrying the speed, brightness and sensitivity of VSDs with genetic targeting. The Fromherz lab describes the design and synthesis of an electrochromic VSD with long alkyl chains containing terminal phosphate groups.[33-35] The hydrophilic precursor dye requires a cell-surface alkaline phosphatase to remove the anionic groups before localizing to the lipid bilayer of plasma membrane. Selective staining is demonstrated in HEK cells without any functional data. Hybrid voltage sensor (hVOS) indicators designed by the Bezanilla lab and others is a FRET pair consisting of a membrane-anchored GFP and voltage-sensitive dipicrylamine (DPA).[36-38] Movement of DPA in the membrane ensuing V_m changes affects the FRET efficiency between DPA and GFP. While action potential can be recorded in cultured neurons and tissue slices, one major concern is the increased membrane capacitance due to DPA addition. A similar strategy, FlareFRET, that utilizes FRET between a rhodopsin domain Ace2N and fluorophore is developed by the Zou lab, in which a lipoic acid ligase fused to Ace2N labels a cell-impermeant fluorophore via copper-catalyzed click reaction.[39] While great membrane-bound fluorescence and voltage sensitivity were seen in HEK cells, toxicity in cultured neurons due to copper addition inhibits application in monitoring action potentials and neuronal activity. Another chemigenetic approach, Voltron, proposed by the Schreiter lab, is composed of Ace2N and a self-labeling enzyme HaloTag.[40] Membrane potential-dependent FRET occurs between Ace2N and a Janelia Fluor (JF) dye bound to HaloTag, providing a turn-off probe of 23% ΔF/F per 100 mV. The advantageous brightness and photo-stability of the JF dye allow for high-resolution voltage imaging in live animals. The Sames lab recently assembled a complex containing

VSD, dextran and a ligand targeting dopamine transporter (hDAT), a system named as VoLDeMo or Voltage Sensor-Ligand-Dextran Targeted to Monoaminergic Neurons (ChemRxiv preprint). Dextran improves the solubility of lipophilic VSDs while the ligand enables binding to endogenous receptors for staining a specific class of neurons and can be modulated. Selective staining and voltage sensitivity have been shown in hDAT-HEK cells but staining targeting endogenous receptors in tissue slice was inconclusive and not supported with functional characterization. Furthermore, the potential effect of binding native receptors on cellular physiology is not discussed.

In more recent years, efforts in the Miller lab have also been invested to incorporate the targeting feature to VF dyes so that they can be effectively employed in more complex tissues. When applied to a biological sample, VF dyes indiscriminately label all the membranes, which not only lacks cellular and subcellular resolution but also raises background signal that compromises sensitivity in imaging. Two approaches have been designed and tested, including fluorogenic activation and covalent labeling, to accomplish genetic targeting of VF dyes to selected cells (Figure 1-4). The central idea of fluorogenic activation is the use of a protecting group to quench the fluorescence of the parent dye until light- or enzyme-mediate removal to restore fluorescence and voltage sensitivity. Ideally, the protecting group cannot be too big or hydrophobic; otherwise, the caged dye might cross the plasma membrane, thus reducing the membrane-associated signal while raising the background cytosolic noise. On the other hand, in the covalent labeling scheme, a small ligand is synthetically fused to the dye of interest. A self-labeling enzyme expressed on the cell surface can react with the ligand such that the VF dye can more efficiently localize to the plasma membrane due to proximity. This process directly competes with the spontaneous insertion of the bright VF dye into the membrane; thus, enzymes with fast and selective reaction kinetics are needed. Also, a low concentration of dye is usually required to minimize background signal.

For fluorogenic activation, our lab first attempted light-controlled uncaging of a dim and inactivated dye. Using the first generation dye VF2.1.Cl as a proof of principle, we first chose dimethoxy-*o*-nitrobenzyle (DMNB) as a photo-labile protecting group, to yield SPOT or small-molecule photoactivatable optical sensors of transmembrane potential.[41] Immediate fluorescence turn-on was observed with 390 nm illumination in selected cells while other untargeted cells remained minimally fluorescent. When uncaged at neuronal processes distant from the soma, the dye successfully diffused back to cell body, allowing for connectivity tracing in a complex neuronal network. The need of UV light precludes SPOT's application in deeper tissue due to problems with scattering and penetration. Other photo-cages responsive to longer wavelengths are available and can be adapted to VF dyes for in viv*o* imaging.

Instead of light, enzyme-mediated unmasking is favored since many fluorogenic probes that can be activated by enzymes ranging from hydrolases, transferases to oxidoreductases have been designed and applied in biological imaging. [42-44] Enzyme expression is easily manipulated by protein engineering to enable specificity in cell-types or subcellular localization, thus controlling fluorescence turn-on in targeted areas of interest. The Lavis group has previously reported a selective esterase-ester pair for targeted small molecule delivery in cultured cells and tissue preparations.[45] Inspired by the remarkable selectivity and rapid reaction kinetics in their system, we appended a cyclopropylmethyl acetoxymethyl ester to reduce the fluorescence of VF2.1.Cl and

engineered a pig liver esterase (PLE) for cell-surface expression that specifically cleaves off the ester to reveal the parent dye.[46] The VF-EX dyes (VoltageFluors targeted by esterase expression) exhibit staining of appreciable contrast in both HEK cells and cultured neurons while maintaining good sensitivity. In particular, VF-EX2 outperforms GEVIs including ASAP1 and Ace2N-mNeon by displaying greatly enhanced signal to noise. More importantly, this strategy can be extended to other VF dyes. A red-shifted and more sensitive dye, carboVF, is similarly alkylated at the phenolic oxygen to diminish fluorescence, followed by PLE-directed turn-on in targeted cells.[47]

One caveat of this PLE/ester method is the bulky and hydrophobic cyclopropyl ester, which inevitably decreases water solubility of the decorated dye and limits its effective concentration and thus fluorescence signal on cells. We noticed this problem while working with the doubly protected carboVF, which showed no detectable cellular staining despite the usage of solubilizing detergent. To circumvent the issue, we have initiated projects to examine other enzyme/substrate pairs; one of which is to use galactosidase to unmask galactose as a quenching group while the hydrophilic hydroxyl groups increase solubility in aqueous buffer. Another limitation of fluorogenic activation is the background fluorescence in non-expressing cells, which primarily comes from the incomplete quenching of parent dye. Thus, the low contrast between transfected and non-transfected cells in this strategy did not generate fruitful results in preliminary experiments with tissue slices.

In the covalent tethering approach, our lab has utilized several self-labeling enzymes including SpyCatcher, SNAP-tag and HaloTag, all of which can successfully label VF dyes to specific cells of interest. Specifically, the small bacterial enzyme SpyCatcher is expressed on cell surface to capture the SpyTag ligand attached to VF2.1.Cl. At a low nanomolar concentration, more than 30 fold contrast ratio was observed in cells expressing SpyCatcher compared to non-expressing cells.[32] Another exciting feature of SpyCatcher-mediated labeling strategy is that subcellular structures can be clearly distinguished from the surrounding, an accomplishment not achieved by VF-EX dyes due to low contrast. Evoked action potentials were detected in single trials in dendritic spines, highlighting the potential to analyze electrical signals in very defined positions. Projects focused on SNAP-tag and HaloTag are undergoing in the lab, which have demonstrated promising high-contrast staining in vivo, a further breakthrough of genetic targeting of VF dyes.

This thesis mainly describes work on PLE-mediated fluorogenic activation using VF2.1.Cl and carboVF as well as attempts and progress on covalent labeling using the HaloTag system. In Chapter 2, the design, synthesis and application of VF-EX is described. In Chapter 3, efforts on generalizing the PLE/ester activation strategy to carboVF and isoVF2.2.Cl(OMe) are discussed. In addition, targeting PLE to other neuron types or subcellular locations is reviewed. In chapter 4, the development of HaloTag enzyme for covalent tethering and the translation of this selective staining to ex vivo slices and in vivo animal are described. In chapter 5, the success of adapting BeRST 1 and VF2.1.Cl for HaloTag labeling as well as the design of a soma-targeted HaloTag to confine dye staining to cell body for enhanced contrast in tissue slice is demonstrated. Fluorogenic activation using other enzyme/substrate pair is presented in Appendix 1 and 2. Appendix 3 focuses on initial efforts to design and use HaloTag virus to increase enzyme expression and dye labeling.

Figures & Schemes

Figure 1-1. *Schemes of genetically encoded voltage indicators (GEVIs).*

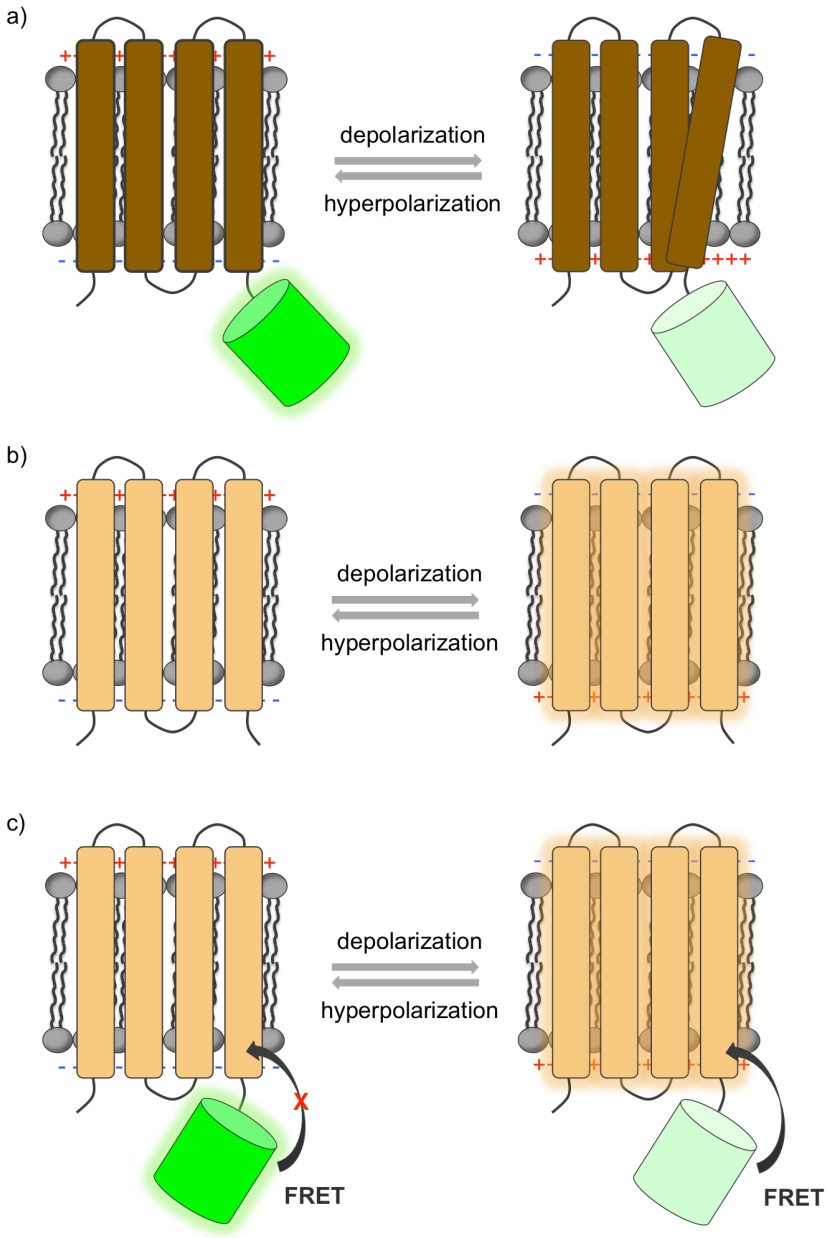

Figure 1-1. Scheme of protein-based voltage sensors. (a) Fusion protein of voltage sensitive domain to a fluorescent protein. (b) Microbial rhodopsin-based sensor. (c) Fusion protein of opsin to a fluorescent protein.

Figure 1-2. *Structures of representative small molecule voltage sensitive dyes.*

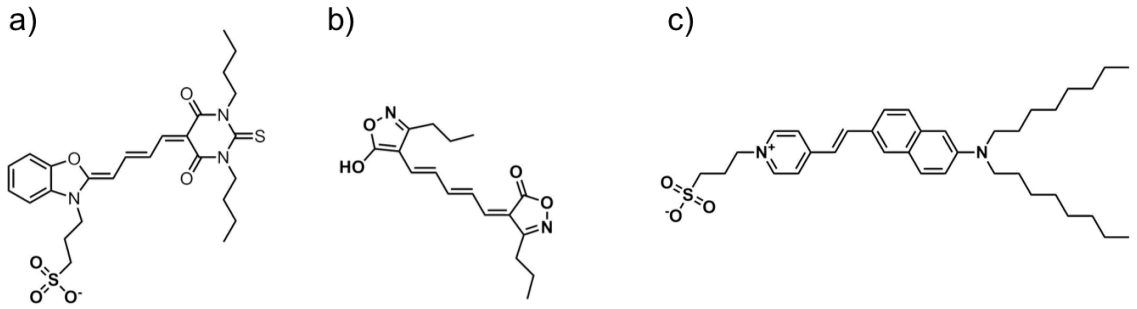

Figure 1-2. Traditional VSDs to track voltage changes include slow but sensitive dyes such as (a) merocyanine 540 and (b) oxonol VI or fast, electrochromic dyes such as (c) Di-8-ANEPPS.

Figure 1-3. *VoltageFluors represent a new class of voltage sensitive dyes for monitoring membrane potential changes.*

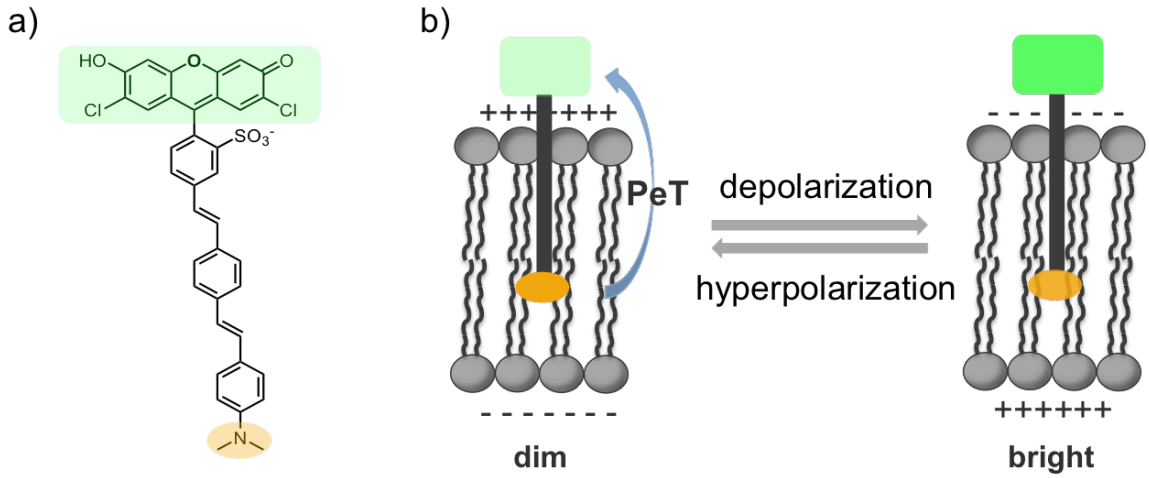

Figure 1-3. VoltageFluors dyes function through a photo-induced electron transfer mechanism. (a) Structure of the first-generation VF dye VF2.1.Cl. (b) PeT-based mechanism of voltage sensing in VF dyes.

Figure 1-4. *Scheme of genetic targeting of VoltageFluor dyes.*

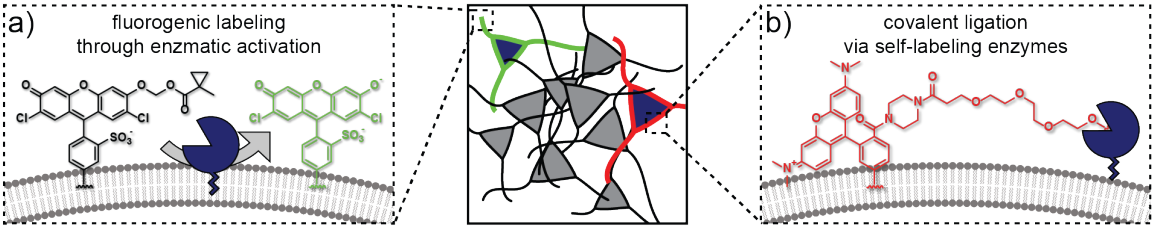

Figure 1-4. Strategies of genetic targeting of VF dyes to cell of interest. (a) Fluorogenic activation by a cell-surface enzyme to remove the masking group and release the active VF dye. (b) Covalent attachment of VF dyes by a self-labeling enzyme that reacts with a ligand synthetically linked to the dye.

Reference

1. Yang, M.; Brackenbury, W. J., *Front. Physiol.* **2013**, *4*, 185.
2. Kadir, L. A.; Stacey, M.; Barrett-Jolley, R., *Front. Physiol.* **2018**, *9*, 1661.
3. Sundelacruz, S.; Levin, M.; Kaplan, D. L., *Stem Cell Rev.* **2009**, *5* (3), 231-246.
4. Miller, E. W., *Curr. Opin. Chem. Biol.* **2016**, *33*, 74-80.
5. Kulkarni, R. U.; Miller, E. W., Biochemistry, 2017, 56, 5171-7.
6. Xu, Y.; Zou, P; Cohen, A. E.; *Curr. Opin. Chem. Biol*. **2017**, *39*, 1-10.
7. Cao, G.; Platisa, J.; Pieribone, V. A.; Raccuglia, D.; Kunst, M.; Nitabach, M. N., *Cell* **2013**, *154* (4), 904-913.
8. Jin, L.; Han, Z.; Platisa, J.; Wooltorton, J. R.; Cohen, L. B.; Pieribone, V. A., *Neuron* **2012**, *75* (5), 779-785.
9. St-Pierre, F.; Marshall, J. D.; Yang, Y.; Gong, Y.; Schnitzer, M. J.; Lin, M. Z., *Nat. Neurosci.* **2014,** *17* (6), 884-9.
10. Yang, H. H.; St-Pierre, F.; Sun, X.; Ding, X.; Lin, M. Z.; Clandinin, T.R., *Cell* **2016**, *166* (1), 245–257.
11. Chamberland, S.; Yang, H. H.; Pan, M. M.; Evans, S. W.; Guan, S.; Chavarha, M.; Yang, Y.; Salesse, C.; Wu, H.; Wu, J. C.; Clandinin, T. R.; Toth, K.; Lin, M. Z.; St-Pierre, F., *Elife* **2017**, *6*, e25690.
12. Kralj, J. M.; Douglass, A. D.; Hochbaum, D. R.; Maclaurin, D.; Cohen, A. E., *Nat. Methods* **2011**, *9*, 90-95.
13. Flytzanis, N. C.; Bedbrook, C. N.; Chiu, H., Engqvist, M. K.; Xiao, C.; Chan, K. Y.; Sternberg, P. W.; Arnold, F. H.; and Gradinaru, V. V., *Nat. Commun.* **2014**, *5*, 4894.
14. Gong, Y.; Li, J. Z.; and Schnitzer, M. J., *PLoS One* **2014**, *8*, e66959.
15. Hochbaum, D. R.; Zhao, Y.; Farhi, S. L.; Klapoetke, N.; Werley, C. A.; Kapoor, V.; Zou, P.; Kralj, J. M.; Maclaurin, D.; Smedemark-Margulies, N.; Saulnier, J. L.; Boulting, G. L.; Straub, C.; Cho, Y. K.; Melkonian, M.; Wong, G. K.; Harrison, D. J.; Murthy, V. N; Sabatini, B. L.; Boyden, E. S.; Campbell, R. E.; Cohen, A. E., *Nat. Methods* **2014**, *11* (8), 825-833.
16. Zou, P.; Zhao, Y.; Douglass, A. D.; Hochbaum, D. R.; Brinks, D.; Werley, C. A.; Harrison, D. J.; Campbell, R. E.; Cohen, A. E.; *Nat. Commun.* **2014**, *5*, 4625.
17. Gong, Y.; Huang, C.; Li, J. Z.; Grewe, B. F.; Zhang, Y.; Eismann, S.; Schnitzer, M. J., *Science* **2015**, *350* (6266), 1361-1366.
18. Kannan, M.; Vasan, G.; Huang, C.; Haziza, S.; Li, J. Z.; Inan, H.; Schnitzer, M. J.; Pieribone, V. A., *Nat. Methods* **2018**, *15* (12),1108-1116
19. Fluhler, E.; Burnham, V. G.; Loew, L. M., *Biochemistry* **1985**, *24* (21), 5749-5755.
20. Loew, L. M.; Simpson, L. L., *Biophys. J.* **1981**, *34* (3), 353-365.
21. Smith, J. C.; Russ, P.; Cooperman, B. S.; Chance, B., *Biochemistry* **1976**, *15* (23), 5094-5105.
22. Cohen, L. B.; Salzberg, B. M.; Davila, H. V.; Ross, W. N.; Landowne, D.; Waggoner, A. S.; Wang, C. H., *J. Membr. Biol.* **1974**, *19* (1), 1-36.
23. Easton, T. G.; Valinsky, J. E.; Reich, E., *Cell* **1978**, *13* (3), 475-486.
24. Davila, H.V.; Salzberg, B. M.; Cohen, L. B.; Waggoner, A. S., *Nat. New. Biol.* **1973**, *241* (109), 159-160.
25. Miller, E. W.; Lin, J. Y.; Frady, E. P.; Steinbach, P. A.; Kristan, W. B., Jr.; Tsien, R. Y., *Proc Natl Acad Sci U S A* **2012,** *109* (6), 2114-9.

26. Woodford, C. R.; Frady, E. P.; Smith, R. S.; Morey, B.; Canzi, G.; Palida, S. F.; Araneda, R. C.; Kristan, W. B.; Kubiak, C. P.; Miller, E. W.; Tsien, R. Y., *J. Am. Chem. Soc.* **2015**, *137* (5), 1817.
27. Deal, P. E.; Kulkarni, R. U.; Al-Abdullatif, S. H.; Miller, E. W., *J. Am. Chem. Soc.* **2016**, *138* (29), 9085-9088.
28. Huang, Y. L.; Walker, A. S.; Miller, E. W., *J. Am. Chem. Soc.* **2015**, *137* (33), 10767-10776.
29. Boggess, S. C.; Gandhi, S. S.; Siemons, B. A.; Huebsch, N.; Healy, K. E.; Miller, E. W., *ACS Chem. Biol.* **2019**, *14* (3) 390-396.
30. Kulkarni, R. U.; Kramer, D. J.; Pourmandi, N.; Karbasi, K.; Bateup, H. S.; Miller, E. W., *Proc. Natl. Acad. Sci. U. S. A.* **2017**, *114* (11), 2813-2818.
31. Kulkarni, R. U.; Yin, H.; Pourmandi, N.; James, F.; Adil, M. M.; Schaffer, D. V.; Wang, Y.; Miller, E. W., *ACS Chem. Biol,* **2017**, *12* (2), 407-413.
32. Grenier, V.; Daws, B. R.; Liu, P; Miller, E. W., *J. Am. Chem. Soc.* **2019**, *141* (3), 1349-1358.
33. Hinner, M. J.; Hübener, G.; Fromherz, P., *Chembiochem*. **2006**, *7* (3), 495-505.
34. Ng, D. N.; Fromherz, P., *ACS Chem. Biol.* **2011**, *6* (5), 444-445.
35. Hinner, M. J.; Hbener, G.; Fromherz, P., *J. Phys. Chem. B.* **2004**, *108* (7), 2445-2453.
36. Chanda, B.; Blunck, R.; Faria, L. C.; Schweizer, F. E.; Mody, I.; Bezanilla, F., *Nat. Neurosci.* **2005**, *8* (11), 1619-1626.
37. Wang, D.; Zhang, Z.; Chanda, B.; Jackson, M. B., *Biophys. J.* **2010**, *99* (7), 2355-2365.
38. DiFranco, M.; Capote, J.; Quiñonez, M.; Vergara, J. L., *J. Gen. Physiol.* **2007**, *130* (6), 581-600.
39. Xu, Y.; Peng, L.; Wang, S.; Wang, A.; Ma, R.; Zhou, Y.; Yang, J.; Sun, D. E.; Lin, W.; Chen, X.; Zou, P., *Angew. Chem. Int. Ed. Engl.* **2018**, *57* (15), 3949-3953.
40. Abdelfattah, A. S.; Kawashima, T.; Singh, A.; Novak, O.; Liu, H.; Shuai, Y.; Huang, Y. C.; Campagnola, L.; Seeman, S. C.; Yu, J.; Zheng, J.; Grimm, J. B.; Patel, R.; Friedrich, J.; Mensh, B. D.; Paninski, L.; Macklin, J. J.; Murphy, G. J.; Podgorski, K.; Lin, B. J.; Chen, T. W.; Turner, G. C.; Liu, Z.; Koyama, M.; Svoboda, K.; Ahrens, M. B.; Lavis, L. D.; Schreiter, E. R., *Science* **2019**. pii: eaav6416.
41. Grenier, V.; Walker, A. S.; Miller, E. W., *J. Am. Chem. Soc.* **2015,** *137* (34), 10894-10897.
enzyme-mediate fluorogenic probe
42. Chyan, W.; Raines, R. T., *ACS Chem. Biol*. **2018**, *13* (7), 1810-1823.
43. Liu, H. W.; Chen, L.; Xu, C.; Li, Z.; Zhang, H.; Zhang, X. B.; Tan, W., *Chem. Soc. Rev*. **2018**, *47* (18), 7140-7180.
44. Drake, C. R.; Miller, D. C.; Jones, E. F., *Curr. Org. Synth.* **2011**, *8* (4), 498-520.
45. Tian, L.; Yang, Y. L.; Wysocki, L. M.; Arnold, A. C.; Hu, A.; Ravichandran, B.; Sternson, S. M.; Looger, L. L.; Lavis, L. D., *Proc Natl Acad Sci U S A* **2012**, *109* (13), 4756-4761.
46. Liu, P.; Grenier, V.; Hong, W.; Muller, V. R.; Miller, E. W., *J. Am. Chem. Soc.* **2017**, *139*, 17334-17340.
47. Ortiz, G.; Liu, P.; Naing, S. H. H.; Muller, V. R.; Miller, E. W., *J. Am. Chem. Soc.* **2019**, *141* (16), 6621-6638.

Chapter 2:

Fluorogenic Targeting of Voltage Sensitive Dyes to Neurons

This work has published in the following scientific journal:

P. Liu, V. Grenier, W. Hong, V.R. Muller and E.W. Miller, Fluorogenic Targeting of Voltage-Sensitive Dyes to Neurons, *J. Am. Chem. Soc.*, **2017**, 139, 17334-17340.

Portions of this work were performed in collaboration with the following persons:
Synthesis was assisted by Vince Grenier and Wootack Hong
Cloning was assisted by Vikram Muller

Abstract

We present a method to target voltage-sensitive fluorescent dyes to specified cells using an enzyme-catalyzed fluorogenic reaction on cell surfaces. The dye/enzyme hybrids are composed of a photoinduced electron transfer (PeT)-based fluorescent voltage indicator and complementary enzyme expressed on the cell surface. Action of the exogenous enzyme on the dye results in fluorogenic activation of the dye, enabling fast voltage imaging in defined neurons, with sensitivity surpassing purely genetically-encoded approaches. We employ a bulky cyclopropylmethyl acetoxymethyl ester to diminish the fluorescence of a PeT-based voltage-sensitive dye, or VoltageFluor. The hydrolytically stable ester can be removed by the action of porcine liver esterase (PLE) to reveal the bright, unmodified VoltageFluor. We established that the chemically modified VoltageFluor is a substrate for PLE in vitro and in live cells. When PLE is targeted to the external face of cell membranes, it controls the apparent staining of cells. Use of neuron-specific promoters can direct staining to mammalian neurons to provide clear detection of neuronal action potentials in single trials. All of the new VoltageFluors targeted by esterase expression report single spikes in cultured mammalian neurons. The best, VF-EX2, does so with a signal-to-noise ratio (SNR) nearly double that of comparable genetically-encoded voltage reporters. By targeting PLE to neurons, VF-EX2 can interrogate the neuromodulatory effects of serotonin in cultured hippocampal neurons. Together, we show that a combination of synthetic chemistry and biochemistry enables bright and fast voltage imaging from genetically-defined neurons in culture.

Introduction

Direct visualization of changes in membrane potential using fluorescent indicators offers a powerful method for probing voltage dynamics in neurons with unprecedented spatial and temporal resolution.[1] Despite the promise of voltage imaging, key challenges of speed, sensitivity, brightness and localization remain. Purely genetically-encoded approaches based on fluorescent proteins or opsins afford the opportunity to target neuronal cell types of interest in complex brain contexts, providing exquisite fluorescence contrast between the cell of interest and its surroundings.[2-6] However, brightness, speed, or sensitivity often limit the wide-spread application of these powerful new genetically-encoded methods. To address these limitations, we have been developing fluorescent voltage indicators that rely on photoinduced electron transfer (PeT) as a membrane potential dependent trigger to control the emission of a fluorescent dye.[7] PeT-based dyes, or VoltageFluors (VF dyes), display voltage sensitive fluorescence, owing to modulation of the rate of PeT within the VF scaffold by the transmembrane electric field.[8] VF dyes therefore possess the requisite speed and sensitivity to report on action potentials in neurons in single trials. Although VF dyes localize to the outer leaflet of cell membranes to sense voltage,[9-10] one current limitation of chemically-synthesized dyes is their inability to discriminate between membranes of different cells. This precludes cell-specific targeting, which significantly erodes signal to noise and cellular resolution compared to genetically encoded approaches.[9-10] To marry the speed, sensitivity, and brightness of synthetic VF dyes with the cell-type specificity enabled by genetically encoded approaches, we combine VF dyes with a genetically encoded component to enable high-contrast imaging in defined neurons. We achieve this with a fluorogenic approach, in which the parent VF dye is chemically modified to be minimally fluorescent

and must be enzymatically activated prior to imaging. The dim VF dye localizes to all cellular membranes where it remains weakly fluorescent until enzymatic cleavage of the chemical modification by an exogenously expressed enzyme (Scheme 2-1). This results in bright, localized fluorescence only in the cells which express the cognate enzyme. Based on our previous photoactivation studies,[11] we hypothesized that a hydrolytically stable, bulky acetoxymethyl ester[12] appended to the phenolic oxygen of VoltageFluor2.1.Cl (VF2.1.Cl)[10] would diminish VF fluorescence. Previous studies showed that intracellular porcine liver esterase (PLE) is capable of unmasking bulky acetoxymethyl esters inside living cells.[12]

Results

VF-EX1 and VF-EX2 (Scheme 2-2) are synthesized in a single step from VF2.1.Cl. Addition of iodo-1-methylcyclopropanecarboxylate to VF2.1.Cl in N,N-dimethylformamide (DMF) in the presence of N,N-diisopropylethylamine (DIPEA) gave VF-EX1 (stoichiometric iodoalkane) or VF-EX2 (excess iodoalkane) (Scheme 2-2). The two different products were characterized by NMR, HPLC, and mass spectrometry. Both VF-EX1 and VF-EX2 display optical properties consistent with O-alkylated fluoresceins[13] – a weak absorbance at λ = 500 nm (Figure 2-1a/d, see Figure 2-2 for excitation spectra). VF-EX1 and VF-EX2 are minimally fluorescent, with quantum yields of 0.004 and 0.013, respectively (HBSS, pH 7.4). Compared to VF2.1.Cl, which has a quantum yield of 0.08 under identical conditions, this represents a 19- and 6.7- fold decrease in fluorescence intensity (Figure 2-1b/e). VF-EX0, in which only the sulfonic acid is esterified (Scheme 2-3), has a quantum yield of 0.24, consistent with a 3-fold increase in quantum efficiency for sulfonate esters (VF-EX0, VF-EX2) compared to their cognate acids (VF2.1.Cl, VF-EX1, Table 2).

We confirmed that purified porcine liver esterase (PLE, Sigma, E2884) hydrolyzes VF-EX1 and VF-EX2 in vitro. The action of PLE on VF-EX1 or VF-EX2 results in a 53- and 11-fold increase in fluorescence after 3 hr. The fluorescence increase is accompanied by a restoration of a fluorescein-like absorption and emission profile (Figure 2-1a,b and d,e). HPLC analysis revealed VF2.1.Cl as the product of PLE-mediated hydrolysis reactions (Figure 2-3). Both substrates show saturation-type enzymatic kinetics with PLE. The Michaelis constant, K_M, for VF-EX1 is 1.2 ± 0.5 μM and for VF-EX2 is 0.12 ± 0.03 μM, (Figure 2-1c,f and Table 2) comparable to the reported values of 0.5 μM for biscyclopropylacetoxymethylfluorescein.[12] VF-EX2 is a better substrate than VF-EX1, as evidenced by the larger k_{cat}/K_M for VF-EX2 (1.3×10^6 $M^{-1}s^{-1}$) vs. VF-EX1 (2.1×10^5 $M^{-1}s^{-1}$) (Table 2). We hypothesize that masking of the anionic sulfonate charge in the case of VF-EX2 makes it a better substrate for PLE.

Having confirmed VF-EX1 and VF-EX2 as substrates for PLE, we next set out to target and express PLE to the surface of eukaryotic cells. Although trafficking to the endoplasmic reticulum (ER) is required for proper cellular PLE activity,[12] we found that removal of the PLE-associated ER retention signal, addition of a transmembrane domain (platelet-derived growth factor receptor, PDGFR, from pDisplay)[14] or glycophosphatidyl inositol anchor signal (GPI, from decay accelerating factor, DAF),[15] and inclusion of a secretion signal derived from immunoglobulin K (IgK) results in clear membrane localization on HEK cells as determined by immunostaining fixed cells (Figure 2-4 and 2-5). Bath application of VF-EX1 or VF-EX2 (500 nM, 30 minutes) to HEK cells

transiently transfected with PLE-DAF or PLE-pDisplay results in clear membrane-associated fluorescence in transfected cells (indicated by nuclear-localized mCherry, Figure 2-6a-d, g-j).

Cells in the same culture that do not express mCherry (and therefore do not express PLE) show negligible levels of membrane-associated fluorescence (Figure 2-6a,c and g,i, Scheme 2-1). Membrane targeting of VF-EX dyes with DAF gave the brightest cells and the largest contrast between PLE-expressing and PLE(-) cells (Figure 2-7, see Figure 2-8 for quantification). DAF-mediated targeting was therefore used for subsequent studies. We examined a number of flexible linker lengths (GGGGS repeats) between PLE and the DAF sequence and found no correlation between linker length and contrast between transfected and control HEK cells treated with VF-EX2 (Figure 2-9). We therefore used the smallest linker length for future studies. Quantification of the difference in fluorescence intensity for PLE-expressing cells vs. controls indicates a contrast of 7-fold between PLE-expressing cells and control cells for VF-EX1 and 17 for VF-EX2, which we attribute to the higher k_{cat}/K_M value for VF-EX2 (Figure 2-1f, Table 2). Longer incubation times with VF-EX2 at 500 nM (up to 2 hours) increased overall fluorescence, but lowered contrast between transfected and untrasfected cells on account of increasing fluorescence in untransfected cells (Figure 2-10a,b). This increase in fluorescence in untransfected cells is due to accumulation of weakly fluorescent VF-EX2 in membranes and not to uncatalyzed hydrolysis, since cells that had been loaded with VF-EX2 for 30 minutes (500 nM), washed, and then monitored over time showed no increase in fluorescence from untransfected cells (Figure 2-10c,d).

The fluorescence associated with PLE-expressing HEK cells was voltage-sensitive; VF-EX1 and VF-EX2 displayed high, linear voltage sensitivities of 19 ± 0.3 and 21 ± 0.3% ΔF/F per 100 mV, comparable to 27% measured for VF2.1.Cl (Figure 2-6e,f and k,l). We additionally confirmed that cell-surface PLE uncages VF-EX2 only within the cell membrane of the cell which expresses PLE (in cis) and not on neighboring cells (in trans). HEK cells expressing PLE on the cell surface and mCherry in the nucleus were plated on top of a monolayer of HEK cells that did not express PLE and had previously been loaded with VF-EX2. If PLE acted in trans, we predicted that addition of PLE-expressing HEK cells to the non-expressing, dye-loaded cells would result in an increase in fluorescence, similar to what we observe when we add purified PLE to HEK cells loaded with VF-EX2 (Figure 2-11a-d). However, if PLE only acts in cis, then addition of PLE-expressing HEK cells will not result in an increase in fluorescence. We observe no increase in fluorescence upon addition of PLE expressing HEK cells to cells loaded with VF-EX (Figure 2-11e-j), confirming both that cell-surface localized PLE cannot act in trans, and that VF-EX2 does not diffuse out of membranes to cells expressing PLE. Importantly, a positive control experiment demonstrates that the harvested PLE-expressing HEK cells can turn-over VF-EX1 if the VF-EX1 is added directly to these PLE-expressing cells (Figure 2-11k). Previous studies establish that the product of VF-EX2 uncaging, VF2.1.Cl, diffuses primarily within membranes and not across membranes.[11] We also established that VF-EX2 does not cross plasma membranes, as HEK cell expressing ER-targeted PLE do not accumulate internal fluorescence (Figure 2-12).

VoltageFluor-EX dyes provide enhanced contrast in neurons. Fixed-cell immunofluorescence established efficient cell-surface targeting of PLE in rat

hippocampal neurons transfected with PLE-DAF under the neuron-specific synapsin promoter (Syn, Figure 2-13, Figure 2-4) or calmodulin kinase II promoter (CaMKII, Figure 2-14, Figure 2-4). Use of a strong, non-specific promoter construct from pCAGS, results in primarily neuronal expression with some glial expression, as assayed by co-localization with glial fibrillary acid protein, GFAP (Figure 2-15). Live cell staining with VF-EX1 and VF-EX2 (1 μM, 1 hour) results in clear enhancement of membrane-associated fluorescence in transfected neurons, with a 4.1- and 4.8-fold increase in fluorescence for Syn-PLE expressing neurons stained with VF-EX1 and VF-EX2 (Figure 2-16a-d, Figure 2-17a-d) and a 3.0- and 3.7- fold increase in fluorescence for CaMKII-PLE expressing neurons with VF-EX1 and VF-EX2 (Figure 2-16e-h, Figure 2-17e-h), respectively (Table 2, Figure 2-18a). The cell-type specific membrane associated fluorescence with VF-EX1 and VF-EX2 is voltage sensitive. Like the parent VF dyes,[8,10,16] VF-EX1 and 2 give clear responses to field-stimulation electrode-evoked action potentials (Figure 2-19a) and the ability to record spontaneous spiking in hippocampal cultures (Figure 2-16i, Figure 2-17i). We selected VF-EX2 for future use in neurons because of its greater brightness in neurons (Figure 2-18b,c). Longer incubation times with VF-EX2 (1 μM, up to 120 minutes), increased the relative fluorescence intensity of PLE-expressing cells (Figure 2-18d). The overall contrast between PLE and wild-type neurons decreased slightly as a result of increased accumulation of VF-EX2 in cell membranes (Figure 2-18d,e). As with HEK cells (Figure 2-10), this is due to nonspecific accumulation of VF-EX2 and not hydrolysis, as neurons loaded for 30 minutes (1 μM VF-EX2) followed by a wash show negligible increases in fluorescence from non-transfected neurons (Figure 2-18f).

We compared the performance of VF-EX2/Syn-PLE to genetically-encoded fluorescent voltage indicators: ASAP1,[2] based on circularly permuted green fluorescent protein (cpGFP), or Ace2N-mNeon (here abbreviated Ace2N),[4] which uses mNeon.[17] VF-EX2/PLE compared favorably to both ASAP1 and Ace2N, displaying improved membrane associated fluorescence relative to ASAP1 and Ace2N (Figure 2-19a-c, Figure 2-21), turn-on responses to spontaneous action potentials (both ASAP1 and Ace2N show turn-off responses to action potentials, Figure 2-19e,f), and an average 7.3 ± 0.8% ΔF/F per spike (20 ± 2.7 SNR) for evoked action potentials compared to -6.5 ± 0.3% for ASAP1 (4.9 ± 0.6 SNR) and -2.9 ± 0.1% for Ace2N (11 ± 0.7 SNR) (132, 62, and 106 action potentials from 16, 7, and 13 separate neurons, respectively (Figure 2-19g,h, Figure 2-20). Under the identical illumination conditions, VF-EX2 has photo-stability comparable to that of ASAP1 and Ace2N (Figure 2-20 and 2-21). The improved fluorescence staining on the cell membrane results from the use of the hybrid chemical-genetic approach. Although genetically-encoded fluorescent proteins traffic to the cell surface, a significant portion of the fluorescent protein-based indicator remains in the cellular export pathways and contributes to unresponsive background fluorescence. In contrast, while membrane-targeted PLE is also making its way through the cellular export pathways, it is non-fluorescent.

The ability of the VF-EX2/PLE system to label specific, genetically-defined cells, coupled with its high voltage sensitivity, make it a promising candidate for interrogating membrane potential dynamics in complex neuronal systems. For example, the neuromodulator serotonin (5-hydroxytryptamine, or 5-HT) exerts diverse effects within the brain and body, depending upon cell type, 5-HT receptor (5-HTR) subtype, and pre-

or post-synaptic localization of the receptor. Numerous serotonergic neurons project onto the hippocampus in the rat brain, delivering 5-HT to modulate neuronal activity. The complex expression pattern of the 14 distinct 5-HTR subtypes[18] in the hippocampus complicates the dissection of molecular pathways involved in mediating the effects of 5-HT. Treatment of hippocampal cultures stained with VF-EX2/PLE exclusively in neurons (CaMKII promoter) with 5-HT (10 μM) shows decreased spiking rates, from 2.5 ± 0.7 Hz to 1.5 ± 0.5 Hz in 5-HT (Figure 2-22 and Figure 2-23).[19] Washout of 5-HT results in a recovery of neuronal spiking to 2.4 ± 0.4 Hz (Figure 2-22a). The decrease in firing rate could be mediated through a number of different pathways: the action of 5-HT1 receptors coupling to inward rectifying potassium channels (K_{ir} channels) via G-protein coupled receptors (GPCRs), resulting in a direct hyperpolarization; the activation of 5-HT2 receptors coupling to release of Ca^{2+} stores via phospholipase C (PLC) and activating inhibitory neurons to decrease overall firing; or through the opening of ion channel-type 5-HT3 receptors causing a depolarization of inhibitory cells. To resolve some of these ambiguities, we again assessed the neuromodulatory effect of 5-HT on the activity of hippocampal neurons using VF-EX2/PLE. Pre-treatment with the 5-HT1A-selective antagonist, WAY 100635 (10 nM; 1.4 nM IC_{50}),[20] prior to 5-HT addition causes a complete loss of the serotonin-mediated decrease in activity in neurons (Figure 2-22b and Figure 2-23). These results suggest the decrease in firing in hippocampal neurons accompanied by serotonin treatment is mediated primarily through 5-HT1A receptors. In support of this model, pre-treatment with ketanserin (100 nM; 2 nM K_i),[21] an antagonist with specificity for 5-HT2 receptors, has no effect on the serotonin-mediated decrease in firing (Figure 2-22c and Figure 2-23). Importantly, firing rates for all neurons were uniform prior to and after washout of 5-HT ($p > 0.1$, across all pair-wise comparisons, Figure 2-23). The use of cell type-specific expression of VoltageFluor-EX system enables a rapid method for dissection of complex neurobiological signaling pathways.

Discussion

In summary, we present the design, synthesis, evaluation, and application of the VoltageFluor-EX hybrid system for fluorogenic targeting of PeT-based fluorescent voltage indicators to specific cells. Fluorogenic targeting using a hybrid small molecule/enzymatic activation approach combines the speed and sensitivity of PeT-based voltage indicators with the cellular specificity of genetic encoding. We show that two VoltageFluor derivatives, VF-EX1 and VF-EX2, with methylcyclopropylacetoxymethyl ester modifications, provide an efficient means of generating high contrast fluorescence in individual neurons. While enzymatic targeting has been employed previously to improve membrane localization of electrochromic dyes,[22-24] these strategies have never been deployed in neurons for functional imaging. Alternative hybrid approaches rely on lipophilic fluorescence quenchers[25] that introduce prohibitive capacitance to the neurons under observation.[26] Here we demonstrate that the VoltageFluor-EX system enables the use of fast, sensitive, non-disruptive VoltageFluor2.1.Cl[8] in specified cells to report on neuronal action potentials with large, linear turn-on responses surpassing the signal-to-noise and sensitivity achieved with fluorescent protein and FRET-opsin voltage indicators under identical conditions. We show that targeting VF-EX2 to neurons enables the dissection of the neuromodulatory effects of serotonin in hippocampal neurons.

When compared to their genetically encoded counterparts, VF-EX dyes lag behind in terms of contrast between transfected and untransfected neurons. Low contrast for VF-EX/PLE in neurons relative to HEK cells may be due, in part, to the lower expression levels of PLE achieved under specific, but weaker promoters like synapsin and CaMKIIα. This may be partially addressed by coupling strong promoters (i.e. CMV) to genetic methods for obtaining cell-type specificity. Improvements can also be made on the chemical side. The dynamic range between caged and uncaged fluorophore can be tuned by altering the amount of PeT between the fluorophore and pendant aryl ring.[27] Larger spectral separation between the excitation maxima of the caged and free dye would also improve contrast. Further improvement in cellular contrast is likely needed for routine usage in vivo. Taken together, this methodology sets the stage for employing fast, sensitive, fluorogenic PeT-based voltage indicators in intact brain tissues, and efforts are underway in our lab to apply this method both to new targeting modalities using complementary substrate/enzyme pairs, expand the palette of fluorogenic voltage indicators, and deploy these probes to intact brains in vivo.

Experimental section

General Synthetic and Analytical Methods

Anhydrous sodium iodide and diisopropylethylamine were purchased from Sigma-Aldrich. Anhydrous solvents (acetonitrile, dichloromethane and N,N-dimethylformamide) were purchased from Acros Organics. VF2.1.Cl and chloromethyl 1-methylcyclopropanecarboxylate were synthesized according to literature procedures.[11,12]

^{1}H and ^{13}C NMR spectra were collected in $(CD_3)_2SO$ (anhydrous, Alfa Aesar, Ward Hill, MA or Cambridge Isotope Laboratories, Cambridge, MA) or $CDCl_3$ (Cambridge Isotope Laboratories, Cambridge, MA) at 25 °C on a Bruker AV-600 spectrometer at the College of Chemistry NMR Facility at the University of California, Berkeley, or at the QB3 Central California 900 MHz NMR Facility. All chemical shifts are reported in the standard δ notation of parts per million using the peak of residual proton signals of $(CD_3)_2SO$ or $CDCl_3$ as an internal reference. Low resolution LC/ESI-MS was performed on an Advion Expression LC-MS coupled to an Agilent Infinity 1220 HPLC, with a Phenomenex Luna 5 µm C18(2) 75 x 4.6 mm column. Semi-preparative HPLC was performed on a Perkin Elmer Series 200 HPLC, with a Phenomonex Luna 5 µm C18(2) 150 x 10 mm column. In both cases water (eluent A) and acetonitrile (eluent B) were employed as the mobile phase, with 0.05% trifluoroacetic acid present as an additive. For analytical HPLC the mobile phase was ramped from 10 to 100% eluent B over eight minutes, then held at 100% B for two minutes at a flow rate of 1.0 mL/minute. For semi-preparative HPLC the mobile phase was ramped from 10 to 100% eluent B over twenty minutes at 5.0 mL/minute. High resolution mass spectra (HR-ESI-MS) were acquired at the QB3/Chemistry Mass Spectrometry Facility at the University of California, Berkeley.

Synthetic Procedures

Example preparation of iodomethyl 1-methylcyclopropanecarboxylate

In a 4 mL dram vial chloromethyl 1-methylcyclopropanecarboxylate (205 mg, 1.38 mmol) and sodium iodide (221 mg, 1.47 mmol) were dissolved in 1 mL of anhydrous acetonitrile. The reaction was stirred under N_2 for 23 hours, at which time a small aliquot was drawn and the reaction was found to have reached completion by ^{1}H NMR. The reaction was diluted with 2 mL of anhydrous dichloromethane and filtered through a cotton plug. Solvents were removed under reduced pressure at 25 °C to yield a golden liquid over residual salts. The supernatant was carefully pipetted into a tared vial to obtain 228 mg (0.706 mmol) of pure iodommethyl 1-methylcyclopropanecarboxylate. The reagent was then employed neat, or as a 1.00 M solution in anhydrous N,N-dimethylformamide for use in subsequent reactions.

^{1}H NMR (600 MHz, $CDCl_3$) δ 5.90 (s, 2H), 1.29 (s, 3H), 1.27 (dd, J = 7.5, 3.9 Hz, 2H), 0.73 (dd, J = 7.6, 4.0 Hz, 2H).

^{13}C NMR (151 MHz, $CDCl_3$) δ 173.86, 31.36, 31.34, 18.98, 17.00.

Synthesis of ((2,7-dichloro-9-(4-((E)-4-((E)-4-(dimethylamino)styryl)styryl)phenyl)-3-oxo-3H-xanthen-6-yl)oxy)methyl-1-methylcyclopropane-1-carboxylate (VF-EX1)

In a 4 mL dram vial VF2.1.Cl (25.1 mg, 36.7 μmol, 1 equivalent) was dissolved in 175 μL of anhydrous N,N-dimethylformamide and 25.6 μL of diisopropylethylamine (147 μmol, 4 equivalents), followed by addition of 36.6 uL of a 1.00 M solution of iodomethyl 1-methylcyclopropanecarboxylate in anhydrous N,N-dimethylformamide (36.6 μmol, 1 equivalent). The reaction was stirred under N_2 at room temperature and monitored by LC-MS. After one hour approximately 50% of the starting material had been consumed. An additional 0.75 equivalents of iodomethyl 1-methylcyclopropanecarboxylate were added. One hour later approximately 15% VF2.1.Cl remained and the reaction was neutralized with 50 μL acetic and diluted with 2 mL of dimethylsulfoxide. The diluted reaction was purified by semi-preparative HPLC without further workup to obtain 4.77 mg of product (5.99 μmol) following evaporation of the mobile phase at a bath temperature of 60 °C and drying under high vacuum.

^{1}H NMR (900 MHz, $(CD_3)_2SO$) δ 8.17 (s, 1H), 7.80 (d, *J* = 7.8 Hz, 1H), 7.67 (d, *J* = 7.8 Hz, 2H), 7.59 (s, 1H), 7.57 (d, *J* = 7.9 Hz, 2H), 7.48 (d, *J* = 8.0 Hz, 2H), 7.44 (s, 1H), 7.40 (d, *J* = 16.6 Hz, 1H), 7.28 (d, *J* = 7.7 Hz, 1H), 7.21 (d, *J* = 16.3 Hz, 1H), 7.07 (s, 1H), 7.03 (d, *J* = 16.3 Hz, 1H), 6.98 (s, 1H), 6.80 (s, 2H), 6.47 (s, 1H), 6.00 (s, 2H), 2.96 (s, 6H), 1.25 (s, 3H), 1.18 – 1.14 (m, 2H), 0.84 – 0.82 (m, 2H).

^{13}C NMR (226 MHz, $(CD_3)_2SO$) δ 176.25, 173.74, 158.18, 158.02, 157.86, 157.75, 155.20, 151.41, 151.07, 147.36, 138.54, 137.63, 135.19, 132.45, 130.08, 130.06, 129.75, 129.74, 128.82, 128.81, 127.65, 127.62, 127.27, 127.19, 126.63, 126.52, 126.25, 125.31, 118.41, 118.22, 117.07, 104.15, 102.84, 84.99, 54.90, 18.65, 18.29, 16.79, 16.76.

Analytical HPLC retention time: 6.36 minutes.

HR-ESI-MS $[M-H]^-$ calculated 794.1388, found 794.1381

Synthesis of ((9-(4-((E)-4-((E)-4-(dimethylamino)styryl)styryl)-2-((((1-methylcyclopropane-1-carbonyl)oxy)methoxy)sulfonyl)phenyl)-3-oxo-3H-xanthen-6-yl)oxy)methyl 1-methylcyclopropane-1-carboxylate (VF-EX2)

In a 4 mL vial VF2.1.Cl (23.2 mg, 33.89 μmol, 1 equivalent) was dissolved in 203 μL of a 1.00 M solution of iodomethyl 1-methylcyclopropanecarboxylate in anhydrous N,N-dimethylformamide (203 μmol, 6 equivalents) and 35.4 μL of diisopropylethylamine (203 μmol, 6 equivalents). The reaction was stirred under N_2 at room temperature and monitored by LC-MS. After two and a half hours VF-EX2 and VF-EX1 were present in an approximately 1:1 ratio. An additional 4 equivalents of iodomethyl 1-methylcyclopropanecarboxylate were added. Two hours later the reaction was found to have reached completion. The reaction was neutralized with 50 μL of acetic acid and diluted with 2 mL of dimethylsulfoxide. The diluted reaction was purified by semi-preparative HPLC without further workup to obtain 9.83 mg of product (10.8 μmol) following evaporation of the mobile phase at a bath temperature of 60 °C and drying under high vacuum.

^{1}H NMR (900 MHz, $(CD_3)_2SO$) δ 8.20 (s, 1H), 7.93 (d, J = 8.4 Hz, 2H), 7.86 (d, J = 8.3 Hz, 2H), 7.81 (d, J = 7.7 Hz, 1H), 7.75 (d, J = 7.8 Hz, 2H), 7.68 (d, J = 7.8 Hz, 2H), 7.59 (s, 1H), 7.51 (d, J = 16.5 Hz, 1H), 7.49 (d, J = 16.4 Hz, 1H), 7.44 (d, J = 16.4 Hz, 1H), 7.40 (d, J = 16.4 Hz, 1H), 7.29 (d, J = 7.6 Hz, 1H), 7.07 (s, 1H), 6.98 (s, 1H), 6.46 (s, 1H), 6.00 (s, 2H), 5.72 (s, 2H), 3.64 (s, 6H), 1.24 (s, 3H), 1.18 – 1.14 (m, 2H), 1.11 (s, 3H), 0.95 (m, 2H), 0.83 (m, 2H), 0.78 – 0.75 (m, 2H).

^{13}C NMR (226 MHz, $(CD_3)_2SO$) δ 176.23, 173.73, 172.35, 158.15, 157.98, 157.73, 155.20, 151.41, 150.97, 147.38, 141.41, 139.18, 138.35, 136.79, 136.16, 132.45, 130.98, 130.09, 129.80, 129.71, 127.63, 127.51, 127.46, 127.27, 127.23, 126.64, 126.20, 125.45, 122.02, 118.41, 118.20, 117.03, 104.16, 102.83, 84.98, 84.01, 51.01, 18.64, 18.28, 18.24, 17.97, 17.01, 16.78, 16.75.

Analytical HPLC retention time: 6.29 minutes. A minor peak (5.5% peak area by integration at 254 nm) with retention time 6.67 minutes can be observed eluting after the main product peak. This minor peak also has the correct product mass. It has been our experience that installing bulky esters at the 3 position of xanthene-based VoltageFuors leads to the formation of conformational isomers, and we believe that this is the case here.[28]

HR-ESI-MS $[M+H]^+$ calculated 908.2057, found 908.2079

Spectrum 1-1. ^{1}H NMR of iodomethyl 1-methylcyclopropanecarboxylate.

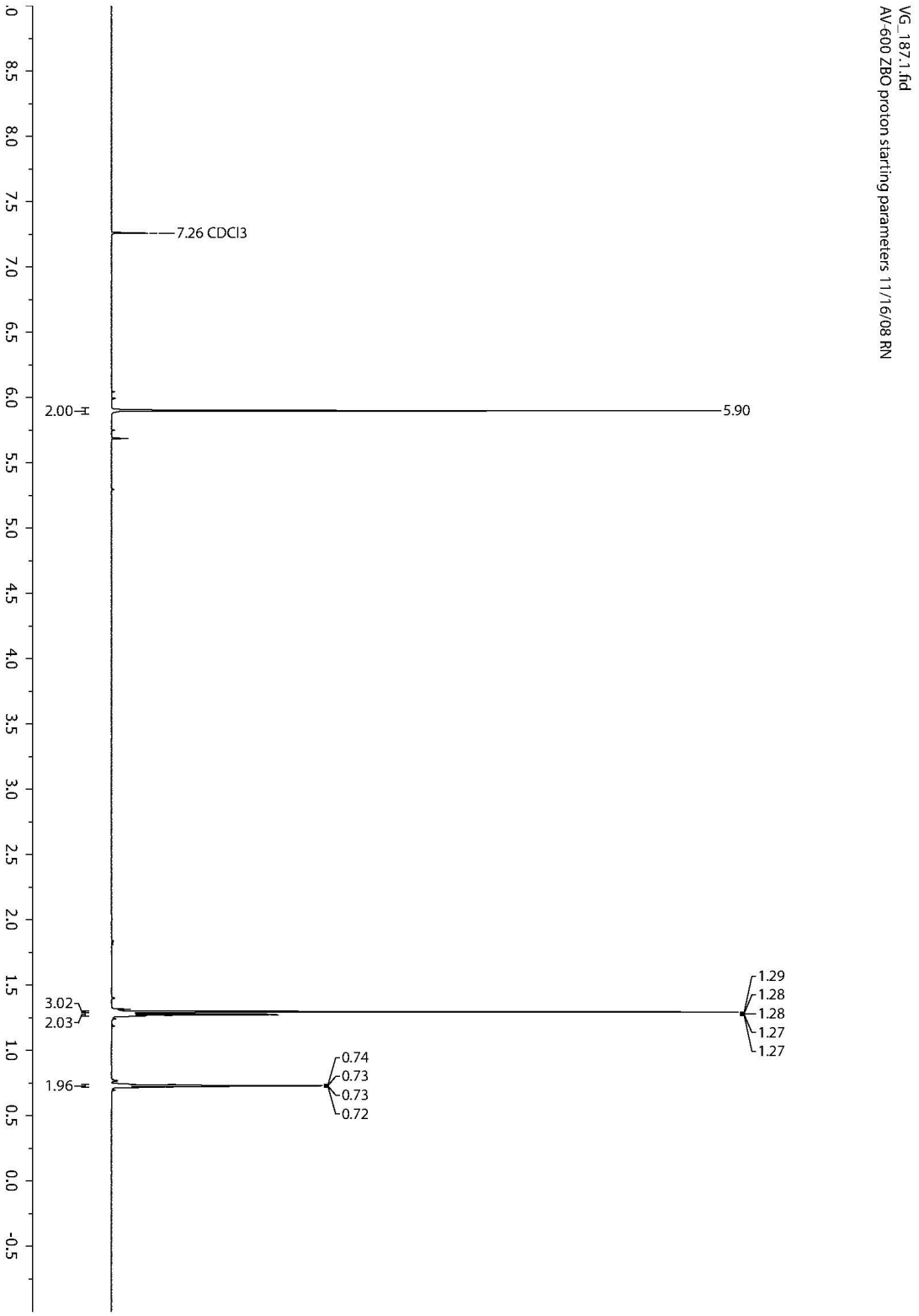

Spectrum 1-2. ^{13}C NMR of iodomethyl 1-methylcyclopropanecarboxylate.

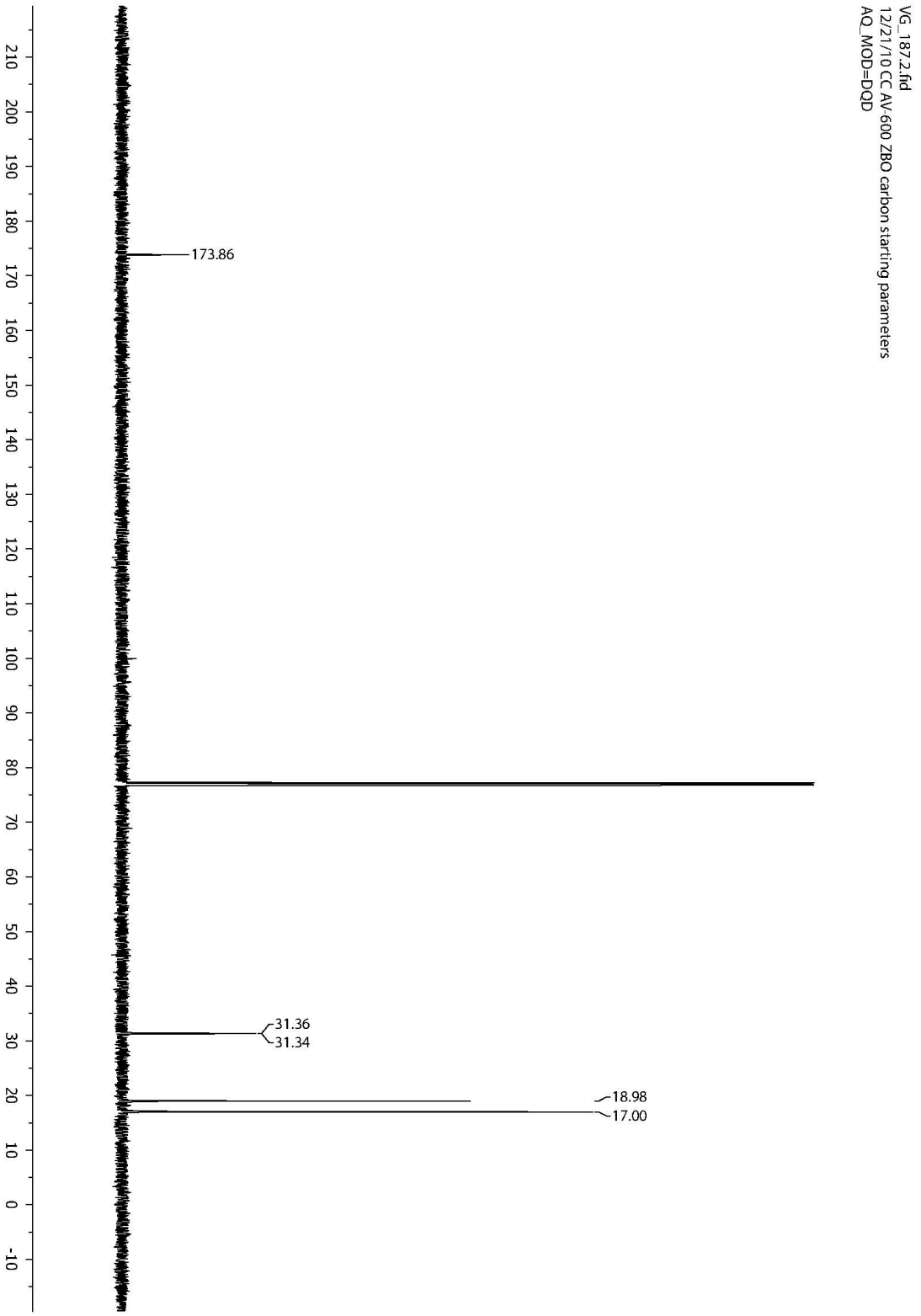

Spectrum 1-3. ^{1}H NMR of VF-EX1.

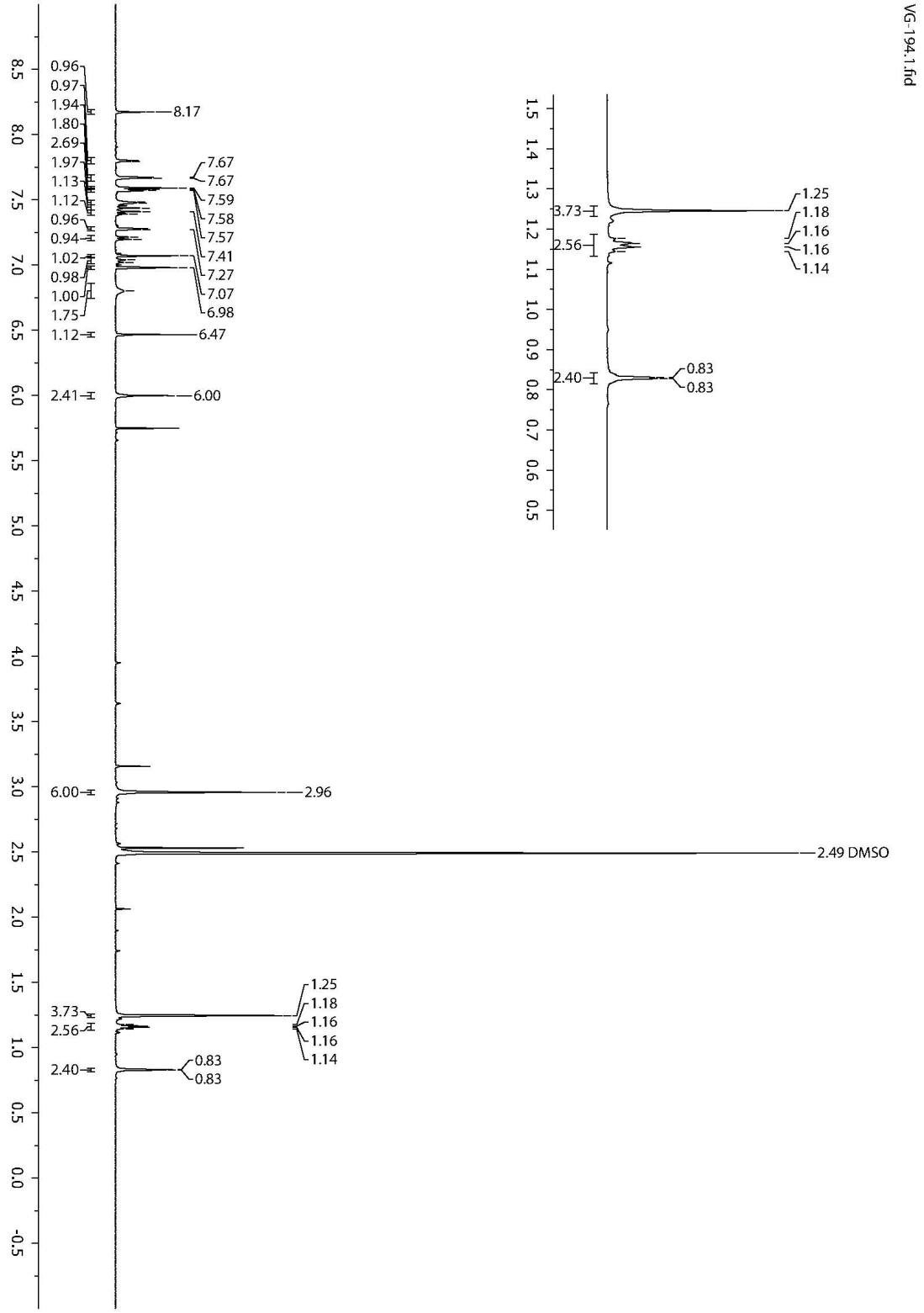

Spectrum 1-4. ^{13}C NMR of VF-EX1.

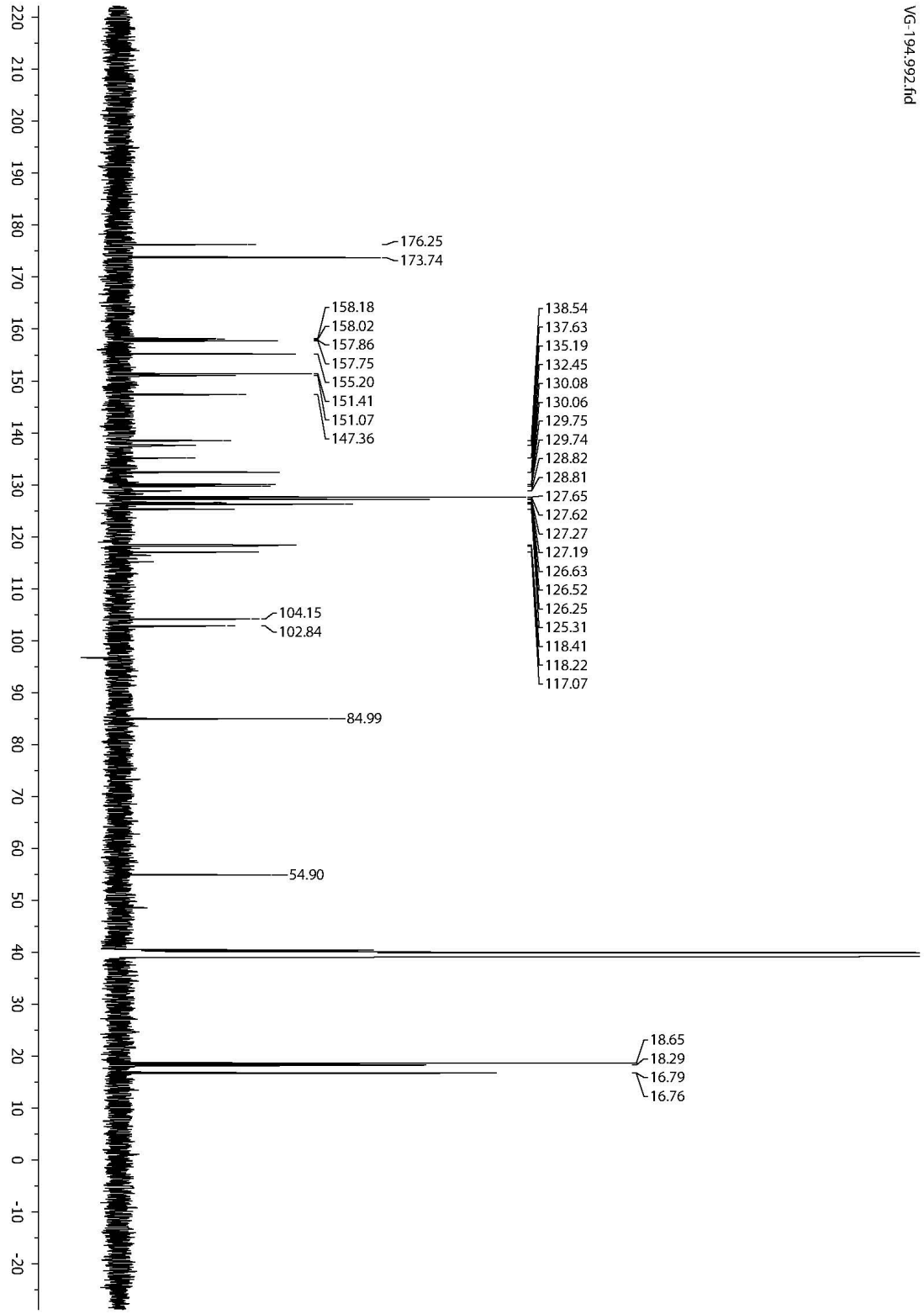

Spectrum 1-5. LC-MS of VF-EX1.

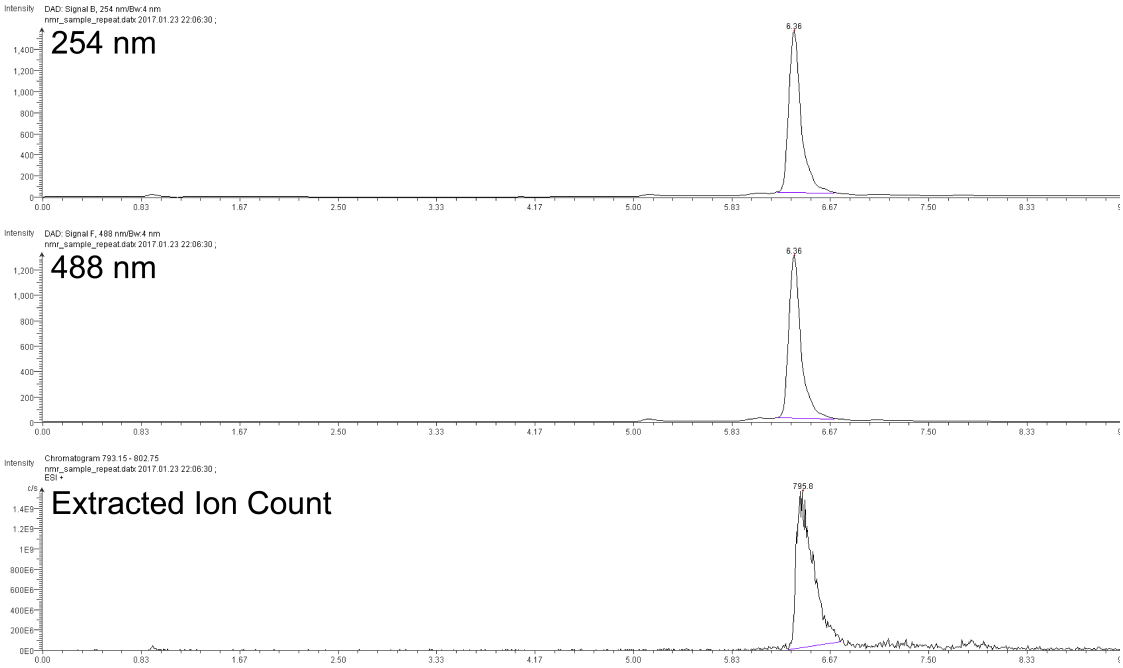

Spectrum 1-6. ^{1}H NMR of VF-EX2.

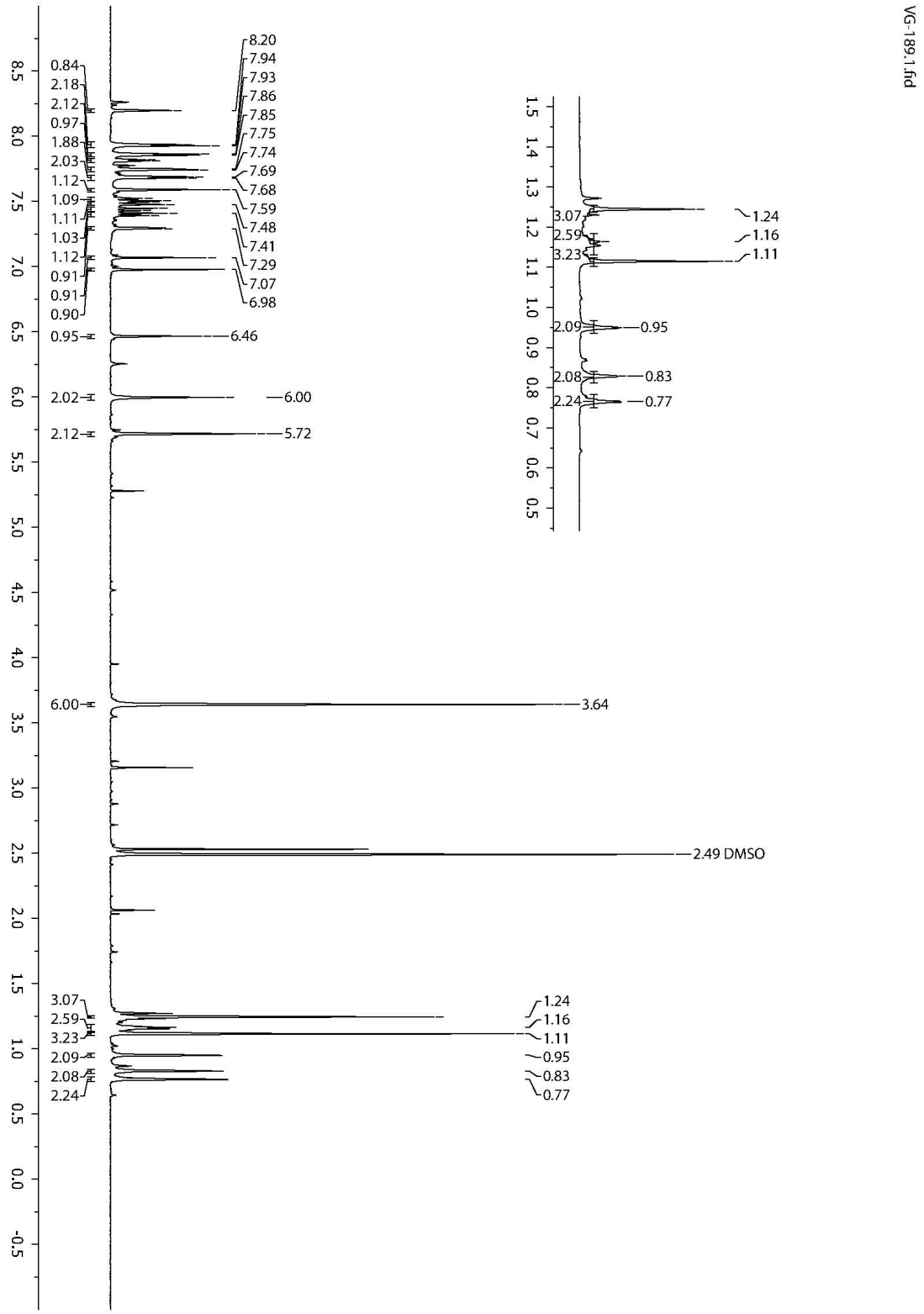

Spectrum 1-7. ^{13}C NMR of VF-EX2.

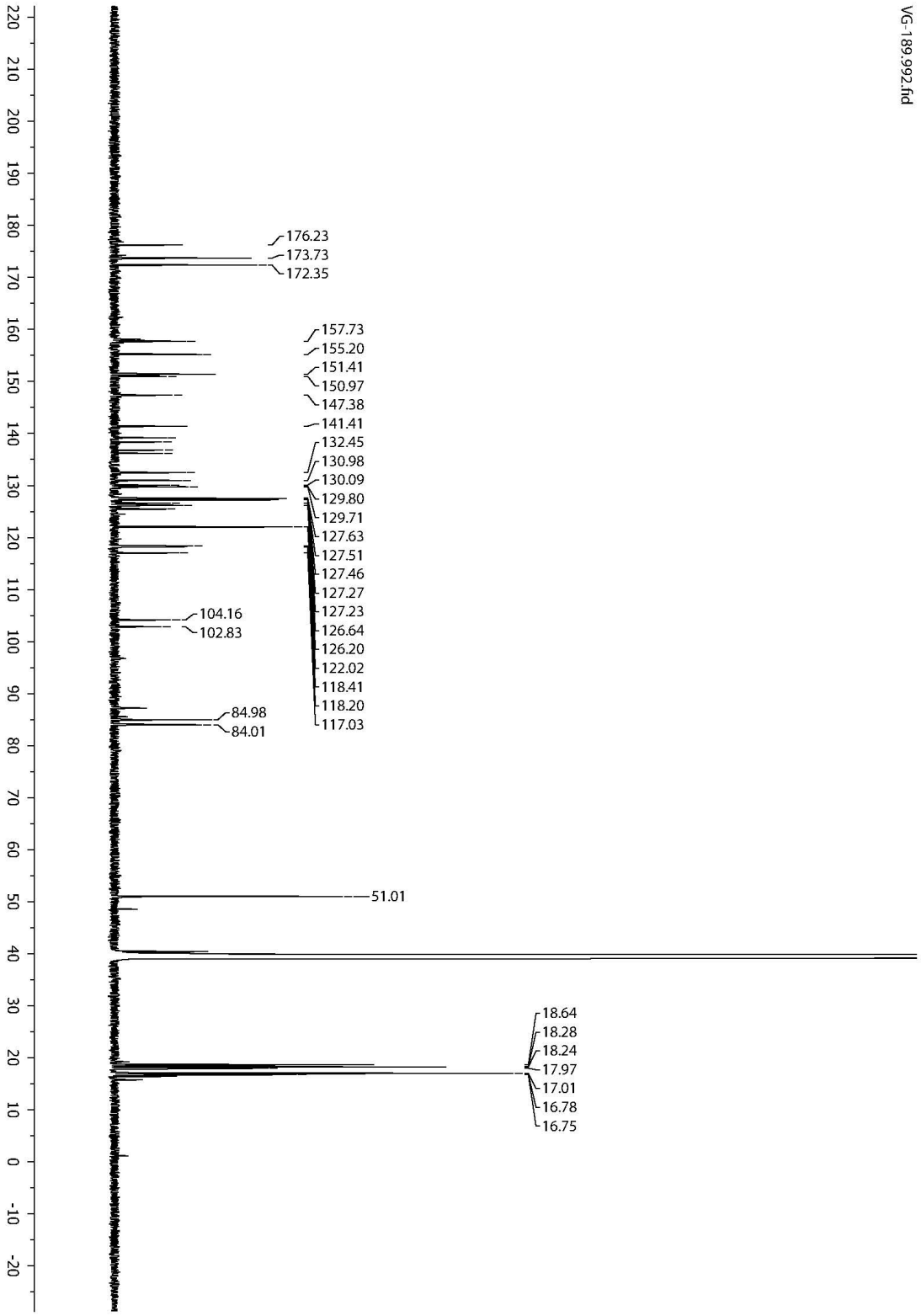

Spectrum 1-8. LC-MS of VF-EX2.

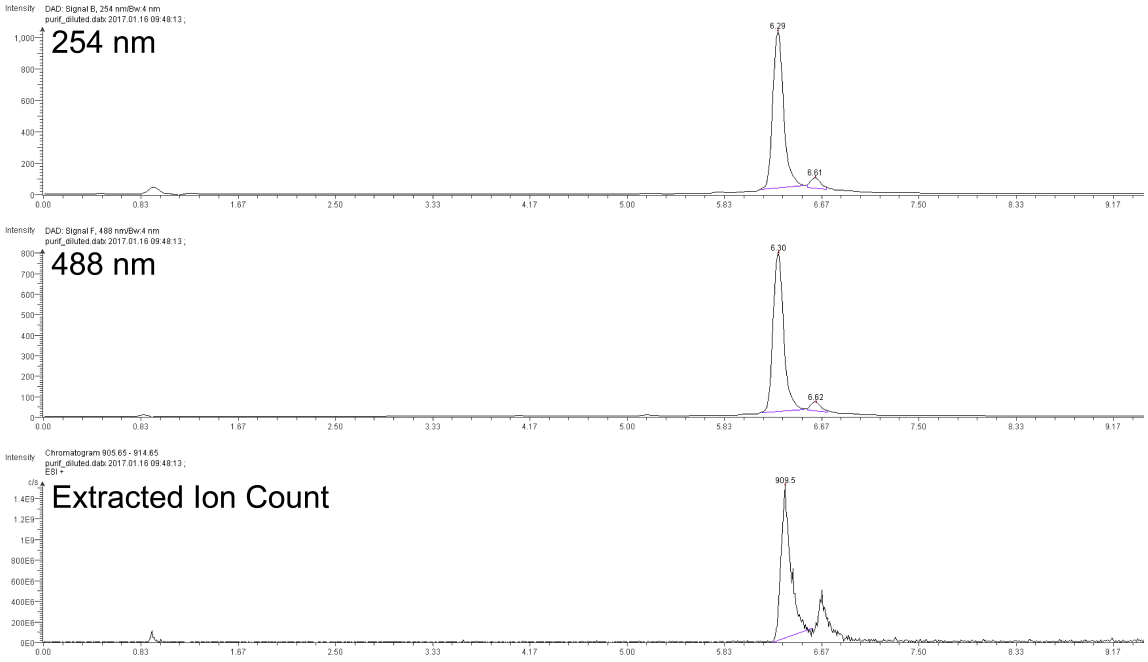

Synthesis of
2-(2,7-dichloro-6-((4-methoxybenzyl)oxy)-3-oxo-3H-xanthen-9-yl)-5-((E)-4-((E)-4-(dimethylamino)styryl)styryl)benzenesulfonic acid (VF2.1.Cl-PMB)

In a 20 mL scintillation vial dissolved VF2.1.Cl (107 mg, 156 μmol) and cesium carbonate (112 mg, 343 μmol) in 1 mL anhydrous dimethylformamide, followed by addition of 109 μL of 4-methoxybenzyl bromide (780 μmol). After stirring for 4 hours the reaction was diluted with 10 mL of H_2O which resulted in the precipitation of an orange solid. The precipitate was recovered by vacuum filtration and washed with approximately 5 mL of diethyl ether.

The orange solid was collected and dissolved in 4.5 mL of dimethylformamide and 1.5 mL of 1.0 M aqueous lithium hydroxide. The solution was stirred under N_2 for five hours at 50 °C. The reaction was then diluted with 20 mL of H_2O and acidified with 1.75 mL of 1.0 M aqueous HCl. The aqueous solution was extracted with 40 mL of 10% isopropanol in dichloromethane. The organic phase was collected and washed twice with 10 mL of H_2O. The organic phase was dried over magnesium sulfate and solvents removed under reduced pressure. The resulting gum was then dissolved in 5 mL of dichloromethane. Addition of an equal volume of hexanes led to precipitation of an orange solid and solvents were again removed under reduced pressure. Obtained **VF2.1.Cl-PMB** (96.1 mg, 77%) as an orange solid.

^{1}H NMR (900 MHz, $(CD_3)_2SO$) δ 8.17 (s, 1H), 7.79 (d, J = 7.6 Hz, 1H), 7.66 (d, J = 7.8 Hz, 2H), 7.58 – 7.54 (m, 3H), 7.48 – 7.41 (m, 5H), 7.41 – 7.38 (m, 2H), 7.25 (d, J = 7.9 Hz, 1H), 7.19 (d, J = 16.5 Hz, 1H), 7.06 (s, 1H), 7.04 (d, J = 8.5 Hz, 1H), 7.01 (d, J = 8.5 Hz, 1H), 7.00 – 6.95 (m, 3H), 6.42 (s, 1H), 5.33 (s, 2H), 3.75 (s, 3H), 2.94 (s, 6H).

^{13}C NMR (226 MHz, $(CD_3)_2SO$) δ 176.08, 160.56, 159.32, 157.79, 157.63, 151.95, 151.62, 147.35, 138.49, 137.71, 135.10, 134.47, 132.45, 132.15, 130.04, 129.66, 129.36, 128.94, 127.60, 127.36, 127.18, 126.57, 126.46, 126.19, 125.34, 119.72, 118.46, 117.46, 115.62, 114.26, 114.21, 114.02, 113.61, 103.90, 101.64, 55.26, 55.09.

Analytical HPLC retention time: 6.68 minutes.
HR-ESI-MS [M-H]- calculated 802.1439, found 802.1411

Synthesis of
(((2-(2,7-dichloro-6-hydroxy-3-oxo-3H-xanthen-9-yl)-5-((E)-4-((E)-4-(dimethylamino)styryl)styryl)phenyl)sulfonyl)oxy)methyl 1-methylcyclopropane-1-carboxylate (VF-EX0)

In a 20 mL scintillation vial dissolved VF2.1.Cl-PMB (83.9 mg, 104 μmol) and iodomethyl 1-methylcyclopropanecarboxylate (108 mg, 417 μmol) in 1 mL of anhydrous dimethylformamide, followed by addition of 72.6 μL of diisopropylethylamine (417 μmol). After stirring for 16 hours at room temperature the reaction was diluted with water and concentrated under reduced pressure at a bath temperature of 60 °C. The resulting gum was dissolved in approximately 1 mL of dichlorometane and precipitation induced by addition of approximately 3 mL of hexanes. The flocculent precipitate was collected by vacuum filtration to obtain VF-EX0 (45.3 mg, 47% crude yield) as an orange solid. Workup was accompanied by concomitant hydrolysis of the phenolic p-methoxybenzyl

protecting group. A small aliquot for characterization was purified by semi-preparative HPLC.

^{1}H NMR (900 MHz, $(CD_3)_2SO$) δ 8.19 (s, 1H), 7.93 (d, J = 8.4 Hz, 2H), 7.86 (d, J = 8.3 Hz, 2H), 7.80 (d, J = 7.9 Hz, 1H), 7.75 (d, J = 7.8 Hz, 2H), 7.69 (d, J = 7.9 Hz, 2H), 7.51 (d, J = 16.6 Hz, 1H), 7.49 (d, J = 16.6 Hz, 1H), 7.43 (d, J = 16.4 Hz, 1H), 7.40 (d, J = 16.5 Hz, 1H), 7.26 (d, J = 7.8 Hz, 1H), 7.13 (s, 1H), 7.08 (s, 1H), 7.02 (s, 1H), 5.72 (s, 2H), 3.64 (s, 6H), 1.12 (s, 3H), 0.95 (s, 2H), 0.77 (s, 2H).

^{13}C NMR (226 MHz, $(CD_3)_2SO$) δ 172.83, 158.12, 157.99, 152.35, 147.80, 141.87, 139.65, 138.66, 137.34, 137.29, 136.61, 131.46, 130.57, 130.26, 130.24, 130.20, 130.18, 128.27, 128.13, 127.92, 127.74, 127.69, 127.02, 126.65, 125.97, 122.50, 84.47, 51.45, 18.71, 18.44, 17.47.

Analytical HPLC retention time: 5.19 minutes.
HR-ESI-MS [M+H]+ calculated 796.1533, found 796.1526

Spectrum 1-9. ^{1}H NMR of VF-EX0.

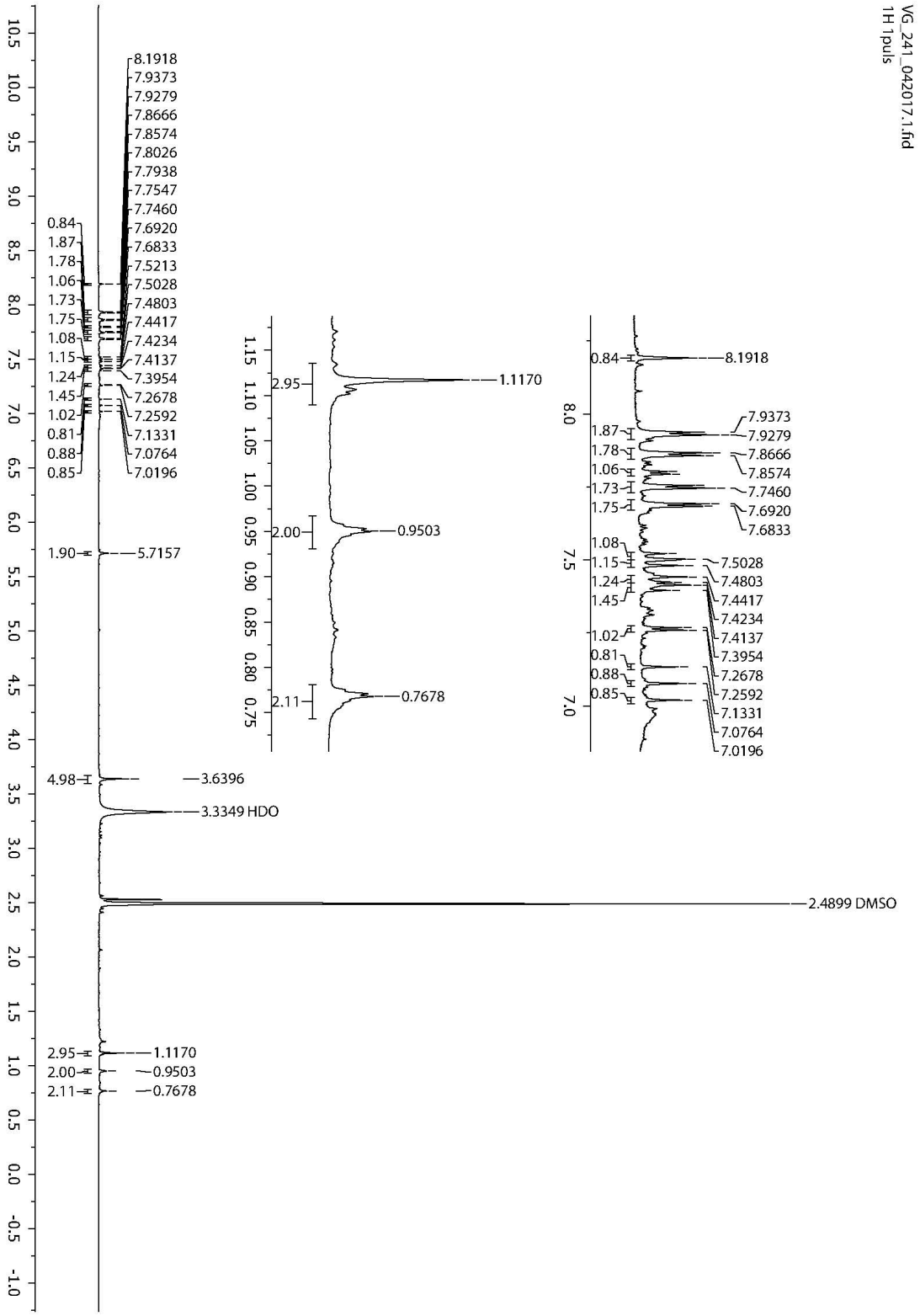

Spectrum 1-10. ^{13}C NMR of VF-EX0**.**

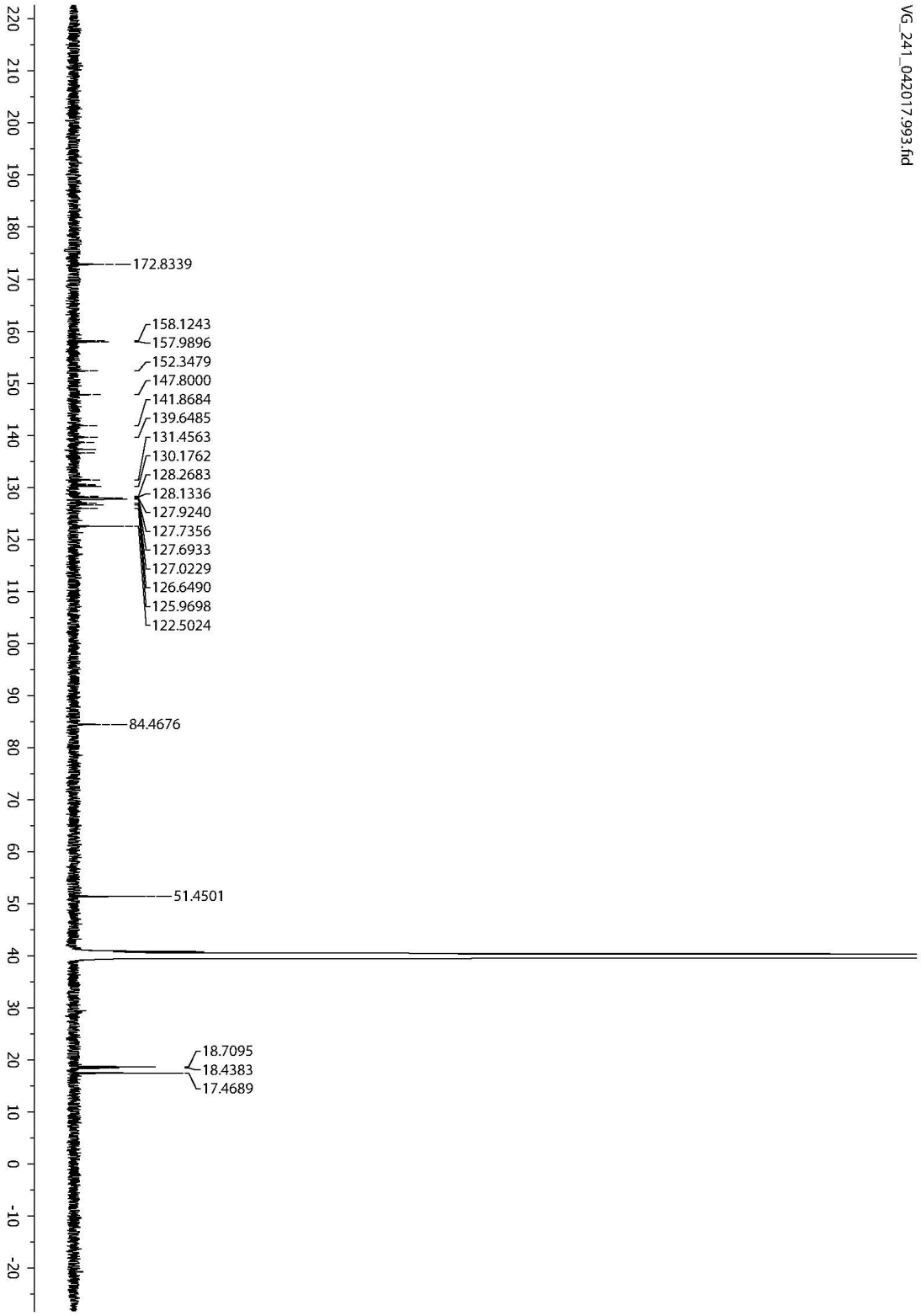

Spectrum 1-11. LC MS of VF-EX0**.**

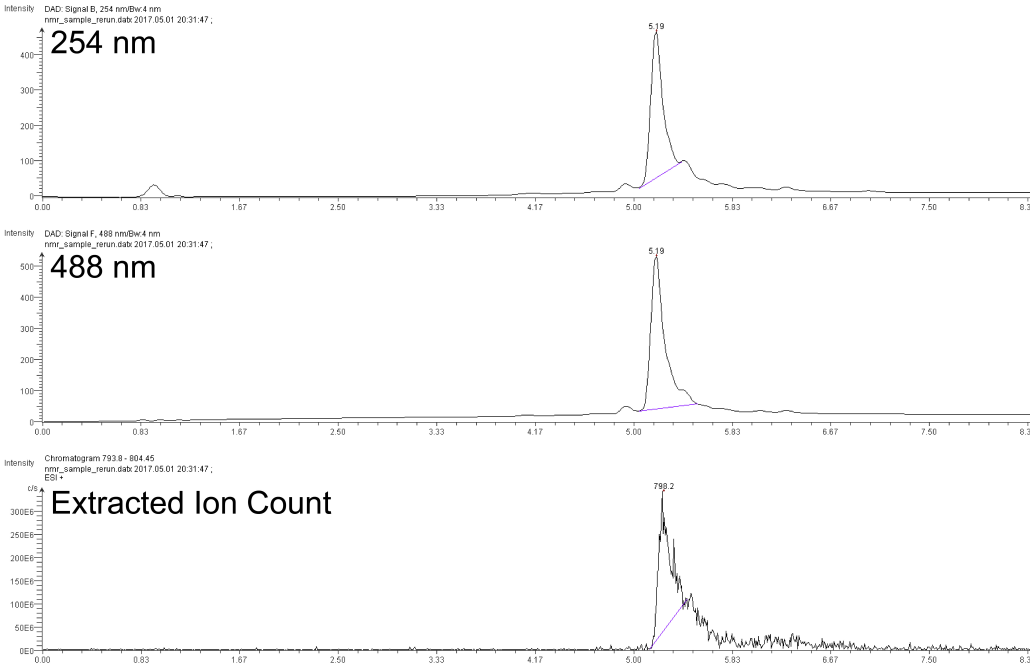

Spectroscopic studies

Stock solutions of dyes were prepared in DMSO (2 mM) and diluted with HBSS (zero Ca^{2+}, zero Mg^{2+}, no phenol red, pH 7.4). UV-Vis absorbance and fluorescence spectra were recorded using a Shimadzu 2501 Spectrophotometer (Shimadzu) and a Quantamaster Master 4 L-format scanning spectrofluorometer (Photon Technologies International). The fluorometer is equipped with an LPS-220B 75-W xenon lamp and power supply, A-1010B lamp housing with integrated igniter, switchable 814 photon-counting/analog photomultiplier detection unit, and MD5020 motor driver. Samples were measured in 1-cm path length quartz cuvettes (Starna Cells). All measurements were done at room temperature.

In vitro PLE reactions and characterization

Commercially purified pig liver esterase (PLE, MW = 168 kDa) was obtained from Sigma-Aldrich (E2884) as a suspension in 3.2 M $(NH_4)_2SO_4$, and was diluted from a stock solution of 28.1 mg/mL to appropriate concentrations in HBSS, pH 7.4. For the enzymatic reaction, 1 μL dyes (final concentration of 50 μM) were incubated with 1 μL PLE (final concentration of 0.7025 mg/mL) and 1 μL Pluronic F-127 (20% solution in DMSO) in 40 μL HBSS at 37 °C for ~ 3 h. The enzymatic products were characterized by spectroscopy and HPLC and compared with the starting materials. For characterization by spectroscopy, the reaction mixture was diluted to 1 mL HBSS (total volume) for measurement. For HPLC characterization, 40 μL of acetonitrile (1:1) was added, followed by centrifugation to precipitate the enzyme. Supernatant was extracted and filtered for HPLC injection. Absorbance was collected from 300 nm to 700 nm. For emission scans, the samples were excited at 520 nm and emission was collected from 525 nm to 700 nm. Excitation scans were collected by monitoring emission at 550 nm when exciting from 300 to 540 nm. To obtain fluorescence turn-on over time, dyes were diluted to 1 μM in 1 mL HBSS in a cuvette and incubated with PLE (100 ng/mL) at 37 °C.

Enzyme kinetics experiments were performed in black, clear-bottom, 96-well polystyrene microplates from Corning. Plates were read from the bottom on a Molecular Devices SpectraMax Paradigm Multi-Mode detection platform plate reader (λ_{ex} 520 nm, λ_{em} 560 nm). All the measurements were done at 37 °C. Enzyme (200 ng/mL) was added to the substrates at t=5 min and more data were collected for another 5 min. To obtain the kinetic constants, the data were fit to the Michaelis-Menten equation $v = \frac{V_{max}[S]}{K_M+[S]}$ (GraphPad Prism).

Cell culture, transfection, and dye loading

All animal procedures were approved by the UC Berkeley Animal Care and Use Committees and conformed to the NIH Guide for the Care and Use of Laboratory Animals and the Public Health Service (PHS) Policy.

Human embryonic kidney 293T (HEK) cells were maintained in Dulbecco's modified eagle medium (DMEM) supplemented with 4.5 g/L D-glucose, 10% fetal bovine serum (FBS; Thermo Scientific) and 1% GlutaMax (Invitrogen) at 37 °C in a humidified incubator with 5 % CO_2. Cells were passaged and plated in DMEM (as above) at a density of 750,000 cells per well in a 6-well plate. Transfection of plasmids was carried out using Lipofectamine 3000 (Invitrogen) ~18-24 h after plating. The cells were split again 48 h after transfection and plated onto 12 mm glass coverslips pre-coated

with Poly-D-Lysine (PDL; 1 mg/ml; Sigma-Aldrich) at a density of 75,000 cells per coverslip in DMEM supplemented with 1 g/L D-glucose, 10% FBS and 1% GlutaMax. Imaging was performed 12-18 h after plating.

Hippocampi were dissected from embryonic day 19 Sprague Dawley rats (Charles River Laboratory) in cold, sterile HBSS (zero Ca^{2+}, zero Mg^{2+}, phenol red). All dissection products were supplied by Invitrogen, unless otherwise stated. Hippocampal tissue was treated with trypsin (2.5%) for 15 min at 37 °C. The tissue was triturated using fire polished Pasteur pipettes, in minimum essential media (MEM) supplemented with 5% FBS, 2% B-27, 2% 1M dextrose (Fisher Scientific) and 1% GlutaMax. The dissociated cells were plated onto 12 mm diameter coverslips (Fisher Scientific) pre-treated with PDL (as above) at a density of 25-30,000 cells per coverslip in MEM supplemented media (as above). Neurons were maintained at 37 °C in a humidified incubator with 5 % CO_2. At 1 day in vitro (DIV) half of the MEM supplemented media was removed and replaced with Neurobasal media containing 2% B-27 supplement and 1% GlutaMax. Transfection of plasmids was carried out using Lipofectamine 3000 (without P3000 reagent) at 6-7 DIV. Imaging was performed on mature neurons 12-14 DIV.

Unless stated otherwise, for loading of HEK cells and hippocampal neurons, DMSO stock solutions of dyes (2 mM) were diluted with 1:1 Pluronic F-127 (20% solution in DMSO) and then further diluted in HBSS to working concentrations. For HEK cells, the typical working concentration was 500 nM. For neurons, the working concentration was 1 μM. HEK cells were incubated with dye for 30 minutes at 37 °C before exchanging dye/HBSS for HBSS without any dye. Neurons were treated identically, but for 60 minutes before exchanging dye/HBSS for HBSS without dye. All imaging was performed in HBSS at room temperature.

Epifluorescence microscopy

Imaging was performed on an AxioExaminer Z-1 (Zeiss) equipped with a Spectra-X Light engine LED light (Lumencor), controlled with Slidebook (v6, Intelligent Imaging Innovations). Images were acquired with a W-Plan-Apo 20x/1.0 water objective (20x; Zeiss). Images were focused onto either an OrcaFlash4.0 sCMOS camera (sCMOS; Hamamatsu) or an eVolve 128 EMCCD camera (EMCCD; Photometrix). For dye imaging, excitation light was delivered at 475 nM (LED, 475 nm, 34 nm bandpass) and emission was collected with a 540/50 nm bandpass filter after passing through a 510 nm longpass dichroic.

Image analysis

For image intensity measurements, regions of interest were drawn around cells or neuronal cell bodies and the mean fluorescence was calculated in ImageJ (FIJI, NIH). Background fluorescence was subtracted by measuring the fluorescence where no cells grew. The fold turn-on was calculated by taking the ratio of transfected cells fluorescence and untransfected cells fluorescence, both background subtracted. At least 15-20 cells were quantified for each coverslip and 3 coverslips were examined to get the average fold turn-on. See Figure 2-8 for an example of regions of interest.

Analysis of voltage sensitivity in HEK cells was performed using ImageJ (FIJI). Briefly, a region of interest (ROI) was selected automatically based on fluorescence intensity and applied as a mask to all image frames. Fluorescence intensity values were calculated at known baseline and voltage step epochs. For analysis of voltage responses

in neurons, regions of interest encompassing cell bodies (all of approximately the same size) were drawn in ImageJ and the mean fluorescence intensity for each frame extracted. ΔF/F values were calculated by first subtracting a mean background value from all raw fluorescence frames, to give a background subtracted trace (bkgsub). A baseline fluorescence value (F_{base}) is calculated from the median of all the frames, and was subtracted from each timepoint of the bkgsub trace to yield a ΔF trace. The ΔF was then divided by F_{base} to give ΔF/F traces. No averaging has been applied to any voltage traces. To get spike rates for serotonin experiments, the fluorescence trace of one movie was first converted to a ΔF/F trace as explained above. The number of spikes were counted manually and divided by 5 s to obtain the frequency. For each ROI, two movies were taken and an average frequency was obtained.

Electrophysiology/Imaging parameters

For electrophysiological experiments, pipettes were pulled from borosilicate glass (Sutter Instruments, BF150-86-10), with a resistance of 5–6 MΩ, and were filled with an internal solution; 115 mM potassium gluconate, 10 mM BAPTA tetrapotassium salt, 10 mM HEPES, 5 mM NaCl, 10 mM KCl, 2 mM ATP disodium salt, 0.3 mM GTP trisodium salt (pH 7.25, 275 mOsm). Recordings were obtained with an Axopatch 200B amplifier (Molecular Devices) at room temperature. The signals were digitized with a Digidata 1440A, sampled at 50 kHz and recorded with pCLAMP 10 software (Molecular Devices) on a PC. Fast capacitance was compensated in the on-cell configuration. For all electrophysiology experiments, recordings were only pursued if series resistance in voltage clamp was less than 30 MΩ. For whole-cell, voltage clamp recordings in HEK 293T cells, cells were held at -60 mV and hyper- and de- polarizing steps applied from -100 to +100 mV in 20 mV increments.

Extracellular field stimulation was delivered by a SD9 Grass Stimulator connected to a recording chamber containing two platinum electrodes (Warner), with triggering provided through the same Digidata 1332A digitizer and pCLAMP 9 software (Molecular Devices) that ran the electrophysiology. Action potentials were triggered by 1 ms 60 V field potentials delivered at 5 Hz. To prevent recurrent activity, the HBBS bath solution was supplemented with synaptic blockers; 10 μM 2,3-Dioxo-6-nitro-1,2,3,4-tetrahydrobenzo[f]quinoxaline-7-sulfonamide (NBQX; Santa Cruz Biotechnology) and 25 μM DL-2-Amino-5-phosphonopentanoic acid (APV; Sigma-Aldrich). For both evoked action potentials and spontaneous activity, images were binned 4x4 to allow sampling rates of 0.5 kHz and 2500 frames (5 s) were acquired for each recording. For serotonin experiments, two 5 s movies of spontaneous activity were taken for each ROI.

Plasmid construction

For expression in HEK cells, PLE with an IgK leader sequence on the N-terminal and an HA tag on the C-terminal was subcloned into a pcDNA3 vector with a cytomegalovirus (CMV) promoter. For expression in neurons, PLE was subcloned into a pcDNA3 vector with a human synapsin promoter (Syn), or calmodulin-dependent protein kinase II promoter (CaMKIIa) and a regulatory element from the woodchuck hepatitis virus (WPRE). Nuclear-targeted mCherry (NLS-mCherry) was inserted downstream of PLE, separated by an internal ribosome entry site (IRES) sequence. All constructs were verified by sequencing. The following sequences were used (5' to 3').

IgK
ATGGAGACAGACACACTCCTGCTATGGGTACTGCTGCTCTGGGTTCCAGGTTC
CACTGGTGAC

PLE (minus ER retention signal)
ATGGTGTGGCTGCTGCCTCTGGTGCTGACCAGCCTGGCCAGCAGCGCCACCT
GGGCCGGCCAGCCCGCCAGCCCTCCCGTGGTGGACACCGCCCAGGGCAGGGT
GCTGGGCAAGTACGTGAGCCTGGAGGGCCTGGCCCAGCCCGTGGCCGTGTTC
CTGGGCGTGCCCTTCGCCAAGCCTCCCTTGGGCAGCCTGAGGTTCGCTCCTCC
TCAGCCTGCTGAGCCCTGGAGCTTCGTGAAGAACACCACCAGCTACCCTCCC
ATGTGCTGCCAGGATCCCGTGGTGGAGCAGATGACCAGCGACCTGTTCACCA
ACGGCAAGGAGAGGCTGACCCTGGAGTTCAGCGAGGACTGCCTGTACCTGAA
CATCTACACACCCGCCGACCTGACCAAGAGAGGCAGGCTGCCCGTGATGGTG
TGGATCCACGGCGGCGGCCTGGTGCTGGGCGGCGCTCCCATGTACGACGGCG
TGGTGCTGGCCGCCCACGAGAACGTGGTGGTGGTGGCCATCCAGTACAGGCT
GGGCATCTGGGGCTTCTTCAGCACCGGCGACGAGCACAGCAGgGGCAACTGG
GGCCACCTGGACCAGGTGGCCGCCCTGCACTGGGTGCAGGAGAACATCGCCA
ACTTCGGCGGCGATCCCGGCAGCGTGACCATCTTCGGCGAGAGCGCCGGCGG
CGAGAGCGTGAGCGTGCTGGTGCTGAGCCCTCTGGCCAAGAACCTGTTCCAC
AGGGCCATCAGCGAGAGCGGCGTGGCCCTGACCGTGGCCCTGGTGAGGAAG
GACATGAAGGCCGCCGCCAAGCAGATCGCCGTGCTGGCCGGCTGCAAGACC
ACCACCAGCGCCGTGTTCGTGCACTGCCTGAGGCAGAAGAGCGAGGACGAG
CTGCTGGACCTGACCCTGAAGATGAAGTTCCTGACCCTGGACTTCCACGGCG
ACCAGAGGGAGAGCCATCCCTTCCTGCCCACCGTGGTGGACGGCGTGCTGCT
GCCCAAGATGCCCGAGGAGATCCTGGCCGAGAAGGACTTCAACACCGTGCCC
TACATCGTGGGCATCAACAAGCAGGAGTTCGGCTGGCTGCTGCCCACTATGA
TGGGCTTCCCTCTGAGCGAGGGCAAGTTGGACCAGAAGACCGCCACCAGCCT
GCTGTGGAAGAGCTATCCCATCGCCAACATTCCCGAGGAGCTGACACCCGTG
GCCACCGACAAGTACCTGGGCGGCACCGACGATCCCGTGAAGAAGAAGGAC
CTGTTCCTGGACCTGATGGGCGACGTGGTGTTCGGCGTGCCCAGCGTGACCGT
GGCCAGGCAGCACAGGGACaCCGGCGCTCCCACCTACATGTACGAGTTCCAG
TACAGGCCCAGCTTCAGCAGCGACAAGAAGCCCAAGTCCGTGATCGGCGACC
ACGGCGACGAGATCTTCAGCGTGTTCGGCTTCCCTCTGCTGAAGGGCGACGC
TCCCGAGGAGGAGGTGAGCCTGAGCAAGACCGTGATGAAGTTCTGGGCCAAC
TTCGCCAGGAGCGGCAATCCCAACGGCGAGGGCCTGCCTCACTGGCCCATGT
ACGACCAGGAGGAGGGCTACCTGCAGATCGGCGTGAACACCCAGGCCGCCA
AGAGGCTGAAGGGCGAGGAGGTGGCCTTCTGGAACGACCTGCTGAGCAAGG
AGGCCGCCAAGAAGCCTCCTAAGATCAAG

HA
TATCCATATGATGTTCCAGATTATGCT

DAF
CCAAATAAAGGAAGTGGAACCACTTCAGGTACTACCCGTCTTCTATCTGGGC
ACACGTGTTTCACGTTGACAGGTTTGCTTGGGACGCTAGTAACCATGGGCTTG
CTGACTTAG

pDisplay
GCTGTGGGCCAGGACACGCAGGAGGTCATCGTGGTGCCACACTCCTTGCCCT
TTAAGGTGGTGGTGATCTCAGCCATCCTGGCCCTGGTGGTGCTCACCATCATC
TCCCTTATCATCCTCATCATGCTTTGGCAGAAGAAGCCACGT

IRES
GCCCCTCTCCCTCCCCCCCCCCTAACGTTACTGGCCGAAGCCGCTTGGAATAA
GGCCGGTGTGCGTTTGTCTATATGTTATTTTCCACCATATTGCCGTCTTTTGGC
AATGTGAGGGCCCGGAAACCTGGCCCTGTCTTCTTGACGAGCATTCCTAGGG
GTCTTTCCCCTCTCGCCAAAGGAATGCAAGGTCTGTTGAATGTCGTGAAGGA
AGCAGTTCCTCTGGAAGCTTCTTGAAGACAAACAACGTCTGTAGCGACCCTTT
GCAGGCAGCGGAACCCCCCACCTGGCGACAGGTGCCTCTGCGGCCAAAAGCC
ACGTGTATAAGATACACCTGCAAAGGCGGCACAACCCCAGTGCCACGTTGTG
AGTTGGATAGTTGTGGAAAGAGTCAAATGGCTCTCCTCAAGCGTATTCAACA
AGGGGCTGAAGGATGCCCAGAAGGCACCCCATTGTATGGGATCTGATCTGGG
GCCTCGGTGCACATGCTTTACATGTGTTTAGTCGAGGTTAAAAAAACGTCTAG
GCCCCCCGAACCACGGGGACGTGGTTTTCCTTTGAAAAACACGATGATAATA
TGGCCACA

NLS-mCherry
ATGGTGCCCAAGAAGAAGAGGAAAGTCGTGAGCAAGGGCGAGGAGGACAAC
ATGGCCATCATCAAGGAGTTCATGCGCTTCAAGGTGCACATGGAGGGCTCCG
TGAACGGCCACGAGTTCGAGATCGAGGGCGAGGGCGAGGGCCGCCCCTACG
AGGGCACCCAGACCGCCAAGCTGAAGGTGACCAAGGGCGGCCCCCTGCCCTT
CGCCTGGGACATCCTGTCCCCTCAGTTCATGTACGGCTCCAAGGCCTACGTGA
AGCACCCCGCCGACATCCCCGACTACTTGAAGCTGTCCTTCCCCGAGGGCTTC
AAGTGGGAGCGCGTGATGAACTTCGAGGACGGCGGCGTGGTGACCGTGACCC
AGGACTCCTCCCTGCAGGACGGCGAGTTCATCTACAAGGTGAAGCTGCGCGG
CACCAACTTCCCCTCCGACGGCCCCGTAATGCAGAAGAAGACCATGGGCTGG
GAGGCCTCCTCCGAGCGGATGTACCCCGAGGACGGCGCCCTGAAGGGCGAG
ATCAAGCAGAGGCTGAAGCTGAAGGACGGCGGCCACTACGACGCCGAGGTC
AAGACCACCTACAAGGCCAAGAAGCCCGTGCAGCTGCCCGGCGCCTACAAC
GTCAACATCAAGCTGGACATCACCTCCCACAACGAGGACTACACCATCGTGG
AACAGTACGAGCGCGCCGAGGGCCGCCACTCCACCGGCGGCATGGACGAGC
TGTACAAG

WPRE
GCTTATCGATAATCAACCTCTGGATTACAAAATTTGTGAAAGATTGACTGGTA
TTCTTAACTATGTTGCTCCTTTTACGCTATGTGGATACGCTGCTTTAATGCCTT
TGTATCATGCTATTGCTTCCCGTATGGCTTTCATTTTCTCCTCCTTGTATAAAT
CCTGGTTGCTGTCTCTTTATGAGGAGTTGTGGCCCGTTGTCAGGCAACGTGGC
GTGGTGTGCACTGTGTTTGCTGACGCAACCCCCACTGGTTGGGGCATTGCCAC
CACCTGTCAGCTCCTTTCCGGGACTTTCGCTTTCCCCCTCCCTATTGCCACGGC
GGAACTCATCGCCGCCTGCCTTGCCCGCTGCTGGACAGGGGCTCGGCTGTTG
GGCACTGACAATTCCGTGGTGTTGTCGGGGAAATCATCGTCCTTTCCTTGGCT
GCTCGCCTGTGTTGCCACCTGGATTCTGCGCGGGACGTCCTTCTGCTACGTCC

CTTCGGCCCTCAATCCAGCGGACCTTCCTTCCCGCGGCCTGCTGCCGGCTCTG
CGGCCTCTTCCGCGTCTTCGCCTTCGCCCTCAGACGAGTCGGATCTCCCTTTG
GGCCGCCTCCCCGCATCGATACCG

Synapsin Promoter
GTGTCTAGACTGCAGAGGGCCCTGCGTATGAGTGCAAGTGGGTTTTAGGACC
AGGATGAGGCGGGGTGGGGGTGCCTACCTGACGACCGACCCCGACCCACTG
GACAAGCACCCAACCCCCATTCCCCAAATTGCGCATCCCCTATCAGAGAGGG
GGAGGGGAAACAGGATGCGGCGAGGCGCGTGCGCACTGCCAGCTTCAGCAC
CGCGGACAGTGCCTTCGCCCCCGCCTGGCGGCGCGCGCCACCGCCGCCTCAG
CACTGAAGGCGCGCTGACGTCACTCGCCGGTCCCCCGCAAACTCCCCTTCCC
GGCCACCTTGGTCGCGTCCGCGCCGCCGCCGGCCCAGCCGGACCGCACCACG
CGAGGCGCGAGATAGGGGGGCACGGGCGCGACCATCTGCGCTGCGGCGCCG
GCGACTCAGCGCTGCCTCAGTCTGCGGTGGGCAGCGGAGGAGTCGTGTCGTG
CCTGAGAGCGCAGTCGAGA

CaMKIIα Promoter
CATTATGGCCTTAGGTCACTTCATCTCCATGGGGTTCTTCTTCTGATTTTCTAG
AAAATGAGATGGGGGTGCAGAGAGCTTCCTCAGTGACCTGCCCAGGGTCACA
TCAGAAATGTCAGAGCTAGAACTTGAACTCAGATTACTAATCTTAAATTCCAT
GCCTTGGGGGCATGCAAGTACGATATACAGAAGGAGTGAACTCATTAGGGCA
GATGACCAATGAGTTTAGGAAAGAAGAGTCCAGGGCAGGGTACATCTACACC
ACCCGCCCAGCCCTGGGTGAGTCCAGCCACGTTCACCTCATTATAGTTGCCTC
TCTCCAGTCCTACCTTGACGGGAAGCACAAGCAGAAACTGGGACAGGAGCCC
CAGGAGACCAAATCTTCATGGTCCCTCTGGGAGGATGGGTGGGGAGAGCTGT
GGCAGAGGCCTCAGGAGGGGCCCTGCTGCTCAGTGGTGACAGATAGGGGTG
AGAAAGCAGACAGAGTCATTCCGTCAGCATTCTGGGTCTGTTTGGTACTTCTT
CTCACGCTAAGGTGGCGGTGTGATATGCACAATGGCTAAAAAGCAGGGAGA
GCTGGAAAGAAACAAGGACAGAGACAGAGGCCAAGTCAACCAGACCAATTC
CCAGAGGAAGCAAAGAAACCATTACAGAGACTACAAGGGGGAAGGGAAGG
AGAGATGAATTAGCTTCCCCTGTAAACCTTAGAACCCAGCTGTTGCCAGGGC
AACGGGGCAATACCTGTCTCTTCAGAGGAGATGAAGTTGCCAGGGTAACTAC
ATCCTGTCTTTCTCAAGGACCATCCCAGAATGTGGCACCCACTAGCCGTTACC
ATAGCAACTGCCTCTTTGCCCCACTTAATCCCATCCCGTCTGTTAAAAGGGCC
CTATAGTTGGAGGTGGGGGAGGTAGGAAGAGCGATGATCACTTGTGGACTAA
GTTTGTTCGCATCCCCTTCTCCAACCCCCTCAGTACATCACCCTGGGGGAACA
GGGTCCACTTGCTCCTGGGCCCACACAGTCCTGCAGTATTGTGTATATAAGGC
CAGGGCAAAGAGGAGCAGGTTTTAAAGTGAAAGGCAGGCAGGTGTTGGGGA
GGCAGTTACCGGGGCAACGGGAACAGGGCGTTTCGGAGGTGGTTGCCATGGG
GACCTGGATGCTGACGAAGGCTCGCGAGGCTGTGAGCAGCCACAGTGCCCTG
CTCAGAAGCCCCAAGCTCGTCAGTCAAGCCGGTTCTCCGTTTGCACTCAGGA
GCACGGGCAGGCGAGTGGCCCCTAGTTCTGGGGGCAGCGG

CMV promoter
GACATTGATTATTGACTAGTTATTAATAGTAATCAATTACGGGGTCATTAGTT
CATAGCCCATATATGGAGTTCCGCGTTACATAACTTACGGTAAATGGCCCGCC

TGGCTGACCGCCCAACGACCCCCGCCCATTGACGTCAATAATGACGTATGTT
CCCATAGTAACGCCAATAGGGACTTTCCATTGACGTCAATGGGTGGACTATTT
ACGGTAAACTGCCCACTTGGCAGTACATCAAGTGTATCATATGCCAAGTACG
CCCCCTATTGACGTCAATGACGGTAAATGGCCCGCCTGGCATTATGCCCAGT
ACATGACCTTATGGGACTTTCCTACTTGGCAGTACATCTACGTATTAGTCATC
GCTATTACCATGGTGATGCGGTTTTGGCAGTACATCAATGGGCGTGGATAGC
GGTTTGACTCACGGGGATTTCCAAGTCTCCACCCCATTGACGTCAATGGGAGT
TTGTTTTGGCACCAAAATCAACGGGACTTTCCAAAATGTCGTAACAACTCCGC
CCCATTGACGCAAATGGGCGGTAGGCGTGTACGGTGGGAGGTCTATATAAGC
AGAGCT

Benchling links for constructs

CMV-IgK-PLE-HA-DAF-IRES-mCherry
https://benchling.com/s/H8lrjABb

CMV-IgK-PLE-HA-pDisplay-IRES-mCherry
https://benchling.com/s/KczxHl33

Synapsin-IgK-PLE-HA-DAF-IRES-mCherry-WPRE
https://benchling.com/s/ZQVd5dJP

CaMKIIα-IgK-PLE-HA-DAF-IRES-mCherry-WPRE
https://benchling.com/s/ziwgvSJ9

Immunocytochemistry

To detect expression and localization of PLE and other protein markers, HEK cells or neurons were fixed with 4% paraformaldehyde in PBS for 10 min and permeabilized (if required) with 0.3% v/v Triton-X100 (Sigma Aldrich) in PBS for 2 min. Blocking was done in 5% w/v bovine serum albumin (BSA; Sigma Aldrich) in PBS for 1 h. Primary antibody was incubated at 4 °C overnight, followed by AlexaFluor secondary antibody (Life Technologies) at room temperature for 2 h. All antibodies were used at 1:1000 dilution.

Name	Primary/ Secondary	Manufacturer	Catalog #	Isotype
Anti-HA	Primary	CST	3724S	Rabbit IgG
Anti-HA	Primary	CST	2367S	Mouse IgG1
Anti-CamKIIa	Primary	EMD Millipore	05-532	Mouse IgG1
Anti-Synapsin	Primary	Synaptic Systems	106001	Mouse IgG1
Anti-GFAP	Primary	EMD Millipore	MAB360	Mouse IgG1
Anti-GABA	Primary	Sigma-Aldrich	A2052	Rabbit IgG

Anti-rabbit 647	Secondary	Life Technologies	A21244	Goat IgG
Anti-rabbit 488	Secondary	Life Technologies	A11008	Goat IgG
Anti-mouse 488	Secondary	Life Technologies	A11001	Goat IgG

Figures and Schemes

Scheme 2-1. *Design of VoltageFluor targeted by esterase expression (VF-EX).*

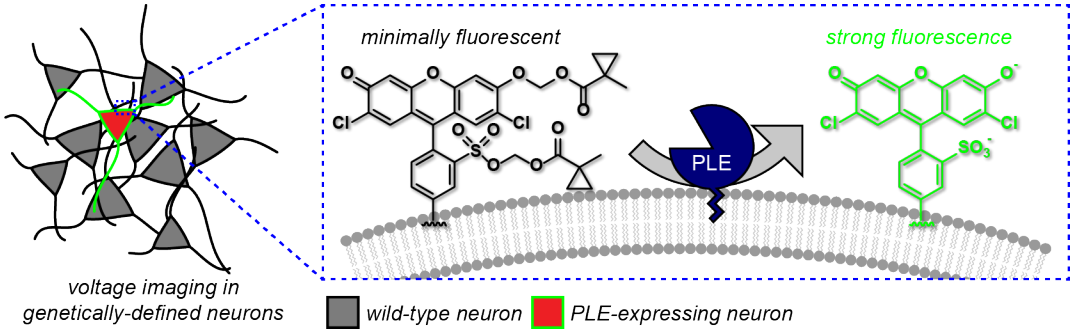

Scheme 2-1. Scheme of neuron-specific targeting with ester/esterase pairs (components are not to scale).

Scheme 2-2. *Synthesis of VF-EX dyes.*

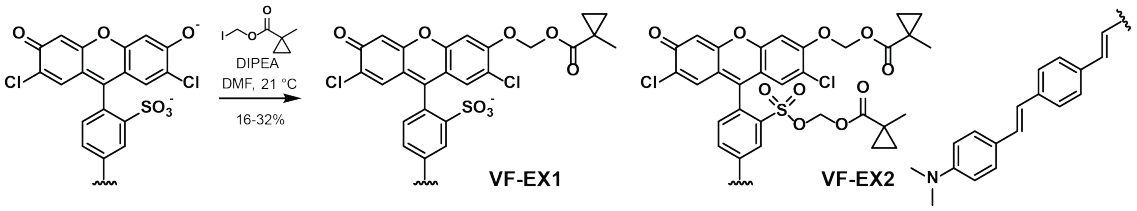

Scheme 2-2. Synthesis of VoltageFluor-EX 1 and 2.

Scheme 2-3. *Synthesis of VE-EX0.*

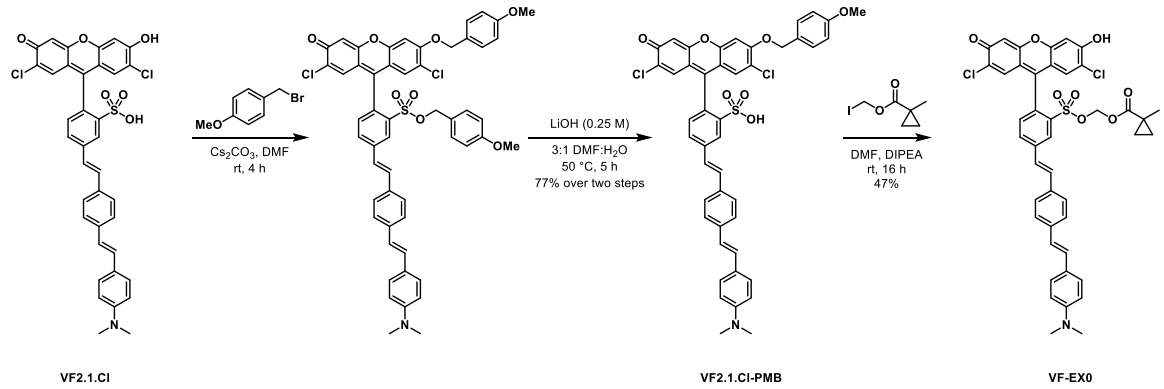

Scheme 2-3. Synthesis of VF-EX0.

Table 2. *Summary of Voltage Indicator Properties.*

				contrast[c]				ΔF/F (%)		SNR
	Φ[a]	K_M[b] (μM)	k_{cat}/K_M[b] ($M^{-1}s^{-1}$)	*in vitro*[d]	HEK[e]	neurons (Syn)[e]	neurons (CaMKII)[e]	HEK[f]	neurons[g]	neurons
VF-EX1	0.004	1.2	$2.1x10^5$	53	7	4.1	3.0	19	---	---
VF-EX2	0.013	0.12	$1.3x10^6$	11	17	4.8	3.7	21	7.2	20
VF-EX0	0.24	---	---	---	---	---	---	---	---	---
VF2.1.Cl	0.08	---	---	---	---	---	---	---	---	---
ASAP 1	---	---	---	---	---	>50	---	---	-6.5	4.9
Ace2N	---	---	---	---	---	>50	---	---	-2.9	11

--- = not determined or not applicable. [a] Quantum yield of fluorescence. Measured in HBSS (pH 7.4). [b] Determined by reaction of dye with purified PLE in HBSS (pH 7.4). [c] Ratio of VF-EX1 or VF-EX2 fluorescence in PLE-expressing cells (or PLE-containing buffer, for *in vitro*) to cells not expressing PLE. [d] After 3 hours in buffer, with or without PLE. [e] After 30 min (HEK cells) or 60 min (neurons) at 37 °C. [f] Per 100 mV depolarization, in HEK cells. [g] Per action potential evoked by field stimulation. All constructs are under the control of the Syn promoter.

.

Figure 2-1. *Spectroscopic characterization of VoltageFluor-EX 1 and 2.*

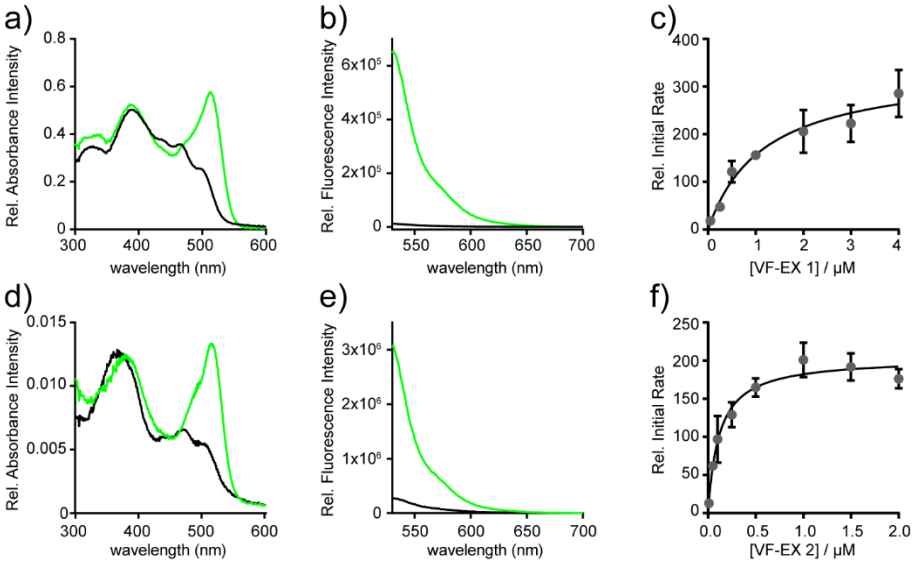

Figure 2-1. (a,d) UV/vis absorption and (b,e) fluorescence emission spectra of VF-EX1 (a,b) or VF-EX2 (d,e) in the absence (black line) or presence (green line) of purified porcine liver esterase (PLE, 0.7 mg/mL, 3 h). Excitation provided at 520 nm. (c,f) Plot of relative initial rate vs. substrate concentration for the reaction of PLE (200 ng/mL) with (c) VF-EX1 or (f) VF-EX2. Data points are mean ± S.E.M. for n = 4 independent measurements. Solid line is the line of best-fit to the Michaelis-Menten equation (Graphpad).

Figure 2-2. *Excitation spectra of VF-EX1 and 2.*

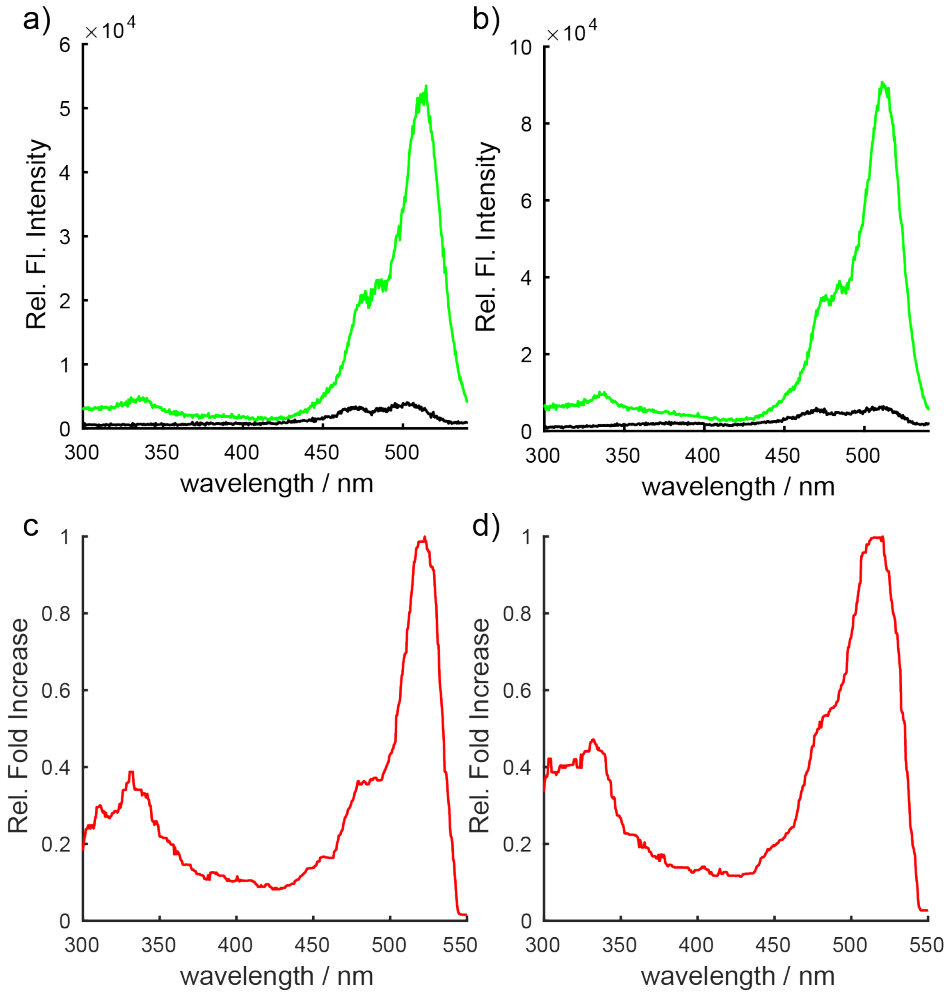

Figure 2-2. Excitation scans of (a) VF-EX1 and (b) VF-EX2 (both at 2 μM, in HBSS. Excitation wavelength was from 300 to 540 nm and emission was monitored at 550 nm. Green line represents presence of PLE for 3 hours and black line represents absence of PLE for the same amount of time. c) and d) Relative increase in fluorescence intensity for (c) VF-EX1 and (d) VF-EX2. For each plot, the (+) PLE values (green) were divided by the (-) PLE values (black). The result was smoothed using a median filter (moving average of ±6 points) and normalized to the maximum value. The largest fold turn-on is near the excitation maximum of 525 nm. Lower fold turn-on values are found centered at 475 nm.

Figure 2-3. *HPLC analysis of PLE reaction with VF-EX1 and VF-EX2.*

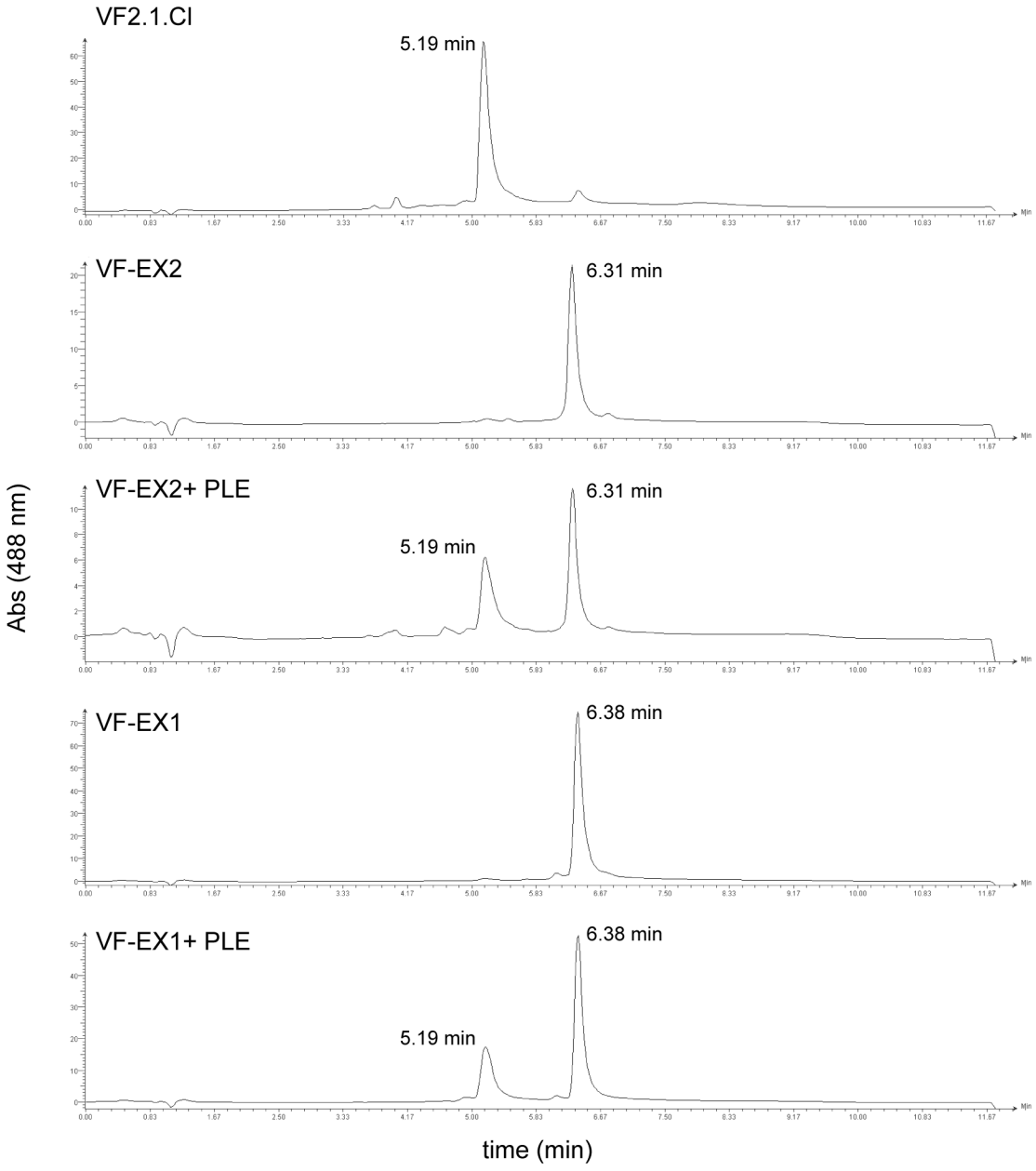

Figure 2-3. HPLC traces of the parent dye VF2.1.Cl and VF-EX dyes with and without PLE reaction.

Figure 2-4. *PLE constructs used in this study.*

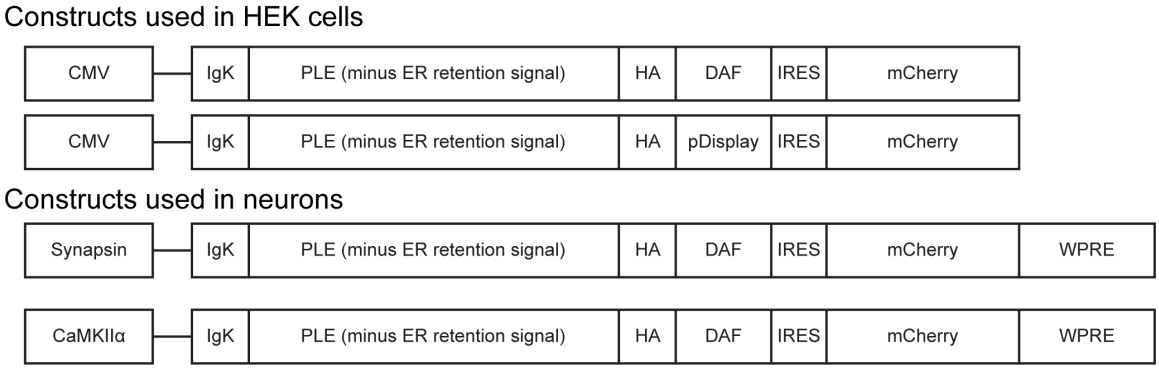

Figure 2-4. PLE constructs used in this study.

Figure 2-5. *Characterization of PLE expression in HEK cells by immunohistochemistry.*

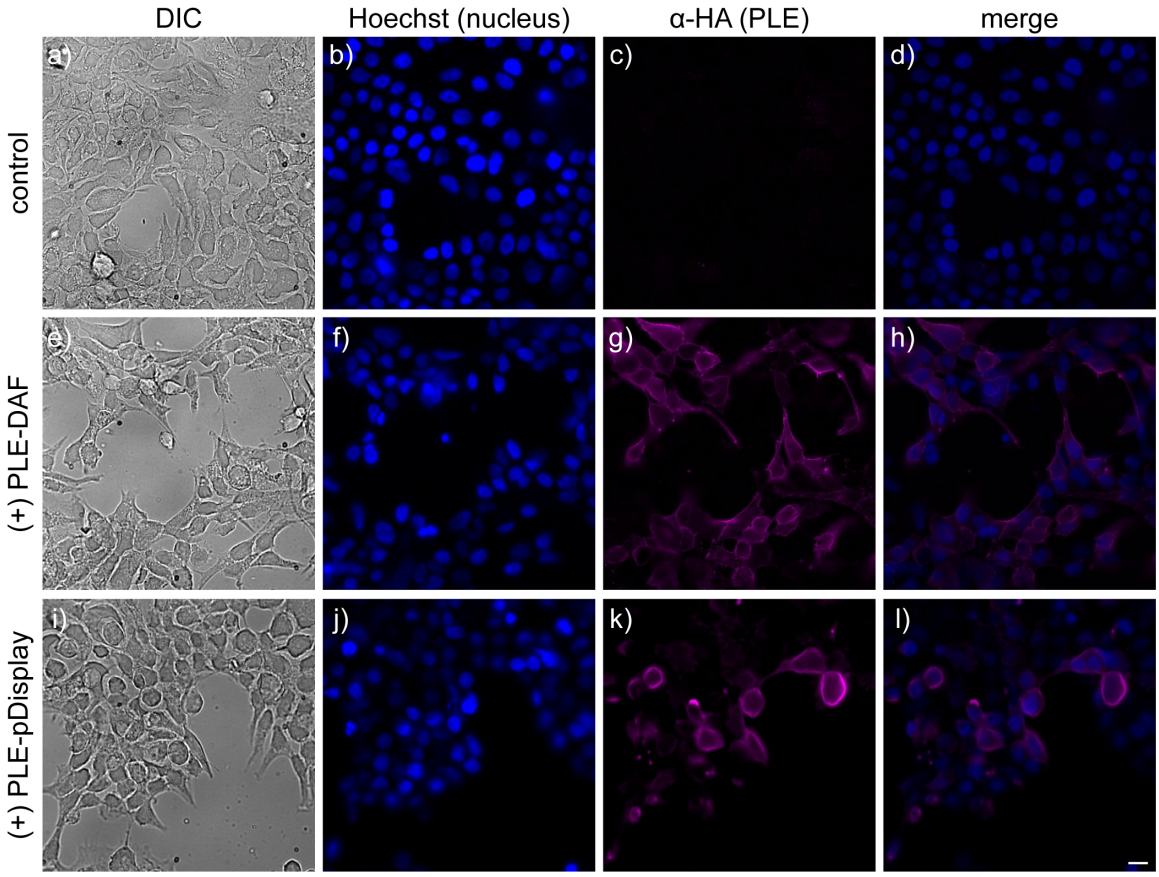

Figure 2-5. Fixed-cell, wide-field immunofluorescence in HEK cells. a-d) Control HEK cells (a) show clear nuclei with Hoechst 33342 (b) and no membrane-associated fluorescence as assayed by anti-HA (α-HA) immunofluorescence (c,d). In contrast, HEK cells expressing PLE-DAF (e-h) and PLE-pDisplay (i-l) show clear membrane-associated fluorescence when probed against the presence of the HA epitope (α-HA, g and k). Scale bar is 20 μm.

Figure 2-6. *Cellular and functional characterization of VoltageFluor-EX 1 and 2.*

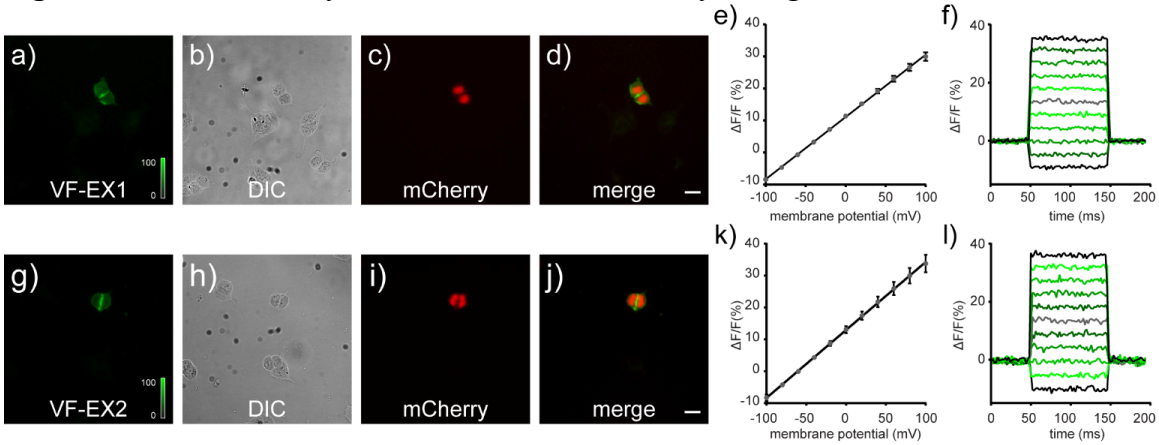

Figure 2-6. Widefield fluorescence microscopy of HEK cells stained with (a-d) VF-EX1 (500 nM, 30 min) or (g-j) VF-EX2 (500 nM 30 min) show membrane-associated fluorescence only in cells expressing cell-surface PLE (indicated by mCherry fluorescence). (a,g) Epifluorescence images showing VoltageFluor-associated fluorescence. (b,h) Transmitted light image of HEK cells. (c,i) Fluorescence image of nuclear-localized mCherry indicating PLE expression. (d,j) Merged imaging showing overlay of both VoltageFluor and mCherry fluorescence. Scale bars are 20 μm. (e,k) Plot of fractional change in fluorescence (ΔF/F) vs. final membrane potential for (e) VF-EX1 and (k) VF-EX2 in HEK cells under whole-cell voltage-clamp conditions. Data are mean ±S.E.M. for 6 cells (VF-EX1) and 8 cells (VF-EX2). (f,l) Representative plots of fractional change in fluorescence (ΔF/F) vs. time for a series of hyper- and de-polarizing steps from a holding potential of -60 mV to ±100 mV in voltage-clamped HEK cells loaded with (f) VF-EX1 or (l) VF-EX2.

Figure 2-7. *Characterization of VF-EX1 and VF-EX2 with DAF- and pDisplay-PLE in HEK cells.*

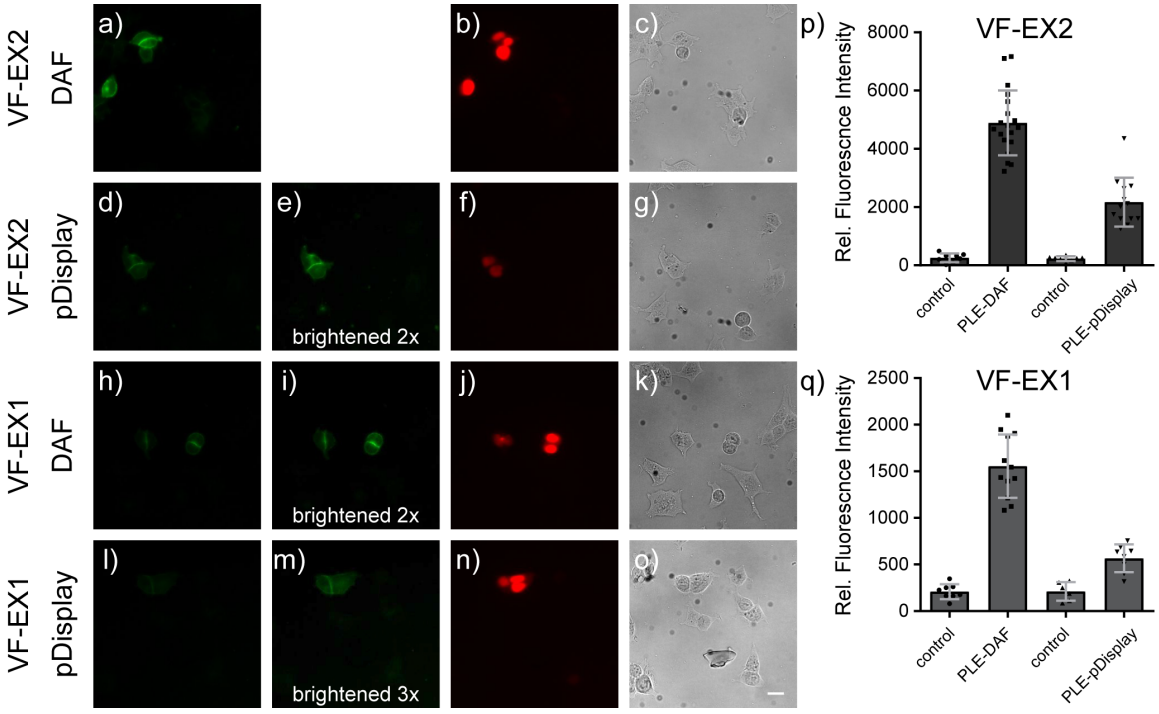

Figure 2-7. Live-cell fluorescence imaging of VoltageFluor-EX dyes in HEK cells. 500 nM of either VF-EX2 or VF-EX1 was incubated with HEK cells transfected with either PLE-DAF or PLE-pDisplay. (a-c) Live-cell, wide-field fluorescence images of VF-EX2 (a) in PLE-DAF expressing HEK cells (marked by mCherry, b). (c) DIC images show cells without mCherry/PLE expression. (d-g) Live-cell, wide-field fluorescence images of (d) VF-EX2 in PLE-pDisplay expressing HEK cells (marked by mCherry, f). (g) DIC images show cells without mCherry/PLE expression. Panel (e) shows the cells in (d), but brightened 2x. (h-k) Live-cell, wide-field fluorescence images of VF-EX1 (h) in PLE-DAF expressing HEK cells (marked by mCherry, j). (k) DIC images show cells without mCherry/PLE expression. Panel (i) shows the cells in (h), but brightened 2x. (l-o) Live-cell, wide-field fluorescence images of VF-EX1 (l) in PLE-DAF expressing HEK cells (marked by mCherry, n). (o) DIC images show cells without mCherry/PLE expression. Panel (m) shows the cells in (l), but brightened 3x. Scale bar is 20 μm. Acquisition and display setting are identical for panels a,d,h, and l. (p-q) Quantification of cell membrane-associated fluorescence for (p) VF-EX2 with DAF/pDisplay constructs and (q) VF-EX1with DAF/pDisplay constructs. Data are mean ± S.E.M. for n = 8-19 regions of interest comprising at least 2-3 cells each (individual values for the ROIs are indicated by markers).

Figure 2-8. *Quantification of contrast between PLE-expressing (DAF-targeted) and untransfected HEK cells stained with VF-EX1 or VF-EX2.*

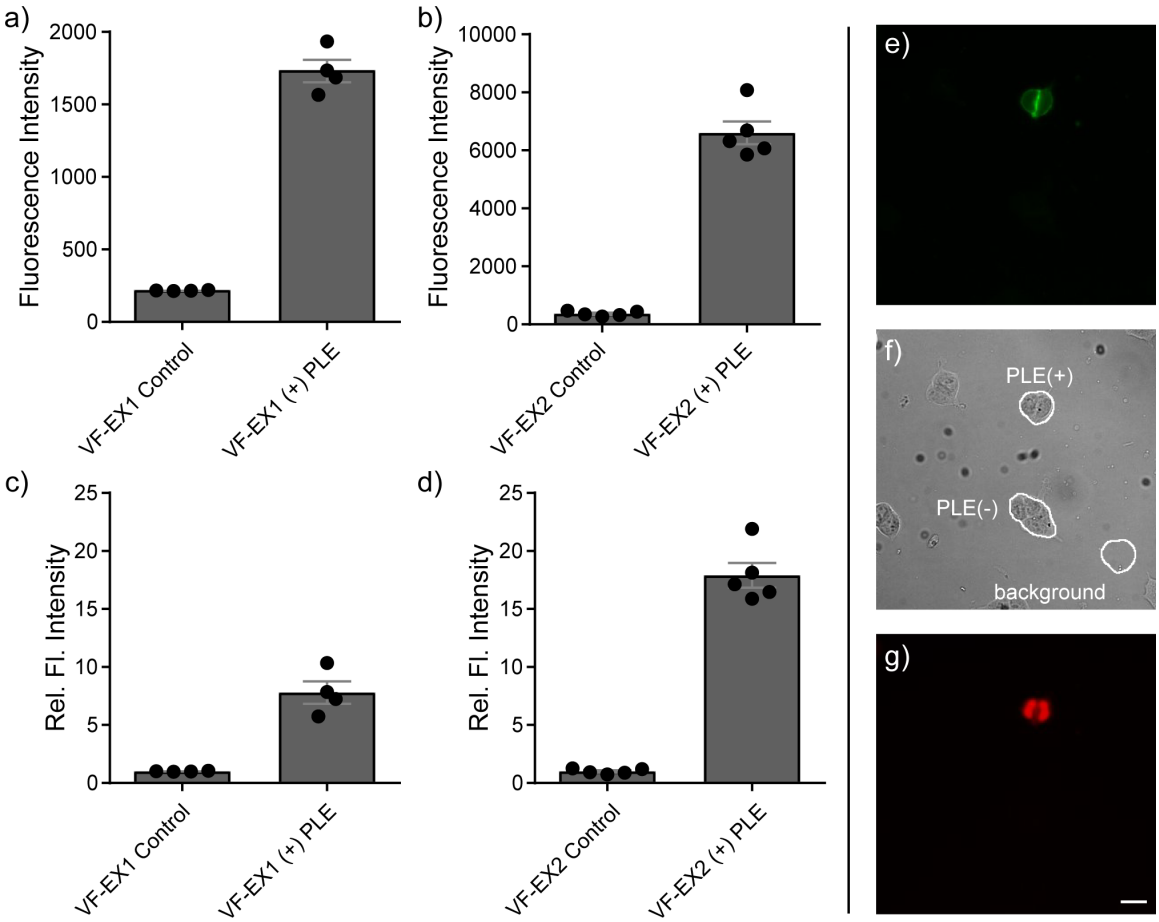

Figure 2-8. 500 nM of either VF-EX2 or VF-EX1 was incubated for 30 minutes at 37 °C with HEK cells transfected with PLE-DAF, replaced with dye-free HBSS and imaged. Panels (a) and (b) show the measured 16-bit grey values. Panels (c) and (d) show the relative contrast (fold turn-on) between control and transfected cells. Panels (e-g) show representative regions of interest used to calculate the mean fluorescence in cells. Data are mean grey values ±S.E.M. for 4 to 5 independent coverslips of cells. Each coverslip comprises 3 fields of view with regions of interest made up of PLE(+) and PLE(-) cells (30-40 cells per coverslip).

Figure 2-9. *Examination of PLE-[linker]-DAF length dependence on VF-EX2 staining.*

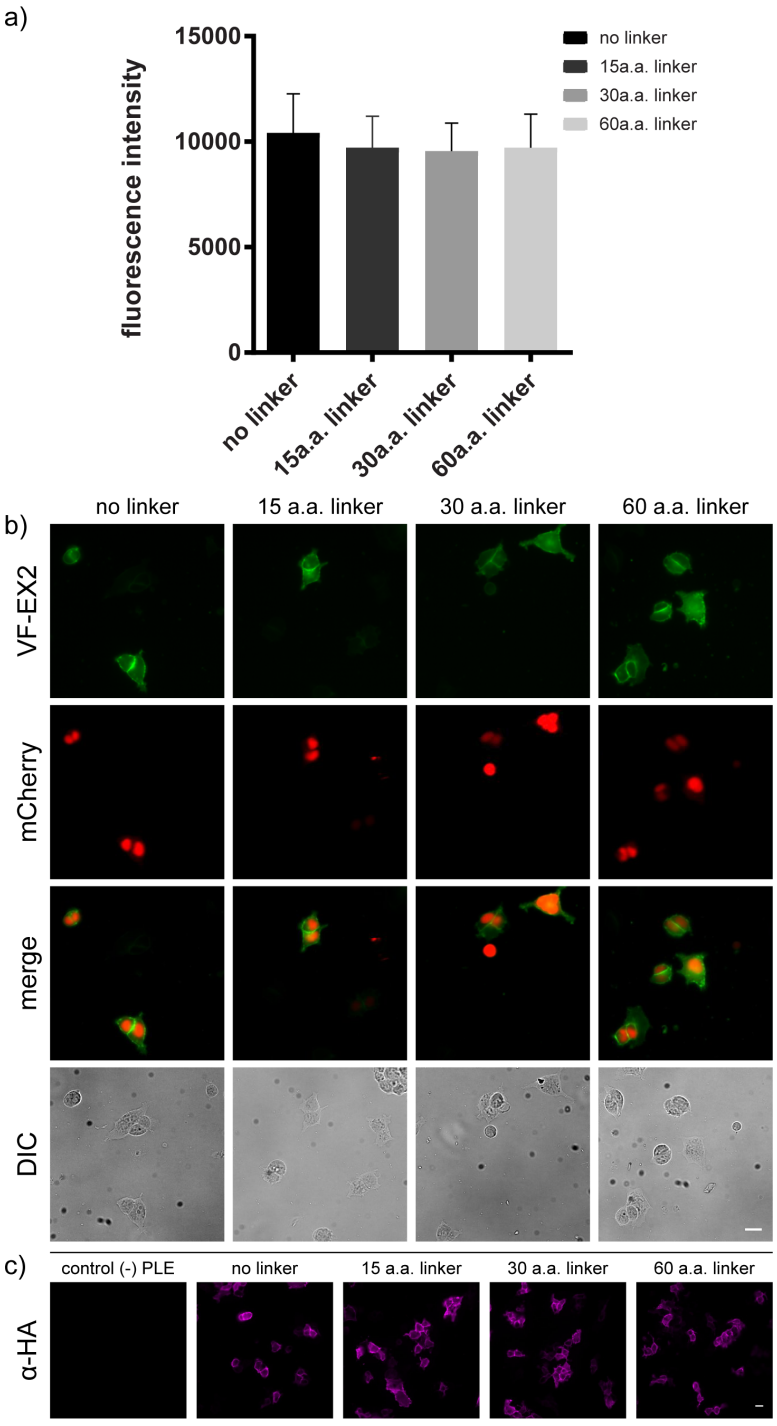

Figure 2-9. (a) Fluorescence intensity of PLE-expressing HEK cells stained with 500 nM VF-EX2. The average fluorescence intensity of PLE-expressing cells (i.e. mCherry-positive) for n = 40-70 ROIs. Values are mean ± standard deviation. (b) Epifluorescence images of HEK cells expressing PLE and stained with VF-EX2. (c) Epifluorescence images of fixed cells stained against HA for the presence of PLE. Scale bar is 20 μm.

Figure 2-10. *Timecourse of VF-EX2 accumulation in HEK cells expressing PLE-DAF.*

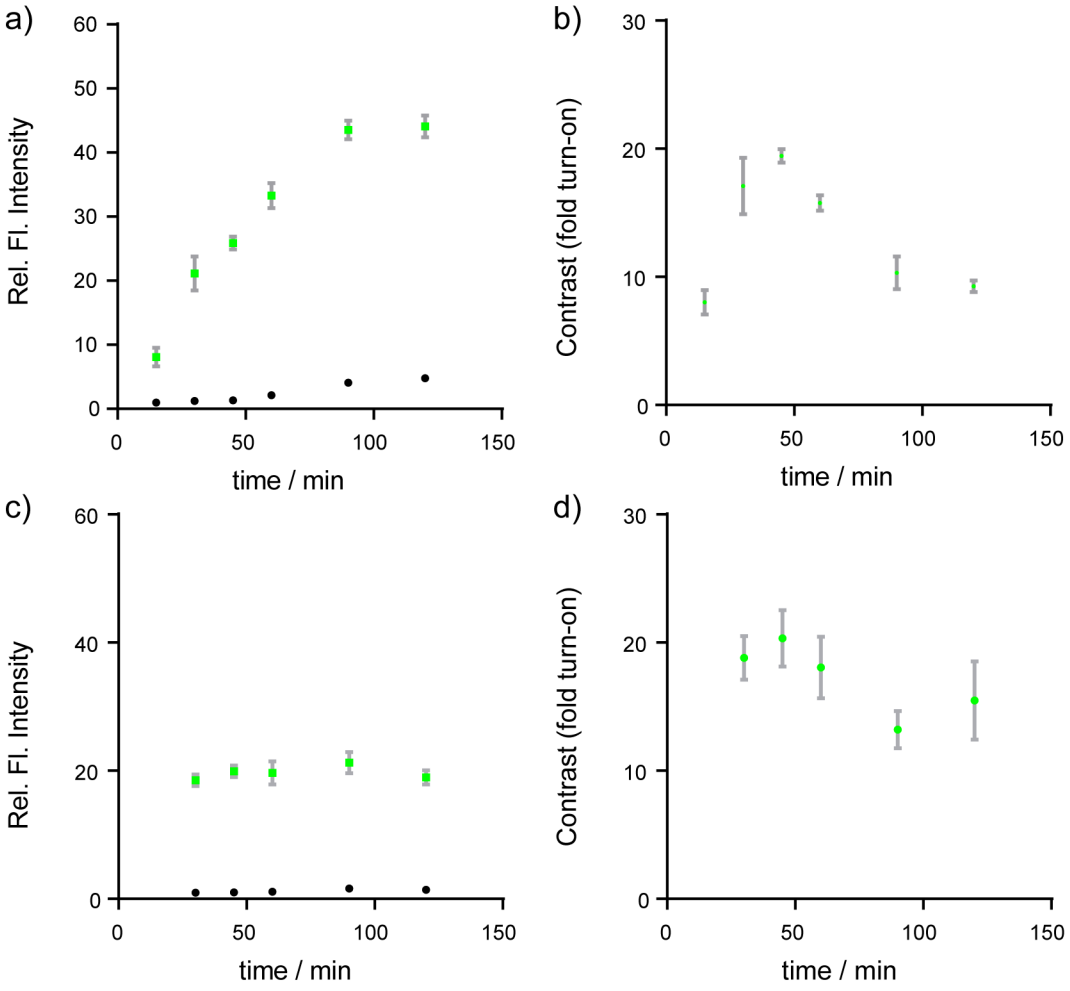

Figure 2-10. (a) The relative fluorescence intensity of HEK cells with (green) or without (black) PLE-DAF and loaded with VF-EX2 (500 nM) incubated at 37 °C for the indicated amount of time prior to exchanging into dye-free HBSS. Values are normalized to the first timepoint (15 min) for the untransfected cells. (b) Contrast, or fold turn-on, for cells in panel a. Contrast is calculated by dividing the relative fluorescence intensity for the PLE(+) by the PLE(-) cells. (c) The relative fluorescence intensity of HEK cells with (green) or without (black) PLE-DAF and loaded with VF-EX2 (500 nM) incubated at 37 °C for 30 minutes, washed into dye-free HBSS and maintained at 37 °C for 0, 15, 30, 60, or 90 minutes (x-axis indicates incubation time of 30 min + wash time). Values are normalized to the first timepoint (30 min) for the untransfected cells. (d) Contrast, or fold turn-on, for cells quantified in panel c. Contrast is calculated by dividing the relative fluorescence intensity for the PLE(+) by the PLE(-) cells. Data are mean values for n = 3 separate coverslips of HEK cells. Each coverslip contained intensity values for 50-60 cells. Error bars are S.E.M. (n = 3).

Figure 2-11. *Possible mechanism of cellular uncaging of VF-EX2 in HEK cells.*

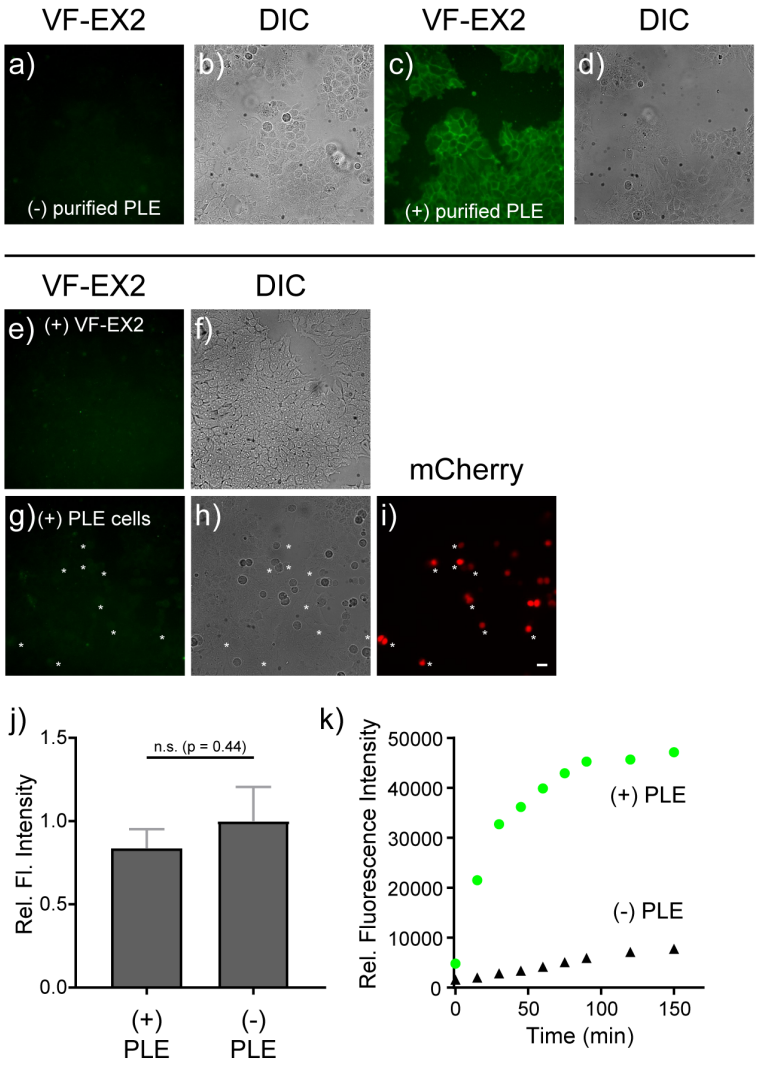

Figure 2-11. Fluorescence imaging in HEK cells with VF-EX2 to probe the mechanism of cellular uncaging.

Upper panel. HEK cells, not expressing cell-surface PLE, loaded with 1 μM VF-EX2 at 37 °C for 15 min show negligible cellular fluorescence (a). A transmitted light/differential interference contrast (DIC) image shows the presence of cells (b). When a large excess of purified PLE (final [PLE] = 28.1 μg/mL, 4.2 units/mL) is added to cells loaded with VF-EX2, membrane-associated fluorescence is observed after 30 min (panels c-d).

Lower panel. HEK cells, not expressing cell-surface PLE, loaded with 1 μM VF-EX2 at 37 °C for 15 min show negligible cellular fluorescence (e-f). Separately, HEK cells expressing cell-surface PLE (and nuclear mCherry) were prepared, harvested, suspended, and plated on the confluent layers of untransfected HEK cells shown in panels e,f. After 30 minutes at 37 °C, the cells were then assayed for increase in membrane-associated fluorescence in the VF-EX2-loaded/untransfected cells (g-i). The green fluorescence intensity proximal to mCherry-positive cells (i, white stars) was compared to green

fluorescence away from mCherry positive cells. (j) There was no statistically significant difference between the regions ($p = 0.44$, two-tailed, paired t-test), consistent with our hypothesis that PLE cannot activate VoltageFluor-EX across cells. Error bars are ±S.E.M. for n = 7 images (each with 6-10 cells)

(k) A positive control confirms that use of trypsin to harvest cells does not destroy PLE activity. Cells expressing surface PLE (green dots, (+) PLE) or not expressing surface PLE (black triangles, (-) PLE) were harvested with trypsin, as in g-i, washed, loaded with 2 μM VF-EX1 and the fluorescence increase over time was analyzed via fluorometer (ex. 520 nm, em. 530nm). PLE(+) cells (green dots) show an increase in fluorescence over time, while PLE (-) cells show negligible fluorescence gains over the course of 2 hours.. Scale bar = 20 μm. White stars indicate the location of mCherry-positive cells.

Figure 2-12. *Cell-surface PLE is required for fluorogenic activation of VF-EX2 dyes.*

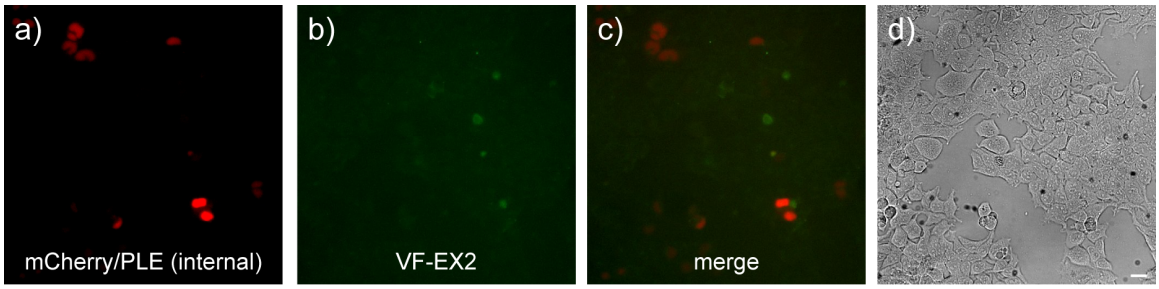

Figure 2-12. Wide-field fluorescence microscopy of HEK cells expressing the original pCAGS-PLE-IRES-NLS-mCherry construct (Lavis and co-workers, *PNAS*, 2012), stained with 500 nM VF-EX2 for 30 min at 37 °C. (a) mCherry expression indicates the expression of ER-localized PLE. (b) Low-levels of background fluorescence are visible from VF-EX2, and (c) fluorescence is not correlated with expression of mCherry/PLE. (d) Visible light image of cells from a-c. Scale bar is 20 μm.

Figure 2-13. *Immunocytochemistry of hippocampal neurons expressing PLE-DAF under control of the Synapsin promoter.*

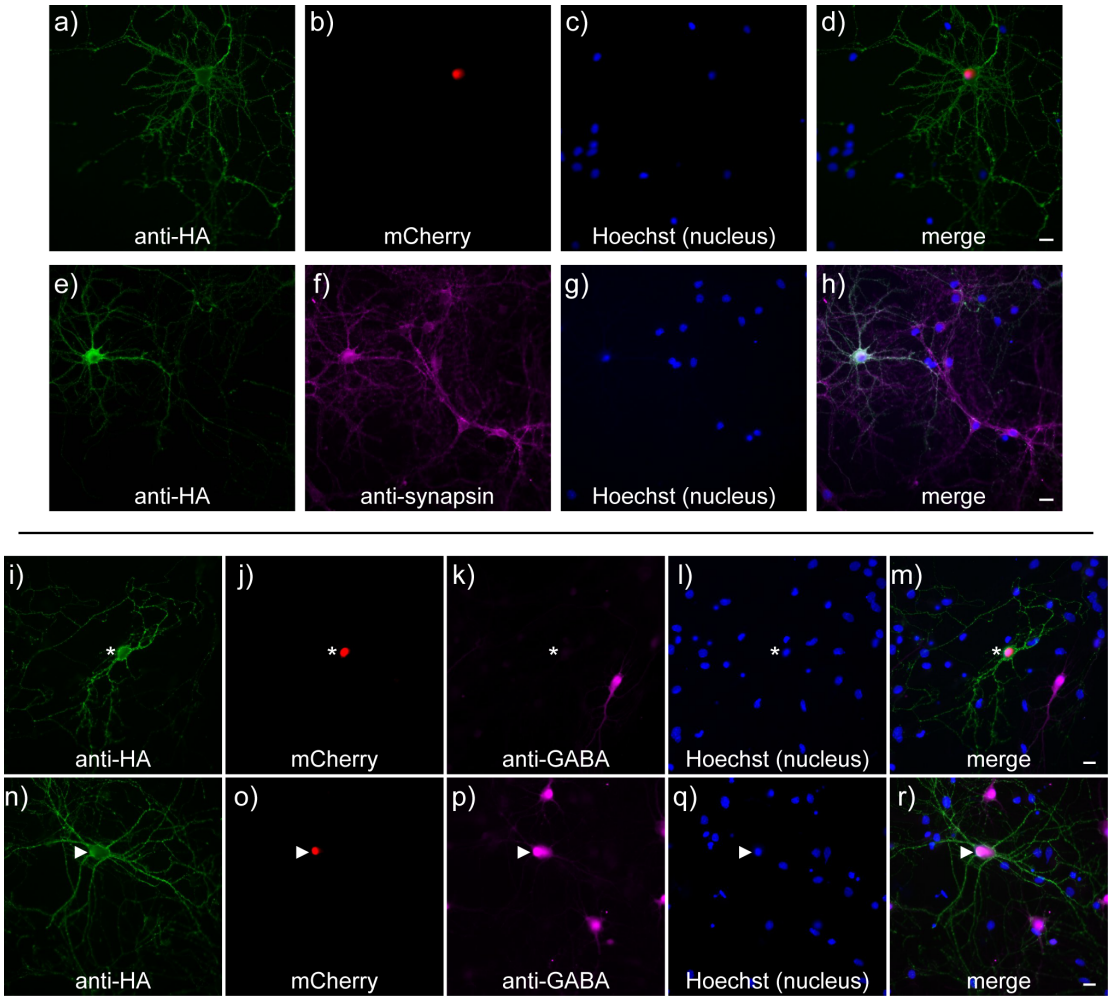

Figure 2-13. Wide-field fluorescence images of fixed neurons.

Upper panels. (a-d) Fixed neurons expressing PLE-DAF under control of the Synapsin (Syn) promoter show good colocalization between neurons positive for cell-surface PLE (anti-HA, green) and nuclear mCherry (red). (e-h) PLE (anti-HA, green) colocalize with synapsin (anti-synapsin, magenta).

Lower panels. Expression of PLE driven by the Syn promoter in both GABA-negative neurons (excitatory) and GABA-positive neurons (inhibitory). (i-m) PLE (anti-HA, green) and mCherry (mCherry, red) expression does not co-localize with GABA (anti-GABA, magenta). White star indicates PLE-(+), but GABA-(-) neuron. (n-r) PLE (anti-HA, green) and mCherry (mCherry, red) expression does co-localize with of GABA (anti-GABA, magenta). White arrowhead indicates PLE-(+) and GABA-(+) neuron. Scale bar = 20 μm and apply to the entire row. Images a-d are under non-permeabilizing conditions and images e-r are under permeabilizing conditions.

Figure 2-14. *Immunocytochemistry of hippocampal neurons expressing PLE-DAF under control of different promoters.*

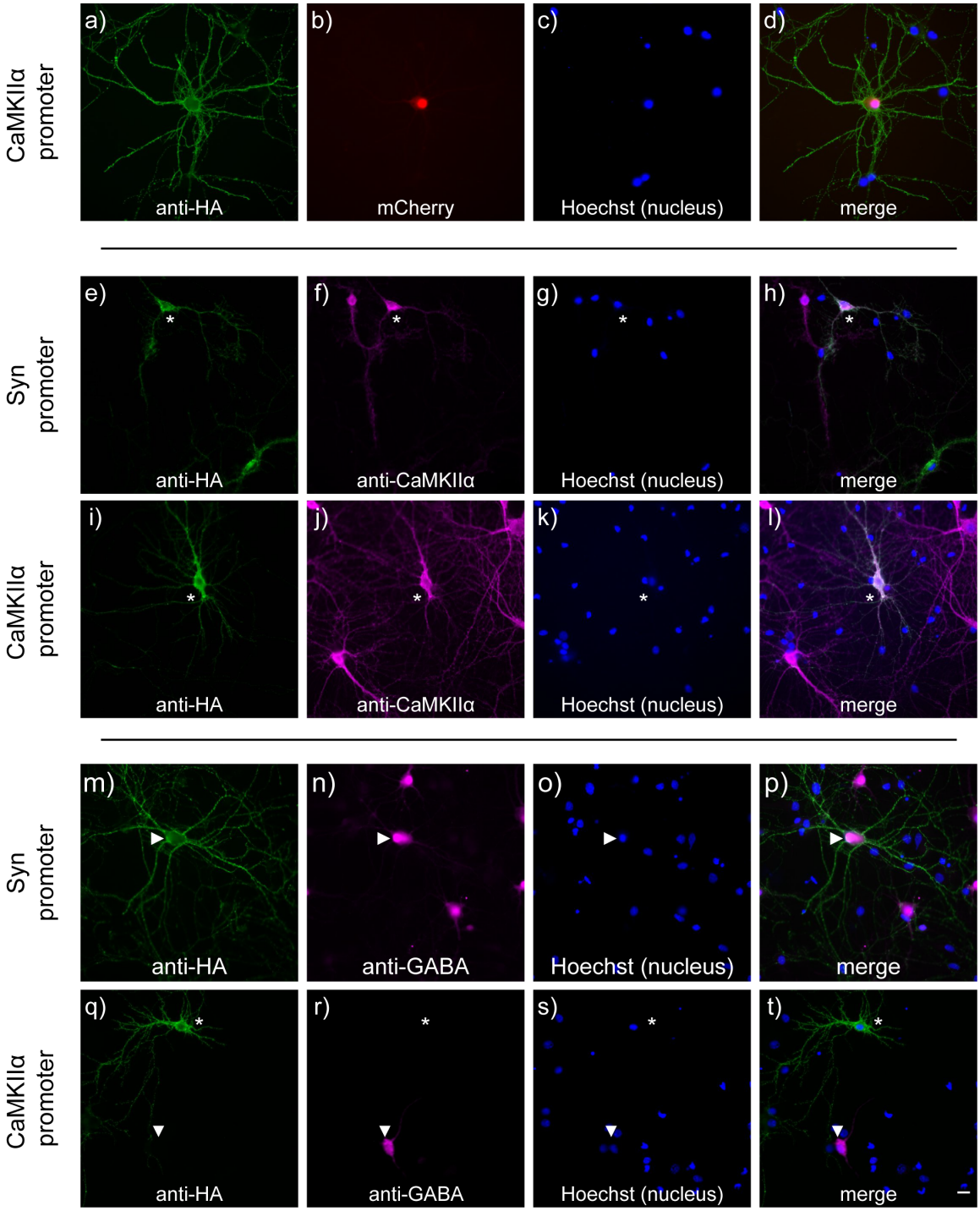

Figure 2-14. Widefield fluorescence images of fixed neurons transfected with Syn-PLE-DAF or CaMKIIα-PLE-DAF.

Upper panels. (a-d) Fixed neurons expressing PLE-DAF under control of the CaMKIIα promoter show good colocalization between neurons positive for cell-surface PLE (anti-HA, green) and nuclear mCherry (red).

Middle panels. (e-h) Expression of PLE driven by the Syn promoter is pan-neuronal. Of the two neurons expressing PLE (anti-HA, green), only one (indicated by the star) is positive for CaMKIIα (anti-CaMKIIα, magenta). (i-l) Expression of PLE (anti-HA, green) driven by the CaMKIIα promoter (targeting excitatory neurons) is restricted to neurons which also express CaMKIIα (anti-CaMKIIα, magenta). The PLE-(+) neuron (white star) also expresses CaMKIIα.

Lower panels. (m-p) Expression of PLE (anti-HA, green) driven by the pan-neuronal Syn promoter results in PLE expression in inhibitory neurons, which are identified by the presence of γ-aminobutyric acid (anti-GABA, magenta). The GABA-(+) neuron (white arrowhead) is also PLE-(+). Images in m-p are reproduced, in part, from Figure1-13n,p,q,r to facilitate comparison. (q-t) Expression of PLE (anti-HA, green) driven by the CaMKIIα promoter (targeting excitatory neurons) does not colocalize with inhibitory neurons, which are identified by the presence of γ-aminobutyric acid (anti-GABA, magenta). The white star indicates a PLE-(+), GABA-(-) neuron and the white arrowhead indicates a PLE-(-), GABA-(+) neuron. Scale bar = 20 μm. Images a-d are under non-permeabilizing conditions and images e-t are under permeabilizing conditions.

Figure 2-15. *Immunocytochemistry of hippocampal neurons expressing PLE-DAF under control of different promoters.*

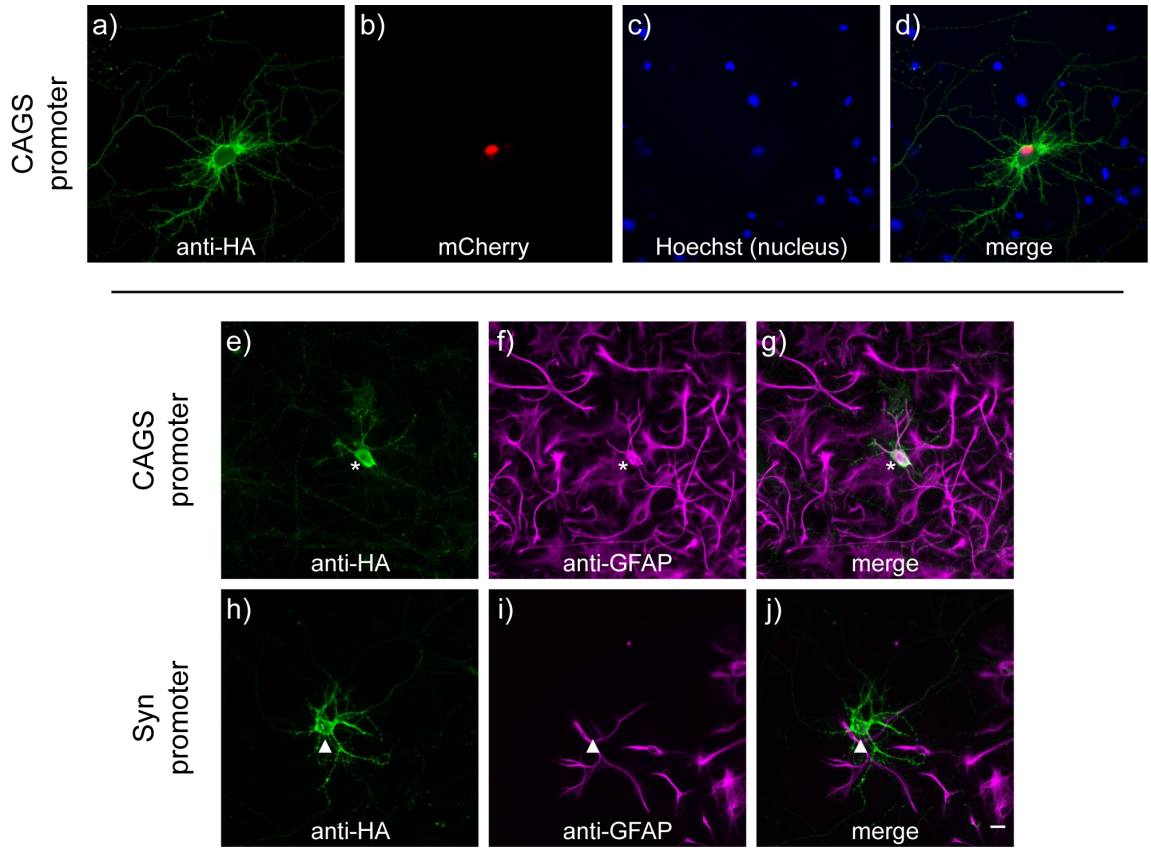

Figure 2-15. Widefield fluorescence images of fixed neurons transfected with pCAGS-PLE-DAF.

Upper panels. (a-d) Fixed neurons expressing PLE-DAF under control of the CAGS promoter show good colocalization between neurons positive for cell-surface PLE (anti-HA, green) and nuclear mCherry (red).

Lower panels. (e-g) Expression of PLE driven by the CAGS promoter results in PLE expression (anti-HA, green) in non-neuronal cell types, as identified by the expression of glial fibrillary acid protein, GFAP (anti-GFAP, magenta). White star indicates a PLE-(+) and GFAP-(+) cell. (h-j) In contrast, expression of PLE driven by the neuron specific Syn promoter results in PLE expression (anti-HA, green) that never colocalizes with GFAP (anti-GFAP, magenta). White arrowhead indicates PLE-(+) and GFAP-(-) cell. Scale bar = 20 μm. Images a-d are under non-permeabilizing conditions and images e-j are under permeabilizing conditions.

Figure 2-16. *Functional imaging in hippocampal neurons with VoltageFluor-EX 1.*

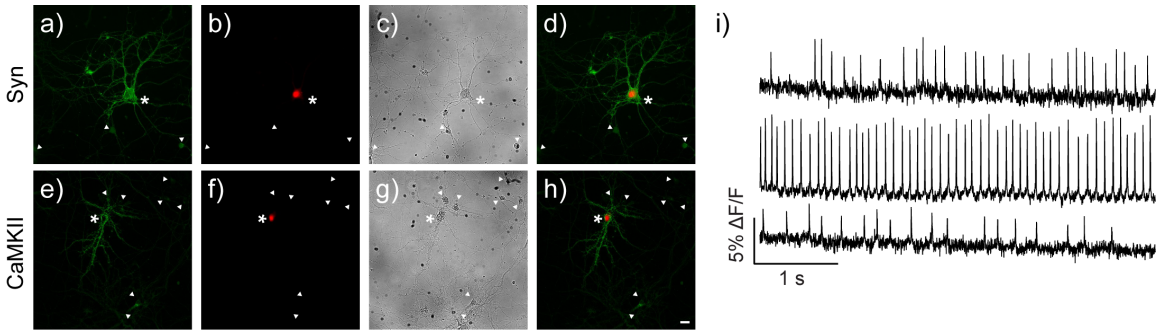

Figure 2-16. Pan- and excitatory-neuron targeting with VF-EX1. (a-h) Live-cell, widefield fluorescence images of rat hippocampal neurons stained with 1 μM VF-EX1 and expressing PLE-DAF under control of the (a-d) synapsin or (e-h) CaMKIIα promoter show clear membrane-associated fluorescence. (a,e) Widefield fluorescence image of membrane-associated VF fluorescence in PLE-expressing neurons. (b,f) Nuclear-localized mCherry confirms PLE expression in defined neurons. (c,g) DIC images of neurons. (d,h) Merged images of VF and mCherry fluorescence confirms good association between bright, membrane-associated fluorescence and mCherry/PLE expression. Scale bars are 20 μm. Asterisks indicate mCherry/PLE-positive neurons while arrowheads indicate untransfected neurons. (i) Representative ΔF/F traces for rat hippocampal neurons stained with VF-EX1 and transfected with Syn-PLE. Traces are ΔF/F from regions of interest at the cell bodies of neurons after background offset and are uncorrected for bleaching. Images are acquired at 500 Hz and represent single trial acquisitions.

Figure 2-17. *Functional imaging in hippocampal neurons with VoltageFluor-EX 2.*

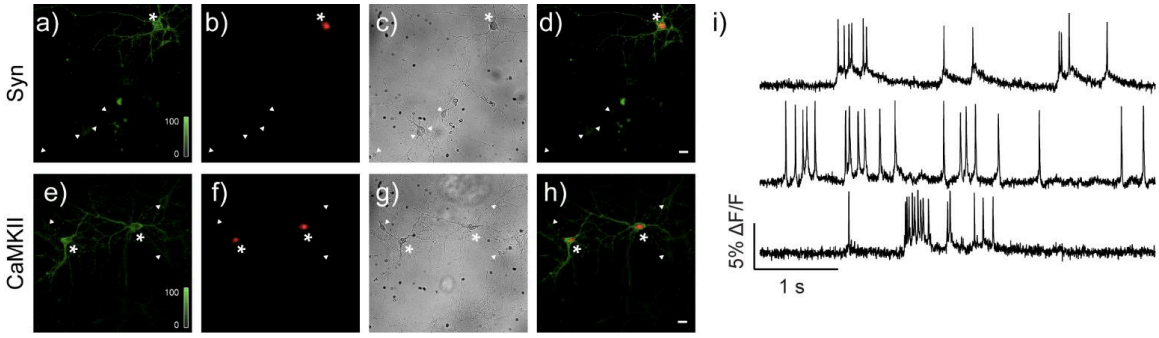

Figure 2-17. Pan- and excitatory-neuron targeting with VF-EX 2. (a-h) Live cell, widefield fluorescence images of rat hippocampal neurons stained with 1 μM VF-EX2 (60 min.) and expressing PLE-DAF under control of the (a-d) synapsin or (e-h) CaMKIIα promoter show clear membrane-associated fluorescence. (a,e) Widefield fluorescence image of membrane-associated VF fluorescence in PLE-expressing neurons. (b,f) Nuclear-localized mCherry confirms PLE expression in defined neurons. (c,g) Differential interference contrast (DIC) images of neurons. (d,h) Merged images of VF and mCherry fluorescence confirms good association between bright, membrane-associated fluorescence and mCherry/PLE expression. Scale bars are 20 μm. Asterisks indicate mCherry/PLE-positive neurons while arrowheads indicate untransfected neurons. (i) Representative ΔF/F traces for rat hippocampal neurons stained with VF-EX2 and transfected with Syn-PLE. Traces are ΔF/F from regions of interest at the cell bodies of neurons after background offset and are uncorrected for bleaching. Images are acquired at 500 Hz and represent single trial acquisition.

Figure 2-18. *Quantification of VF-EX1 and VF-EX2 / PLE in live neurons.*

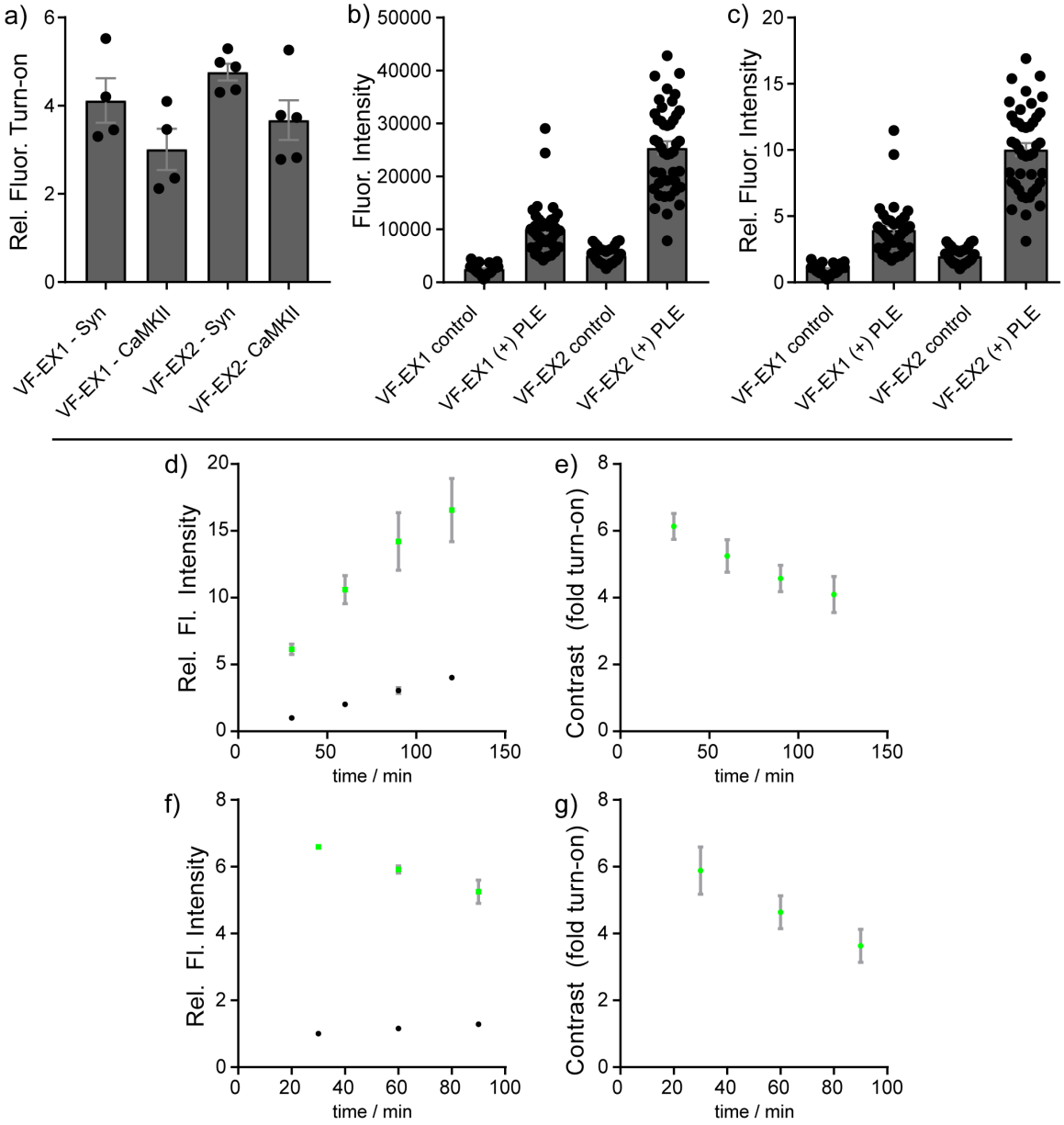

Figure 2-18. Quantification of VF-EX1 and VF-EX2 / PLE in live neurons.

Upper Panel (a) Quantification of the relative fluorescence turn-on in neurons stained with either VF-EX1 or VF-EX2 and expressing PLE-DAF under control of the synapsin or CaMKII promoter relative to control cells. Individual points are the average contrast ratio between for 6-10 neurons expressing PLE and 6-10 neurons not expressing PLE, on a single coverslip. Error bars are ±S.E.M. (b) Comparison of the fluorescence intensity (pixel grey values, 16-bit scale) of VF-EX1 and VF-EX2 in neurons expressing PLE-DAF under control of the synapsin promoter. Each point represents an individual neuron. (c) Comparison of the relative fluorescence intensity of VF-EX1 and VF-EX2 in neurons

expressing PLE-DAF under control of the synapsin promoter. Each point represents an individual neuron. Error bars are ±S.E.M.

Lower Panel. Timecourse of VF-EX2 accumulation in neurons expressing PLE-DAF (synapsin). (d) The relative fluorescence intensity of neurons with (green) or without (black) PLE-DAF and loaded with VF-EX2 (1 μM) incubated at 37 °C for the indicated amount of time prior to exchanging into dye-free HBSS. Values are normalized to the first timepoint (30 min) for the untransfected cells. (e) Contrast, or fold turn-on, for cells in panel d. Contrast is calculated by dividing the relative fluorescence intensity for the PLE(+) by the PLE(-) cells. (f) The relative fluorescence intensity of neurons with (green) or without (black) PLE-DAF and loaded with VF-EX2 (1 μM) incubated at 37 °C for 30 minutes, washed into dye-free HBSS and maintained at 37 °C for 0, 30, or 60 minutes (x-axis indicates incubation time of 30 min + wash time). Values are normalized to the first timepoint (30 min) for the untransfected cells. (g) Contrast, or fold turn-on, for cells quantified in panel f. Contrast is calculated by dividing the relative fluorescence intensity for the PLE(+) by the PLE(-) cells. Data are mean values for n = 3 separate coverslips of neurons. Each coverslip contained intensity values for 15-20 cells. Error bars are S.E.M. (n = 3).

Figure 2-19. *Spiking events recorded optically by VF-EX2/PLE, ASAP 1, and Ace2N.*

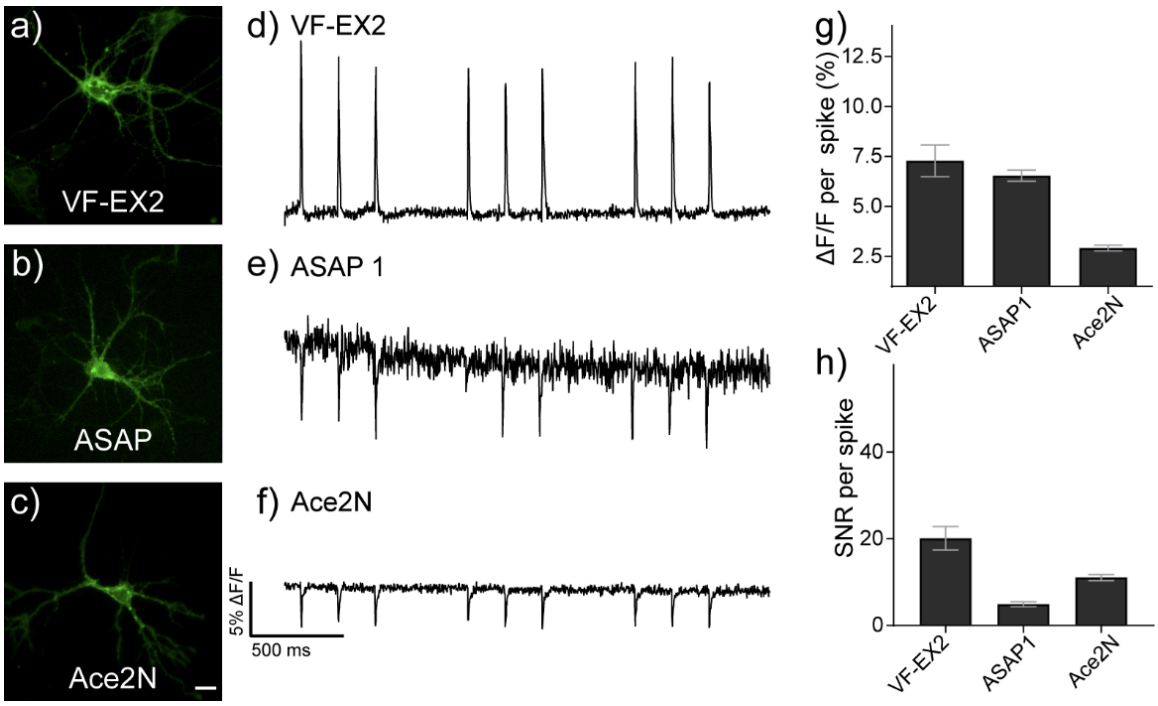

Figure 2-19. Comparison of VoltageFluor-EX2 to genetically encoded voltage indicators. (a-c) Live-cell, widefield fluorescence imaging of neurons expressing (a) PLE and stained with 1 μM VF-EX2 (60 min.), (b) ASAP 1, or (c) Ace2N-mNeon (Ace2N) under control of the Syn promoter. Scale bar is 20 μm. (d-f) ΔF/F vs. time plots for action potentials evoked and optically recorded with either (d) VF-EX2/PLE, (e) ASAP 1, or (f) Ace2N. (d)g-h) Quantification of (g) ΔF/F and (h) signal-to-noise (SNR). Data are mean ±S.E.M. for n = 16, 7, and 13 neurons (each neuron is the average of 9 evoked action potentials).

Figure 2-20. *Spiking events recorded optically by VF-EX2/PLE, ASAP 1, and Ace2N.*

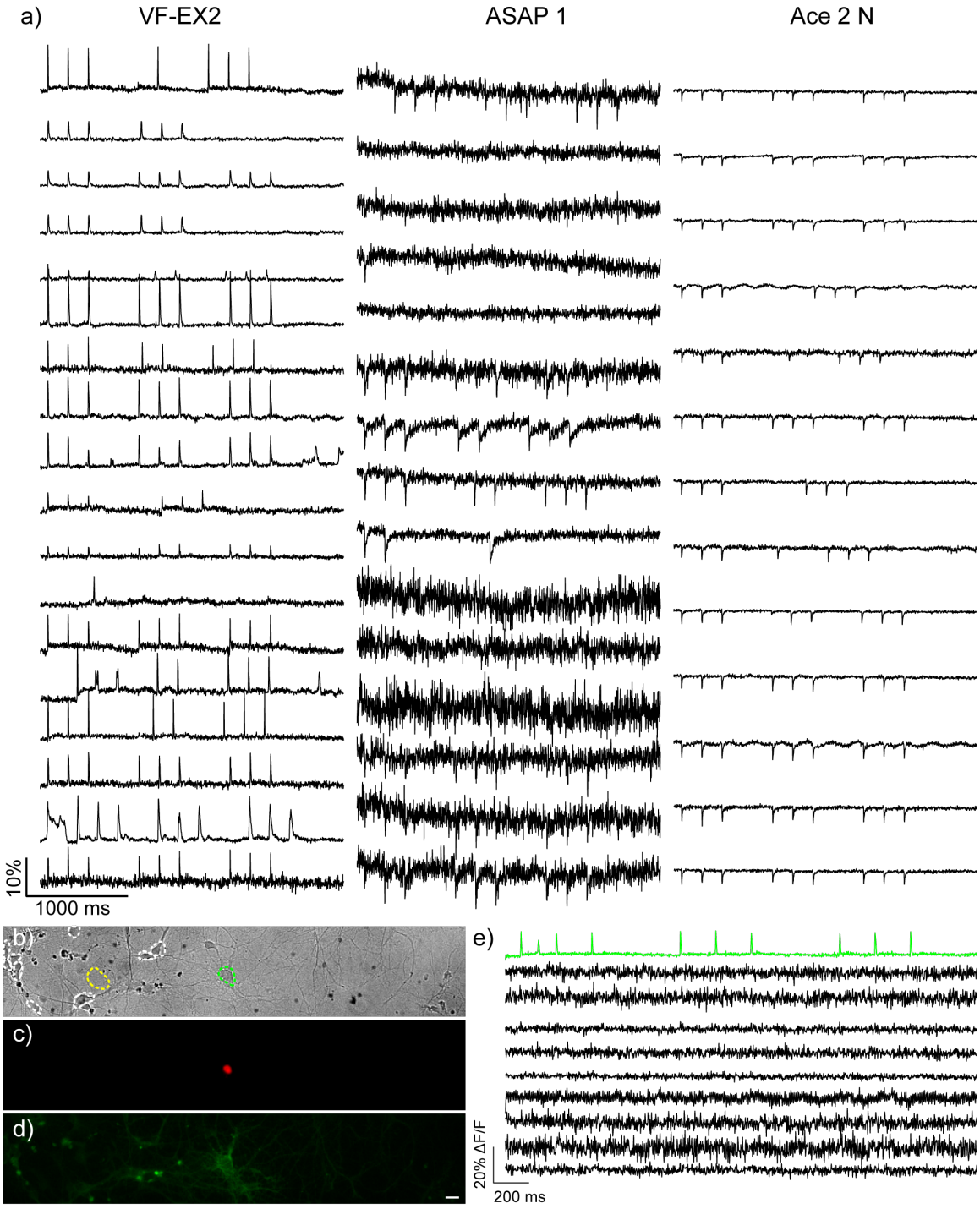

Figure 2-20. Compare evoked action potentials recorded optically by VF-EX2/PLE, ASAP 1, and Ace2N. (a) Representative data used to construct plots in Figure 4d-f in the main text. Plots show ΔF/F vs time for rat hippocampal neurons expressing the indicated constructs under control of the synapsin promoter. (b-d) Representative images showing neurons expressing PLE (syn) and stained with VF-EX2. (b) PLE-negative ROIs are

indicated in white, and the background ROI is in yellow on the DIC image. The green ROI is the PLE-positive cell. (c) mCherry image reveals a single PLE-positive cell. (d) The PLE(+) neuron is brighter than the surrounding neurons. Scale bar is 20 μm. (e) Evoked activity across the entire field of view can only be observed in the PLE positive neuron (green trace); the other cells do not have enough fluorescence signal.

Figure 2-21. *Spontaneous activity in rat hippocampal neurons and quantification of cellular vs. membrane-associated fluorescence.*

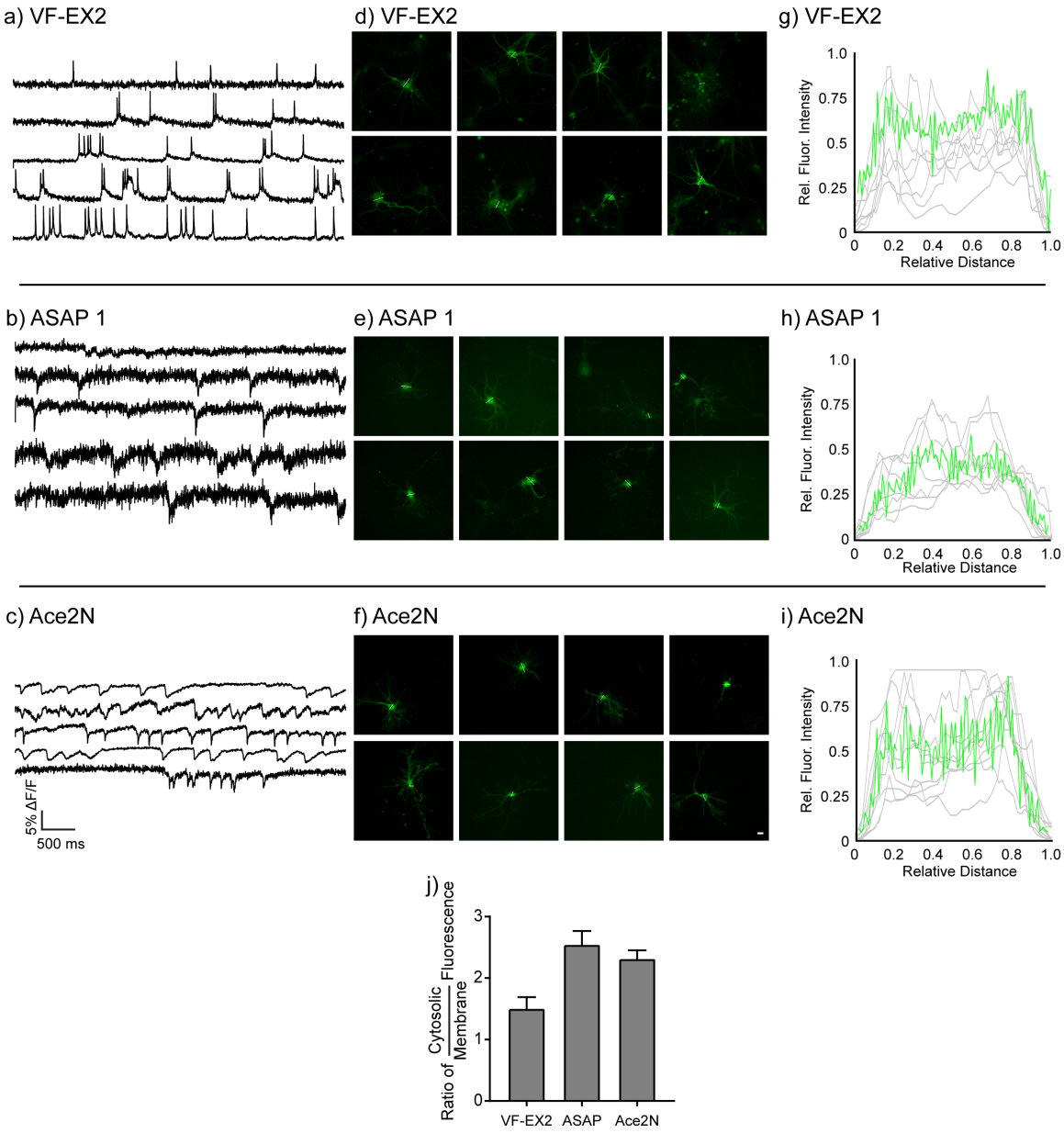

Figure 2-21. Compare spontaneous activity and fluorescence localization of VF-EX2, ASAP 1 and Ace2N in cultured neurons.

Left panel. Representative ΔF/F traces for rat hippocampal neurons (a) transfected with Syn-PLE and stained with VF-EX2 or just transfected with (b) ASAP 1, or (c) Ace2N. Images were acquired at 500 Hz and ΔF/F was computed by plotting the intensity at an ROI encompassing the cell body divided by the initial fluorescence intensity.

Middle panel. To quantify the relative amount of membrane-associated fluorescence, intensity profiles were acquired for at least 8 neurons from (d) VF-EX2/PLE, (e) ASAP 1, and (f) Ace2N.

Right and lower panel. For each intensity profile, the distance was normalized (0 to 1.0) and rounded to the nearest 0.01 increment. The normalized fluorescence for each profile was plotted (grey traces, g-i) and then averaged (green traces, g-i). The ratio of inner fluorescent to outer fluorescence was quantified in the following manner. Inner fluorescence was defined as the average fluorescence intensity from 0.2 to 0.8 along the cell profile. Outer fluorescence was defined as the average fluorescence from 0 to 0.2 and from 0.8 to 1.0 along the cell profile. The ratio for each cell was calculated and plotted in panel j. Error bars are ±S.E.M. for n = 8 (VF-EX2/PLE or ASAP 1) or 10 cells (Ace2N).

Figure 2-22. *Interrogation of the neuromodulatory effects of serotonin on neurons from the rat hippocampus.*

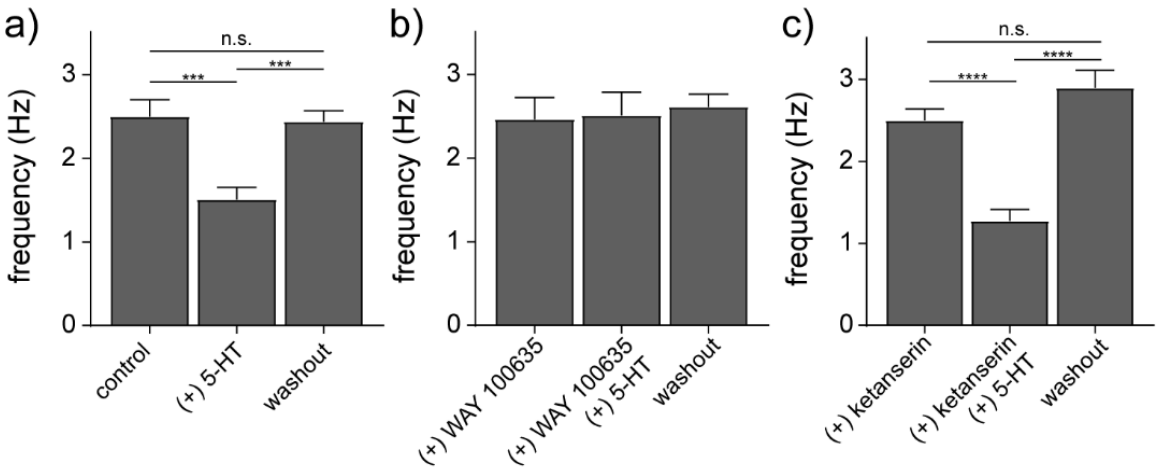

Figure 2-22. Optical recording of neuronal activity using VF-EX2 in cultured hippocampal neurons upon various drug treatment. (a-c) Hippocampal neurons expressing PLE (CaMKIIα-PLE) and stained with 1 μM VF-EX2 (60 min.) were treated with (a) 5-HT (10 μM) alone, (b) in the presence of WAY 100635 (10 nM), or (c) in the presence of ketanserin (100 nM). The firing rate of neurons was measured before (left bars), during (middle bars), and after (right bars) washout of 5-HT. Data are mean ± S.E.M. for the average firing rate of 8-10 different coverslips of neurons. Each coverslip's average firing frequency was measured from between 5-8 individual neurons, for a total of between 46-93 neurons for each condition. Two-tailed Mann-Whitney tests were used to determine statistical significance.
*** indicates $p < 0.005$; **** indicates $p < 0.001$.

Figure 2-23. *Interrogation of the neuromodulatory effects of serotonin on neurons from the rat hippocampus.*

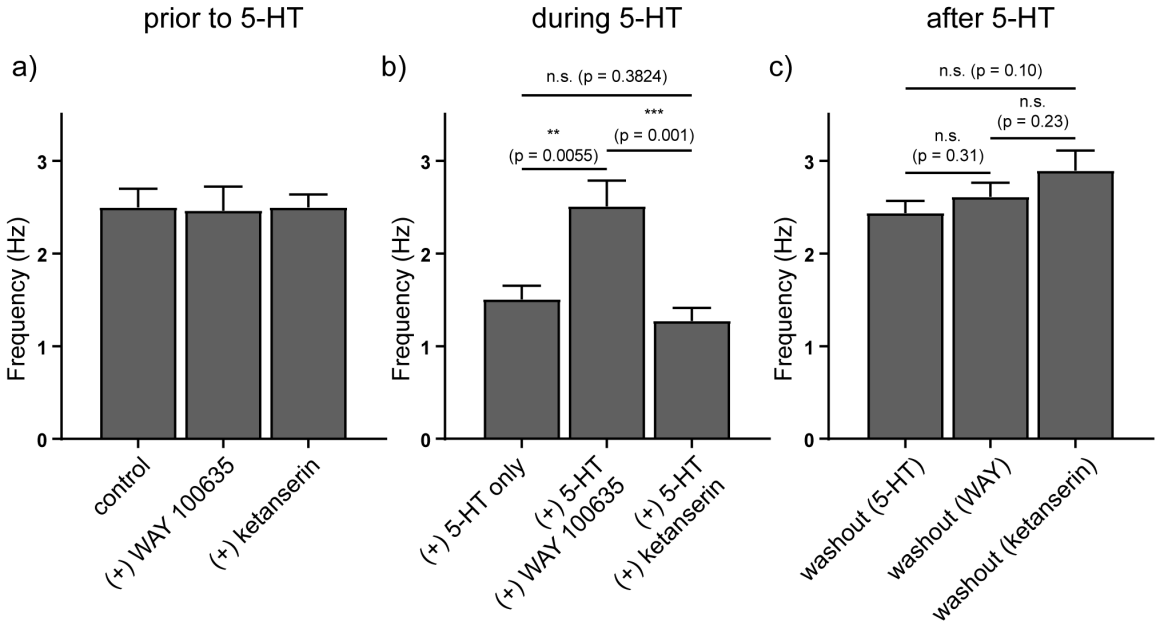

Figure 2-23. Optical recording of neuronal activity using VF-EX2 in cultured hippocampal neurons upon various drug treatment. (a) Prior to 5-HT treatment, all neurons show similar firing rates, even in the presence of WAY 100635 or ketanserin. (b) During 5-HT treatment, cells treated only with 5-HT or cells treated with 5-HT in the presence of ketanserin showed a decrease in the spike frequency. There was no statistical difference between neurons with and without ketanserin. The presence of the 5-HT_{1A} inhibitor, WAY 100635, blocked the effect of 5-HT. (c) After washout of drugs (both 5-HT and inhibitors), cells return to normal firing frequencies which are statistically indistinguishable from one another. Plots show mean ±S.E.M. for n = 12, 8, and 9 coverslips (control, WAY 100635, and ketanserin treatment). Each coverslip represents the average firing frequency of 5-8 neurons. A two-tailed Mann-Whitney test for statistical significance was employed; p-values are indicated in comparisons across conditions.

Reference

1. Peterka, D. S.; Takahashi, H.; Yuste, R., *Neuron* **2011,** *69* (1), 9-21.
2. St-Pierre, F.; Marshall, J. D.; Yang, Y.; Gong, Y.; Schnitzer, M. J.; Lin, M. Z., *Nat Neurosci* **2014,** *17* (6), 884-9.
3. Hochbaum, D. R.; Zhao, Y.; Farhi, S. L.; Klapoetke, N.; Werley, C. A.; Kapoor, V.; Zou, P.; Kralj, J. M.; Maclaurin, D.; Smedemark-Margulies, N.; Saulnier, J. L.; Boulting, G. L.; Straub, C.; Cho, Y. K.; Melkonian, M.; Wong, G. K. S.; Harrison, D. J.; Murthy, V. N.; Sabatini, B. L.; Boyden, E. S.; Campbell, R. E.; Cohen, A. E., *Nature Methods* **2014,** *11* (8), 825-833.
4. Gong, Y. Y.; Huang, C.; Li, J. Z.; Grewe, B. F.; Zhang, Y. P.; Eismann, S.; Schnitzer, M. J., *Science* **2015,** *350* (6266), 1361-1366.
5. Abdelfattah, A. S.; Farhi, S. L.; Zhao, Y.; Brinks, D.; Zou, P.; Ruangkittisakul, A.; Platisa, J.; Pieribone, V. A.; Ballanyi, K.; Cohen, A. E.; Campbell, R. E., *J Neurosci* **2016,** *36* (8), 2458-72.
6. Jin, L.; Han, Z.; Platisa, J.; Wooltorton, J. R. A.; Cohen, L. B.; Pieribone, V. A., *Neuron* **2012,** *75* (5), 779-785.
7. Miller, E. W., *Curr Opin Chem Biol* **2016,** *33*, 74-80.
8. Miller, E. W.; Lin, J. Y.; Frady, E. P.; Steinbach, P. A.; Kristan, W. B., Jr.; Tsien, R. Y., *Proc Natl Acad Sci U S A* **2012,** *109* (6), 2114-9.
9. Kulkarni, R. U.; Kramer, D. J.; Pourmandi, N.; Karbasi, K.; Bateup, H. S.; Miller, E. W., *Proc Natl Acad Sci U S A* **2017,** *114* (11), 2813-2818.
10. Woodford, C. R.; Frady, E. P.; Smith, R. S.; Morey, B.; Canzi, G.; Palida, S. F.; Araneda, R. C.; Kristan, W. B., Jr.; Kubiak, C. P.; Miller, E. W.; Tsien, R. Y., *J Am Chem Soc* **2015,** *137* (5), 1817-24.
11. Grenier, V.; Walker, A. S.; Miller, E. W., *J. Am. Chem. Soc.* **2015,** *137* (34), 10894-10897.
12. Tian, L.; Yang, Y. L.; Wysocki, L. M.; Arnold, A. C.; Hu, A.; Ravichandran, B.; Sternson, S. M.; Looger, L. L.; Lavis, L. D., *Proc Natl Acad Sci U S A* **2012**, *109* (13), 4756-4761.
13. Kawaguchi, M.; Okabe, T.; Okudaira, S.; Hanaoka, K.; Fujikawa, Y.; Terai, T.; Komatsu, T.; Kojima, H.; Aoki, J.; Nagano, T., *J. Am. Chem. Soc.* **2011**, *133* (31), 12021-30.
14. Chesnut, J. D.; Baytan, A. R.; Russell, M.; Chang, M. P.; Bernard, A.; Maxwell, I. H.; Hoeffler, J. P., *J Immunol Methods* **1996**, *193* (1), 17-27.
15. Medof, M. E.; Walter, E. I.; Roberts, W. L.; Haas, R.; Rosenberry, T. L., *Biochemistry* **1986**, *25* (22), 6740-7.
16. Huang, Y. L.; Walker, A. S.; Miller, E. W., *J. Am. Chem. Soc.* **2015**, *137* (33), 10767-10776.
17. Shaner, N. C.; Lambert, G. G.; Chammas, A.; Ni, Y.; Cranfill, P. J.; Baird, M. A.; Sell, B. R.; Allen, J. R.; Day, R. N.; Israelsson, M.; Davidson, M. W.; Wang, J., *Nat Methods* **2013**, *10* (5), 407-9.
18. Hoyer, D.; Hannon, J. P.; Martin, G. R., *Pharmacol Biochem Behav* **2002**, *71* (4), 533-54.
19. Mahgoub, M. A.; Sara, Y.; Kavalali, E. T.; Monteggia, L. M., *J Pharmacol Exp Ther* **2006**, *317* (1), 88-96.

20. Fletcher, A.; Forster, E. A.; Bill, D. J.; Brown, G.; Cliffe, I. A.; Hartley, J. E.; Jones, D. E.; McLenachan, A.; Stanhope, K. J.; Critchley, D. J.; Childs, K. J.; Middlefell, V. C.; Lanfumey, L.; Corradetti, R.; Laporte, A. M.; Gozlan, H.; Hamon, M.; Dourish, C. T., *Behav Brain Res* **1996**, *73* (1-2), 337-53.
21. Leysen, J. E.; Awouters, F.; Kennis, L.; Laduron, P. M.; Vandenberk, J.; Janssen, P. A., *Life Sci* **1981**, *28* (9), 1015-22.
22. Hinner, M. J.; Hubener, G.; Fromherz, P., *Chembiochem* **2006**, *7* (3), 495-505.
23. Hinner, M. J.; Hubener, G.; Fromherz, P., *J Phys Chem B* 2004, 108 (7), 2445-2453.
24. Ng, D. N.; Fromherz, P., *Acs Chem Biol* **2011**, *6* (5), 444-451.
25. Chanda, B.; Blunck, R.; Faria, L. C.; Schweizer, F. E.; Mody, I.; Bezanilla, F., *Nat Neurosci* **2005**, *8* (11), 1619-26.
26. Wang, D.; Zhang, Z.; Chanda, B.; Jackson, M. B., *Biophys J* 2010, 99 (7), 2355-65.
27. Urano, Y.; Kamiya, M.; Kanda, K.; Ueno, T.; Hirose, K.; Nagano, T., *J Am Chem Soc* **2005**, *127* (13), 4888-94.
28. Deal, P. E.; Kulkarni, R. U.; Al-Abdullatif, S. H.; Miller, E. W., *J. Am. Chem. Soc.* **2016**, *138*, 9085–9088.

Chapter 3:

Application of PLE-based Fluorogenic Activation

Part of this work has published in the following scientific journal:

G. Ortiz, P. Liu, S.H.H. Naing, V.R. Muller and E.W. Miller, Synthesis of Sulfonated Carbofluoresceins for Voltage Imaging, *J. Am. Chem. Soc.,* **2019**, 141(16), 6621-6638.

Portions of this work were performed in collaboration with the following persons:
Synthesis was assisted by Gloria Ortiz, Su Naing, Rishi Kulkarni and Vince Grenier
Cloning was assisted by Vikram Muller

Abstract

Given the success of the VF-EX approach described in chapter 2, we aim to further optimize the system from both the protein and chemical side, to enhance the contrast of targeted staining as well as to expand the scope of targeting to other cell types or specific cellular locations. The enzyme-mediated activation strategy can be extended to any dyes with a phenolic oxygen, thus we have chosen two dyes with better photo-physical properties, carboVoltageFluor and isoVF2.2.Cl(OMe), as candidates for masking. While both dyes' fluorescence were effectively quenched by cyclopropyl ester, only the former was a substrate, displaying fluorescence turn-on and voltage sensitivity in cultured HEK cells and neurons. On the other hand, we also attempted to vary the PLE construct for expression with cell type-specificity and subcellular precisions. To enable expression in inhibitory neurons, GAD65 and GAD67 promoters were used but the immunostaining data to determine their specificity were inconclusive and there was also insufficient enzyme expression to allow for contrast in staining. We then changed the targeting sequences for pre- and post-synaptic localization but immunostaining showed uniform signal across the cellular membrane instead of the expected punctate staining pattern.

Introduction

We previously showed that fluorescein-based VoltageFluor dyes could be adapted to cell-specific targeting through a fluorogenic approach. Alkylation of the phenolic oxygen of VF2.1.Cl with either a photo-labile nitrobenzyl protecting group[1] or a hydrolytically-stable cyclopropylmethyl acetoxy methyl ether[2] results in decreased fluorescence, which can be restored by photo-uncaging[1] or the action of an exogenously expressed esterase[2]. Localization of porcine liver esterase (PLE) on the cell surface results in VF fluorescence restricted to cells that express PLE. This hybrid approach consisted of small molecule protection and cell-surface enzymatic activation combines the speed and sensitivity of PeT-based voltage indicators with the cellular specificity of genetic encoding. The VF-EX system described in chapter 2 is a proof-of-concept that demonstrates the ability of fluorogenic activation strategy to record neuronal activity in cells of interest with high spatial and temporal resolution by our voltage sensitive dye.

This chapter describes the efforts and progress towards improving the system and generalizing the strategy to dyes of different colors, increased voltage sensitivity or enhanced photo-physical properties, which would eventually boost the contrast between cells of interest and background, non-specific cells and potentially achieve targeting in complex tissues such as ex vivo slices. We have chosen two dyes, carboVoltageFluor (carboVF) and isoVF2.2.Cl(OMe), which both exhibit superior performance in both HEK cells and neurons, compared to the first generation dye VF2.1.Cl used in the original VF-EX system.

Carbofluoresceins are an attractive target for responsive probes because they maintain oxygen substitution patterns at the 3' and 6' positions, similar to fluorescein, while simultaneously possessing excitation and emission profiles red-shifted nearly 50 nm compared to fluorescein. Co-workers in the lab have shown that inclusion of a sulfonic acid functional group prevents the spirocyclization typical of carbofluoresceins. Dichloro-substituted sulfone carbofluoresceins incorporated into a PeT-based voltage-sensing scaffold, carboVF2.1(OMe).Cl, possesses >30% $\Delta F/F$ response to 100 mV

depolarizations in HEK cells, has excitation and emission spectra >560 nm, and readily reports on action potentials in mammalian neurons.[3] The use of sulfone carbofluoresceins in the context of voltage sensing enables complementation with a growing toolkit of strategies for fluorogenic targeting. Meanwhile, isoVF2.2.Cl(OMe) has similar spectral properties as VF2.1.Cl, as both are fluorescein-based. Nonetheless, modifications on the aniline electron-rich donor and position of phenylenevinylene molecular wire relative to the fluorophore head significantly improve the voltage sensitivity and signal to noise in isoVF2.1.Cl(OMe) with 48% ΔF/F per 100 mV and D' of 150, relative to 27% ΔF/F per 100 mV and D' of 22 for VF2.1.Cl (unpublished data). Hence, we believe that both dyes are ideal candidates for cyclopropyl ester-based quenching on phenolic oxygen and PLE-mediated activation in cells of interest to achieve targeting.

In addition to the modifications on the chemical side, we are also working on enzyme expression by switching the membrane targeting domain and the promoter sequences, to achieve high-contrast voltage imaging at specific cell types and subcellular structures. This chapter also presents some preliminary data on inhibitory cell targeting as well as pre- and post-synaptic targeting of PLE in cultured hippocampal neurons.

Results & Discussions

3-1: Application of PLE-based fluorogenic activation to carboVoltageFluor

Carbo-VoltageFluors targeted by esterase expression (carboVF-EX) are synthesized in a single step from carboVF2.1(OMe).Cl (Scheme 3-1-1). Addition of stoichiometric (EX 1) or excess (EX 2) iodo-1-methylcyclopropane-carboxylate in DMF using N,N-diisopropylethylamine as a base provides the singly and doubly protected carboVF-EX derivatives. Alkylation results in a hypsochromatic shift in the absorption spectrum, from a maximum at 550 nm for carboVF2.1(OMe).Cl to 420 nm for carboVF-EX 1 (Figure 3-1-1a). Alkylation of the phenolic oxygen of carboVF2.1(OMe).Cl results in a 12-fold decrease in fluorescence quantum yield (Table 3-1-1).

The carboVF-EX dyes are substrates for purified PLE (Sigma, E2884). CarboVF-EX1 and EX2 are hydrolyzed by PLE, resulting in a 45- or 21- fold increase in fluorescence, respectively, after 2h. Release of the caged species results in carboVF2.1(OMe).Cl-like absorbance and emission profiles (Figure 3-1-1a,b, Figure 3-1-2a,b). HPLC analysis reveals carboVF2.1(OMe).Cl as the product of PLE-mediated hydrolysis reactions (Figure 3-1-3). Both carboVF-EX 1 and 2 show saturation-type enzymatic kinetics with PLE (Table 3-1-1, Figure 3-1-1c, Figure 3-1-2c). The Michaelis constant, K_M, for carboVF-EX 1 is 6.4 ± 1 μM and 0.16 ± 0.06 μM for carboVF-EX 2. These values correspond reasonably well with the values we obtained for the fluorescein-based VF-EX 1 (1.2 ± 0.5 μM) and VF-EX 2 (0.12 ± 0.03 μM).[2] All of these values are within the range for the reaction of bis(cyclopropylacetoxymethy)-fluorescein, 0.5 μM.[4] The double-protected carboVF-EX 2 is a better substrate for PLE than the singly-protected carboVF-EX 1: the k_{cat}/K_M for carboVF-EX 2 is 4.9×10^5 $M^{-1}s^{-1}$, nearly 5-fold larger than the value for carboVF-EX 1 (1.3×10^5 $M^{-1}s^{-1}$). Again, the measured k_{cat}/K_M values for carboVF-EX dyes closely match the values obtained for fluorescein VF-EX dyes (Table 3-1-1).[2]

We next sought to determine if we could elicit a similar turn-on phenomenon in living cells. CarboVF-EX 1 (500 nM, 30 min or 1 h) was bath applied to HEK cells

transfected with cell-surface PLE anchored via a glycophosphatidyl inositol, GPI, anchor (GPI sequence derived from decay-accelerating factor, DAF; Figure 3-1-4, Figure 3-1-5). CarboVF-EX 1 was uncaged by PLE on the cell surface, displaying membrane-associated fluorescence in transfected cells (as indicated by nuclear-localized GFP fluorescence, Fig. 5a-c). CarboVF-EX 2 did not elicit a turn-on response when bath-applied to PLE-expressing HEK cells (data not shown). We hypothesize that due to the extra carbon dimethyl group ($C(CH_3)_2$), carboVF-EX 2 is more lipophilic than VF-EX 2 and does not properly load into cell membranes. Due to these results, we carried carboVF-EX 1 forward in our studies.

HEK cells expressing PLE-DAF and stained with carboVF-EX 1 show a 8.9 (±0.7) fold turn-on after 30 mins, respectively, when compared to non-transfected cells from the same culture (Figure 3-1-6a-c). These results match the observed 7-fold increase in fluorescence after uncaging of VF-EX 1 in HEK cells. As with fluorescein-based VF-EX 1, longer incubation times with carboVF-EX 1 increases the overall fluorescence associated with carboVF-EX 1 in PLE-expressing cells, but decreases the contrast due to accumulation of uncaged carboVF-EX 1 in untransfected cells. Following enzymatic uncaging, carboVF-EX 1 was voltage sensitive in PLE-DAF expressing HEK cells, displaying an 18% ΔF/F per 100 mV, lower than the 31% ΔF/F displayed by carboVF2.1(OMe).Cl (Figure 3-1-6d,e). The lower fractional voltage sensitivity may be a result of increased background staining with carboVF-EX 1 compared to carboVF2.1(OMe).Cl.

We observe selective staining of neurons expressing PLE-DAF under the neuron-specific synapsin promoter (Syn) using carboVF-EX 1 (Figure 3-1-7a-c, Figure 3-1-4). Bath-application of carboVF-EX 1 using 500 nM, 1 μM, or 2 μM results in 2.4-, 2.3, and 1.9-fold turn-on after 30 minutes. We also loaded 500 nM carboVF-EX1 for 1 hr, but saw a decrease in contrast with a 1.8-fold turn-on. Our results are comparable to those obtained with VF-EX1 (1 μM), which exhibits a 4.1-fold turn-on in neurons after 1 hr.[2] The membrane fluorescence associated with carboVF-EX 1 in neurons is voltage-sensitive. CarboVF-EX1 responds to field stimulation electrode-evoked action potentials with a voltage sensitivity of 8.4% ΔF/F (SNR = 12 ± 0.8, n = 9 cells, Figure 3-1-8) and was able to record spontaneous spiking events in cultured neurons transfected with PLE-DAF (Figure 3-1-7d) – comparable to the values of VF-EX2 / PLE in cultured neurons that we previously reported (7.3 ± 0.8%, SNR = 20 ± 2.7).[2]

3-2: Application of PLE-based fluorogenic activation to isoVF2.2.Cl(OMe)

We appended a cyclopropylmethyl acetoxy methyl ether to the phenolic oxygen of isoVF2.2.Cl(OMe) to obtain cp-isoVF2.2.Cl(OMe) (isoVF2.2.Cl(OMe) synthesis was conducted by Dr. Rishi Kulkarni and cp-isoVF2.2.Cl(OMe) synthesis was conducted by Dr. Vincent Grenier). We used the same CMV-PLE-DAF construct in the VF-EX system in which a nuclear mCherry acts as a marker for PLE expression (Scheme 3-2-1). The ester successfully quenched the fluorescence of the parent dye, as demonstrated in the absorption and emission spectra of cp-isoVF2.2.Cl(OMe) (Figure 3-2-1). Unfortunately, the masked dye is not a good substrate for PLE. When the dye was reacted with purified pig liver esterase (excess, 37 °C for 2 h), negligible absorbance turn-on was observed at λ = 520 nm, the absorption maximum for the parent dye isoVF2.2.Cl(OMe) (Figure 3-2-2a). There was a 5-fold increase in fluorescence (Figure 3-2-2b), which is minimal

compared to the more than 20-fold turn-on in both VF-EX and carboVF-EX systems.[2-3] We also confirmed the ineffective conversion by checking the HPLC traces, revealing that most of starting material, cp-isoVF2.2.Cl(OMe), remained in the reaction mixture after reaction with excess PLE (Figure 3-2-3). Nonetheless, we still moved on to HEK cells to evluate the efficiency of PLE unmasking the dye. Again, the cyclopropyl ester indeed masked and quenched the fluorescence of the parent dye with minimal signal from the cells not expressing PLE (Figure 3-2-4a), compared to the bright, membrane-associated fluorescence in the parent dye (Figure 3-2-4c). However, in cells expressing cell-surface PLE, we did not observe any fluorescence turn-on, suggesting that cp-isoVF2.2.Cl(OMe) is a poor substrate for the enzyme (Figure 3-2-4b). We hypothesize that the kinked shape of cp-isoVF2.2.Cl(OMe) due to the wire orientation prevents the enzyme from incorporating the dye into its active site to remove the ester. To verify this, we would need to synthesize a few other masked dyes of different wire orientations or conduct modeling studies to probe the substrate-active site structure in the PLE enzyme.

3-3: Targeting PLE to inhibitory neurons

Since we have successfully expressed PLE in excitatory neurons under the control of a CaMKIIα promoter and saw desirable fluorescence turn-on in targeted cells[2], we next explored the possibility of achieving a similar contrast in inhibitory neurons. We have chosen the glutamate decarboxylase (GAD) promoter since the GAD enzyme is known to decarboxylate glutamate to GABA, the important inhibitory neurotransmitter.[5-6] There are two isoforms of the enzyme, GAD_{65} and GAD_{67}, which differ in their molecular weight as their names suggest. Both function at different locations and developmental stages and differ at their functions slightly. While GAD_{65} synthesizes GABA to be used as neurotransmitters, GAD_{65} is found almost exclusively at nerve terminals and expressed later during synapse development. On the other hand, GAD_{67} is present uniformly in the cells and throughout development to produce GABA for cellular functions other than neurotransmission.[7-11] The promoter sequences for both were extracted using PCR from rat genomic DNA to prepare two different PLE constructs (Figure 3-3-1).

We first performed immunohistochemistry on the constructs by staining against the HA tag, which is indicative of PLE expression (Figure 3-3-2). Using permeablizing conditions, we observed that PLE expression under the GAD67 promoter was mostly cytosolic and concentrated in the cell body while that under the GAD65 promoter exhibited membrane-bound signal in both the cell body and processes. We also stained for all the inhibitory neurons in the culture with an anti-GABA antibody. While most anti-HA staining (i.e. PLE expression) matched anti-GABA fluorescence (Figure 3-3-3a,b for GAD65, Figure 3-3-3d for GAD67), a small portion of PLE-expressing cells did not have GABA expression (Figure 3-3-3c for GAD65, Figure 3-3-3e for GAD67), suggesting non-inhibitory cell types. These data to verify the expression pattern are inconclusive so far; thus, additional staining against anti-CaMKIIα, marker for excitatory neurons, or an alternative inhibitory marker such as anti-GAD, would be necessary to confirm the cell-type specificity, if any, for both GAD65 and GAD67 promoters.

Despite the ambiguous results in immunohistochemistry, we tested the constructs with VF-EX2 for live cell staining (Figure 3-3-4). Unfortunately, all the neurons in the field view, for both constructs, seemed to have similar fluorescence staining, which is

probably cellular auto-fluorescence or minimal background fluorescence from the incompletely quenched dye. These results are consistent with the immunostaining data that PLE expression on the cell surface under these inhibitory promoters is basically inefficient, leading to negligible enzymatic activity for fluorogenic activation. Future work involves investigating other inhibitory promoters or alternative PLE analogs.

3-4: Targeting PLE to pre- and post-synaptic terminals

We also tried targeting PLE to specific subcellular locations, including pre- and post-synaptic terminals. Electrical activities at these structures are challenging to study due to their micrometer sizes, that is significantly smaller than a tip of patch pipette in electrophysiology. Fluorescent signal in these areas can be easily concealed in the background or non-specific staining in all cells; as a result, targeting our dye to those subcellular structures with contrast above the background would be necessary to record activities with enough signal-to-noise ratio.

We used the signal peptides and localization sequences from a split GFP-based construct mGRASP, which enables synapse imaging.[12] When a synapse is formed, the GFP fragments reconstitute and fluoresce. By simply replacing the GFP fragments in the pre- and post-synaptic constructs with our PLE sequence, we generated four constructs under synapsin and CAG promoter (Figure 3-4-1). Cytosolic mCherry was used to better visualize the expected punctate staining along the neuronal processes. In cultured neurons, expression of PLE under the synapsin promoter was so weak that no fluorescence turn-on was seen in cells expressing mCherry (Figure 3-4-2a,b and Figure 3-4-3a,b). CAG promoter enhanced the enzyme expression as evidenced by selective staining and contrast in PLE-expressing neurons (Figure 3-4-2c,d and Figure 3-4-3c,d). However, the staining was uniform throughout the membrane, while punctate staining should be expected, suggesting that either PLE was not targeted to the desired locations or the uncaged dye diffused quickly across the cellular membrane. We then did immunostaining on the CAG constructs, confirming that PLE was not expressed at pre- or post-synaptic terminals; instead it was trafficked to the cell surface without any specificity from the targeting moieties (Figure 3-4-4). Future work on targeting to subcellular structures involves exploring other signal peptides, targeting domains or promoters.

Conclusion

In this chapter, we have demonstrated that PLE/cyclopropyl ester-based activation strategy can be applied to selected dyes of improved photo-physical properties. In particular, carboVF-EX 1 is the first long-wavelength voltage sensitive dye targeted to specific cells via enzyme-mediated fluorogenic activation, providing voltage imaging performance rivaling that of previous enzyme-activated voltage indicators (VF-EX), but at long wavelengths compatible with GFP. Nonetheless, the low contrast ratio between PLE-expressing cells and wild-type cells needs to be addressed, by both decreasing the brightness of caged cVF-EX1-type dyes and improving singly-protected cVF-EX1-type dyes as substrates for PLE. On the other hand, the isoVF dye with a kinked molecular wire, did not seem to fit into the enzyme activate site for ester removal, though more studies are required to provide clearer explanations. Attempts at targeting PLE to

inhibitory cells, pre- and post-synaptic terminals yielded little positive results, but a variety of signal peptides and targeting sequences are yet to be examined.

Experimental Section

Spectroscopic studies

UV-Vis absorbance and fluorescence spectra were recorded using a 2501 Spectrophotometer (Shimadzu) and a Quantamaster Master 4 L-format scanning spectrofluorometer (Photon Technologies International). The fluorometer is equipped with an LPS-220B 75-W xenon lamp and power supply, A-1010B lamp housing with integrated igniter, switchable 814 photon-counting/analog photomultiplier detection unit, and MD5020 motor driver. Samples were measured in 1-cm path length quartz cuvettes (Starna Cells). The maximum absorption wavelength (λ_{max}) and maximum emission wavelength (λ_{em}) were taken in HBSS (zero Ca^{2+}, zero Mg^{2+}, no phenol red, pH 7.4) using stock solutions of dyes in DMSO (0.5-2 mM). Absorbance was collected from 300 nm to 700 nm for both carboVF and isoVF dyes. For emission scans, carboVF dyes were excited at 565 nm and emission was collected from 570 nm to 800 nm while isoVF dyes were excited at 520 nm and emission was collected from 525 nm to 700 nm.

In vitro PLE reactions and characterization

Commercially purified pig liver esterase (PLE, MW = 168 kDa) was obtained from Sigma-Aldrich (E2884) as a suspension in 3.2 M $(NH_4)_2SO_4$, and was diluted from a stock solution of 28.1 mg/mL to appropriate concentrations in HBSS (pH 7.4). For the enzymatic reaction with carboVF-EX and isoVF-ED dyes, the dyes (final concentration of 50 μM) were incubated with 1 μL PLE (final concentration of 0.70 mg/mL) and 1 μL Pluronic F-127 (20% w/v in DMSO) in 40 μL HBSS at 37 °C for ~ 2 h. For characterization by spectroscopy, the reaction mixture was diluted to 1 mL HBSS (total volume) for measurement. For HPLC characterization, 40 μL of acetonitrile (1:1) was added, followed by centrifugation to precipitate the enzyme. Supernatant was extracted and filtered for HPLC injection.

Enzyme kinetics experiments for carboVF-EX dyes were performed in black, clear-bottom, 96-well polystyrene microplates from Corning. Plates were read from the bottom on a Molecular Devices SpectraMax Paradigm Multi-Mode detection platform plate reader (λ_{ex} 560 nm, λ_{em} 610 nm). All the measurements were done at 37 °C. Enzyme (168 ng/mL) was added to the substrates at t = 5 min and more data were collected for another 5 min. To obtain the kinetic constants, the data were fit to the Michaelis-Menten equation $v = \frac{V_{max}[S]}{K_M+[S]}$ (GraphPad Prism).

Cell culture

All animal procedures were approved by the UC Berkeley Animal Care and Use Committees and conformed to the NIH Guide for the Care and Use and Laboratory Animals and the Public Health Policy.

Human embryonic kidney 293T (HEK) cells were maintained in Dulbecco's modified eagle medium (DMEM) supplemented with 4.5 g/L D-glucose, 10% fetal bovine serum (FBS; Thermo Scientific) and 1% GlutaMax (Invitrogen) at 37 °C in a humidified incubator with 5% CO_2. Cells were passaged and plated in DMEM (as above) at a density of 750,000 cells per well in a 6-well plate. Transfection of plasmids was carried out using Lipofectamine 3000 (Invitrogen) ~18-24 h after plating. The cells were split again 48 h after transfection and plated onto 12 mm glass coverslips pre-coated with

Poly-D-Lysine (PDL; 1 mg/ml; Sigma-Aldrich) at a density of 75,000 cells per coverslip in DMEM supplemented with 1 g/L D-glucose, 10% FBS and 1% GlutaMax. Imaging was performed 12-18 h after plating.

Hippocampi were dissected from embryonic day 19 Sprague Dawley rats (Charles River Laboratory) in cold, sterile HBSS (zero Ca^{2+}, zero Mg^{2+}, phenol red). All dissection products were supplied by Invitrogen, unless otherwise stated. Hippocampal tissue was treated with trypsin (2.5%) for 15 min at 37 °C. The tissue was triturated using fire polished Pasteur pipettes, in minimum essential media (MEM) supplemented with 5% FBS, 2% B-27, 2% 1M dextrose (Fisher Scientific) and 1% GlutaMax. The dissociated cells were plated onto 12 mm diameter coverslips (Fisher Scientific) pre-treated with PDL (as above) at a density of 25-30,000 cells per coverslip in MEM supplemented media (as above). Neurons were maintained at 37 °C in a humidified incubator with 5% CO_2. At 1 day in vitro (DIV) half of the MEM supplemented media was removed and replaced with Neurobasal media containing 2% B-27 supplement and 1% GlutaMax. Transfection of plasmids was carried out using Lipofectamine 3000 (without P3000 reagent) at 6-7 DIV. Imaging was performed on mature neurons 13-16 DIV.

For loading the dyes in HEK cells and hippocampal neurons, DMSO stock solutions were diluted first with 1:1 Pluronic F-127 (20% w/v in DMSO) and then further diluted in HBSS to working concentrations. Cells were incubated with dyes in HBSS at 37 °C in the incubator before exchanging dye/HBSS for HBSS without any dye. All imaging was performed in HBSS at room temperature.

Epifluorescence microscopy

Imaging was performed on an AxioExaminer Z-1 (Zeiss) equipped with a Spectra-X Light engine LED light (Lumencor), controlled with Slidebook (v6, Intelligent Imaging Innovations). Images were acquired with a W-Plan-Apo 20x/1.0 water objective (20x; Zeiss). Images were focused onto either an OrcaFlash4.0 sCMOS camera (sCMOS; Hamamatsu) or an eVolve 128 EMCCD camera (EMCCD; Photometrix). For carboVF images, the excitation light was delivered from a LED at 575/35 nm and emission was collected with a triple emission filter (473/22, 543/19, 648/98 nm) after passing through a triple dichroic mirror (475/30, 540/25, 642/96 nm). For isoVF dyes, excitation light was delivered at 475 nM (LED, 475 nm, 34 nm bandpass) and emission was collected with a 540/50 nm bandpass filter after passing through a 510 nm longpass dichroic.

Image analysis

For image intensity measurements, regions of interest were drawn around cells or neuronal cell bodies and the mean fluorescence was calculated in ImageJ (FIJI, NIH). Background fluorescence was subtracted by measuring the fluorescence where no cells grew. The fold turn-on was calculated by taking the ratio of transfected cells fluorescence and untransfected cells fluorescence, both background subtracted. At least 15-20 cells were quantified for each coverslip and 4 coverslips were examined to get the average fold turn-on.

Analysis of voltage sensitivity in HEK cells was performed using ImageJ (FIJI). Briefly, a region of interest (ROI) was selected automatically based on fluorescence intensity and applied as a mask to all image frames. Fluorescence intensity values were calculated at known baseline and voltage step epochs. For analysis of voltage responses

in neurons, regions of interest encompassing cell bodies (all of approximately the same size) were drawn in ImageJ and the mean fluorescence intensity for each frame extracted. ΔF/F values were calculated by first subtracting a mean background value from all raw fluorescence frames, to give a background subtracted trace (bkgsub). A baseline fluorescence value (Fbase) is calculated from the median of all the frames, and subtracted from each timepoint of the bkgsub trace to yield a ΔF trace. The ΔF was then divided by Fbase to give ΔF/F traces. No averaging has been applied to any voltage traces.

Electrophysiology/Imaging parameters

For electrophysiological experiments, pipettes were pulled from borosilicate glass (Sutter Instruments, BF150-86-10), with a resistance of 4–6 MΩ, and were filled with an internal solution; 115 mM potassium gluconate, 10 mM BAPTA tetrapotassium salt, 10 mM HEPES, 5 mM NaCl, 10 mM KCl, 2 mM ATP disodium salt, 0.3 mM GTP trisodium salt (pH 7.25, 275 mOsm). Recordings were obtained with an Axopatch 200B amplifier (Molecular Devices) at room temperature. The signals were digitized with a Digidata 1440A, sampled at 50 kHz and recorded with pCLAMP 10 software (Molecular Devices) on a PC. Fast capacitance was compensated in the on-cell configuration. For all electrophysiology experiments, recordings were only pursued if series resistance in voltage clamp was less than 30 MΩ. For whole-cell, voltage clamp recordings in HEK cells, cells were held at -60 mV and hyper- and de- polarizing steps applied from -100 to +100 mV in 20 mV increments.

Extracellular field stimulation was delivered by a SD9 Grass Stimulator connected to a recording chamber containing two platinum electrodes (Warner), with triggering provided through the same Digidata 1332A digitizer and pCLAMP 9 software (Molecular Devices) that ran the electrophysiology. Action potentials were triggered by 1 ms 60 V field potentials delivered at 5 Hz. To prevent recurrent activity, the HBBS bath solution was supplemented with synaptic blockers; 10 μM 2,3-Dioxo-6-nitro-1,2,3,4-tetrahydrobenzo[f]quinoxaline-7-sulfonamide (NBQX; Santa Cruz Biotechnology) and 25 μM DL-2-Amino-5-phosphonopentanoic acid (APV; Sigma-Aldrich). For both evoked action potentials and spontaneous activity, images were binned 4x4 to allow sampling rates of 0.5 kHz and 2500 frames (5 s) were acquired for each recording.

Rat genomic DNA extraction

Extraction of rat genomic DNA was done following a phenol/chloroform-based DNA isolation protocol from the Jackson laboratory (https://www.jax.org/jax-mice-and-services/customer-support/technical-support/genotyping-resources/dna-isolation-protocols). Briefly, place about 0.5 cm of rat tail (from pregnant female used in the neuron prep) in a 2 mL Eppendorf tube and add 0.5 mL of DNA digestion buffer (50 mM Tris-HCl pH 8, 100 mM EDTA pH 8.0, 100 mM NaCl and 1% SDS) with proteinase K (0.5 mg/ml final concentration). Incubate at 55 °C with shaking for overnight. Add 0.7 ml phenol/chloroform/isoamyl alcohol (25:24:1) and mix well (no vortex). Centrifuge the mixture at max speed for 5 minutes and transfer 0.5 mL of the top phase to a new tube. Add 1 mL 100% ethanol and mix well until DNA precipitate forms. Centrifuge the tube at max speed for 5 minutes and remove the supernatant. Wash the precipitate with 0.5 mL cold 70% ethanol, centrifuge for 5 minutes, remove the supernatant and air dry at room temperature. Re-dissolve the DNA in EB and it can be used directly in PCR.

Immunocytochemistry

To detect expression and localization of PLE and other protein markers, HEK cells or neurons were fixed with 4% paraformaldehyde in PBS for 10 min and permeabilized (if required) with 0.3% v/v Triton-X 100 (Sigma Aldrich) in PBS for 2 min. Blocking was done in 5% w/v bovine serum albumin (BSA; Sigma Aldrich) in PBS for 1 h. Primary antibody was incubated at 4 °C overnight, followed by AlexaFluor secondary antibody (Life Technologies) at room temperature for 2 h. All antibodies were used at 1:1000 dilution.

Name	**Primary/ Secondary**	**Manufacturer**	**Catalog #**	**Isotype**
Anti-HA	Primary	CST	3724S	Rabbit IgG
Anti-HA	Primary	CST	2367S	Mouse IgG1
Anti-GABA	Primary	Sigma-Aldrich	A2052	Rabbit IgG
Anti-rabbit 647	Secondary	Life Technologies	A21244	Goat IgG
Anti-rabbit 488	Secondary	Life Technologies	A11008	Goat IgG
Anti-mouse 488	Secondary	Life Technologies	A11001	Goat IgG

Plasmid construction

All plasmids were constructed using Gibson Assembly and were confirmed by sequencing. The following sequences were used (5' to 3').

IgK

ATGGAGACAGACACACTCCTGCTATGGGTACTGCTGCTCTGGGTTCCAGGTTC
CACTGGTGAC

PAT3

CCACCTTCTACTAGTCTTTTGTTGCTTGCTGCACTTCTCCCCTTCGCTCTTCCC
GCTTCAGATTGGAAGACAGGAGAAGTCACCGCTTCC

PLE (minus ER retention signal)

ATGGTGTGGCTGCTGCCTCTGGTGCTGACCAGCCTGGCCAGCAGCGCCACCT
GGGCCGGCCAGCCCGCCAGCCCTCCCGTGGTGGACACCGCCCAGGGCAGGGT
GCTGGGCAAGTACGTGAGCCTGGAGGGCCTGGCCCAGCCCGTGGCCGTGTTC
CTGGGCGTGCCCTTCGCCAAGCCTCCCTTGGGCAGCCTGAGGTTCGCTCCTCC
TCAGCCTGCTGAGCCCTGGAGCTTCGTGAAGAACACCACCAGCTACCCTCCC
ATGTGCTGCCAGGATCCCGTGGTGGAGCAGATGACCAGCGACCTGTTCACCA
ACGGCAAGGAGAGGCTGACCCTGGAGTTCAGCGAGGACTGCCTGTACCTGAA
CATCTACACACCCGCCGACCTGACCAAGAGAGGCAGGCTGCCCGTGATGGTG
TGGATCCACGGCGGCGGCCTGGTGCTGGGCGGCGCTCCCATGTACGACGGCG
TGGTGCTGGCCGCCCACGAGAACGTGGTGGTGGTGGCCATCCAGTACAGGCT
GGGCATCTGGGGCTTCTTCAGCACCGGCGACGAGCACAGCAGgGGCAACTGG

GGCCACCTGGACCAGGTGGCCGCCCTGCACTGGGTGCAGGAGAACATCGCCA
ACTTCGGCGGCGATCCCGGCAGCGTGACCATCTTCGGCGAGAGCGCCGGCGG
CGAGAGCGTGAGCGTGCTGGTGCTGAGCCCTCTGGCCAAGAACCTGTTCCAC
AGGGCCATCAGCGAGAGCGGCGTGGCCCTGACCGTGGCCCTGGTGAGGAAG
GACATGAAGGCCGCCGCCAAGCAGATCGCCGTGCTGGCCGGCTGCAAGACC
ACCACCAGCGCCGTGTTCGTGCACTGCCTGAGGCAGAAGAGCGAGGACGAG
CTGCTGGACCTGACCCTGAAGATGAAGTTCCTGACCCTGGACTTCCACGGCG
ACCAGAGGGAGAGCCATCCCTTCCTGCCCACCGTGGTGGACGGCGTGCTGCT
GCCCAAGATGCCCGAGGAGATCCTGGCCGAGAAGGACTTCAACACCGTGCCC
TACATCGTGGGCATCAACAAGCAGGAGTTCGGCTGGCTGCTGCCCACTATGA
TGGGCTTCCCTCTGAGCGAGGGCAAGTTGGACCAGAAGACCGCCACCAGCCT
GCTGTGGAAGAGCTATCCCATCGCCAACATTCCCGAGGAGCTGACACCCGTG
GCCACCGACAAGTACCTGGGCGGCACCGACGATCCCGTGAAGAAGAAGGAC
CTGTTCCTGGACCTGATGGGCGACGTGGTGTTCGGCGTGCCCAGCGTGACCGT
GGCCAGGCAGCACAGGGACaCCGGCGCTCCCACCTACATGTACGAGTTCCAG
TACAGGCCCAGCTTCAGCAGCGACAAGAAGCCCAAGTCCGTGATCGGCGACC
ACGGCGACGAGATCTTCAGCGTGTTCGGCTTCCCTCTGCTGAAGGGCGACGC
TCCCGAGGAGGAGGTGAGCCTGAGCAAGACCGTGATGAAGTTCTGGGCCAAC
TTCGCCAGGAGCGGCAATCCCAACGGCGAGGGCCTGCCTCACTGGCCCATGT
ACGACCAGGAGGAGGGCTACCTGCAGATCGGCGTGAACACCCAGGCCGCCA
AGAGGCTGAAGGGCGAGGAGGTGGCCTTCTGGAACGACCTGCTGAGCAAGG
AGGCCGCCAAGAAGCCTCCTAAGATCAAG

HA
TATCCATATGATGTTCCAGATTATGCT

DAF
CCAAATAAAGGAAGTGGAACCACTTCAGGTACTACCCGTCTTCTATCTGGGC
ACACGTGTTTCACGTTGACAGGTTTGCTTGGGACGCTAGTAACCATGGGCTTG
CTGACTTAG

neurexin-1
GTACGCTACAAGTATCGCAACAGGGATGAGGGATCTTACCACGTTGACGAAT
CTAGGAACTATATCAGTAACAGCGCTCAGAGTAATGGCGCCGTGGTTAAAGA
GAAACAGCCCTCCAGCGCCAAATCAGCAAACAAAAACAAGAAAAACAAGGA
TAAAGAGTACTACGTAAGATCT

CD4-2
GTCGACTTTCAGAAAGCTAGCTCTATTGTTTATAAGAAGGAGGGGGAACAGG
TGGAGTTCAGTTTCCCATTGGCCTTCACAGTCGAGAAGCTCACAGGATCAGG
AGAGTTGTGGTGGCAGGCCGAAAGAGCCTCCTCCAGCAAGAGTTGGATCACT
TTTGATCTGAAAAACAAAGAAGTGAGCGTGAAGAGAGTCACACAGGACCCT
AAGCTGCAGATGGGCAAGAAGTTGCCTTTGCACTTGACACTCCCCCAAGCCC
TGCCCCAGTATGCTGGCTCCGGGAACCTCACCCTCGCCTTGGAGGCTAAGAC
CGGAAAGTTGCATCAGGAGGTCAACCTCGTGGTGATGAGGGCAACACAGCTG
CAGAAGAACCTGACCTGCGAAGTGTGGGGTCCCACCTCACCTAAACTGATGC

TGTCTCTGAAGCTGGAGAATAAGGAGGCTAAAGTCAGTAAAAGAGAGAAGG
CTGTGTGGGTCCTTAACCCGGAGGCAGGGATGTGGCAGTGTCTTCTTAGCGA
CTCTGGACAGGTGCTGCTGGAGAGCAACATCAAGGTGCTTCCTACTTGGTCA
ACACCAGTACAGCCGATGGCCCTGATCGTACTCGGGGGAGTCGCCGGCCTGC
TTCTGTTTATCGGCCTGGGCATCTTCTTCTGC

Neuroligin-1 (N-terminal)
ATGGCACTTCCTAGATGTATGTGGCCTAATTATGTATGGCGAGCTATGATGGC
CTGCGTGGTGCACCGAGGGAGTGGCGCCCCACTTACACTCTGCCTGTTGGGTT
GCCTCCTCCAGACTTTCCACGTTCTTTCACAGAAGCTGGATGAC

Neuroligin-1 (C-terminal)
GGGACGCTCGAGCTGGTGCCCCACTTGCATAACCTCAATGACATCAGCCAAT
ACACAAGTACAACCACCAAGGTCCCAAGCACTGACATCACCCTTCGACCAAC
TCGGAAAAACTCAACCCCTGTGACCAGCGCATTTCCAACCGCTAAGCAAGAC
GACCCCAAACAACAGCCTAGTCCATTTAGCGTAGACCAAAGGGACTACAGCA
CAGAGCTGTCCGTGACCATAGCTGTAGGAGCTTCCCTGCTTTTCCTGAACATT
CTGGCTTTCGCGGCCCTCTATTACAAGAAGGACAAAAGGCGCCACGACGTAC
ATAGGAGATGTAGTCCGCAACGAACTACAACCAATGATCTTACGCACGCACC
TGAGGAGGAGATCATGAGTCTTCAGATGAAACACACAGACCTGGACCACGA
GTGTGAATCCATCCATCCCCATGAGGTGGTGCTGAGGACAGCATGCCCTCCG
GACTATACCCTGGCAATGCGCCGAAGCCCAGACGACATTCCCCTGATGACAC
CCAATACCATAACCATGATTCCCAACACTATTCCAGGAATCCAGCCTCTCCAC
ACTTTCAACACATTCACTGGTGGACAGAATAATACTCTCCCTCATCCGCATCC
ACACCCCCACTCCCACAGCACAACACGGGTGGGTGGCAGCGGTGGCAGATCT

IRES
GCCCCTCTCCCTCCCCCCCCCCTAACGTTACTGGCCGAAGCCGCTTGGAATAA
GGCCGGTGTGCGTTTGTCTATATGTTATTTTCCACCATATTGCCGTCTTTTGGC
AATGTGAGGGCCCGGAAACCTGGCCCTGTCTTCTTGACGAGCATTCCTAGGG
GTCTTTCCCCTCTCGCCAAAGGAATGCAAGGTCTGTTGAATGTCGTGAAGGA
AGCAGTTCCTCTGGAAGCTTCTTGAAGACAAACAACGTCTGTAGCGACCCTTT
GCAGGCAGCGGAACCCCCCACCTGGCGACAGGTGCCTCTGCGGCCAAAAGCC
ACGTGTATAAGATACACCTGCAAAGGCGGCACAACCCCAGTGCCACGTTGTG
AGTTGGATAGTTGTGGAAAGAGTCAAATGGCTCTCCTCAAGCGTATTCAACA
AGGGGCTGAAGGATGCCCAGAAGGCACCCCATTGTATGGGATCTGATCTGGG
GCCTCGGTGCACATGCTTTACATGTGTTTAGTCGAGGTTAAAAAAACGTCTAG
GCCCCCCGAACCACGGGGACGTGGTTTTCCTTTGAAAAACACGATGATAATA
TGGCCACA

T2A
GAGGGTCGGGGCTCTCTGCTCACATGTGGCGACGTCGAGGAGAATCCCGGAC
CGGCCCCGGGGTCGACA

Nuclear Localization Sequencing

ATGGTGCCCAAGAAGAAGAGGAAAGTCGTGAGCAAGGGCGAGGAGGACAAC
ATGGCCATCATCAAGGAGTTCATGCGCTTCAAGGTGCAC

mCherry

ATGGAGGGCTCCGTGAACGGCCACGAGTTCGAGATCGAGGGCGAGGGCGAG
GGCCGCCCCTACGAGGGCACCCAGACCGCCAAGCTGAAGGTGACCAAGGGC
GGCCCCCTGCCCTTCGCCTGGGACATCCTGTCCCCTCAGTTCATGTACGGCTC
CAAGGCCTACGTGAAGCACCCCGCCGACATCCCCGACTACTTGAAGCTGTCC
TTCCCCGAGGGCTTCAAGTGGGAGCGCGTGATGAACTTCGAGGACGGCGGCG
TGGTGACCGTGACCCAGGACTCCTCCCTGCAGGACGGCGAGTTCATCTACAA
GGTGAAGCTGCGCGGCACCAACTTCCCCTCCGACGGCCCCGTAATGCAGAAG
AAGACCATGGGCTGGGAGGCCTCCTCCGAGCGGATGTACCCCGAGGACGGC
GCCCTGAAGGGCGAGATCAAGCAGAGGCTGAAGCTGAAGGACGGCGGCCAC
TACGACGCCGAGGTCAAGACCACCTACAAGGCCAAGAAGCCCGTGCAGCTG
CCCGGCGCCTACAACGTCAACATCAAGCTGGACATCACCTCCCACAACGAGG
ACTACACCATCGTGGAACAGTACGAGCGCGCCGAGGGCCGCCACTCCACCGG
CGGCATGGACGAGCTGTACAAG

WPRE

GCTTATCGATAATCAACCTCTGGATTACAAAATTTGTGAAAGATTGACTGGTA
TTCTTAACTATGTTGCTCCTTTTACGCTATGTGGATACGCTGCTTTAATGCCTT
TGTATCATGCTATTGCTTCCCGTATGGCTTTCATTTTCTCCTCCTTGTATAAAT
CCTGGTTGCTGTCTCTTTATGAGGAGTTGTGGCCCGTTGTCAGGCAACGTGGC
GTGGTGTGCACTGTGTTTGCTGACGCAACCCCCACTGGTTGGGGCATTGCCAC
CACCTGTCAGCTCCTTTCCGGGACTTTCGCTTTCCCCCTCCCTATTGCCACGGC
GGAACTCATCGCCGCCTGCCTTGCCCGCTGCTGGACAGGGGCTCGGCTGTTG
GGCACTGACAATTCCGTGGTGTTGTCGGGGAAATCATCGTCCTTTCCTTGGCT
GCTCGCCTGTGTTGCCACCTGGATTCTGCGCGGGACGTCCTTCTGCTACGTCC
CTTCGGCCCTCAATCCAGCGGACCTTCCTTCCCGCGGCCTGCTGCCGGCTCTG
CGGCCTCTTCCGCGTCTTCGCCTTCGCCCTCAGACGAGTCGGATCTCCCTTTG
GGCCGCCTCCCCGCATCGATACCG

Synapsin Promoter

GTGTCTAGACTGCAGAGGGCCCTGCGTATGAGTGCAAGTGGGTTTTAGGACC
AGGATGAGGCGGGGTGGGGGTGCCTACCTGACGACCGACCCCGACCCACTG
GACAAGCACCCAACCCCCATTCCCCAAATTGCGCATCCCCTATCAGAGAGGG
GGAGGGGAAACAGGATGCGGCGAGGCGCGTGCGCACTGCCAGCTTCAGCAC
CGCGGACAGTGCCTTCGCCCCCGCCTGGCGGCGCGCGCCACCGCCGCCTCAG
CACTGAAGGCGCGCTGACGTCACTCGCCGGTCCCCCGCAAACTCCCCTTCCC
GGCCACCTTGGTCGCGTCCGCGCCGCCGCCGGCCCAGCCGGACCGCACCACG
CGAGGCGCGAGATAGGGGGGCACGGGCGCGACCATCTGCGCTGCGGCGCCG
GCGACTCAGCGCTGCCTCAGTCTGCGGTGGGCAGCGGAGGAGTCGTGTCGTG
CCTGAGAGCGCAGTCGAGA

CAG Promoter

TCGAGGTGAGCCCCACGTTCTGCTTCACTCTCCCCATCTCCCCCCCCTCCCCA
CCCCCAATTTTGTATTTATTTATTTTTTAATTATTTTGTGCAGCGATGGGGGCG
GGGGGGGGGGGGGGGCGCGCGCCAGGCGGGGCGGGGCGGGGCGAGGGGCG
GGGCGGGGCGAGGCGGAGAGGTGCGGCGGCAGCCAATCAGAGCGGCGCGCT
CCGAAAGTTTCCTTTTATGGCGAGGCGGCGGCGGCGGCGGCCCTATAAAAAG
CGAAGCGCGCGGCGGGCG

GAD65 Promoter

GAGATTTCTGGGTGGCGTGAACAAGGAATAGGTAATCCCACAAAACCTTGCA
GTGGGCTATTCTGGAGATTTTGGCGTGGGTCTCCTACTTTAGAGGGGAAGCTA
TAGTCTTGGTTCCCAGTCTGCTGCCTCCTTTGTGAACTAATGACTGTAATTATT
ACCTCCCAGAGCTCTTTTGTTATCAACAACCAGGAGCCTGGGGGGGATGGGC
CCTTTGGGGAAAGGGGAAAAAATTTACAAAGCAAATTGCTGTCTAGGAAGGG
TTGGAATTTTTTTAAAAAGACAAACCCAATTTCAGCCTGTATCCGAAGTGGGG
AGTGGCAATGTTTTTTAATGTAAATATCATTAGATTTTTAAAAAAATTCTCAG
AGCTGTGGATTCAATTGCATTTCAACAGTACTGCTTTAAGTCACTATTTTTGA
CGAAGTTAAATTCAGATGTTGAGAGTCTGTCCTCTTGTTTTCATCCATTTCTTC
CTTGTGAGGTGTGTGTGTGTGTGTGTGTGTGTGTGTGTGTTTATGAACCAT
TTTATTTCTGACCACTCATCCGTGGTAAAAAGCTTCAACCCCAGCCAGCTGGC
TTGAAGAGAGAATTATTTGCAGGATTTGGTATGGATTTAAACAAAGACCCAG
GCTCTCCAAGTCCTGTTGGCAAGGCTGGGTGGAGAGAGTGCCCAGCATTCCA
GGAGATGTTGCCTCTGCCAACCGAAGTCACCAGGCCTGGAGTACCCTAAAGA
TTGACCAAGTTAAGGCGTAGGGTCAAGATGACTACCTTCCCTCAACATGCTCC
TGCTTTTGGCTTAGAGACGTGCCTGGGTAGCACCTCAACAGGGTCAATCACA
CTCCCCACGCCTCCCTAGTCCCGCGACTTCTGTGGGCATCCACTATCTAGATC
CTCCCTGGCCGTCAGGATTCTGGCAACTGGGAAGAAGTAAAGCTTTGGGGAG
AGAATGCACTTGGAGGCCCAAGACTTGGGCTTCTGTACAGTTACCCGAGGTC
TCAGGATCCCTAACAAAATAAGTGATCCTGGTCGCCAAAACCAAGTAGGGTC
CCTGCTCAGGCAAGAGCTTTGGTGCCTTTTTTGAAAACTCAAAAGAAGGAAC
GAAGAAATGCTGTGGAGACCAGGGAGACTGCAGCCCCTTGCTCAGGGAGCG
CAGGAAAGGAGATCCGGATGGCTGAAAGCAGCACCTTCCCGCTAGTCTTTCT
TGAGCTATGTGTAAATCGGAAACCAAGGGTCTAGTATAAGCGAGCCAAAACA
AAGCGGAGTCCGAGGGCCCCACATCTTCCTTAAGGCGCTGTCCCGCAGTTTA
TGGGCCTTTAGGGAAGAGAAAACAGAAAGGATTGTTTCATTCCTTTATTAGA
AAACACAAACGAAACTACTTCTCTCTGGGCCGGGAAATTGCCAATCTTGCGT
TCCTAGGCACCTCCTGACCTTAAGGACTCTTCTGGGGGAGGGGAGAGGTCAG
TGGTTTCAGTACTCCTGAAACTACCCGAGTGCCTTTTCTCCTGGAATTTGAAA
GTCTGGTTTGCTTACTTCGAAAACCCCTGAATCCCGCCTAAGCACAGGTGCAT
AAGCAGCAAGCCAAGGTCACCAAGTAACCGGATCCCCTCCCCCATCAACCAT
AAATCCTGTGGTCTGTGTCAGCTCTCCGCTGCTCCCTTTCAAGAAGTTTCTGTT
CGTTTTATTTATTTAATTTTTCCCAGCCTGAGGTCCTCAGTGATAGACTCCAGC
GTGGATTTTAATTGCTTCAATCAGCAGTCTTTCTCCTCAGCCGTCAGTCAAAA
CCTGGACGGTGGGTCTGGGGACTCAGCGCTTGACTGCACAGGAAGTGGACGA
CCCCCCCAGGCTGGCTCAGCTCAGTAGGCAGACGTTTTTAGGCTCGGCTAAG
GAAGGAGATGAAATGAGTCCGTCGGCGTGGAAGCGATACACCTTCCTCCCTC
TTTGGTTCCTTCCCCGTGCTCTGGAGCTCTGCCTGATTGCGGCCAGGTGGCCT

GGGCTCTTGAGGTCACAGCGACCTCCGCACGGGTTTGGAGGAAGGAGGGTGC
GAAAACCGCTTTTGCTCGGCCGGCCTCAGCCAGAGACAGCTCTCAAACAATG
AGCCAATCGCTGCACATGTGAAGTCGCTTTCAGTCACCCCCCAAGATTGTCA
AGGTCTCCCTGGTGCCCAGGGTCACCGAGGCCAGCGTGCAGCGGGCTGCGGT
AGCACCCTGGACAGCGCGTCCCGGCCGAAGAGGACCTGGAGCGCCTGTGGCT
GGGTCAGCGCTGCGCAGGCACGCCTCCCACCCCCGCATCTGACTCGCGCTCA
AACGCACAGCCTCGCACCTCACGACCCAGCTCCTCCATTTCCCTTTCGTCACT
CTCTGGTCTCCCCACCAAACTCCTCTCCCTAAAAATTCTCTTGGGTCCTTTCCA
CTTTCCAATCTCCAGACTGCGAGGATCAGGCTACTCCCCCATTTAACCACCGC
GCAGAGCACAACGGCTCGTCCCTACGCCCTGACTCGAACACTCACACGCACG
AGCACTGGCATACGCAGACAGCACGTTTCCTGTCCCTGTGTGACACCCACCCT
CGTCGCGCGGCTGCTCCAGCCCTCGCGCGGTGCCCTCCTCCCGCCACACACAC
TCGCACACGCACGCAGGCGCGTGCAGGGTCGAGCCGAAGGCAGCTTGCCCGC
AGCCACTCGGAGGCGACCAGCGCCAGACTAGCAGAACCC

GAD67 Promoter

GTCTCTGTGTGTTTGGCGCCCTCTGGTGGAAAATTTTCCCAAAACCGCCTTTTT
ATGGTGGGGGACTTCACCCCGCTCAGTAAGGTGCTTAAATACTGCCAAAAGA
GAATCATTAAACACCGTGAAACTGAAAAGAAGCGCGGAGAGTGGGCCAAGA
CAAGGAGTGCGGTCCTGGCTTCCCGGAGCCACCCTCCACGCTCCGGTTCCCC
AGGCGTGTGGAGCGGCACTCGTGCATGTTATTAACCTTCAGACATGATCAAT
CACAGAGATTTCTTTTCCCCCTCTCAAGGGAGAGGGCTCAGAGAAAGGGAAA
TAGACCCCTTTCCTCTTTTGGTACCAGGTAGCTGTGTTCGAACGAGGTAGTTT
GGAGATGAACTGGATGAAGATACTGGAGTGCAGAAACTCCACGGTCTGGGTG
GGTGGTCCCCTCAGCTCTGCTTTGCCTGTACAGCCACATTGGCTCACTAGAGC
GCTCCCCATGACACCACCCAGAGAAAACCTTCTGGATTCGCCAATCCAGGAC
AACCACCGGAAATTGATTAAGGCAAAGCAAATATTTTAATCTCCTCCAAGAT
ACGGGAAGGAGGGCAAAAAGGAAGAGAAAGAAGAATCACCCGGTGAGACA
AAATTCTTCGTAAGAATGATTTTTTCCCTTGCTGTCACCCAACATTGCTTATCT
CAAAAATAATTGGGAAAAAAACAAAAAACAGAGCGTGCTGAGTGCATTCTG
GATTACTCATAGGACTTTGTCACACACACCCTCCTTTCTGGTCGCAAACCCAT
GAGCTGGCTTTATCATCGAAATATAAAGCGCCAGAGGCAGTCAGACACCTGC
AAAGGAGCCCCAGGCTGCGCGGACGAGCTGCCCCCGCGAGCAGCGGCTTCGT
GATTCCCCCGCCGAGCGGGTCCCCGCCTCCCCACTCCGCCCCCGCCTCCCCCA
AGCCCAGCGGCGGCCTCTCCGGATCTCTCTCTTCTTCGGGCTCTCCGTGCCGG
ACCAGGGATCCTGCAAGCAAGGAAGCAGCCCCGGGGTGACACCCAGCACGT
ACGTCTGTGGCAGAGCAAAGCCAAGCCCAAGCGGGGGACGCTTCGCGGAGG
AGTCGCGGGAGGGTCCAGCTCGC

CMV Promoter

GACATTGATTATTGACTAGTTATTAATAGTAATCAATTACGGGGTCATTAGTT
CATAGCCCATATATGGAGTTCCGCGTTACATAACTTACGGTAAATGGCCCGCC
TGGCTGACCGCCCAACGACCCCCGCCCATTGACGTCAATAATGACGTATGTT
CCCATAGTAACGCCAATAGGGACTTTCCATTGACGTCAATGGGTGGACTATTT
ACGGTAAACTGCCCACTTGGCAGTACATCAAGTGTATCATATGCCAAGTACG

CCCCCTATTGACGTCAATGACGGTAAATGGCCCGCCTGGCATTATGCCCAGT
ACATGACCTTATGGGACTTTCCTACTTGGCAGTACATCTACGTATTAGTCATC
GCTATTACCATGGTGATGCGGTTTTGGCAGTACATCAATGGGCGTGGATAGC
GGTTTGACTCACGGGGATTTCCAAGTCTCCACCCCATTGACGTCAATGGGAGT
TTGTTTTGGCACCAAAATCAACGGGACTTTCCAAAATGTCGTAACAACTCCGC
CCCATTGACGCAAATGGGCGGTAGGCGTGTACGGTGGGAGGTCTATATAAGC
AGAGCT

Benchling links for constructs

CMV-IgK-PLE-HA-DAF-IRES-EGFP
https://benchling.com/s/seq-MsN0VuNN8tG1ucr6pwUx

Synapsin-IgK-PLE-HA-DAF-IRES-EGFP-WPRE
https://benchling.com/s/seq-0DOcbWomXeGrsHX1SY79

GAD65-IgK-PLE-HA-DAF-IRES-mCherry-WPRE
https://benchling.com/s/1JsffIPZ

GAD67-IgK-PLE-HA-DAF-IRES-mCherry-WPRE
https://benchling.com/s/Ex3xRXLJ

Synapsin-PAT3-PLE-HA -CD42-neurexin1-T2A-mCherry
https://benchling.com/s/1JU7x5Ja

CAG-PAT3-PLE-HA -CD42-neurexin1-T2A-mCherry
https://benchling.com/s/gVycBBch

Synapsin-PLE-HA-neuroligin1-mCherry
https://benchling.com/s/Orv5yCs9

CAG-PLE-HA-neuroligin1-mCherry
https://benchling.com/s/44OO0SWR

Figures and Schemes

Scheme 3-1-1. *Design of fluorogenic activation using a red-shifted VF dye, carboVF, in specific cells of interest.*

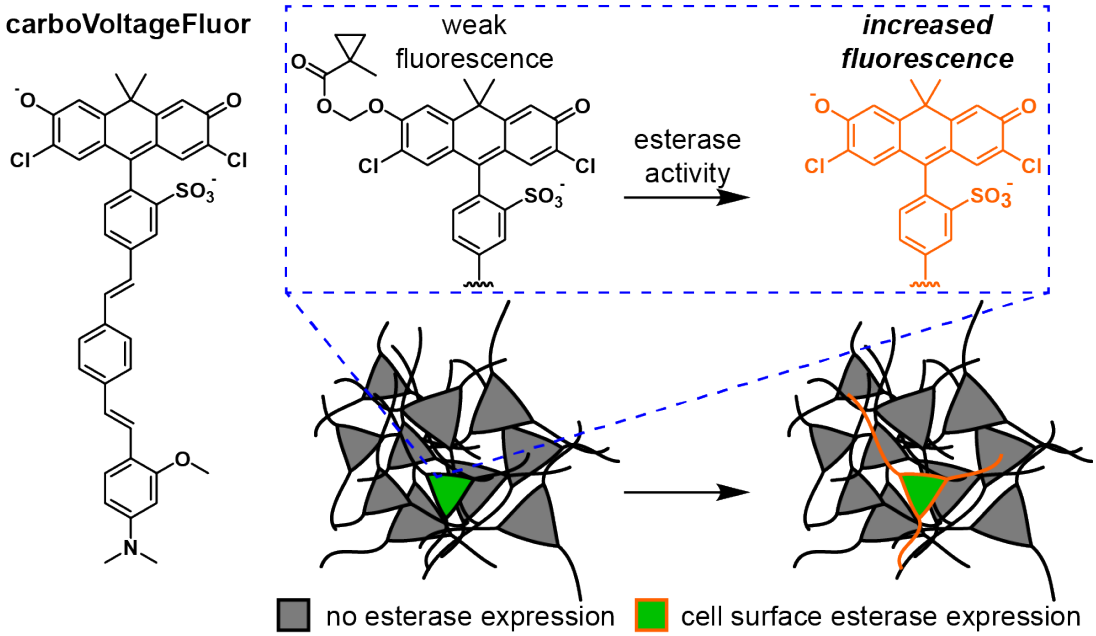

Scheme 3-1-1. Scheme of neuron-specific targeting with cell-surface PLE and carboVoltageFluor (components are not to scale).

Scheme 3-2-1. *Design of fluorogenic activation using a second generation VF dye, isoVF2.2Cl(OMe), in specific cells of interest.*

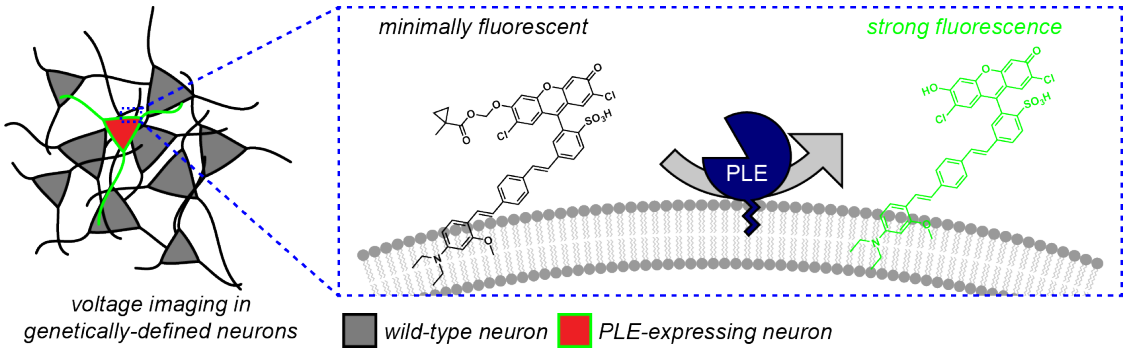

Scheme 3-2-1. Scheme of neuron-specific targeting with cell-surface PLE and cp-isoVF2.2.Cl(OMe) (components are not to scale).

Figure 3-1-1. *In vitro characterization of carboVF-EX 1.*

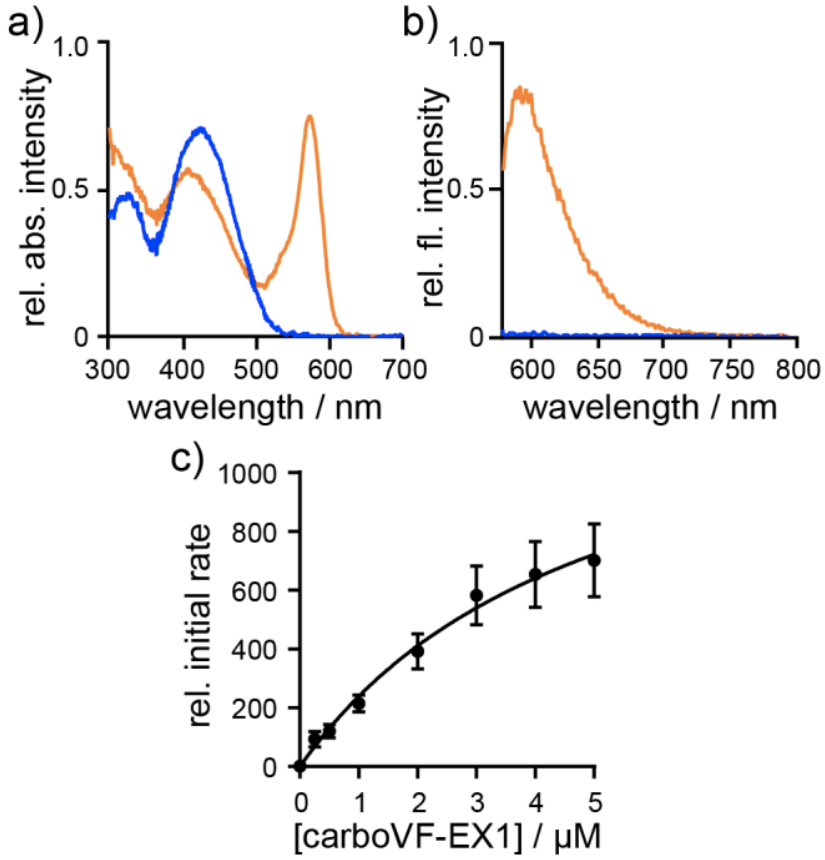

Figure 3-1-1. PLE-mediated uncaging of carboVF-EX 1 in vitro. Normalized (a) absorbance and (b) emission spectra of carboVF-EX 1 (0.5 µM) in HBSS with 0.01% SDS. Spectra are acquired 2h after adding PLE (0.7 mg/mL, orange) or blank (blue). (c) Plot of relative initial rate vs. [carboVF-EX 1]. Error bars are ± S.E.M. for n = 7 independent determinations. [PLE] is 168 ng/mL (1 nM) for saturation kinetics measurements.

Figure 3-1-2. *In vitro characterization of carboVF-EX 2.*

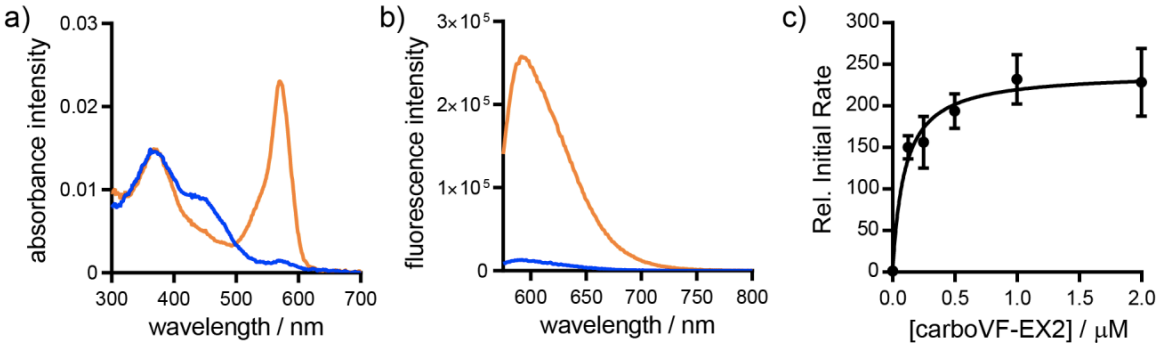

Figure 3-1-2. Spectroscopic characterization of carboVF-EX 2 in vitro. (a) UV-vis absorption and (b) fluorescence emission spectra of carboVF-EX 2 in the absence (blue lines) or presence (orange lines) of PLE (0.7 mg/mL, 2 h). (c) Plot of relative initial rate vs substrate concentration for the reaction of PLE (168 ng/mL) with carboVF-EX 2. Data points are the mean ± S.E.M. for n = 8 independent measurements. The solid line is the best fit to the Michaelis-Menten equation (Graphpad).

Figure 3-1-3. *HPLC analysis of PLE reaction with carboVF-EX 1 and 2.*

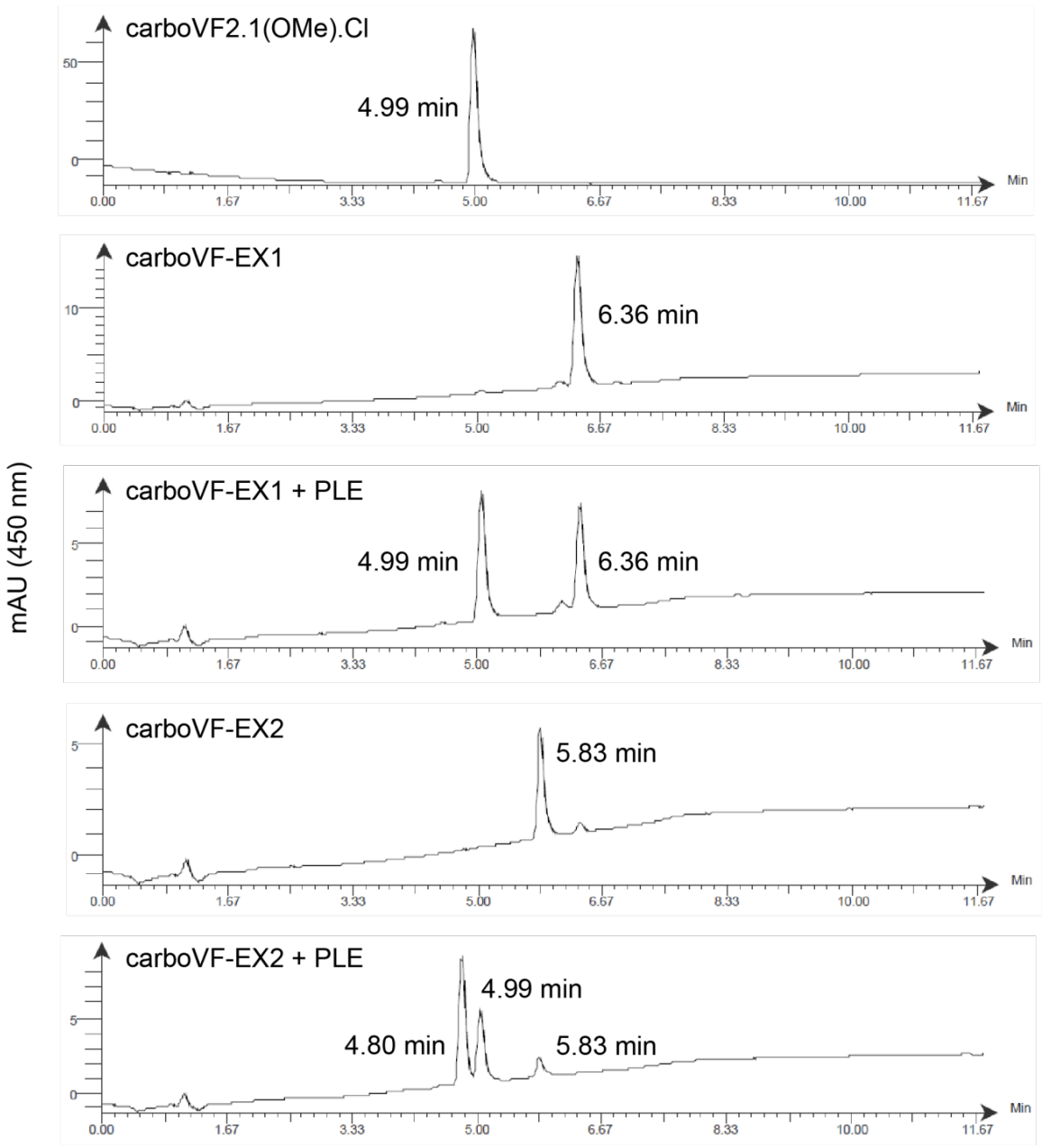

Figure 3-1-3. HPLC analysis of PLE reaction with carboVF-EX 1 and 2. Note: the reaction of carboVF-EX2 + PLE leads to carboVF2.1(OMe).Cl (4.99 min) and the intermediate in which only the sulfonate is esterified (4.80 min).

Figure 3-1-4. *PLE constructs used in this study.*

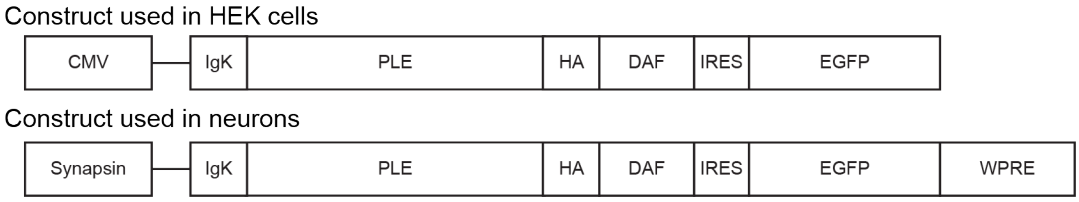

Figure 3-1-4. PLE constructs used in this study.

Figure 3-1-5. *Characterization of cell-surface PLE expression in HEK cells using immunohistochemistry.*

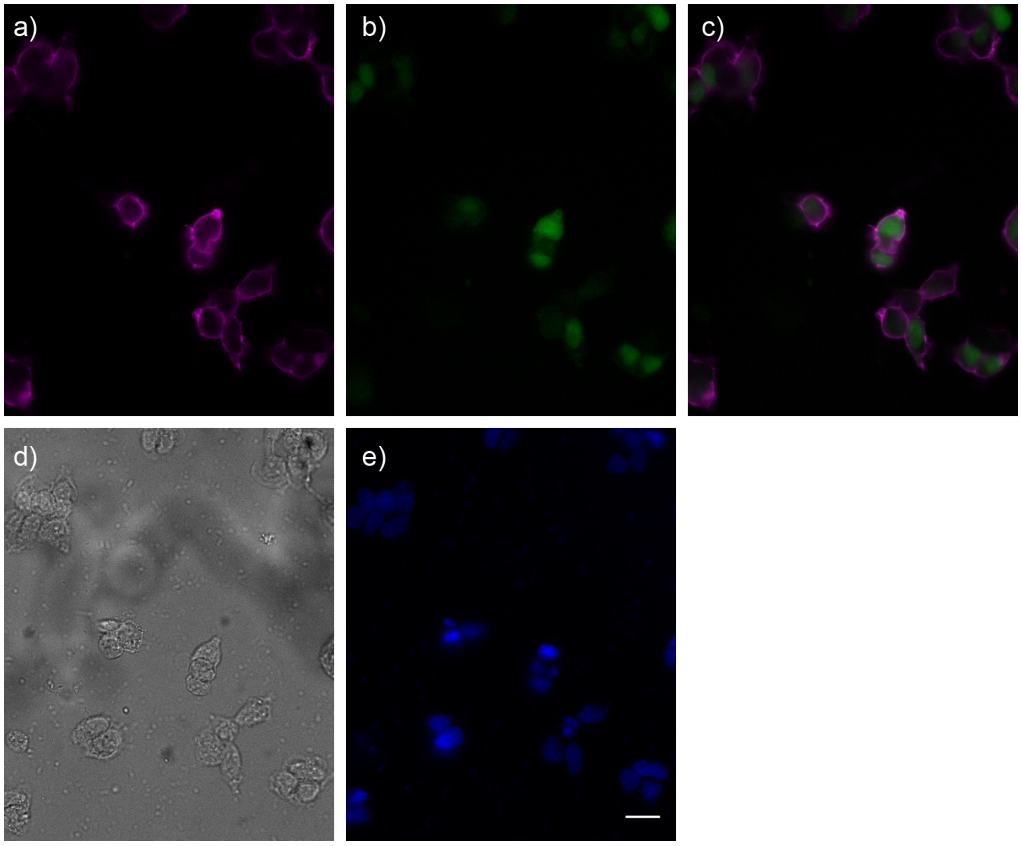

Figure 3-1-5. Immunohistochemistry of cell-surface PLE in HEK cells. (a) Membrane-associated anti-HA staining shows cell-surface PLE expression. (b) PLE expression is indicated by nuclear EGFP. (c) Merged images of anti-HA staining and EGFP. (d) DIC images of fixed cells. (e) Nuclei staining of Hoechst 33342. Scale bar is 20 μm.

Figure 3-1-6. *Characterization of carboVF-EX 1 in HEK cells.*

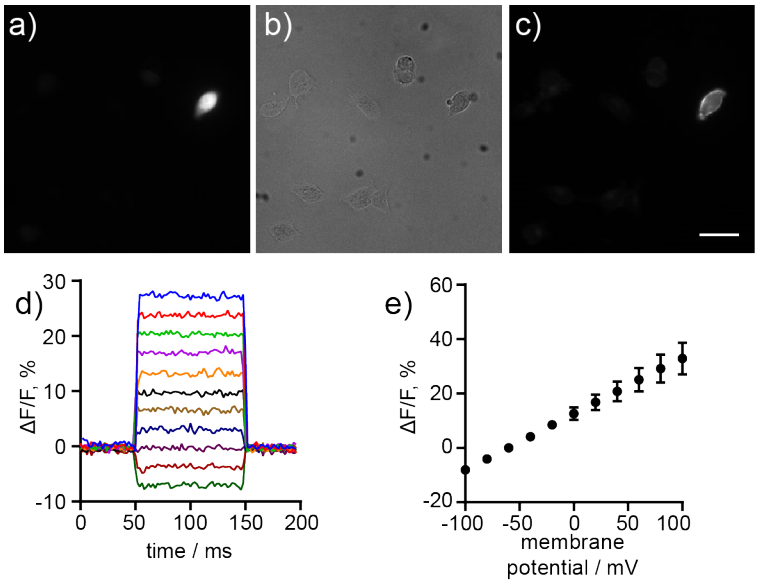

Figure 3-1-6. Cellular characterization of carboVF-EX 1. (a-c) Wide-field fluorescence microscopy of HEK cells stained with carboVF-EX 1 (500 nM, 30 min) shows membrane labeling of the cell expressing cell surface PLE, as indicated by (a) GFP fluorescence. (b) DIC image of HEK cells and (c) epifluorescence image showing carboVF-associated fluorescence in PLE-expressing cell. Scale bar is 10 μm. (d) Voltage sensitivity of carboVF-EX 1 in patch-clamped PLE-expressing HEK cells. (e) Plot of ΔF/F vs membrane potential (in mV) for carboVF-EX 1. Data are mean ± S.D. for five cells.

Figure 3-1-7. *Characterization of carboVF-EX 1 in cultured hippocampal neurons.*

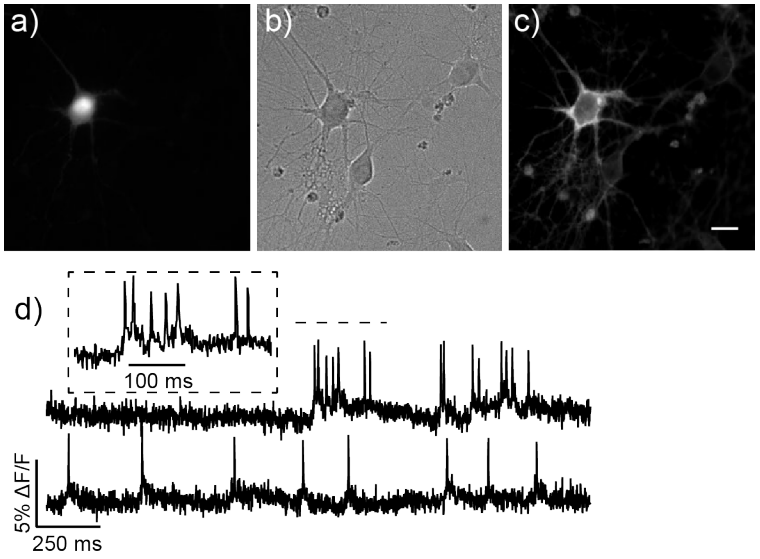

Figure 3-1-7. Cellular characterization of carboVF-EX 1. (a-c) Live cell wide-field images of rat hippocampal neurons expressing PLE-DAF under the control of the synapsin promoter (Syn) and stained with carboVF-EX 1 (500 nM, 30 min). (c) GFP fluorescence indicated PLE expression in neurons shown in the b) DIC image. (a) Membrane-associated fluorescence of carboVF in PLE expressing neuron. Scale bar is 20 μm. (d) Representative ΔF/F traces for spontaneous activity of neurons transfected with Syn-PLE and stained with carboVF-EX 1. Images were acquired at 500 Hz and represent single-trial acquisitions. Inset shows expanded time scale of indicated area of the upper trace.

Figure 3-1-8. *Activity profiling with carboVF-EX1 in neurons.*

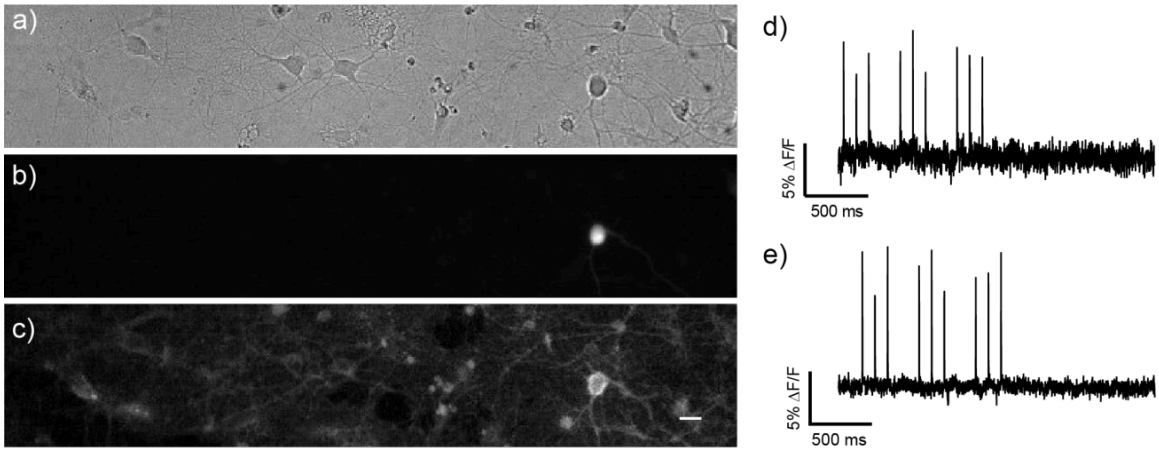

Figure 3-1-8. Field stimulation of neurons expressing PLE and stained with carboVF-EX1. (a) DIC Image of neurons sparsely transfected with PLE and stained with 500 nM carboVF-EX1. (b) EGFP fluorescence image of neurons from panel a. (c) Fluorescence image indicating the selective uncaging of carboVF-EX1 in the presence of PLE. Scale bar is 20 μm. (d-e) Field stimulation of neurons expressing PLE and stained with (d) 500 nM carboVF-EX 1 and (e) 1 μM carboVF-EX 1.

Figure 3-2-1. *In vitro characterization of isoVF2.2.Cl(OMe).*

a)

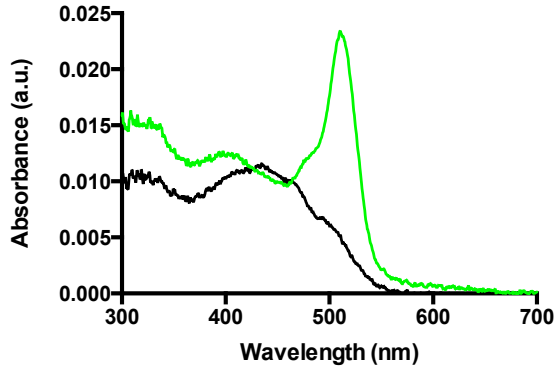

b)

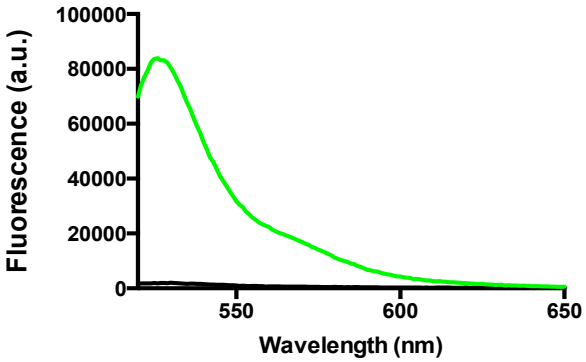

Figure 3-2-1. Characterizing the effect of cyclopropyl ester on quenching the fluorescence of the parent dye. Normalized (a) absorbance and (b) emission spectra of isoVF2.2.Cl(OMe) (green trace) and cp-isoVF2.2.Cl(OMe (black trace).

Figure 3-2-2. *In vitro characterization of PLE reaction with cp-isoVF2.2.Cl(OMe).*
a)

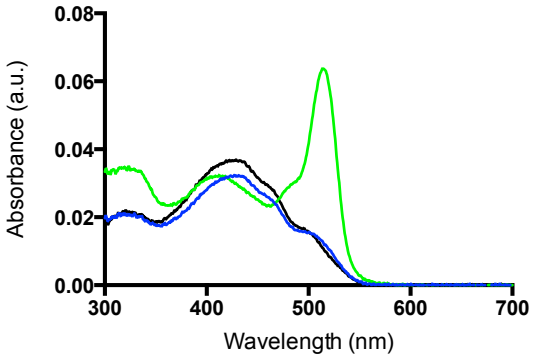

b)

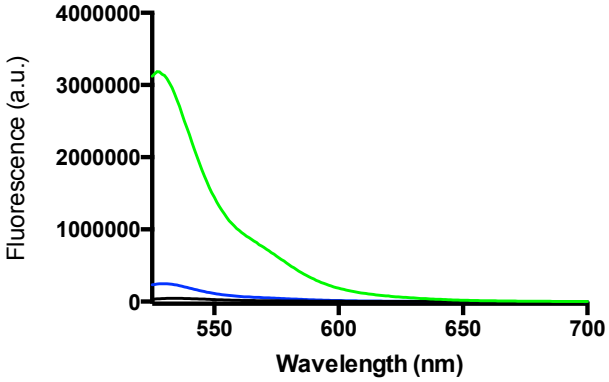

Figure 3-2-2. Spectroscopic characterization of cp-isoVF2.2.Cl(OMe) with PLE reaction in vitro. (a) UV-vis absorption and (b) fluorescence emission spectra of cp-isoVF2.2.Cl(OMe) in the absence (black lines) or presence (blue lines) of PLE (0.7 mg/mL, 2 h). Spectra for the parent dye isoVF2.2.Cl(OMe) are shown in green lines.

Figure 3-2-3. *HPLC analysis of PLE reaction with cp-isoVF2.2.Cl(OMe).*

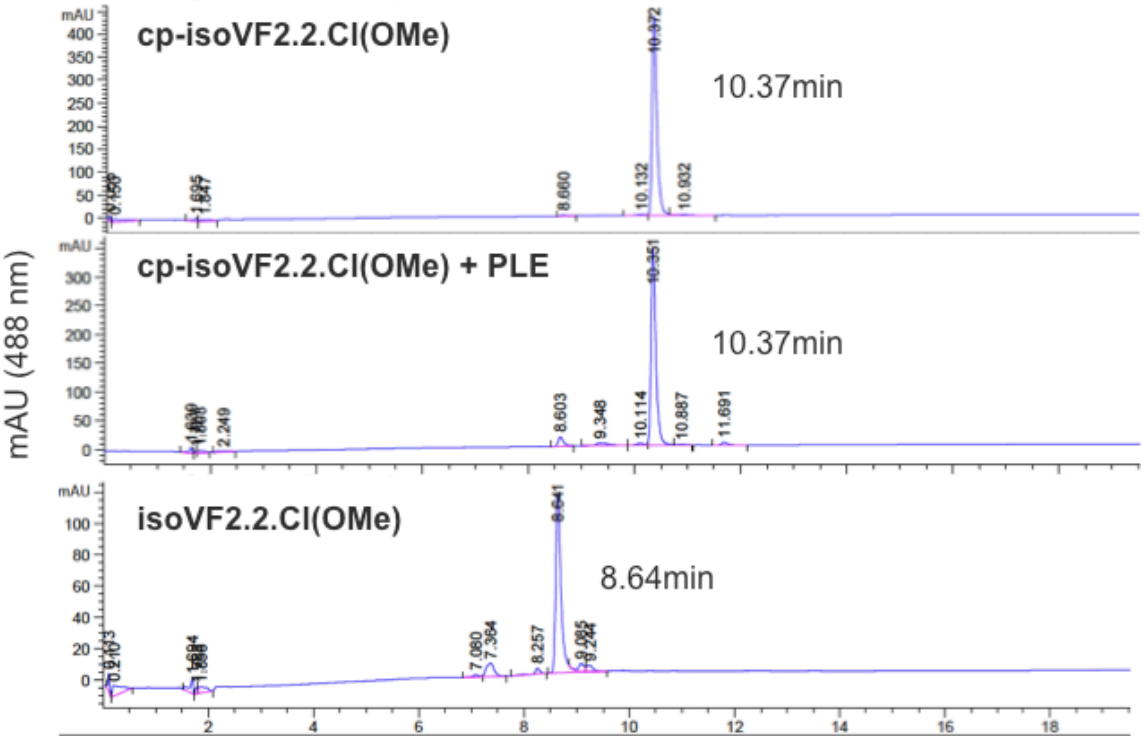

Figure 3-2-3. HPLC analysis of PLE reaction with cp-isoVF2.2.Cl(OMe).

Figure 3-2-4. *Characterization of cp-isoVF2.2.Cl(OMe) in HEK cells.*

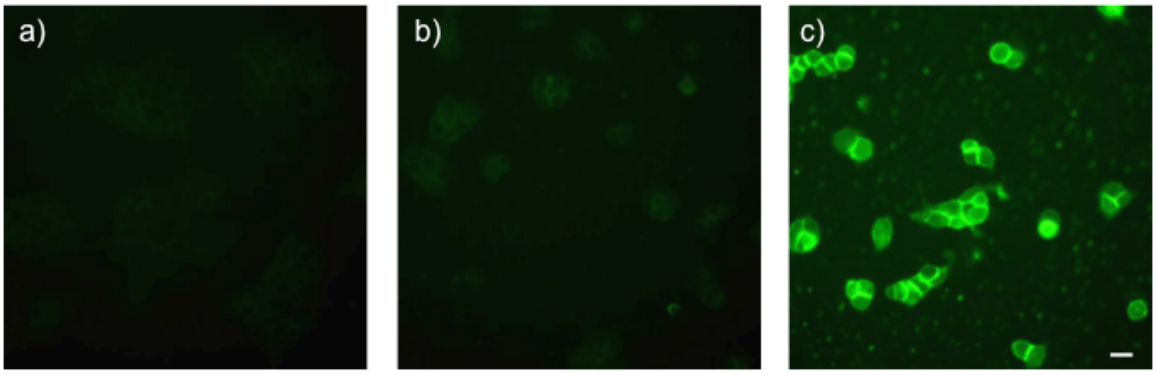

Figure 3-2-4. Live-cell wide-field imaging of HEKs. All images are acquired using the VF channel. (a) Negative control cells without PLE transfection and loaded with 1 μM cp-isoVF2.2.Cl(OMe) at 37 °C for 30 min. (b) HEK cells sparsely transfected with PLE-DAF and loaded with cp-isoVF2.2.Cl(OMe). (c) HEK cells sparsely transfected with PLE-DAF and loaded with 1 μM isoVF2.2.Cl(OMe) at 37 °C for 30 min. Dye concentrations are matched at wire absorbance. Scale bar is 20 μm.

Figure 3-3-1. *PLE constructs used for expression in inhibitory neurons.*

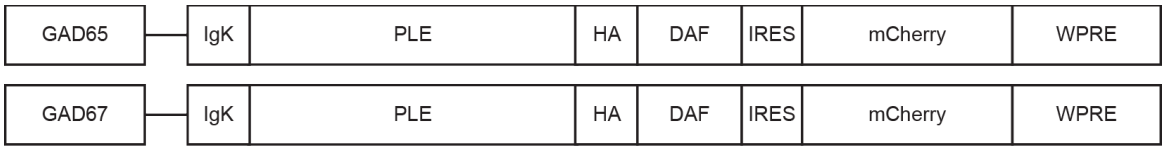

Figure 3-3-1. GAD65 and GAD67 promoters are used for expression in inhibitory neurons.

Figure 3-3-2. *Characterization of inhibitory PLE constructs in cultured neurons using immunohistochemistry.*

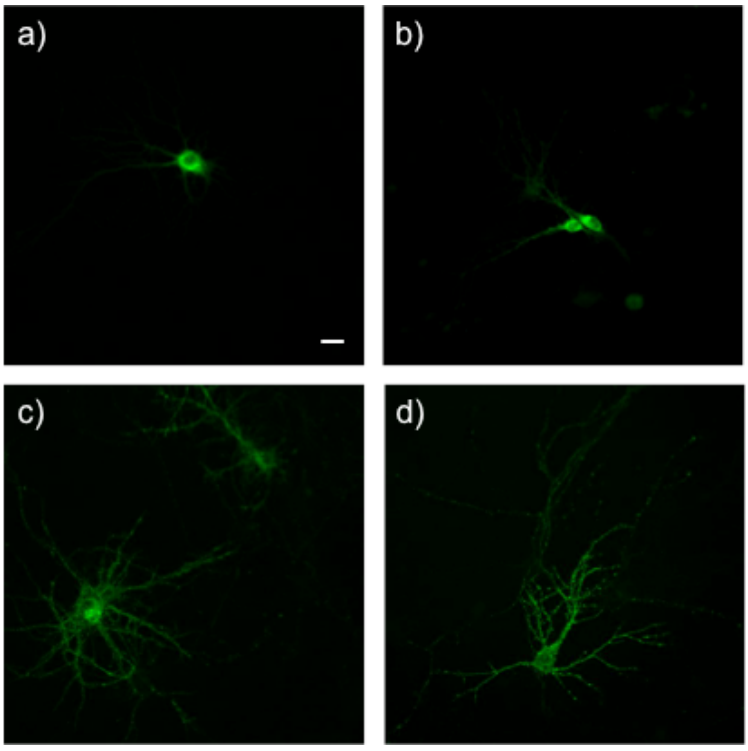

Figure 3-3-2. Fixed cell wide-field images of rat hippocampal neurons expressing (a,b) GAD67-PLE-DAF or (c,d) GAD65-PLE-DAF under permeable conditions. Two representative regions of interest are shown for each construct. Anti-HA staining indicates PLE expression. Scale bar is 20 μm.

Figure 3-3-3. *Characterization of specificity of inhibitory PLE constructus in cultured neurons using immunohistochemistry.*

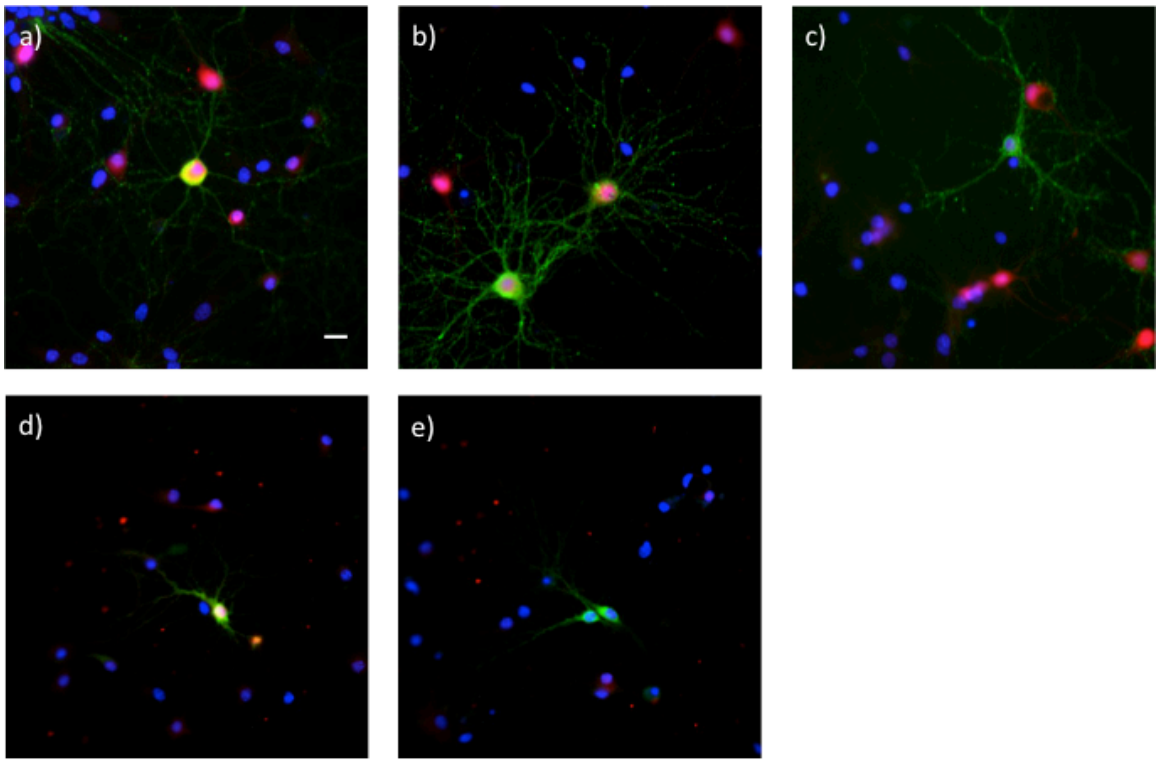

Figure 3-3-3. Representative images of neurons expressing PLE constructs with inhibitory promoters. Fixed cell wide-field images of rat hippocampal neurons expressing (a-c) GAD65-PLE-DAF or (d,e) GAD67-PLE-DAF under permeablizing condition. Blue: Hoechst 33342 stains nucleus. Some PLE-expressing cells also express GABA (a,b,d) while a few do not (c,e). Green: anti-HA staining indicates PLE expression. Red: anti-GABA staining indicates inhibitory cells. Scale bar is 20 μm.

Figure 3-3-4. *Characterization of inhibitory PLE constructs in cultured neurons.*

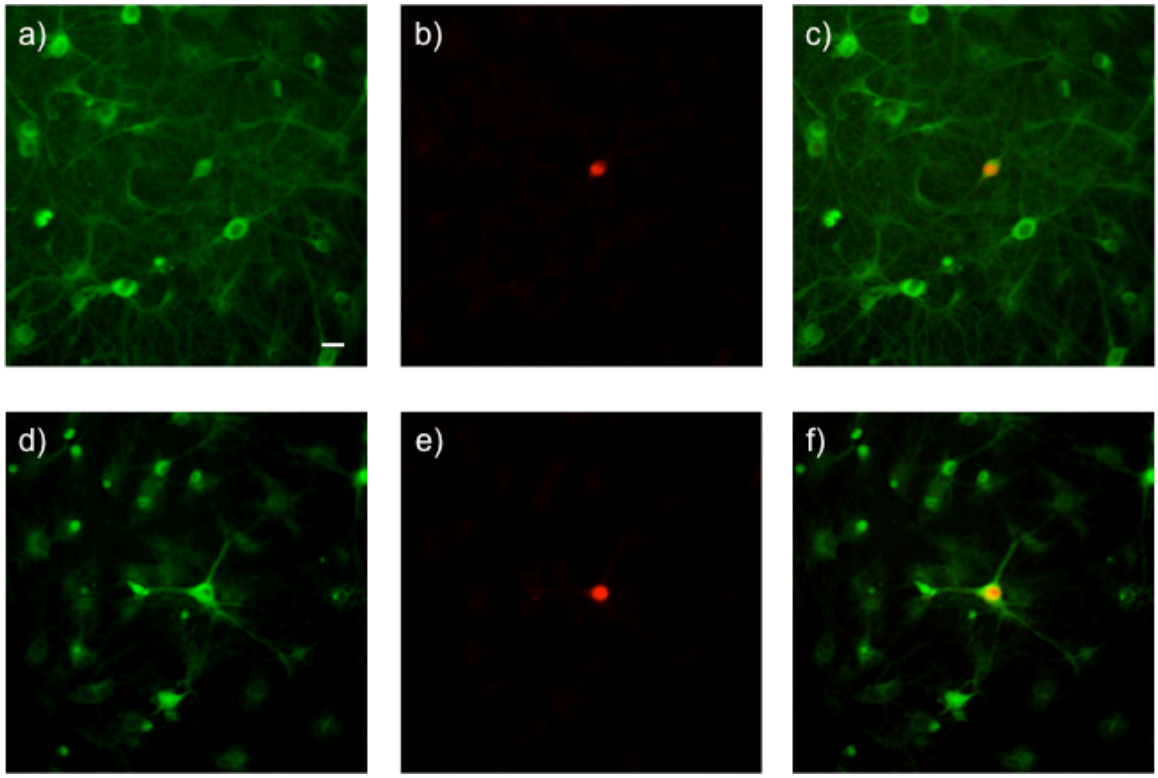

Figure 3-3-4. Cellular characterization of PLE constructs with inhibitory promoters. Live cell wide-field images of rat hippocampal neurons expressing (a-c) GAD67-PLE-DAF or (d-f) GAD65-PLE-DAF and stained with VF-EX 2 (1 μM, 60 min). (a,d) Uniform VF fluorescence was seen in all neurons in the field of view. (b,e) Nuclear mCherry expression indicates PLE expression. (c,f) Merged image of VF and mCherry fluorescence. Scale bar is 20 μm.

Figure 3-4-1. *PLE constructs used for expression in subcellular structures.*

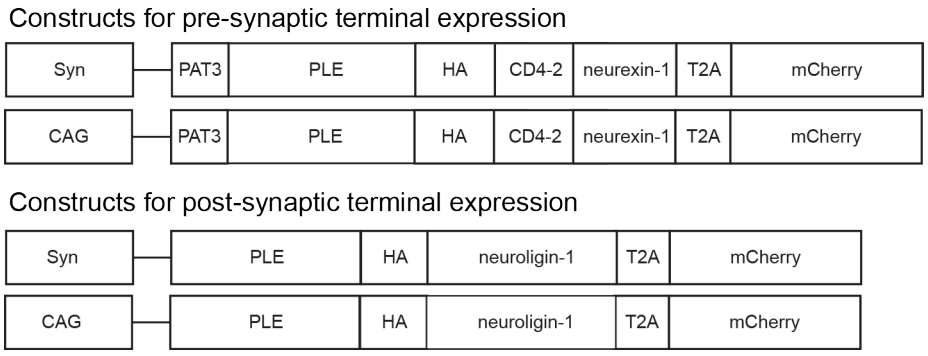

Figure 3-4-1. Constructs used to target PLE to pre- and post-synaptic terminals.

Figure 3-4-2. *Characterization of presynaptic PLE constructs in cultured neurons*

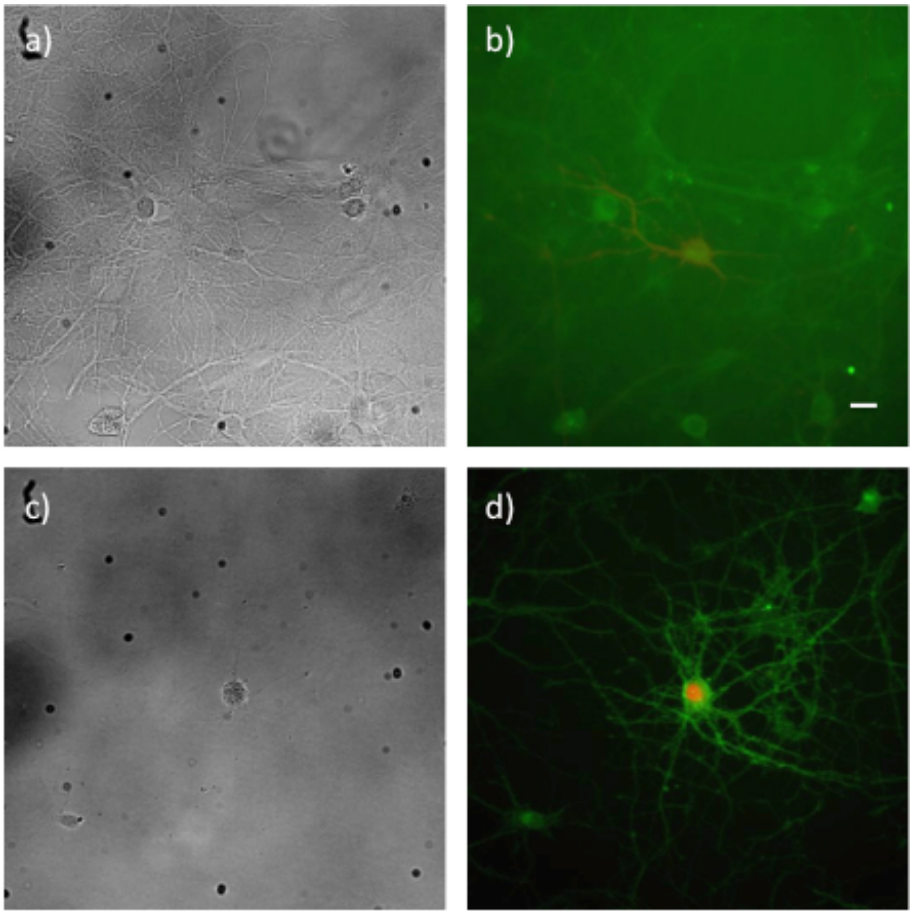

Figure 3-4-2. Cellular characterization of PLE constructs expressing presynaptic terminal targeting sequences. Live cell wide-field images of rat hippocampal neurons expressing (a,b) Syn-presynaptic-PLE or (c,d) CAG-presynaptic-PLE and stained with VF-EX 2 (1 μM, 60 min). (a,c) DIC images of neurons. (b, d) Merge image of mCherry fluorescence (PLE expression) and VF staining. (b) Uniform and dim VF fluorescence was seen in all neurons. (d) Selective VF staining in the cell expressing PLE but fluorescence is seen throughout the cellular membrane. Scale bar is 20 μm.

Figure 3-4-3. *Characterization of postsynaptic PLE constructs in cultured neurons*

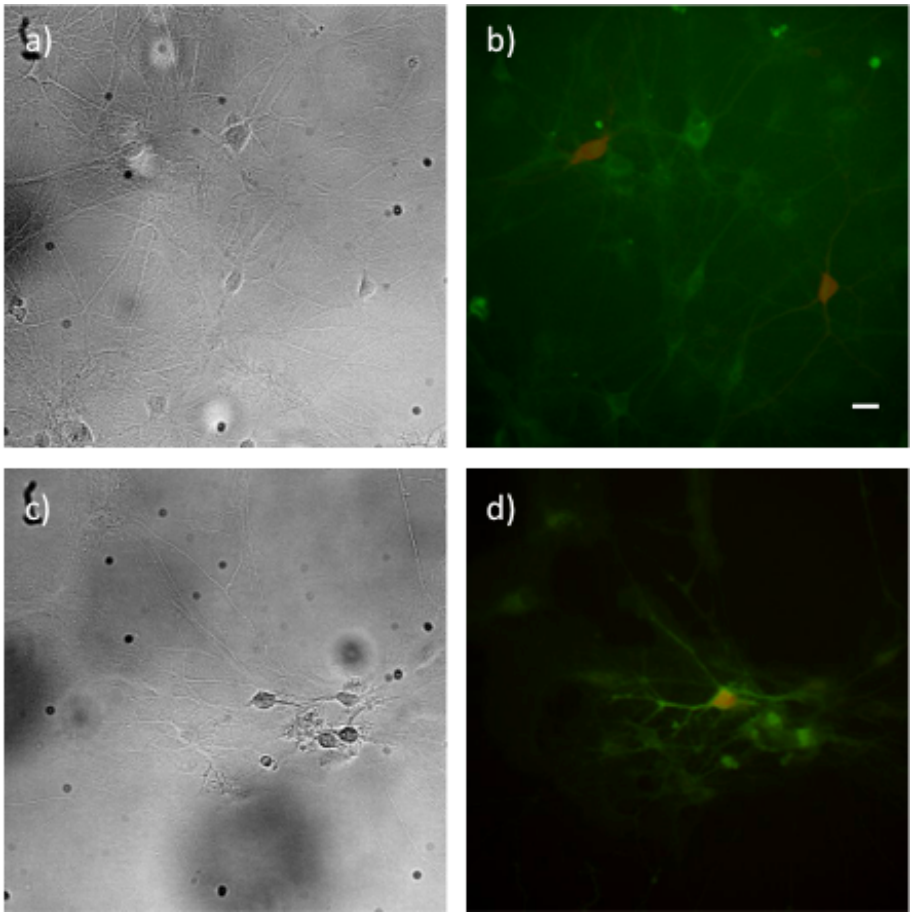

Figure 3-4-3. Cellular characterization of PLE constructs expressing postsynaptic terminal targeting sequences. Live cell wide-field images of rat hippocampal neurons expressing (a,b) Syn-postsynaptic-PLE or (c,d) CAG-postsynaptic-PLE and stained with VF-EX 2 (1 μM, 60 min). (a,c) DIC images of neurons. (b,d) Merge image of mCherry fluorescence (PLE expression) and VF staining. (b) Uniform and dim VF fluorescence was seen in all neurons. (d) Selective VF staining in the cell expressing PLE but fluorescence is seen throughout the cellular membrane. Scale bar is 20 μm.

Figure 3-4-4. *Characterization of CAG-pre- and postsynaptic PLE constructs in cultured neurons using immunohistochemistry.*

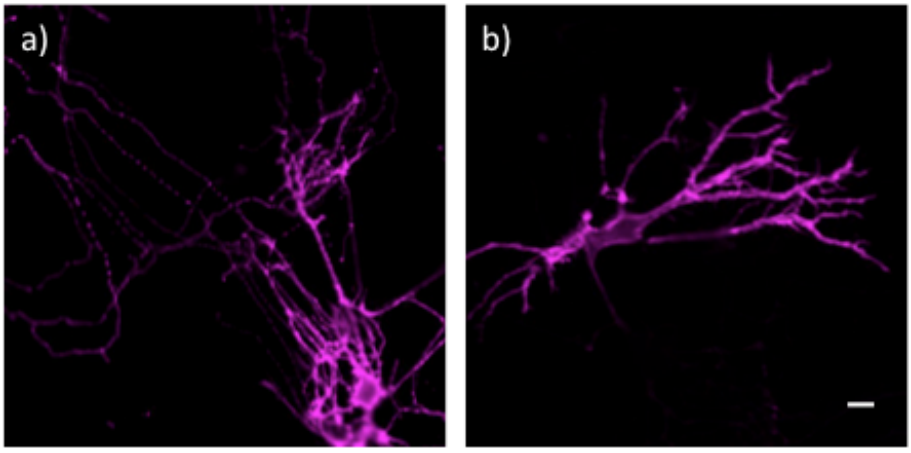

Figure 3-4-4. Fixed cell wide-field images of rat hippocampal neurons expressing (a) CAG-presynaptic-PLE or (b) CAG-postsynaptic-PLE. Anti-HA staining was observed to stain the cellular membrane uniformly. Scale bar is 20 μm.

.

Table 3-1-1. *Properties of carboVF2.1(OMe).Cl and carboVF-EX dyes.*

				contrast[c]			% ΔF/F		SNR
dye	Φ [a]	K_M [b]	K_{cat}/K_M [b]	in vitro[d]	HEK[e]	neurons[e]	HEK[f]	neurons[g]	neurons
cVF	0.0012	---	---	---	---	---	31±2	13.9±1.4	28±1.9
cVF-EX1	0.001	6.4±1.4 μM	1.3 x 10^5 $M^{-1}s^{-1}$	45	8.9±0.7	2.4±0.08	18±3	8.4±0.4	12±0.8
cVF-EX2	0.011	0.16±0.08 μM	4.9 x 10^5 $M^{-1}s^{-1}$	21	---	---	---	---	---

--- = not determined or not applicable. [a] Quantum yield of fluorescence. Measured in HBSS (pH 7.4). [b] Determined by reaction of dye with purified PLE in HBSS (pH 7.4). [c] Ratio of VF-EX 1 or VF-EX 2 fluorescence in PLE-expressing cells (or PLE-containing buffer, for *in vitro*) to cells not expressing PLE. [d] After 2 hours in buffer, with or without PLE. [e] After 30 min using 500 nM cVF-EX 1 at 37 °C. [f] Per 100 mV depolarization, in HEK cells. [g] Per action potential evoked by field stimulation.

References

1. Grenier, V.; Walker, A. S.; Miller, E. W., *J. Am. Chem. Soc.* **2015,** *137* (34), 10894-10897.
2. Liu, P.; Grenier, V.; Hong, W.; Muller, V. R.; Miller, E. W., *J. Am. Chem. Soc.* **2017**, *139*, 17334-17340.
3. Ortiz, G.; Liu, P.; Naing, S. H. H.; Muller, V. R.; Miller, E. W., *J. Am. Chem. Soc.* **2019**, *141* (16), 6621-6638.
4. Tian, L.; Yang, Y. L.; Wysocki, L. M.; Arnold, A. C.; Hu, A.; Ravichandran, B.; Sternson, S. M.; Looger, L. L.; Lavis, L. D., Proc Natl Acad Sci U S A **2012**, *109* (13), 4756-4761.
5. Erlander, M. G.; Tillakaratne, N. J.; Feldblum, S.; Patel, N.; Tobin, A. J.; *Neuron* **1991**, 7 (1), 91–100.
6. Langendorf, C. G.; Tuck, K. L.; Key, T. L.; Fenalti, G.; Pike, R. N.; Rosado, C. J.; Wong, A. S. M.; Buckles, A. M.; Law, R. H. P.; Whisstock, J. C., *Biosci. Rep.* **2013**, *33* (1), 137-144.
7. Esclapez, M.; Tillakaratne, N. J.; Kaufman, D. L.; Tobin, A. J.; Houser, C. R., *J. Neurosci.* **1994**, *14*, 1834-1855.
8. Hendrickson, A. E.; Tillakaratne, N. J.; Mehra, R. D.; Esclapez, M.; Erickson, A.; Vician, L.; Tobin, A. J., *J. Comp. Neurol.* **1994**, *343* (4), 566-581.
9. Kanaani, J.; Lissin, D.; Kash, S. F.; Baekkeskov, S., *J. Biol. Chem.* **1999,** *274* (52), 37200-37209.
10. Kiser, P. J.; Cooper, N. G.; Mower, G. D., *J. Comp. Neurol.* **1998**, *402* (1), 62-74.
11. Varju, P.; Katarova, Z.; Madarász, E.; Szabó, G., *Cell Tissue Res.* **2001**, *305* (2), 239-246.
12. Kim, J.; Zhao, T.; Petralia, R. S.; Yu, Y.; Peng, H.; Myers, E.; Magee, J. C., *Nat. Methods* **2012**, *9*, 96-102.

Chapter 4:

Covalent Labeling of Voltage Sensitive Dyes to Neurons

Portions of this work were performed in collaboration with the following persons:
Synthesis and cellular characterization was assisted by Parker Deal
Cloning was assisted by Vikram Muller
In utero electroporation was assisted by Kiarash Sharmadani
Slice patching and live animal imaging was assisted by Hillel Adesnik

Abstracts

Voltage-sensitive fluorescent dyes (VSDs) are powerful tools that enable the recording of millisecond-scale neuronal dynamics. VSDs are attractive for such measurements due to their extremely fast kinetics, high sensitivities to membrane potential changes, and easily tunable absorbance and emission profiles. Despite these advantages, previously developed VSDs have found limited use in complex tissue preparations, such as brain slice and live animal, because of their indiscriminate staining of all cellular membranes. We addressed this limitation by developing genetically targeted voltage dyes using a HaloTag-based system. It is a hybrid approach, consisting of previously reported tetramethylrhodamine-based voltage reporter RhoVRs coupled to a chloroalkane ligand (RhoVR-HaloTag) and a cell-surface HaloTag protein expressed selectively in cells of interest. We demonstrated that RhoVR-HaloTags can selectively label and record activity from dissociated rat hippocampal neurons and in ex vivo mouse brain slice with single cell resolution. In addition, we showed that the good two-photon cross sections typical of tetramethylrhodamines enabled clear visualization of subcellular structures in slices. These results present the potential of hybrid chemogenetic voltage indicators to combine the optical performance of small-molecule chromophores with the inherent selectivity of genetically-encodable systems, permitting imaging modalities inaccessible to either technique individually.

Introduction

For decades, researchers have been interested in measuring and studying the membrane potential (V_m) changes in cells, in particular neurons, where rapid depolarization of V_m about 100 mV, or action potential, is a key component in neuronal signaling pathways. The traditional method or gold standard to monitor V_m is electrode-based electrophysiology, which offers remarkable speed and sensitivity of measurement. However, it is extremely invasive, low throughput and has limitations in spatial resolution given the relatively large size of patch pipette tip compared to subcellular structures. To resolve some of the problems, optical tools, including small molecule-based[1] and protein-based[2-4], have been explored and developed for voltage sensing in hundreds of cells simultaneously. One class of small molecule fluorescent dye designed by our lab, VoltageFluors (VF)[5], possesses exceptional and readily tunable photo-physical properties (i.e. absorption and emission profiles, photo-stability, brightness, voltage sensitivity, etc.)[6-9], which allows us to evaluate neuronal activity and connectivity with outstanding sensitivity in cultured neurons in a high throughput manner.

On the other hand, a common issue with all small molecule dye imaging, the inability to target to specific cells of interest, remains a challenge to use the dyes in complex biological settings. For instance, our VF dyes indiscriminately labels all membranes and increases unproductive or background fluorescence dominating the desired voltage readout. This high background poses difficulties for voltage imaging in ex vivo brain slice and in vivo live animal. While our lab has developed both photoactivatable[10] and enzymatically uncaged[11-12] VF that reduce off-target fluorescence through fluorogenic activation of the dye in cells of interest, these systems still lacked the specificity necessary to enable in vivo voltage imaging. One explanation is the inefficient quenching at the phenolic oxygen of fluorescein-based VF dyes, contributing to the compromised contrast ratio between transfected and non-transfected cells. In addition,

these strategies are not untranslatable to red-shifted rhodamine-based VF dyes RhoVR 1[6] and BeRST 1[7], which have improved photo-physical properties compared to the first generation fluorescein-based dyes. Alternatively, we have also developed VF dyes that could be ligated directly to cells of interest using self-labeling enzymes like the SpyTag/SpyCatcher system.[13] While contrast has been significantly enhanced, the slow reaction kinetics of SpyCatcher and low fluorescence signal of fluorescein hinder its application in mouse brain slices.

Inspired by the covalent labeling system, we combined the selectivity of genetically-encodable systems with the favorable photo-physics and tunability of VF dyes, using a rhodamine-based voltage reporter (RhoVR) and the protein tagging system HaloTag. We choose to target RhoVR1 due to its red-shifted absorption/emission, large voltage sensitivities (47% ΔF/F per 100 mV), ease of synthesis and functionalization as well as high two-photon cross-section, which is desirable for deep tissue in imaging for in vivo applications. The HaloTag system is selected due to its small enzyme size for engineering and fast kinetics with exceptional affinity and selectivity.[14] By expressing HaloTag on the cell surface and adding RhoVR 1 linked to the HaloTag ligand via a flexible polyethene glycol linker (PEG), we hoped to gain selectivity through the protein component while maintaining the photo-physical properties of RhoVR 1, which would provide sufficient contrast for complicated biological systems (Scheme 4-1).

Results & Discussions

To design the protein component of the hybrid system, we selected the HaloTag system due to its remarkable affinity and selectivity, ease of ligand synthesis and extremely fast kinetics.[14] In order to express the HaloTag enzyme on the cell surface, we fused a transmembrane domain (pDisplay) derived from platelet-derived growth factor receptor (PDGFR)[15] to the C-terminal of the HaloTag sequence (Figure 4-1a). We also appended a secretion signal peptide from immunoglobulin K (IgK) to the N-terminal to enhance extracellular trafficking. To track the protein expression in live cells, we included a nuclear-localized EGFP downstream of HaloTag, separated by an internal ribosome entry site (IRES)[16]. These modifications successfully resulted in cell surface expression of HaloTag in HEK cells, as shown by live cell staining using a cell-impermeant tetramethylrodamine TMR-HaloTag ligand (Figure 4-1b-d). Bath application of TMR-HaloTag at 50 nM for 30 minutes displayed clear membrane-bound fluorescence, which matched EGFP signal in transfected cells.

To improve water solubility and flexibility of the dye-ligand complex, we introduced a polyethylene glycol linker of variable lengths (Scheme 4-2, synthesis conducted by Dr. Parker Deal).[17] We hypothesize that a longer linker for the voltage reporter might be necessary to confer flexibility and the ability to adopt a proper orientation in the membrane for voltage sensing when the dye is covalently tethered to the enzyme. All the dyes localized to the cell surface of HEK cells sparsely transfected with HaloTag-pDipslay (Figure 4-2a). Compared to the control dye RhoVR 1 which stained all membrane indiscriminately, RhoVR-HaloTag dyes exhibited selective staining only in cells expressing HaloTag enzyme. We next conducted whole-cell patch-clamp electrophysiology to evaluate the voltage sensitivity by monitoring the fluorescence change in response to a series of voltage steps from -100 mV to + 100mV with 20 mV increments. We observed an increase in sensitivity (up to 34% ΔF/F per 100 mV for

longest linker n = 25) with an increasing length of linker or flexibility (Figure 4-3). Interestingly, the PEG_0 dye displayed no sensitivity but greater brightness compared to others (Figure 4-2b); we propose that the PEG_0 dye was too closely bound to the HaloTag enzyme and thus probably not in the membrane, explaining the lack of voltage sensitivity and higher brightness due to the absence of membrane-associated PeT quenching effect.

Given the best voltage sensitivity, we decided to carry forward RhoVR1-PEG_{25}-HaloTag for subsequent characterization and experiments. Using confocal microscopy, we imaged RhoVR1-PEG_{25}-HaloTag in HEK cells expressing cell-surface HaloTag (Figure 4-4). Membrane-associated fluorescence was observed in cells expression nuclear EGFP (HaloTag) while non-transfected cells showed minimal background fluorescence when 50 nM of dye was used, indicating that the fast HaloTag reaction outcompetes non-specific insertion of the dye into the membranes. For experiments in cultured hippocampal neurons, we used a human synapsin promoter to enable neuron-specific expression (Figure 4-1a). Again, neurons stained with 50 nM RhoVR1-PEG_{25}-HaloTag displayed exceptional contrast (Figure 4-5) and importantly, spontaneous spiking events can be captured with desirable signal-to-noise (Figure 4-6). We also co-stained the same culture with a far-red dye BeRST 1, which non-selectively labeled all the neurons (Figure 4-7a), RhoVR1-PEG_{25}-HaloTag highlighted specific cells of interest and clearly presented neuronal projections from those cells in a complex network of neuronal processes (Figure 4-7b).

Having demonstrated the effectiveness of RhoVR1-PEG_{25}-HaloTag to record neuronal activity with remarkable contrast, we then compared it to the commonly used GEVIs ASAP1[18] and Ace2N-mNeon (Ace2N)[19]. Our dye outperformed both ASAP1 and Ace2N, exhibiting brighter and red-shifted membrane fluorescence at matched light powers (Figure 4-8a), turn-on responses to action potentials (ASAP1 and Ace2N-mNeon both possess turn-off responses) (Figure 4-8a) and an average $\Delta F/F$ per spike of 10.4% ± 0.2% (SNR= 16.5:1) for evoked action potentials, compared to -4.4% ± 0.1% (SNR= 10:1) per spike for ASAP1 and -1.7% ± 0.1% per spike for Ace2N (SNR= 8:1) (Figure 4-8b,c). The low SNR in the GEVIs can be explained by the appreciable amount of cytosolic fluorescence due to protein trafficking, which contributes to an elevated background or noise level. On the other hand, our genetic component, HaloTag, is non-fluorescent while the dye does not cross the membrane, thus confining all fluorescence signals to the membrane for voltage sensing.

Since the red-shifted absorbance/emission profile of the dye enables application alongside green fluorescent tools, we conducted a dual-color imaging to probe calcium and voltage responses in genetically defined cells by replacing the nuclear EGFP marker with a genetically encode calcium sensor GCaMP6s[20] (Figure 4-1). Cells of interest revealed cytosolic green fluorescence for GCaMP6s and membrane-associated red fluorescence for RhoVR1-PEG_{25}-HaloTag (Figure 4-9b-d). The cells were simultaneously excited with both blue and green light, and the resulting emission was split into GCaMP6s and RhoVR fluorescence channels[6], which allowed us to detect both the rapid changes in membrane potential and the corresponding slower increase in $[Ca^{2+}]$ during spontaneous spiking events (Figure 4-9a). In all cases, the fast voltage spike precedes the subsequent Ca^{2+} transient. Because of the fast kinetics of action potentials compared to Ca^{2+} fluctuations, the voltage trace resolves individual spiking events, which provides more information in neuronal firing, while Ca^{2+} trace lacks such resolution.

Inspired by the performance of RhoVR1-PEG_{25}-HaloTag in cultured cells, we applied the strategy in a more complex biological system. We acquired acute mouse brain slices expressing cell-surface HaloTag using in utero electroporation (IUE). The constructs used in cultured neurons with IRSE-EGFP was not suitable for IUE since the expression of EGFP was too weak to screen in neonates (data not shown); in addition, shortening the construct by removing the unnecessary IRES-EGFP is expected to improve plasmid take-up and expression in neurons (Figure 4-1a). Instead, the new construct is co-injected with either a pCAG-mTagBFP2 or pCAG-EGFP for screening purpose in neonates and in slice preparation.

The slice was loaded with 250 nM RhoVR1-PEG_{25}-HaloTag at room temperature for 15 min and z-stack images from surface of the slice to about 100 μm in depth were taken under a confocal microscopy (Figure 4-10a-c). Sparsely labeled EGFP cells were found in layer 2/3 of the cortex (Figure 4-10a). The dye concentration and brightness of staining decreased as we imaged deeper inside the tissue and was barely visible at 100 μm, suggesting that the small molecule was able to penetrate and diffuse fairly deep in the 15 min loading time (Figure 4-10b). Selective staining in EGFP-positive cells was observed but contrast was not obvious near surface of the slice where effective dye concentration was relatively high that non-specific labeling in background cells was prominent. Deeper in the slice, contrast was greatly enhanced with clear visualization of both the cell bodies and neuronal processes. Interestingly, not all EGFP-positive cells had cell-surface labeling and we hypothesize that it could be a problem with co-injection in which the separate fluorescent protein plasmid tended to express better under a stronger CAG promoter. We also confirmed the voltage sensitivity of the selectively labeled dye by performing current-clamp electrophysiology to evoke activity in the targeted cell. The recorded fluorescence trace revealed approximately 5% $\Delta F/F$ per action potential and individual spikes were resolved in single-trials (Figure 4-10d, e).

Two-photon microscopy has become popular and desirable for in vivo imaging due its long excitation wavelength that increases tissue penetration while minimizing light scattering and phototoxicity.[21-22] Since rhodamine exhibits excellent two-photon absorption[23], we conducted two-photon imaging in the slice labeled with our targeted RhoVR1-PEG_{25}-HaloTag. Although RhoVR1-PEG_{25}-HaloTag absorbs best at around 820 nm (Figure 4-11a), we still managed to visualize the stained cell at 1040 nm (Figure 4-11b), the longest wavelength available on the microscope and a preferred wavelength for in vivo imaging. Upon closer inspection, subcellular structures such as dendritic spines could be distinguished from the background (Figure 4-11c), signifying the potential of monitoring voltage activities at these defined positions. We also compared the selective staining with the non-targeted parent dye RhoVR 1, which stained all cellular membranes indiscriminately and one can only identify the cell bodies as the black holes since the dye did not enter the cytosol (Figure 4-11d). With the resolution conferred by two-photon illumination, we achieved exceptional contrast of staining in selected neurons compared to background cells, which would be useful for analyzing electrical activities in specific subset of cells. We have also conducted preliminary imaging experiments in live anesthetized mouse expressing HaloTag. The RhoVR1-PEG_{25}-HaloTag was delivered by stereotactic injection to the area of BFP marker fluorescence, followed by Z-stack imaging at 860 nm excitation. Only a few numbers of cells including neuronal projections were stained and easily distinguished from the surrounding background (Figure 4-12).

Immediate experiments involve optimizing imaging parameters to detect voltage activity in selectively stained cells in vivo.

Conclusions

We have presented the design and application of genetically targetable tetramethylrhodamine voltage indicator (RhoVR1-PEG_{25}-HaloTag) that marries the specificity of self-labeling protein HaloTag with the favorable photo-physics of small-molecule VSDs. The specificity afforded through this hybrid chemical/genetic approach enabled voltage imaging of single neurons in brain slice, a feat previously impossible with VSDs. We also demonstrated the potential of RhoVR1-PEG_{25}-HaloTag for use with two-photon microscopy that is attractive for in vivo applications due to its higher tissue penetrance and reduced photo-toxicity relative to one-photon microscopy.

Current work focuses on characterizing the voltage sensitivity of targeted RhoVR1-PEG_{25}-HaloTag in two-photon illumination as well as optimizing the labeling protocol in live animal. Meanwhile, we are preparing a HaloTag virus to enable cell-type specific expression by the Cre-loxP system and to boost the enzyme expression. Labeling of cells of interest depends on expression of enzyme on the cell surface. The 1:1 stoichiometry of indicator and enzyme will limit the total number of indicators, and therefore fluorescence intensity, on the cell surface. As a result, using a viral vector with superior transduction and expression efficiency would increase the amount of dye labeled and the signal-to-noise for voltage imaging.

Experimental Sections

Cell Culture

All animal procedures were approved by the UC Berkeley Animal Care and Use Committees and conformed to the NIH Guide for the Care and Use and Laboratory Animals and the Public Health Policy.

Human embryonic kidney 293T (HEK) cells were passaged and plated onto 12 mm glass coverslips pre-coated with Poly-D-Lysine (PDL; 1 mg/ml; Sigma-Aldrich) to provide a confluency of ~15% and 50% for electrophysiology and imaging, respectively. HEK cells were plated and maintained in Dulbecco's modified eagle medium (DMEM) supplemented with 4.5 g/L D-glucose, 10% FBS and 1% Glutamax. Transfection of genetic tools was carried out using Lipofectamine 3000 24 h after plating. Imaging was performed 18-24 h following transfection. For whole-cell patch clamp electrophysiology, cells were plated in DMEM (as above) at a density of 750,000 cells per well in a 6-well plate. Transfection of plasmids was carried out ~18-24 h after plating. The cells were split again 48 h after transfection and plated onto 12 mm glass coverslips pre-coated with Poly-D-Lysine at a density of 75,000 cells per coverslip in DMEM supplemented with 1 g/L D-glucose, 10% FBS and 1% GlutaMax. Imaging was performed 12-18 h after plating.

Hippocampi were dissected from embryonic day 19 Sprague Dawley rats (Charles River Laboratory) in cold sterile HBSS (zero Ca^{2+}, zero Mg^{2+}). All dissection products were supplied by Invitrogen, unless otherwise stated. Hippocampal tissue was treated with trypsin (2.5%) for 15 min at 37 °C. The tissue was triturated using fire polished Pasteur pipettes, in minimum essential media (MEM) supplemented with 5% fetal bovine

serum (FBS; Thermo Scientific), 2% B-27, 2% 1M D-glucose (Fisher Scientific) and 1% Glutamax. The dissociated cells were plated onto 12 mm diameter coverslips (Fisher Scientific) pre-treated with PDL at a density of 30-35,000 cells per coverslip in MEM supplemented media (as above). Neurons were maintained at 37 °C in a humidified incubator with 5 % CO_2. At 1 day in vitro (DIV) half of the MEM supplemented media was removed and replaced with Neurobasal media containing 2% B-27 supplement and 1% Glutamax. Transfection of genetic tools was carried out using Lipofectamine 3000 at 7 DIV. Functional imaging was performed on mature neurons 13-20 DIV.

In utero electroporation

Pregnant mice at E15-16 were anaesthetized with 2.0% isoflurane, the abdomen was cleaned with 70% ethanol and swabbed with iodine, and a small vertical incision was made in the skin and abdominal wall and 8–12 embryos gently exposed. Each embryo was injected with 0.5–1 μl of DNA solution and 0.05% Fast Green dye. We used a pressure-controlled beveled glass pipette (Drummond, Custom Microbeveller) for injection. After each injection, the embryos were moistened with saline and voltage steps via tweezertrodes (BTX, 5 mm round, platinum, BTX electroporator) were applied with the positive electrode placed over the visual cortex and the negative electrode placed under the head of the embryo. Voltage was 40 V for 5 pulses at 1 Hz, each pulse lasting 50 ms. The embryos were returned to the abdomen, which was sutured, followed by suturing of the skin. The procedure typically lasted under 30 min.

Acute brain slice preparation

Mice were deeply anesthetized with isoflurane and quickly decapitated. After removing the scalp and skull, ice-cold artificial cerebrospinal fluid with sucrose (ACSF-sucrose) cutting solution (in mM: NaCl, 83; KCl, 2.5; $MgSO_4$, 3.3; Na_2HPO_4, 1; $NaHCO_3$, 26.2; D-glucose, 22; sucrose, 72; and $CaCl_2$, 0.5) was applied to the brain. BFP fluorescence was checked with a hand held laser before the brain was taken out. The brain was cut into 300 μm thick slices with a DTK-1000 slicer in ice-cold sucrose cutting solution. The cut slices were incubated in sucrose cutting solution, bubbled with 95% O_2 and 5% CO_2, first at 31 °C for about 30 min and then at room temperature until further use. For bath application of the dye and cell staining, a slice was transferred to a 35 mm dish with 3mL sucrose cutting solution (total volume) bubbled with 95% O_2 and 5% CO_2 to which dye stock solution was added (250 nM final concentration). The slice was incubated with the dye at room temperature for 15 min with carbogen. For functional imaging, the slice was transferred to a fresh dish with ACSF recording solution (in mM: NaCl, 119; KCl, 2.5; $MgSO_4$, 1.3; NaH_2PO_4, 1.3; $NaHCO_3$, 26; D-glucose, 20 and $CaCl_2$, 2.5) using a plastic Pasteur pipette and washing is not necessary. A small harp or staple is used to press down the slice to minimize disturbance on the slice during perfusion and to make sure slice is flat for even illumination.

Imaging Parameters

Epifluorescence imaging was performed on an AxioExaminer Z-1 (Zeiss) equipped with a Spectra-X Light engine LED light (Lumencor), controlled with Slidebook (v6, Intelligent Imaging Innovations). Co-incident excitation with multiple LEDs was controlled by Lumencor software triggered through a Digidata 1332A digitizer and pCLAMP 10 software (Molecular Devices). Images were acquired with a W-Plan-

Apo 20x/1.0 water objective (20x; Zeiss). Images were focused onto either an OrcaFlash4.0 sCMOS camera (sCMOS; Hamamatsu) or an eVolve 128 EMCCD camera (EMCCD; Photometrix). More detailed imaging information for each experimental application is expanded below. For RhoVR images, the excitation light was delivered from a LED (1.73-9.72 W/cm^2) at 542/33 (bandpass) nm and emission was collected with a quadruple emission filter (430/32, 508/14, 586/30, 708/98 nm) after passing through a quadruple dichroic mirror (432/38, 509/22, 586/40, 654 nm LP). For EGFP images, excitation light was delivered from a LED (0.82-5.77 W/cm^2) at 475/34 nm and emission was collected with a quadruple emission filter (430/32, 508/14, 586/30, 708/98 nm) after passing through a quadruple dichroic mirror (432/38, 509/22, 586/40, 654 nm LP).

Confocal imaging was performed with a Zeiss LSM 880 NLO AxioExaminer equipped with a Diode 405 nm laser line, Argon 458, 488, and 514 laser lines, a DPSS 561 nm laser line, a HeNe 633 laser line and and a BiG-2 detector with a 690+ dichroic. Images were acquired using a W-Plan-Apo 20x/1.0 water objective and a Zeiss Airyscan detector. For 2P imaging, samples were excited using 820-1040 nm light with 2-5% laser for 820-860 nm and 100% at 1040 nm.

Unless stated otherwise, for loading of HEK cells and hippocampal neurons, 50 μM DMSO stock solutions of were diluted 1:1000 in HBSS for loading, without solubilizing reagents. All imaging experiments were performed in HBSS.

Imaging activity in cultured neurons

For evoked activity, coverslips of neurons were placed in a recording chamber containing two platinum electrodes (Warner), which were connected to a SD9 Grass Stimulator, which delivered the extracellular field stimulation. The triggering was provided through the same Digidata 1332A digitizer and pCLAMP 9 software that ran the electrophysiology. Action potentials were triggered by 1 ms 60 V field potentials delivered at 5 Hz. Synaptic blockers including 10 μM 2,3-Dioxo-6-nitro-1,2,3,4-tetrahydrobenzo[f]quinoxaline-7-sulfonamide (NBQX; Santa Cruz Biotechnology) and 25 μM DL-2-Amino-5-phosphonopentanoic acid (APV; Sigma-Aldrich) were added to the HBSS solution to prevent recurrent activity. For both evoked action potentials and spontaneous activity, images were obtained using the sCMOS camera with a 20x water objective. Images were binned 4x4 to allow sampling rates of 0.5 kHz and 2500 frames (5 s) were acquired for each recording.

In vitro two-photon cross section measurement

Measurement and calculation of two-photon cross section for the dyes were done according to the previously published protocol.[9] Briefly, all measurement were done on a confocal microscope equipped with two-photon laser. Two-photon cross section of RhoVR1-PEG$_{25}$-HaloTag was measured and calculated by comparison to a Rhodamine B standard. The dyes were diluted in PBS with 0.1% SDS (pH 7.4) in a 35 mm imaging dish. Images were acquired using a 20x water objective. The excitation was from 700 nm to 1040 nm with 10 nm increments and power at each wavelength was calculated by multiplying the percentage of laser power used and the total power of laser. Total fluorescence intensity of each acquired image was measured in ImageJ. Brightness per unit power was calculated at each wavelength for both RhoVR1-PEG$_{25}$-HaloTag and Rhodamine B. Two-photon cross section (σ_{TPE}) of a dye at a specific wavelength is

inversely proportional to its quantum yield (ϕ) and directly proportional to photon emitted at that wavelength (F, or brightness per unit power as abovementioned). Thus, σ_{TPE} of RhoVR1-PEG$_{25}$-HaloTag can be calculated according to the following equation with known values of $\phi_{\text{Rhodamine B}}$, $\phi_{\text{RhoVR1-PEG25-HaloTag}}$, $\sigma_{\text{TPE(RhodamineB)}}$ and measured brightness per unit power for both dyes:

$$\sigma_{\text{TPE}_{\text{RhoVR}}} = \frac{\phi_{\text{Rhodamine B}}}{\phi_{\text{RhoVR}}} \times \frac{F_{\text{RhoVR}}}{F_{\text{Rhodamine B}}} \times \sigma_{\text{TPE}_{\text{Rhodamine B}}}$$

where $\phi_{\text{Rhodamine B}} = 0.31$ and $\phi_{\text{RhoVR}} = 0.05$.

Dual-View imaging

Dual-view imaging was preformed using a 20x objective paired with the sCMOS camera. RhoVR1-PEG$_{25}$-HaloTag was excited using the 542 nm LED with a light intensity of 2.40-9.73 W/cm^2 while GCaMP6s was excited simultaneously using a 475 nm LED with a light intensity of 0.82-1.20 W/cm^2. Emission was collected with a QUAD filter and dichroic (see above) used in conjunction with a Dual-View emission splitter (Optical Insights). The Dual-View was equipped with a 585dcxr dichroic (Chroma) and 520/28 nm (Semrock) and 610/75 nm (Chroma) emission filters, which separated the GCaMP6s and RhoVR signals.

Image Analysis

Analysis of voltage sensitivity in HEK cells and neurons was performed using ImageJ (FIJI). Briefly, a region of interest (ROI) was selected automatically based on fluorescence intensity and applied as a mask to all image frames. Fluorescence intensity values were calculated at known baseline and voltage step epochs. ΔF/F values were calculated by first subtracting a mean background value from all raw fluorescence frames, bypassing the noise amplification which arises from subtracting background for each frame, to give a background subtracted trace (bkgsub). A baseline fluorescence value (Fbase) is calculated either from the first several (10-20) frames of the experiment for evoked activity, or from the median for spontaneous activity, and was subtracted from each timepoint of the bkgsub trace to yield a ΔF trace. The ΔF was then divided by Fbase to give ΔF/F traces. No averaging has been applied to any voltage traces.

Electrophysiology

For electrophysiological experiments, pipettes were pulled from borosilicate glass (Sutter Instruments, BF150-86-10), with a resistance of 4–8 MΩ, and were filled with an internal solution; 115 mM potassium gluconate, 10 mM BAPTA tetrapotassium salt, 10 mM HEPES, 5 mM NaCl, 10 mM KCl, 2 mM ATP disodium salt, 0.3 mM GTP trisodium salt (pH 7.25, 275 mOsm). Recordings were obtained with an Axopatch 200B amplifier (Molecular Devices) at room temperature. The signals were digitized with Digidata 1440A, sampled at 50 kHz and recorded with pCLAMP 10 software (Molecular Devices) on a PC. Fast capacitance was compensated in the on-cell configuration. For all electrophysiology experiments, recordings were only pursued if series resistance in voltage clamp was less than 30 MΩ. For whole-cell, voltage clamp recordings in HEK 293T cells, cells were held at -60 mV and 100 ms hyper- and de- polarizing steps applied from -100 to +100 mV in 20 mV increments. Imaging was performed using a 20x objective and the EMCCD camera at a sampling rate of 0.5 kHz. Dyes were excited using

the 542 nm LED with an intensity of 9.73 W/cm^2. For initial voltage characterization emission was collection with the QUAD filter and dichroic (see above). For whole-cell, current clamp in slices, experiments were conducted on the microscope set up for slice patching in the Adesnik lab. Briefly, slices were transferred to the microscope perfusion chamber with ACSF recording solution. Illumination of the samples was done by a spectra-X Light engine LED light (Lumencor), controlled with Matlab script written by the Adesnik lab. Images were acquired with a W-Plan-Apo 20x/1.0 water objective (20x; Zeiss) at a sampling rate of 1 kHz.

DNA constructs

To express the HaloTag protein on the cell surface, an IgK leader sequence was fused to the N-terminal and a transmembrane domain (pDisplay) was added to the C-terminal of the HaloTag sequence. For the purpose of inmmunostaining, an HA tag was inserted. Mammalian expression vector pcDNA3 with either a cytomegalovirus (CMV) promoter or human synapsin promoter (Syn) was used for protein expression in HEK cells and cultured neurons, respectively. To increase expression in neurons, a regulatory element from the woodchuck hepatitis virus (WPRE) was used. In some constructs, nuclear-targeted EGFP (NLS-EGFP) was inserted down stream of HaloTag, separated by an internal ribosome entry site (IRES) sequence, in order to track the expression of HaloTag in live cells. For dual voltage and calcium imaging, a GCaMP6s with an IRES sequence was inserted down stream of HaloTag. The cloned constructs were verified by sequencing. All the constructs were prepared using Qiagen Maxiprep kit, except those with CMV promoter. The following sequences were used (5' to 3'):

IgK

ATGGAGACAGACACACTCCTGCTATGGGTACTGCTGCTCTGGGTTCCAGGTTC
CACTGGTGAC

HaloTag

GCAGAAATCGGTACTGGCTTTCCATTCGACCCCCATTATGTGGAAGTCCTGGG
CGAGCGCATGCACTACGTCGATGTTGGTCCGCGCGATGGCACCCCTGTGCTG
TTCCTGCACGGTAACCCGACCTCCTCCTACGTGTGGCGCAACATCATCCCGCA
TGTTGCACCGACCCATCGCTGCATTGCTCCAGACCTGATCGGTATGGGCAAAT
CCGACAAACCAGACCTGGGTTATTTCTTCGACGACCACGTCCGCTTCATGGAT
GCCTTCATCGAAGCCCTGGGTCTGGAAGAGGTCGTCCTGGTCATTCACGACTG
GGGCTCCGCTCTGGGTTTCCACTGGGCCAAGCGCAATCCAGAGCGCGTCAAA
GGTATTGCATTTATGGAGTTCATCCGCCCTATCCCGACCTGGGACGAATGGCC
AGAATTTGCCCGCGAGACCTTCCAGGCCTTCCGCACCACCGACGTCGGCCGC
AAGCTGATCATCGATCAGAACGTTTTTATCGAGGGTACGCTGCCGATGGGTG
TCGTCCGCCCGCTGACTGAAGTCGAGATGGACCATTACCGCGAGCCGTTCCT
GAATCCTGTTGACCGCGAGCCACTGTGGCGCTTCCCAAACGAGCTGCCAATC
GCCGGTGAGCCAGCGAACATCGTCGCGCTGGTCGAAGAATACATGGACTGGC
TGCACCAGTCCCCTGTCCCGAAGCTGCTGTTCTGGGGCACCCCAGGCGTTCTG
ATCCCACCGGCCGAAGCCGCTCGCCTGGCCAAAAGCCTGCCTAACTGCAAGG
CTGTGGACATCGGCCCGGGTCTGAATCTGCTGCAAGAAGACAACCCGGACCT
GATCGGCAGCGAGATCGCGCGCTGGCTGTCGACGCTCGAGATTTCCGGC

HA
TATCCATATGATGTTCCAGATTATGCT

DAF
CCAAATAAAGGAAGTGGAACCACTTCAGGTACTACCCGTCTTCTATCTGGGC
ACACGTGTTTCACGTTGACAGGTTTGCTTGGGACGCTAGTAACCATGGGCTTG
CTGACTTAG

pDisplay
GCTGTGGGCCAGGACACGCAGGAGGTCATCGTGGTGCCACACTCCTTGCCCT
TTAAGGTGGTGGTGATCTCAGCCATCCTGGCCCTGGTGGTGCTCACCATCATC
TCCCTTATCATCCTCATCATGCTTTGGCAGAAGAAGCCACGT

IRES
GCCCCTCTCCCTCCCCCCCCCCTAACGTTACTGGCCGAAGCCGCTTGGAATAA
GGCCGGTGTGCGTTTGTCTATATGTTATTTTCCACCATATTGCCGTCTTTTGGC
AATGTGAGGGCCCGGAAACCTGGCCCTGTCTTCTTGACGAGCATTCCTAGGG
GTCTTTCCCCTCTCGCCAAAGGAATGCAAGGTCTGTTGAATGTCGTGAAGGA
AGCAGTTCCTCTGGAAGCTTCTTGAAGACAAACAACGTCTGTAGCGACCCTTT
GCAGGCAGCGGAACCCCCCACCTGGCGACAGGTGCCTCTGCGGCCAAAAGCC
ACGTGTATAAGATACACCTGCAAAGGCGGCACAACCCCAGTGCCACGTTGTG
AGTTGGATAGTTGTGGAAAGAGTCAAATGGCTCTCCTCAAGCGTATTCAACA
AGGGGCTGAAGGATGCCCAGAAGGCACCCCATTGTATGGGATCTGATCTGGG
GCCTCGGTGCACATGCTTTACATGTGTTTAGTCGAGGTTAAAAAAACGTCTAG
GCCCCCCGAACCACGGGGACGTGGTTTTCCTTTGAAAAACACGATGATAATA
TGGCCACA

NLS-EGFP
ATGGTGCCCAAGAAGAAGAGGAAAGTCAGCAAGGGCGAGGAGCTGTTCACG
GGGTGGTGCCCATCCTGGTCGAGCTGGACGGCGACGTAAACGGCCACAAGTT
CAGCGTGTCCGGCGAGGGCGAGGGCGATGCCACCTACGGCAAGCTGACCCTG
AAGTTCATCTGCACCACCGGCAAGCTGCCCGTGCCCTGGCCCACCCTCGTGA
CCACCCTGACCTACGGCGTGCAGTGCTTCAGCCGCTACCCCGACCACATGAA
GCAGCACGACTTCTTCAAGTCCGCCATGCCCGAAGGCTACGTCCAGGAGCGC
ACCATCTTCTTCAAGGACGACGGCAACTACAAGACCCGCGCCGAGGTGAAGT
TCGAGGGCGACACCCTGGTGAACCGCATCGAGCTGAAGGGCATCGACTTCAA
GGAGGACGGCAACATCCTGGGGCACAAGCTGGAGTACAACTACAACAGCCA
CAACGTCTATATCATGGCCGACAAGCAGAAGAACGGCATCAAGGTGAACTTC
AAGATCCGCCACAACATCGAGGACGGCAGCGTGCAGCTCGCCGACCACTACC
AGCAGAACACCCCCATCGGCGACGGCCCCGTGCTGCTGCCCGACAACCACTA
CCTGAGCACCCAGTCCGCCCTGAGCAAAGACCCCAACGAGAAGCGCGATCAC
ATGGTCCTGCTGGAGTTCGTGACCGCCGCCGGGATCACTCTCGGCATGGACG
AGCTGTACAAG

GCaMP6s
ATGGGTTCTCATCATCATCATCATCATGGTATGGCTAGCATGACTGGTGGACA

GCAAATGGGTCGGGATCTGTACGACGATGACGATAAGGATCTCGCCACCATG
GTCGACTCATCACGTCGTAAGTGGAATAAGACAGGTCACGCAGTCAGAGCTA
TAGGTCGGCTGAGCTCACTCGAGAACGTCTATATCAAGGCCGACAAGCAGAA
GAACGGCATCAAGGCGAACTTCCACATCCGCCACAACATCGAGGACGGCGG
CGTGCAGCTCGCCTACCACTACCAGCAGAACACCCCCATCGGCGACGGCCCC
GTGCTGCTGCCCGACAACCACTACCTGAGCGTGCAGTCCAAACTTTCGAAAG
ACCCCAACGAGAAGCGCGATCACATGGTCCTGCTGGAGTTCGTGACCGCCGC
CGGGATCACTCTCGGCATGGACGAGCTGTACAAGGGCGGTACCGGAGGGAG
CATGGTGAGCAAGGGCGAGGAGCTGTTCACCGGGGTGGTGCCCATCCTGGTC
GAGCTGGACGGCGACGTAAACGGCCACAAGTTCAGCGTGTCCGGCGAGGGT
GAGGGCGATGCCACCTACGGCAAGCTGACCCTGAAGTTCATCTGCACCACCG
GCAAGCTGCCCGTGCCCTGGCCCACCCTCGTGACCACCCTGACCTACGGCGT
GCAGTGCTTCAGCCGCTACCCCGACCACATGAAGCAGCACGACTTCTTCAAG
TCCGCCATGCCCGAAGGCTACATCCAGGAGCGCACCATCTTCTTCAAGGACG
ACGGCAACTACAAGACCCGCGCCGAGGTGAAGTTCGAGGGCGACACCCTGG
TGAACCGCATCGAGCTGAAGGGCATCGACTTCAAGGAGGACGGCAACATCCT
GGGGCACAAGCTGGAGTACAACCTGCCGGACCAACTGACTGAAGAGCAGAT
CGCAGAATTTAAAGAGGCTTTCTCCCTATTTGACAAGGACGGGGATGGGACA
ATAACAACCAAGGAGCTGGGGACGGTGATGCGGTCTCTGGGGCAGAACCCC
ACAGAAGCAGAGCTGCAGGACATGATCAATGAAGTAGATGCCGACGGTGAC
GGCACAATCGACTTCCCTGAGTTCCTGACAATGATGGCAAGAAAAATGAAAT
ACAGGGACACGGAAGAAGAAATTAGAGAAGCGTTCGGTGTGTTTGATAAGG
ATGGCAATGGCTACATCAGTGCAGCAGAGCTTCGCCACGTGATGACAAACCT
TGGAGAGAAGTTAACAGATGAAGAGGTTGATGAAATGATCAGGGAAGCAGA
CATCGATGGGGATGGTCAGGTAAACTACGAAGAGTTTGTACAAATGATGACA
GCGAAGTGA

WPRE

GCTTATCGATAATCAACCTCTGGATTACAAAATTTGTGAAAGATTGACTGGTA
TTCTTAACTATGTTGCTCCTTTTACGCTATGTGGATACGCTGCTTTAATGCCTT
TGTATCATGCTATTGCTTCCCGTATGGCTTTCATTTTCTCCTCCTTGTATAAAT
CCTGGTTGCTGTCTCTTTATGAGGAGTTGTGGCCCGTTGTCAGGCAACGTGGC
GTGGTGTGCACTGTGTTTGCTGACGCAACCCCCACTGGTTGGGGCATTGCCAC
CACCTGTCAGCTCCTTTCCGGGACTTTCGCTTTCCCCCTCCCTATTGCCACGGC
GGAACTCATCGCCGCCTGCCTTGCCCGCTGCTGGACAGGGGCTCGGCTGTTG
GGCACTGACAATTCCGTGGTGTTGTCGGGGAAATCATCGTCCTTTCCTTGGCT
GCTCGCCTGTGTTGCCACCTGGATTCTGCGCGGGACGTCCTTCTGCTACGTCC
CTTCGGCCCTCAATCCAGCGGACCTTCCTTCCCGCGGCCTGCTGCCGGCTCTG
CGGCCTCTTCCGCGTCTTCGCCTTCGCCCTCAGACGAGTCGGATCTCCCTTTG
GGCCGCCTCCCCGCATCGATACCG

CMV promoter

GACATTGATTATTGACTAGTTATTAATAGTAATCAATTACGGGGTCATTAGTT
CATAGCCCATATATGGAGTTCCGCGTTACATAACTTACGGTAAATGGCCCGCC
TGGCTGACCGCCCAACGACCCCCGCCCATTGACGTCAATAATGACGTATGTT
CCCATAGTAACGCCAATAGGGACTTTCCATTGACGTCAATGGGTGGACTATTT

ACGGTAAACTGCCCACTTGGCAGTACATCAAGTGTATCATATGCCAAGTACG
CCCCCTATTGACGTCAATGACGGTAAATGGCCCGCCTGGCATTATGCCCAGT
ACATGACCTTATGGGACTTTCCTACTTGGCAGTACATCTACGTATTAGTCATC
GCTATTACCATGGTGATGCGGTTTTGGCAGTACATCAATGGGCGTGGATAGC
GGTTTGACTCACGGGGATTTCCAAGTCTCCACCCCATTGACGTCAATGGGAGT
TTGTTTTGGCACCAAAATCAACGGGACTTTCCAAAATGTCGTAACAACTCCGC
CCCATTGACGCAAATGGGCGGTAGGCGTGTACGGTGGGAGGTCTATATAAGC
AGAGCT

Synapsin Promoter
GTGTCTAGACTGCAGAGGGCCCTGCGTATGAGTGCAAGTGGGTTTTAGGACC
AGGATGAGGCGGGGTGGGGGTGCCTACCTGACGACCGACCCCGACCCACTG
GACAAGCACCCAACCCCCATTCCCCAAATTGCGCATCCCCTATCAGAGAGGG
GGAGGGGAAACAGGATGCGGCGAGGCGCGTGCGCACTGCCAGCTTCAGCAC
CGCGGACAGTGCCTTCGCCCCCGCCTGGCGGCGCGCGCCACCGCCGCCTCAG
CACTGAAGGCGCGCTGACGTCACTCGCCGGTCCCCCGCAAACTCCCCTTCCC
GGCCACCTTGGTCGCGTCCGCGCCGCCGCCGGCCCAGCCGGACCGCACCACG
CGAGGCGCGAGATAGGGGGGCACGGGCGCGACCATCTGCGCTGCGGCGCCG
GCGACTCAGCGCTGCCTCAGTCTGCGGTGGGCAGCGGAGGAGTCGTGTCGTG
CCTGAGAGCGCAGTCGAGA

Benchling links for constructs

CMV-IgK-HaloTag-HA-pDisplay-IRES-EGFP
https://benchling.com/s/seq-hnmTQqUI6MJ8uOIEuXa8

Synapsin-IgK-HaloTag-HA-pDisplay-IRES-EGFP-WPRE
https://benchling.com/s/seq-kCT5loPFZtiFqYywoksg

Synapsin-IgK-HaloTag-HA-pDisplay-IRES-GCaMP6s-WPRE
https://benchling.com/s/seq-ibK9qbzeFVNIJeaz6LmV

Synapsin-IgK-HaloTag-HA-pDisplay-WPRE
https://benchling.com/s/seq-zWvHNSFd26mff9OStRXg

Figures and Schemes

Scheme 4-1. *Design of covalent labeling of RhoVR dyes in specific cells of interest.*

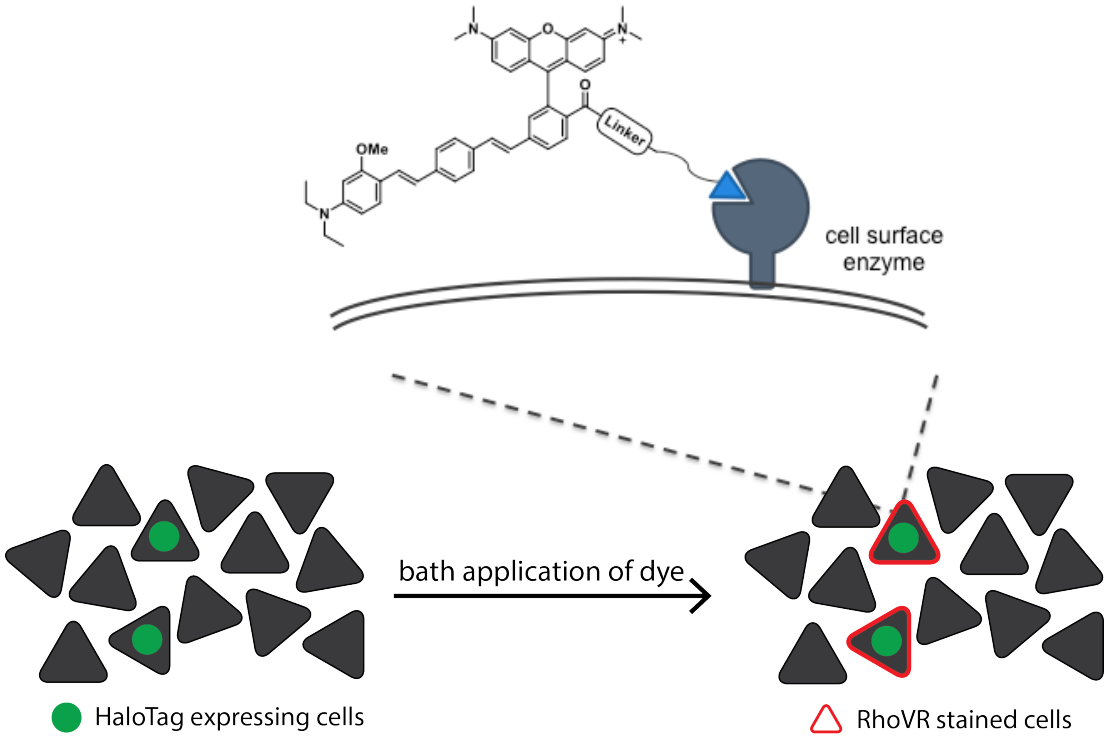

Scheme 4-1. Scheme of neuron-specific targeting with cell-surface HaloTag and RhoVR-HaloTag (components are not to scale).

Scheme 4-2. *Structures of RhoVR-HaloTag dyes used in this study.*

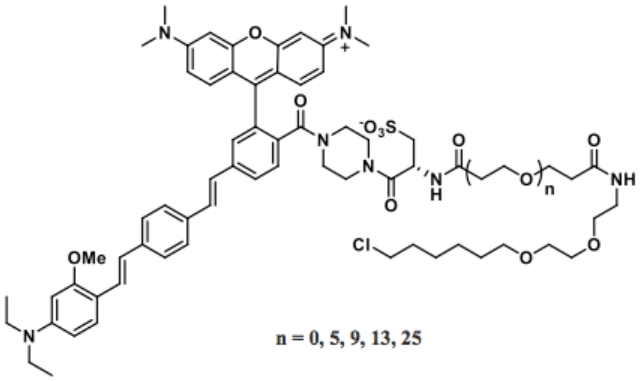

Scheme 4-2. Structures of RhoVR1-PEG$_x$-HaloTag with variable linker size synthesized and tested in the covalent labeling strategy.

Figure 4-1. *HaloTag constructs used in this study and characterization in HEK cells.*

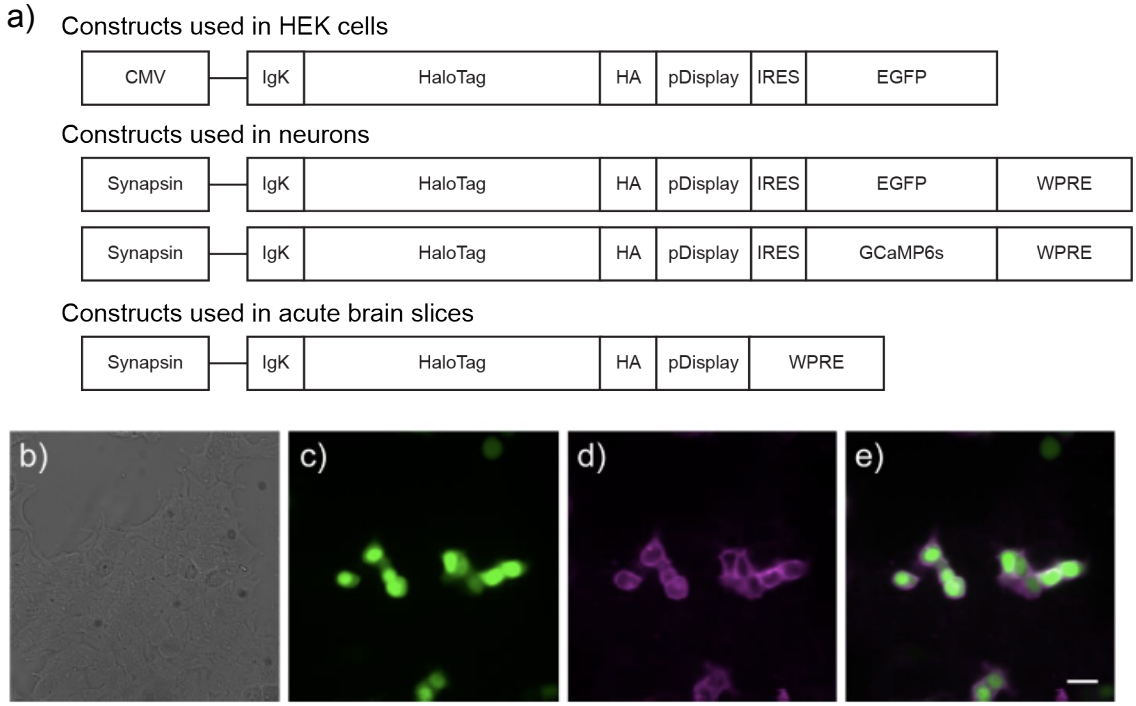

Figure 4-1. Engineering a cell-surface HaloTag for covalent labeling of RhoVR-HaloTag dyes. (a) HaloTag constructs used in this study. (b-e) Selective staining of TMR-PEG_{13}-HaloTag in HEK cells sparsely transfected with HaloTag-pDisplay construct. (b) Differential interference contrast (DIC) images of HEK cells. (c) Nuclear EGFP fluorescence indicates HaloTag expression. (d) Membrane-associated fluorescence is observed in specific cells after bath application of 200 nM dye for 30 min at 37 °C. (e) Merge of EGFP and TMR fluorescence confirms good association between cell-surface staining and HaloTag expression. Scale bar is 20 μm.

Figure 4-2. *Characterization of RhoVR-PEG$_x$- HaloTag brightness in HEK cells.*

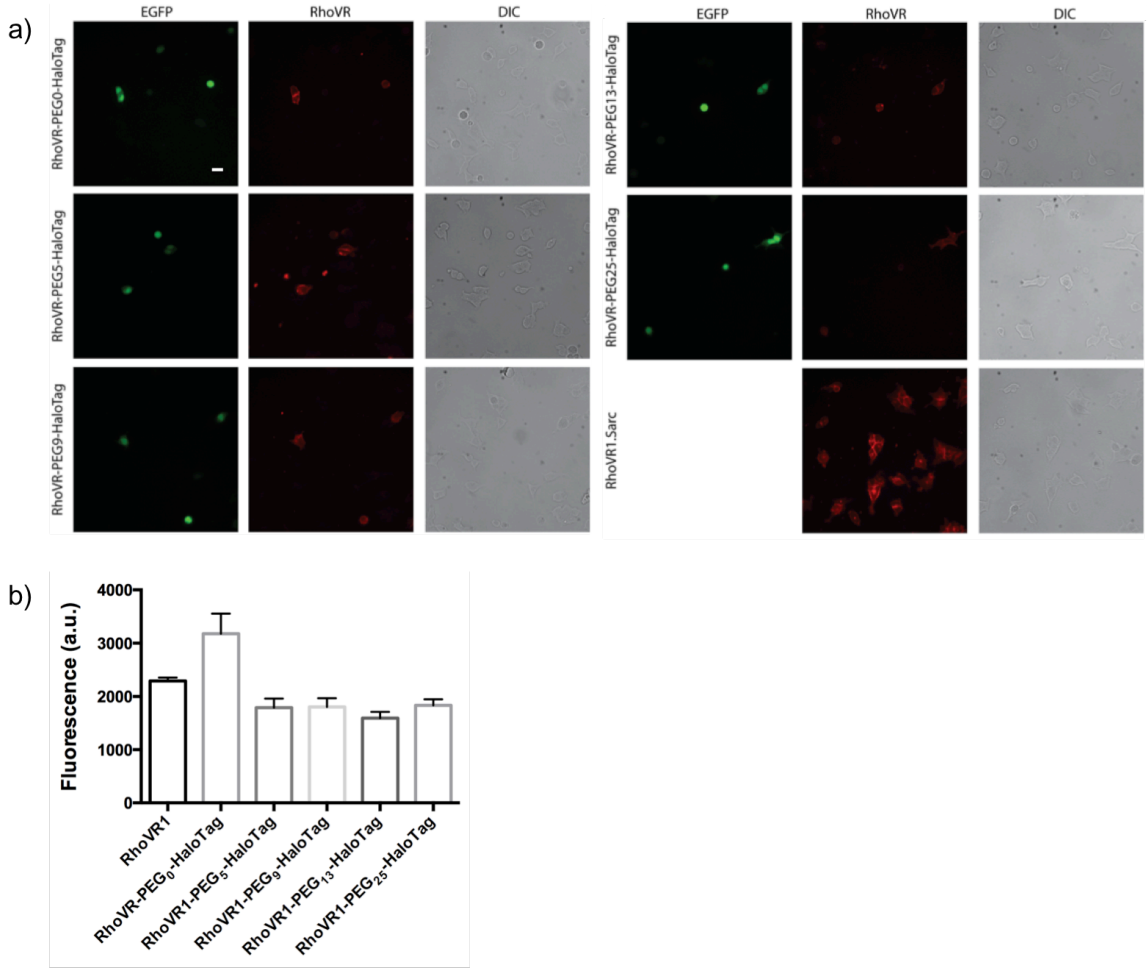

Figure 4-2. Comparing brightness of RhoVR1-PEG$_x$-HaloTag dyes in HEK cells. (a) RhoVR1-PEG$_x$-HaloTag dyes exhibit membrane-associated fluorescence that matches nuclear EGFP, which indicates HaloTag expression. RhoVR1, as a control, stained all cells non-selectively. All dyes were loaded at 50 nM at 37 °C for 30 min. Scale bar is 20 μm. (b) Quantification of fluorescence staining for all the dyes (n = 20 cells for each dye). Error bars are ±S.E.M.

Figure 4-3. *Characterization of RhoVR-PEG$_x$-HaloTag voltage sensitivity in HEK cells.*

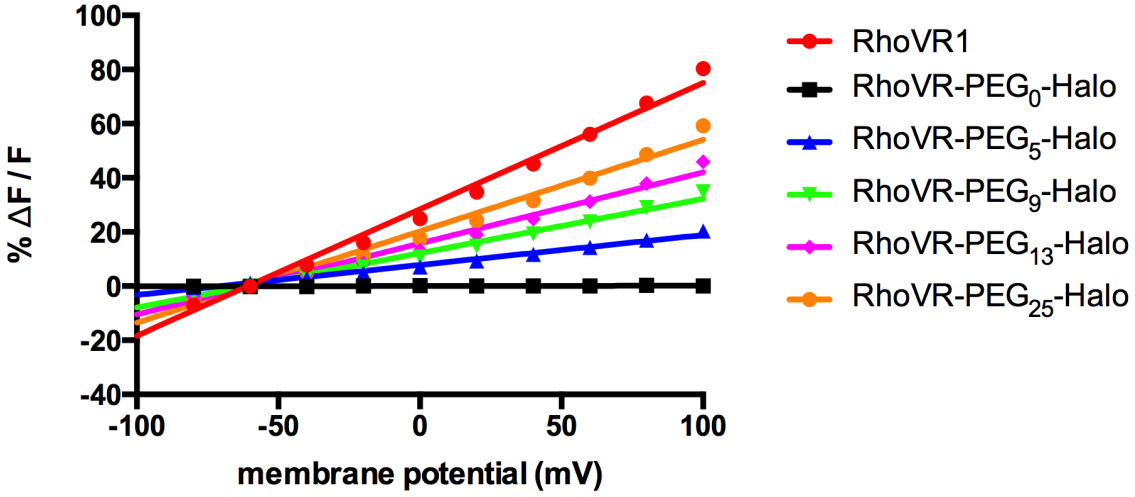

Figure 4-3. Voltage-sensitivity plot (% ΔF/F vs mV) of RhoVR-HaloTag dyes of variable linker lengths. Whole-cell voltage clamp electrophysiology was performed to step the membrane potential from -100 mV to +100 mV with 20 mV increments while fluorescence change was monitored (n = 3-9 cells per dye, error bars not shown). Increasing linker length improved voltage sensitivity with a maximum of 34% % ΔF/F per 100mV for PEG$_{25}$ dye.

Figure 4-4. *Characterization of RhoVR1-PEG$_{25}$-HaloTag localization in HEK cells.*

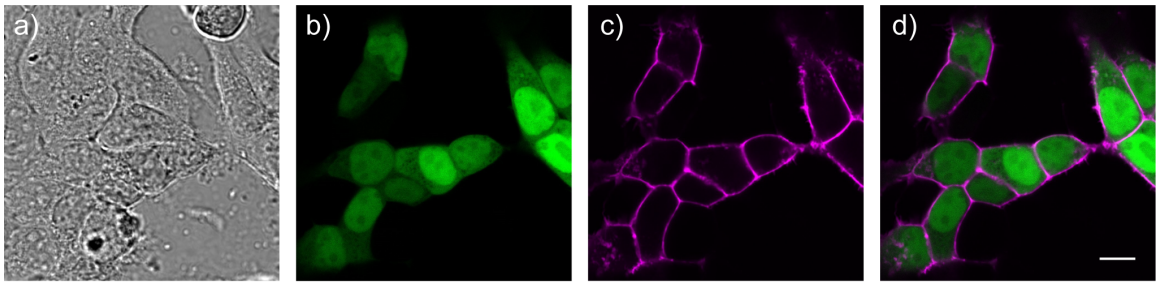

Figure 4-4. Confocal microscope imaging of RhoVR1-PEG$_{25}$-HaloTag in HEK cells. (a) DIC images of HEK cells transfected with HaloTag-pDisplay construct. (b) Nuclear EGFP fluorescence indicates HaloTag expression in a few selected cells among densely packed cells. d) Membrane-associated and high-contrast fluorescence is observed in specific cells after bath application of 50 nM RhoVR1-PEG$_{25}$-HaloTag for 30 min at 37 °C. (e) Merge of EGFP and RhoVR-HaloTag fluorescence confirms good association between bright, cell-surface staining and HaloTag expression. Scale bar is 10 μm.

Figure 4-5. *Characterization of RhoVR1-PEG$_{25}$-HaloTag staining in cultured neurons.*

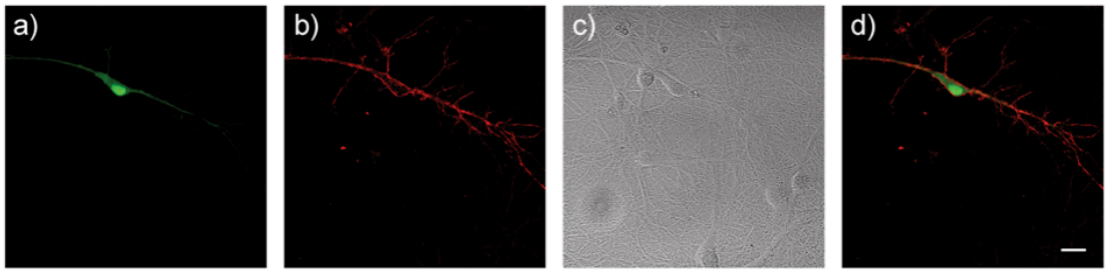

Figure 4-5. Confocal microscopy imaging of RhoVR1-PEG$_{25}$-HaloTag staining in cultured hippocampal neurons. Both dyes were loaded at 50 nM at 37 °C for 30 min. Selective staining of RhoVR1-PEG$_{25}$-HaloTag (a-d) in neuronal culture sparsely transfected with HaloTag. (a) Nuclear EGFP fluorescence indicates HaloTag expression. (b) Membrane-associated and high-contrast fluorescence is observed in a specific cell. (c) DIC images of cultured neurons. (d) Merge of EGFP and RhoVR-HaloTag fluorescence confirms good association between bright, cell-surface staining and HaloTag expression. Scale bar is 20 μm.

Figure 4-6. *Functional imaging with RhoVR1-PEG$_{25}$-HaloTag in cultured neurons.*

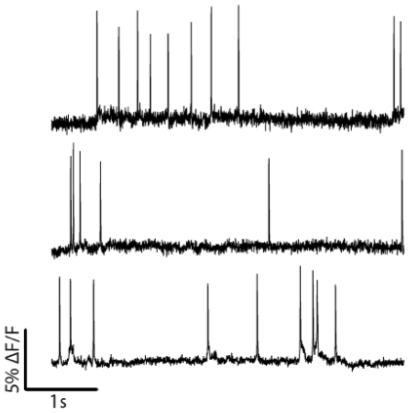

Figure 4-6. Recording neuronal activity by RhoVR1-PEG$_{25}$-HaloTag in cultured hippocampal neurons. Representative traces of spontaneous spiking events in neurons as shown by RhoVR1-PEG$_{25}$-HaloTag.

Figure 4-7. *Characterization of BeRST 1 and RhoVR1-PEG$_{25}$-HaloTag in cultured neurons.*

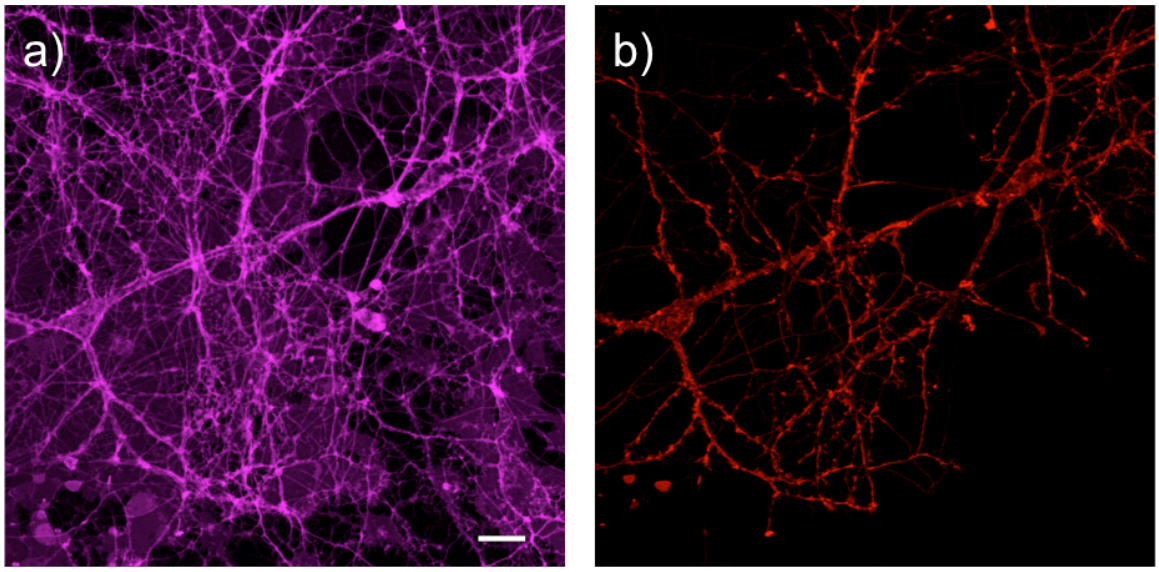

Figure 4-7. Confocal microscopy imaging of (a) non-targeted far-red dye BeRST1 and (b) targeted dye RhoVR1-PEG$_{25}$-HaloTag co-stained in the same neuronal culture. While BeRST1 shows uniform, non-selective staining in the field of view, RhoVR1-PEG$_{25}$-HaloTag highlights only two cells of interest with clear visualization of their respective neuronal projections. Scale bar is 20 μm.

Figure 4-8. *Characterization of RhoVR1-PEG$_{25}$-HaloTag with genetically encoded voltage indicators (GEVIs).*

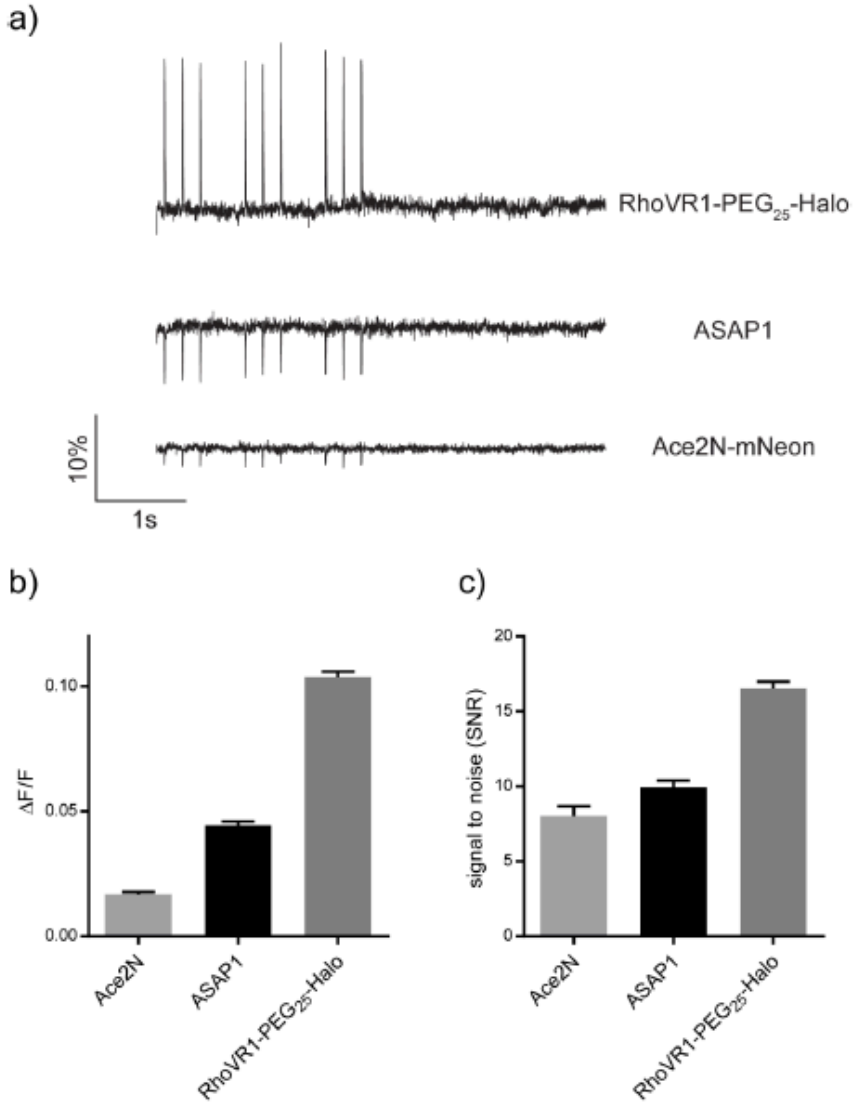

Figure 4-8: Comparing of RhoVR1-PEG$_{25}$-HaloTag with GEVIs ASAP1 and Ace2N-mNeon. (a) Representative voltage recordings of evoked activity measured with the voltage reporters. Voltage traces were acquired with identical parameters and matched light power. RhoVR1-PEG$_{25}$-HaloTag outperforms the GEVIs with improved voltage sensitivities (b) and signal-to-noise ratio (c) measured from averages of individual evoked spike (n=77-205). Error bars are ± S.E.M.

Figure 4-9. *Simultaneous calcium and voltage imaging using GCaMP6s and RhoVR1-PEG_{25}-HaloTag.*

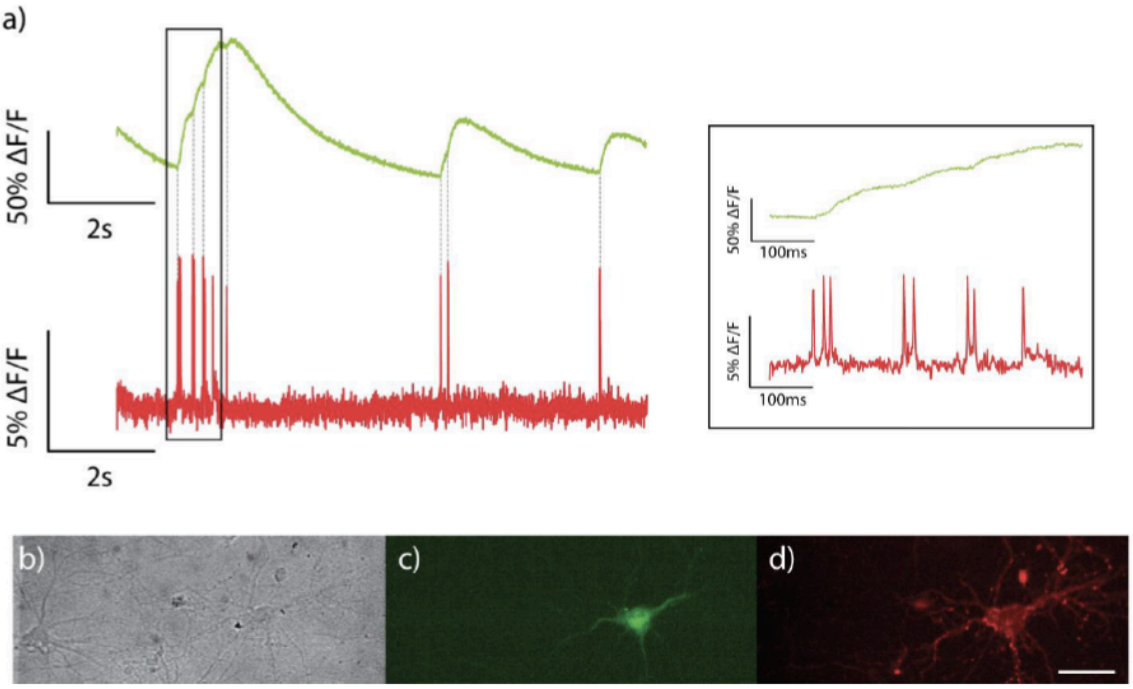

Figure 4-9. Recording spontaneous activity using a dual-view set-up for both calcium and voltage responses. (a) The green trace represents Ca^{2+} fluctuations recorded by a genetically encoded calcium indicator GCaMP6s. The red trace represents voltage changes recorded by RhoVR1-PEG_{25}-HaloTag. The inset shows an expanded time scale of the boxed region. (b) DIC image of cultured neurons. (c) Cytosolic fluorescence from GCaMP6s. (d) Membrane-associated fluorescence from RhoVR1-PEG_{25}-HaloTag. Scale bar is 50 μm.

Figure 4-10. *Imaging RhoVR1-PEG$_{25}$-HaloTag in mouse brain slice.*

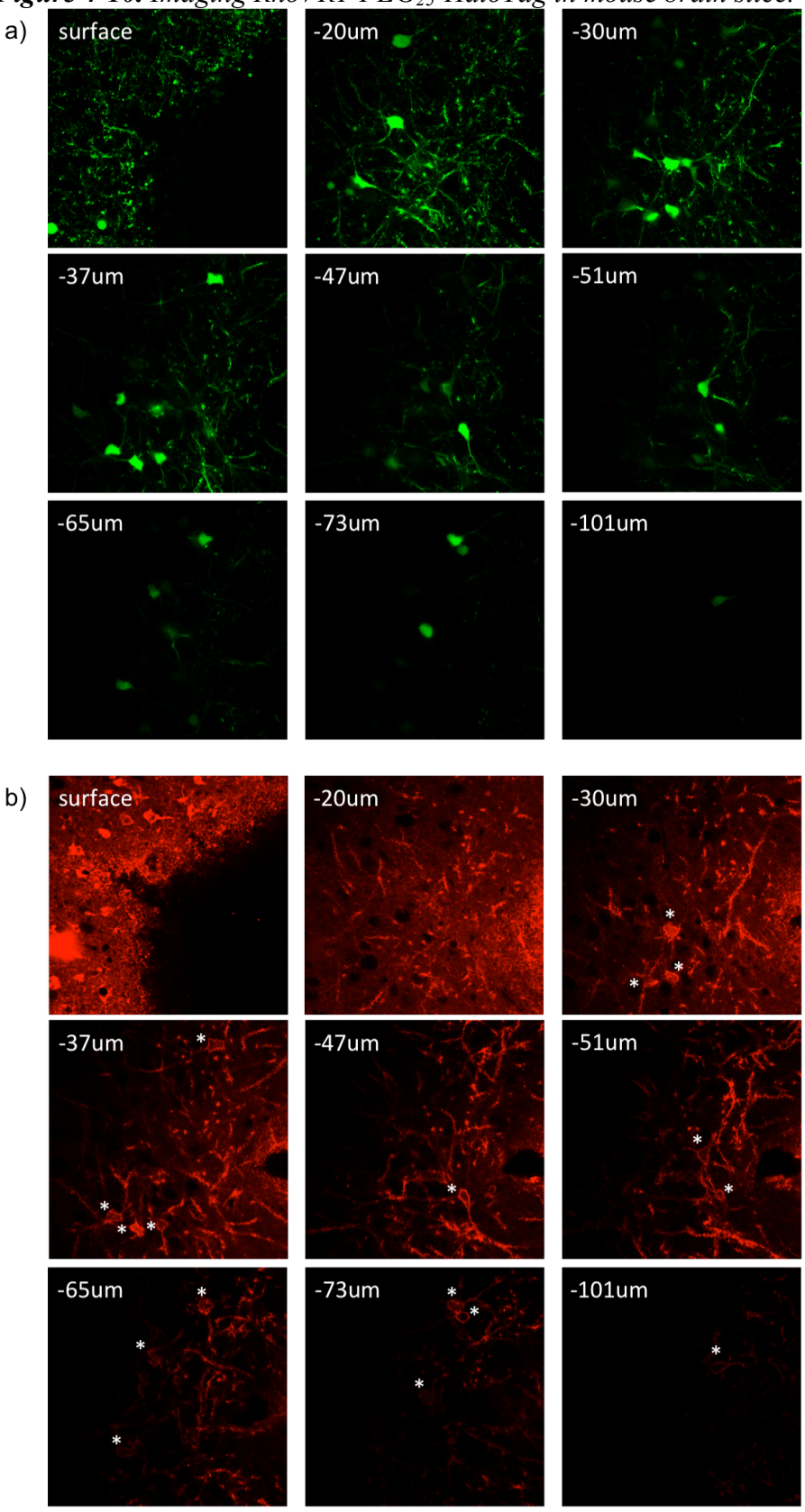

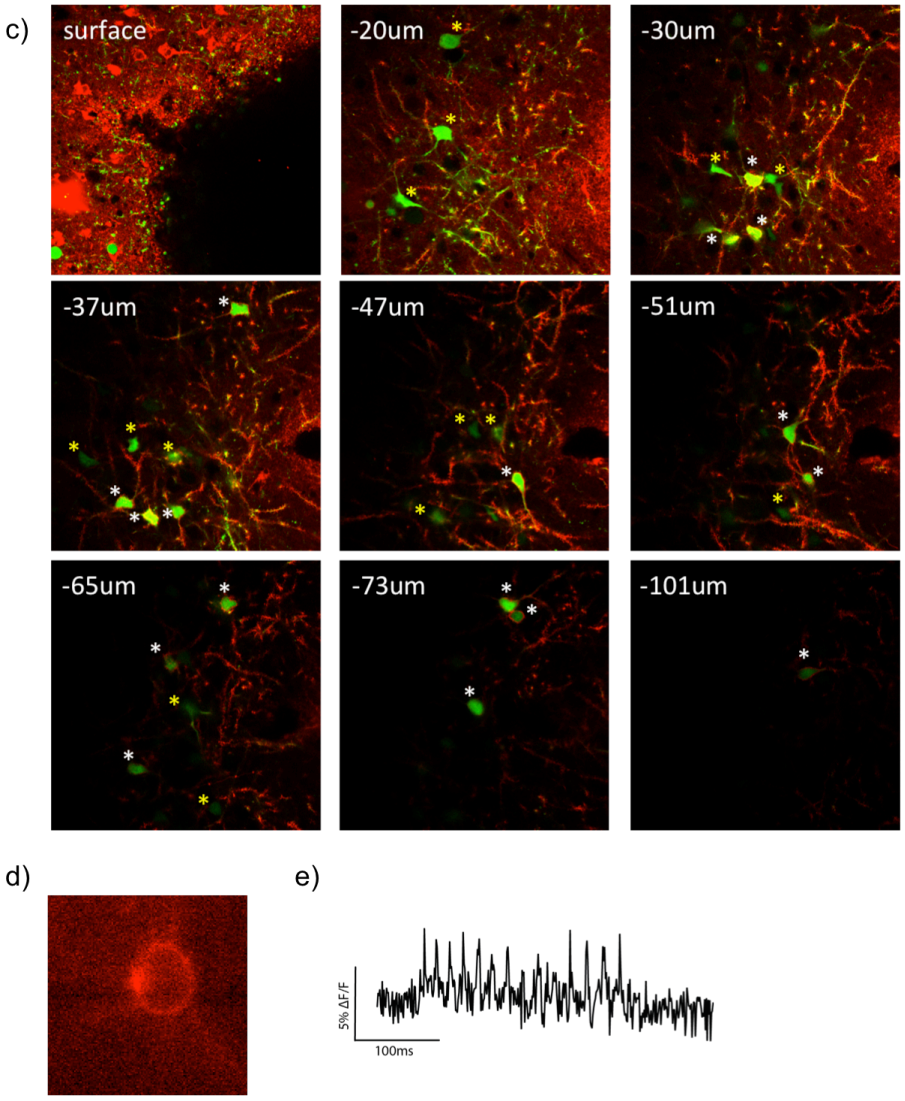

Figure 4-10. One-photon confocal microscopy imaging of RhoVR1-PEG$_{25}$-HaloTag in mouse brain slice expressing HaloTag-pDisplay and pCAG-EGFP following in utero electroporation. Z-stack imaging was conducted from surface of the slice to deeper into the tissue and the depth relevant to the surface was indicated in each image. (a) EGFP was used for screening positive pups and expressing slices. (b) RhoVR staining shows membrane-associated fluorescence in selected cells that express EGFP and exhibits high contrast with respect to background and non-transfected cells. White asterisks indicate cell bodies of neurons with selective staining. (c) Merge images of EGFP and RhoVR channels. Yellow asterisks indicate neurons expressing only EGFP without RhoVR staining. (d) Wide-field fluorescence image of RhoVR stained slice acquired during patch-clamp electrophysiology. (e) Representative ΔF/F trace of evoked voltage activity recorded by RhoVR1-PEG$_{25}$-HaloTag in a neuron patch-clamped for current injection. Images are acquired at 1 kHz and represent single-trial acquisitions.

Figure 4-11. *Two-photon imaging of RhoVR1-PEG$_{25}$-HaloTag mouse brain slice.*

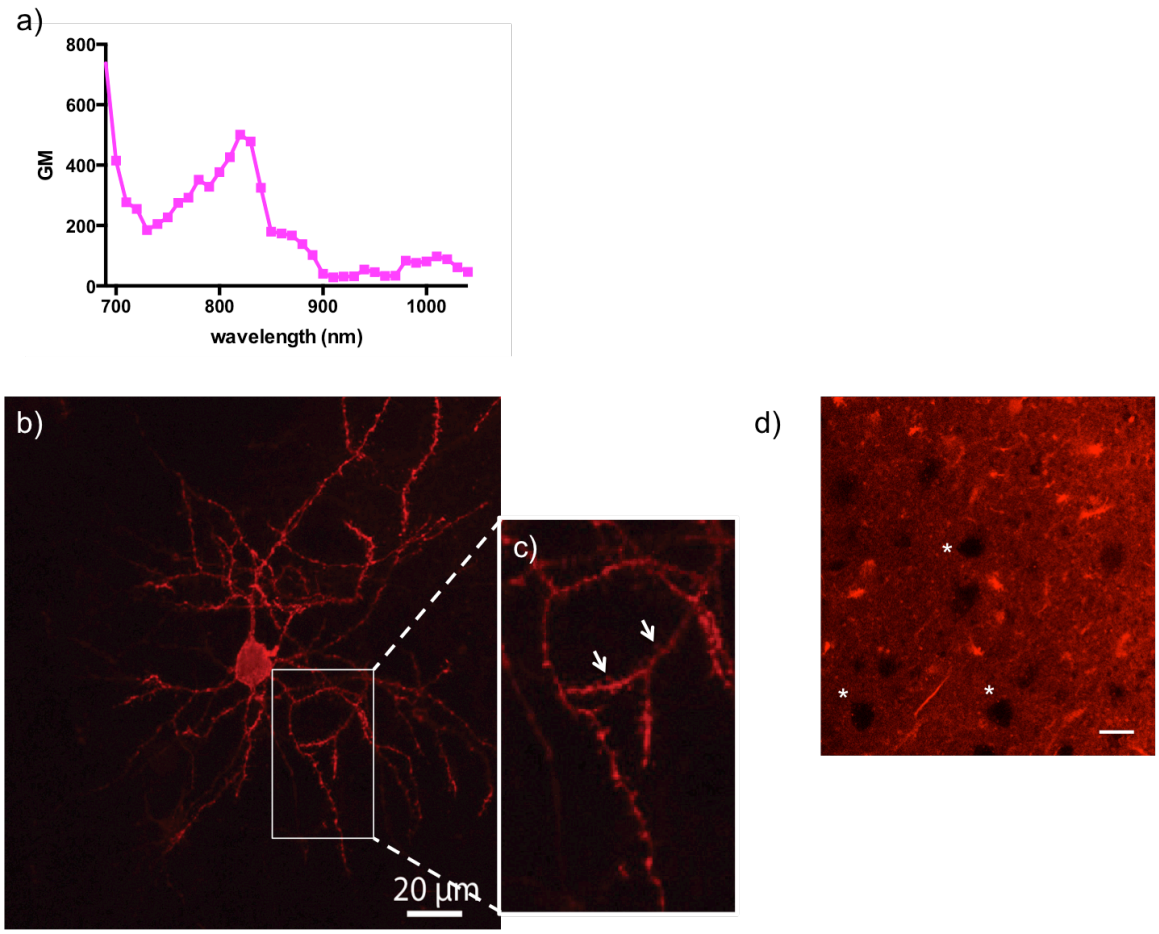

Figure 4-11. Two-photon imaging of RhoVR1-PEG$_{25}$-HaloTag (a) in vitro and (b-c) in mouse brain slice stained (250 nM, 15 min at RT). (a) Two-photon cross-section (GM) was measured at 500 nM in PBS with 0.1% SDS. (b) Two-photon laser at 1040 nm was used to excite and visualize the sample. In this region of interest, only one neuron expresses HaloTag and gets labele. A closer inspection (c) reveals its projections and subcellular structures such as dendritic spines (white arrows). (d) Representative image of non-targeted parent dye RhoVR1 in brain slice White asterisks indicate cell bodies. Scale bar is 20 µm.

Figure 4-12. *Imaging RhoVR1-PEG$_{25}$-HaloTag in live anesthetized mouse.*

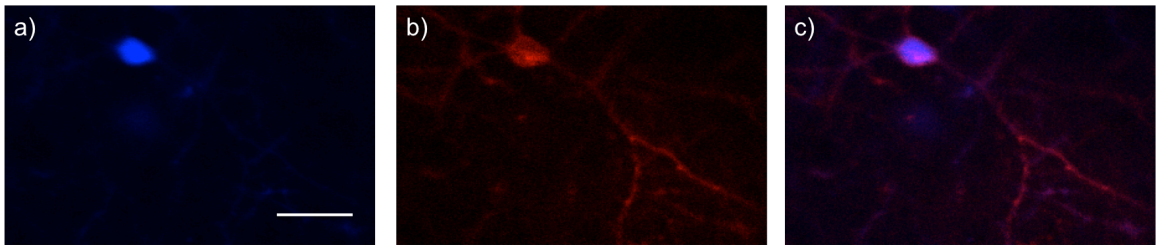

Figure 4-12. Two-photon imaging of RhoVR1-PEG$_{25}$-HaloTag in live anesthetized mouse expressing Syn-HaloTag-pDisplay and pCAG-mTagBFP2. (a) BFP fluorescence indicates HaloTag expression. (b) RhoVR staining shows membrane-associated signal in selected cells with high contrast with respect to background and non-transfected cells. (c) Merge image of cytosolic BFP and membrane-associated RhoVR fluorescence. Scale bar is 20 μm

Reference

1. Miller, E. W., *Curr. Opin. Chem. Biol.* **2016**, *33*, 74-80.
2. Yang, H. H.; St-Pierre, F., *J. Neurosci.* **2016**, *36* (39), 9977-9989.
3. Bando, Y.; Sakamoto, M.; Kim, S.; Ayzenshtat, I.; Yuste, R., Cell Reports **2019**, *26* (3), 802-813.
4. Xu, Y.; Zou, P; Cohen, A. E.; *Curr. Opin. Chem. Biol*. **2017**, *39*, 1-10.
5. Miller, E. W.; Lin, J. Y.; Frady, E. P.; Steinbach, P. A.; Kristan, W. B., Jr.; Tsien, R. Y., *Proc Natl Acad Sci U S A* **2012,** *109* (6), 2114-9.
6. Deal, P. E.; Kulkarni, R. U.; Al-Abdullatif, S. H.; Miller, E. W., *J. Am. Chem. Soc.* **2016**, *138* (29), 9085-9088.
7. Huang, Y. L.; Walker, A. S.; Miller, E. W., *J. Am. Chem. Soc.* **2015**, *137* (33), 10767-10776.
8. Boggess, S. C.; Gandhi, S. S.; Siemons, B. A.; Huebsch, N.; Healy, K. E.; Miller, E. W., *ACS Chem. Biol.* **2019**, *14* (3) 390-396.
9. Kulkarni, R. U.; Kramer, D. J.; Pourmandi, N.; Karbasi, K.; Bateup, H. S.; Miller, E. W., *Proc. Natl. Acad. Sci. U. S. A.* **2017**, *114* (11), 2813-2818.
10. Grenier, V.; Walker, A. S.; Miller, E. W., *J. Am. Chem. Soc.* **2015,** *137* (34), 10894-10897.
11. Liu, P.; Grenier, V.; Hong, W.; Muller, V. R.; Miller, E. W., *J. Am. Chem. Soc.* **2017**, *139*, 17334-17340.
12. Ortiz, G.; Liu, P.; Naing, S. H. H.; Muller, V. R.; Miller, E. W., *J. Am. Chem. Soc.* **2019**, *141* (16), 6621-6638.
13. Grenier, V.; Daws, B. R.; Liu, P; Miller, E. W., *J. Am. Chem. Soc.* **2019**, *141* (3), 1349-1358.
14. Los, G. V.; Encell, L. P.; McDougall, M. G.; Hartzell, D. D.; Karassina, N.; Zimprich, C.; Wood, M. G.; Learish, R.; Ohana, R. F.; Urh, M.; Simpson, D.; Mendez, J.; Zimmerman, K.; Otto, P.; Vidugiris, G.; Zhu, J.; Darzins, A.; Klaubert, D. H.; Bulleit, R. F.; Wood, K. V., *ACS Chem. Biol.* **2008**, *3* (6), 373-382.
15. Chesnut, J. D.; Baytan, A. R.; Russell, M.; Chang, M. P.; Bernard, A.; Maxwell, I. H.; Hoeffler, J. P., *J Immunol Methods* **1996**, *193* (1), 17-27.
16. Pelletier, J.; Sonenberg, N., *Nature* **1998**, *334* (6180), 320–325.
17. Deal, P. E., PhD Dissertation, **2018**.
18. St-Pierre, F.; Marshall, J. D.; Yang, Y.; Gong, Y.; Schnitzer, M. J.; Lin, M. Z., *Nat. Neurosci.* **2014,** *17* (6), 884-9.
19. Gong, Y. Y.; Huang, C.; Li, J. Z.; Grewe, B. F.; Zhang, Y. P.; Eismann, S.; Schnitzer, M. J., *Science* **2015,** *350* (6266), 1361-1366.
20. Chen, T.-W.; Wardill, T. J.; Sun, Y.; Pulver, S. R.; Renninger, S. L.; Baohan, A.; Schreiter, E. R.; Kerr, R. A.; Orger, M. B.; Jayaraman, V.; Looger, L. L.; Svoboda, K.; Kim, D. S., *Nature* **2013**, *499* (7458), 295–300.
21. Denk, W.; Strickler, J. H.; *Science* **1990**, *248* (4951), 73-76.
22. Helmchen, F.; Denk, W., *Nat. Methods* **2005**, *2* (12), 932-940.
23. Xu, C.; Webb, W. W., *J. Opt. Soc. Am. B* **1996***, 13* (3), 481-491.

Chapter 5:

Application of HaloTag-based Covalent Labeling

Portions of this work were performed in collaboration with the following persons:
Synthesis of VF-PEG_{13}-HaloTag was assisted by Vincent Grenier
Synthesis and cellular characterization of mBeRST-PEG_{25}-HaloTag was assisted by Gloria Ortiz
Cloning was assisted by Vikram Muller
In utero electroporation was assisted by Kiarash Shamardani
Slice patch-clamping was assisted by Hillel Adesnik

Abstract

An alternative targeting strategy to fluorogenic activation is covalent labeling, a hybrid approach consisting of a cell surface enzyme expressed on specific cells and a chemically modified dye containing an enzyme-specific ligand. Using HaloTag and RhoVR1-PEG_{25}-HaloTag, we have established high-contrast staining in cultured neurons, mouse brain slice and live animal. To build upon that, we converted two more dyes, VF2.1.Cl and BeRST 1, to VF-HaloTag and mBeRST-HaloTag and proved that both can be targeted to cells expressing HaloTag. While VF-HaloTag is not an ideal target due to its rapid bleaching, mBeRST-HaloTag reports spontaneous spiking events with high signal-to-noise in cultured neurons and exhibits selective staining in mouse brain slice. In addition, targeting voltage dye exclusively to cell bodies was accomplished by utilizing a soma targeting sequence on the HaloTag construct, thus maximizing effective signal for data analysis. These efforts intend to design a HaloTag system that can be eventually used as a practical tool to replace traditional electrophysiology and Ca^{2+}-based imaging to monitor neuronal activity in complex biological system.

Introduction

Covalent labeling of a rhodamine-based voltage sensitive dye (RhoVR 1) by a cell-surface HaloTag permits specific staining to cells of interest. Compared to the esterase-based fluorogenic activation described in Chapter 2 and Chapter 3, contrast has been substantially increased as a result of the fast and high-affinity reaction between the HaloTag enzyme and its ligand, which outcompetes the non-selective labeling process of the hydrophobic molecular wire entering the plasma membrane. Selective staining with remarkable contrast has been achieved in not only cultured cells, but also mouse brain slice and live animal. Encouraged by these results, we have decided to expand the strategy to other dyes, creating the possibility of conducting multi-color targeted staining when combined with other targeting strategies and to optimize the system from the chemical side.

This chapter reports the design and initial data of combining HaloTag with two other dyes, VF2.1.Cl and BeRST 1. Both dyes have different spectral properties and voltage sensitivity from RhoVR 1. VF2.1.Cl is the first generation, fluorescein-based VoltageFluor dye with desirable quantum yield and sensitivity.[1] Its ability to report spontaneous activity was demonstrated in heterogeneous preparations such as leech ganglia but targeting the dye remains a challenge. In the past years, photo-labile[2] or ester[3] groups have been used to diminish its fluorescence and activity but the fluorescence turn-on was not robust enough for tissue applications. As a result, we turned to HaloTag-based covalent labeling strategy to discover a solution.

The key to the performance of HaloTag-based targeting appears to rely on the properties of the chemical dye rather than the enzyme expression. Thus, we selected the one of the best voltage sensitive dyes developed in the lab, Berkeley Red Sensor of Transmembrane potential, or BeRST 1. With its far-red spectral profile and high photo-stability, BeRST 1 enables high-speed and sensitive voltage recording in conjunction with other optogenetic tools such as GCaMP and channelrhodopsin.[4] It would be advantageous to combine BeRST 1 with a protein component to introduce specificity to the dye, in an effort to expand the scope of its application to more complex samples.

Besides switching the dyes, we also worked on targeting HaloTag to precise cellular locations. While HaloTag allows for specific staining in a defined set of neurons, including the extensive neuronal projections, staining of the projections increases the overall signal of the image, thus raising the background noise. For data analysis, soma fluorescence is usually measured as the signal to quantify membrane potential changes; as a result, staining all the membranes reduces signal-to-noise. Therefore, we aimed to restrict all the essential fluorescence signals to the cell body or soma and to eliminate the background fluorescence from neuronal processes. To do so, re-designing the HaloTag construct would be necessary.

Results & Discussions

5-1: Application of HaloTag-based covalent labeling to VF2.1.Cl

VF-HaloTag was synthesized by attaching the HaloTag ligand to VF2.1.Cl connected by a polyethylene glycol (PEG) linker (Scheme 5-1-1b, synthesis was conducted by Dr. Vince Grenier). We modified the plasmid construct used for RhoVR1-HaloTag (Chapter 4, Figure 4-1) by switching to a red fluorescent protein mCherry for spectral separation from the fluorescein-based dye (Figure 5-1-1). Bath application of 50 nM VF-HaloTag to HEK cells sparsely transfected with CMV-HaloTag-pDisplay resulted in clear membrane-associated fluorescence (Figure 5-1-2c) that matched the nuclear mCherry or HaloTag expression (Figure 5-1-2b,d). In a patch of densely packed cells, fluorescence was only observed in specific cells (Figure 5-1-2a,c). The selectivity of staining is remarkable with a 15-fold contrast, which is defined as the ratio of background-subtracted fluorescence from transfected cells to non-transfected cells.

To drive neuron-specific expression in rat hippocampal cultures, a human synapsin promoter was used (Figure 5-1-1). The contrast of VF-HaloTag labeling was maintained in the neuronal culture (Figure 5-1-3a) and cell-surface staining was only visualized in a specific cell expressing nuclear mCherry (Figure 5-1-3b,c). We acquired these VF-HaloTag images 8 days after transfection when the enzyme production increased markedly to capture sufficient dye molecules to provide the contrast. Unlike the RhoVR1-HaloTag system, expression or stained dye signal earlier than that time point was not as robust (data not shown), which might point to a fact that the mCherry construct may not express as well as the EGFP construct. We also varied the dye concentration and noticed only a slight difference in fluorescence intensity between 50 nM and 10 nM (Figure 5-1-3e) since the HaloTag binding site is probably getting saturated at low nano-molar concentrations. The contrast between transfected and non-transfected neurons improved at 10 nM compared to 50 nM, due to a decreased non-specific staining in non-transfected cells. The voltage sensitivity of the targeted dye was confirmed by recording spontaneous activity (Figure 5-1-4), though the signal-to-noise was not ideal. Another observation was that the dye bleached fast when we acquired the activity traces (data not shown), which can be explained by the inherent photo-instability of VF2.1.Cl. Despite the limited application of VF-HaloTag for future studies due to its green spectral profile and inferior photo-physical properties, it is promising that the HaloTag-based strategy is easily transferrable to other dyes.

5-2: Application of HaloTag-based covalent labeling to mBeRST

The original BeRST 1 was modified by shifting the molecular wire from para- to meta- position on the pendant ring to enhance its voltage sensitivity.[5-7] Following that, mBeRST was converted to the HaloTag version by appending a PEG linker and haloalkane ligand to generate mBeRST-PEG_{25}-HaloTag (Figure 5-2-1, synthesis was conducted by Gloria Ortiz).

For characterization in cultured cells, we used the same EGFP constructs as RhoVR1-PEG_{25}-HaloTag (Chapter 4, Figure 4-1). Selective and membrane-associated fluorescence of mBeRST-PEG_{25}-HaloTag was only detected in EGFP-expressing cells in both sparsely transfected HEK cells (Figure 5-2-2a-c) and cultured rat hippocampal neurons (Figure 5-2-3a-c). By whole-cell patch clamp electrophysiology in HEK cells, we calculated a voltage sensitivity of 20.6% ± 1.5% $\Delta F/F$ per 100 mV (n = 7 cells, Figure 5-2-2d). Spontaneous spiking events in cultured neurons were successfully recorded in cells of interest with this targeted dye (Figure 5-2-3d).

Acute brain slices were acquired and stained in a manner similar to that in the RhoVR1-PEG_{25}-HaloTag study (Chapter 4, Experimental Section). Only a few cells were labeled with the dye, displaying bright and membrane-associated fluorescent signal in both cell bodies and neuronal processes (Figure 5-2-4a). We then performed current-clamp electrophysiology to evoke activity while simultaneously monitoring fluorescence change and found out that the stained dye was voltage sensitive to report action potentials (Figure 5-2-4b,c). This again illustrates the generalizability of HaloTag-based selective labeling strategy to another voltage dye of different color, sensitivity and photostability.

5-3: Target mBeRST and RhoVR staining to neuronal cell body

The dendritic K^+ channel $K_v2.1$ is densely expressed on the soma and proximal dendrites. Mutation studies have revealed a 26-amino acid sequence from the cytoplasmic tail of the protein that is responsible for the localization.[8] Thus, we inserted the soma targeting (ST) sequence downstream of pDisplay, the transmembrane domain (Figure 5-3-1). The construct expressed poorly in cultured hippocampal neurons, evidenced by dim and low-contrast RhoVR1-PEG_{25}-HaloTag staining using the same transfection and labeling protocol as Syn-HaloTag-pDisplay (Figure 5-3-2). There seemed to be stronger signal on the cell body compared to the processes, but a co-staining experiment with a dye that labels the cellular membrane uniformly would be necessary to compare the difference in signal.

We next evaluated the expression and localization of this construct in mouse brain slice, as it has been previously reported by the Adesnik lab that the ST sequence does not work as efficiently in cultured cells as in slices (data not shown). Using RhoVR1-PEG_{25}-HaloTag, we only saw staining on the cell body (Figure 5-3-3a-c) and did not observe labeled projections. We also collected a series of z-stack images over a depth of 22 μm to cover not only the cell body but also the surrounding processes, and did a max-intensity projection of the images. The resulting image only showed soma staining, suggesting the specificity of the ST sequencing in slices (Figure 5-3-3d). Repeating the staining with mBeRST-PEG_{25}-HaloTag yielded similar results that only cell body was stained, indicating specific expression of HaloTag on the soma (Figure 5-3-4). Despite the inconclusive results in cultured neurons, the soma targeting sequence indeed localized the HaloTag and therefore the dye staining exclusively on the cell body. Future experiments

include confirming the voltage sensitivity of the stained dye and improving the expression the enzyme to enhance dye labeling and fluorescent signal.

Conclusion

The transformation of a VoltageFluor dye to its HaloTag version is relatively straightforward by simply attaching the haloalkane ligand to the dye via a water-soluble and flexible PEG linker. These modifications do not seem to affect the photo-physical properties of the sensor itself while allowing for specific labeling to cells of interest expressing an engineered cell-surface HaloTag enzyme. We have demonstrated selective staining using both VF2.1.Cl and BeRST1, two dyes of different spectral characteristics and voltage sensitivity, emphasizing the generalizability of this particular strategy. Despite its bright and targeted staining of VF-HaloTag in cultured neurons, its low sensitivity and photo-stability may encounter setbacks in potential applications. On the other hand, BeRST1 is by far one of the best VoltageFluor dyes developed with high speed, sensitivity, photo-stability and long-wavelength fluorescence profiles. We were able to add in the targeting feature that enables staining and voltage imaging in defined cells in cultured neurons and live mouse brain slice. Additional characterization will be useful to optimize the BeRST-HaloTag hybrid approach to probe neuronal activity and connectivity in complex biological settings. We have also added an additional targeting sequence to the transmembrane domain in the HaloTag construct to restrict its expression and RhoVR staining on the cell body, with successful soma staining demonstrated in mouse brain slice. This approach further enhances signal-to-noise ratio for both imaging and data analysis in a complex biological sample by confining all fluorescence to neuronal somas where membrane potential is usually measured. All these preliminary data point to the possibility of wedding the superior photo-physical properties of VoltageFluor dyes and the cellular and subcellular specificity conferred by the HaloTag enzyme to enable high throughput and precise dissection of neural circuits and pathways.

Experimental Section

Cell culture

All animal procedures were approved by the UC Berkeley Animal Care and Use Committees and conformed to the NIH Guide for the Care and Use and Laboratory Animals and the Public Health Policy.

Human embryonic kidney 293T (HEK) cells were maintained in Dulbecco's modified eagle medium (DMEM) supplemented with 4.5 g/L D-glucose, 10% fetal bovine serum (FBS; Thermo Scientific) and 1% GlutaMax (Invitrogen) at 37 °C in a humidified incubator with 5% CO2. Cells were passaged and plated in DMEM (as above) at a density of 750,000 cells per well in a 6-well plate. Transfection of plasmids was carried out using Lipofectamine 3000 (Invitrogen) ~18-24 h after plating. The cells were split again 48 h after transfection and plated onto 12 mm glass coverslips pre-coated with Poly-D-Lysine (PDL; 1 mg/ml; Sigma-Aldrich) at a density of 75,000 cells per coverslip in DMEM supplemented with 1 g/L D-glucose, 10% FBS and 1% GlutaMax. Imaging was performed 12-18 h after plating.

Hippocampi were dissected from embryonic day 19 Sprague Dawley rats (Charles River Laboratory) in cold, sterile HBSS (zero Ca^{2+}, zero Mg^{2+}, phenol red). All dissection products were supplied by Invitrogen, unless otherwise stated. Hippocampal tissue was treated with trypsin (2.5%) for 15 min at 37 °C. The tissue was triturated using fire polished Pasteur pipettes, in minimum essential media (MEM) supplemented with 5% FBS, 2% B-27, 2% 1M dextrose (Fisher Scientific) and 1% GlutaMax. The dissociated cells were plated onto 12 mm diameter coverslips (Fisher Scientific) pre-treated with PDL (as above) at a density of 25-30,000 cells per coverslip in MEM supplemented media (as above). Neurons were maintained at 37 °C in a humidified incubator with 5% CO_2. At 1 day in vitro (DIV) half of the MEM supplemented media was removed and replaced with Neurobasal media containing 2% B-27 supplement and 1% GlutaMax. Transfection of plasmids was carried out using Lipofectamine 3000 (without P3000 reagent) at 6-7 DIV. Imaging was performed on mature neurons 13-16 DIV.

No solubilizing reagent was used for loading the dyes in HEK cells and hippocampal neurons. DMSO stock solutions were diluted directly in HBSS to working concentrations. Cells were incubated with dyes in HBSS at 37 °C in the incubator before exchanging dye/HBSS for HBSS without any dye. All imaging was performed in HBSS at room temperature.

Epifluorescence microscopy

Imaging was performed on an AxioExaminer Z-1 (Zeiss) equipped with a Spectra-X Light engine LED light (Lumencor), controlled with Slidebook (v6, Intelligent Imaging Innovations). Images were acquired with a W-Plan-Apo 20x/1.0 water objective (20x; Zeiss). Images were focused onto an OrcaFlash4.0 sCMOS camera (sCMOS; Hamamatsu). Confocal imaging was performed with a Zeiss LSM 880 NLO AxioExaminer equipped with a Diode 405 nm laser line, Argon 458, 488, and 514 laser lines, and a DPSS 561 nm laser line and a Helium-neon 633nm laser line. Images were acquired using a W-Plan-Apo 20x/1.0 DIC objective and a Zeiss Airyscan detector.

Image analysis

Analysis of voltage sensitivity in HEK cells was performed using ImageJ (FIJI). Briefly, a region of interest (ROI) was selected automatically based on fluorescence intensity and applied as a mask to all image frames. Fluorescence intensity values were calculated at known baseline and voltage step epochs. ΔF/F values were calculated by first subtracting a mean background value from all raw fluorescence frames, to give a background subtracted trace (bkgsub). A baseline fluorescence value (Fbase) is calculated from the median of all the frames, and subtracted from each timepoint of the bkgsub trace to yield a ΔF trace. The ΔF was then divided by Fbase to give ΔF/F traces. No averaging has been applied to any voltage traces.

Electrophysiology/Imaging parameters

For electrophysiological experiments, pipettes were pulled from borosilicate glass (Sutter Instruments, BF150-86-10), with a resistance of 4–6 MΩ, and were filled with an internal solution; 115 mM potassium gluconate, 10 mM BAPTA tetrapotassium salt, 10 mM HEPES, 5 mM NaCl, 10 mM KCl, 2 mM ATP disodium salt, 0.3 mM GTP trisodium salt (pH 7.25, 275 mOsm). Recordings were obtained with an Axopatch 200B amplifier (Molecular Devices) at room temperature. The signals were digitized with a Digidata 1440A, sampled at 50 kHz and recorded with pCLAMP 10 software (Molecular Devices) on a PC. Fast capacitance was compensated in the on-cell configuration. For all electrophysiology experiments, recordings were only pursued if series resistance in voltage clamp was less than 30 MΩ. For whole-cell, voltage clamp recordings in HEK 293T cells, cells were held at -60 mV and hyper- and de- polarizing steps applied from -100 to +100 mV in 20 mV increments. For whole-cell, current clamp in slices, experiments were conducted on the microscope set up for slice patching in the Adesnik lab. Briefly, slices were transferred to the microscope perfusion chamber with ACSF recording solution (in mM: NaCl, 119; KCl, 2.5; $MgSO_4$, 1.3; NaH_2PO_4, 1.3; $NaHCO_3$, 26; D-glucose, 20 and $CaCl_2$, 2.5. To illumination the samples, spectra-X Light engine LED light (Lumencor), controlled with MATLAB script written by the Adesnik lab. Images were acquired with a W-Plan-Apo 20x/1.0 water objective (20x; Zeiss) at a sampling rate of 1 kHz.

In utero electroporation

Pregnant mice at E15-16 were anaesthetized with 2.0% isoflurane, the abdomen was cleaned with 70% ethanol and swabbed with iodine, and a small vertical incision was made in the skin and abdominal wall and 8–12 embryos gently exposed. Each embryo was injected with 0.5–1 μl of DNA solution and 0.05% Fast Green dye. We used a pressure-controlled beveled glass pipette (Drummond, Custom Microbeveller) for injection. After each injection, the embryos were moistened with saline and voltage steps via tweezertrodes (BTX, 5 mm round, platinum, BTX electroporator) were applied with the positive electrode placed over the visual cortex and the negative electrode placed under the head of the embryo. Voltage was 40 V for 5 pulses at 1 Hz, each pulse lasting 50 ms. The embryos were returned to the abdomen, which was sutured, followed by suturing of the skin. The procedure typically lasted under 30 min.

Acute brain slice preparation

Mice were deeply anesthetized with isoflurane and quickly decapitated. After removing the scalp and skull, ice cold sucrose cutting solution (in mM: NaCl, 83; KCl, 2.5; $MgSO_4$, 3.3; Na_2HPO_4, 1; $NaHCO_3$, 26.2; D-glucose, 22; sucrose, 72; and $CaCl_2$, 0.5) was applied to the brain. BFP fluorescence was checked with a hand held 405 nm laser before the brain was taken out. The brain was cut into 300 μm thick slices with a DTK-1000 slicer in ice-cold sucrose cutting solution. The cut slices were incubated in sucrose cutting solution, bubbled with 95% O_2 and 5% CO_2, first at 31 °C for about 30 min and then at room temperature until further use. For bath application of the dye and cell staining, a slice was transferred to a 35 mm dish with sucrose cutting solution bubbled with 95% O_2 and 5% CO_2 to which dye stock solution was added (250 nM final concentration). The slice was incubated with the dye at room temperature for 15 min before imaging.

DNA constructs

To express the HaloTag protein on the cell surface, an IgK leader sequence was fused to the N-terminal and a transmembrane domain (pDisplay) was added to the C-terminal of the HaloTag sequence. For the purpose of inmmunostaining, an HA tag was inserted. Mammalian expression vector pcDNA3 with either a cytomegalovirus (CMV) promoter or human synapsin promoter (Syn) was used for protein expression in HEK cells and cultured neurons, respectively. To increase expression in neurons, a regulatory element from the woodchuck hepatitis virus (WPRE) was used. In some constructs, nuclear-targeted EGFP or mCherry was inserted down stream of HaloTag, separated by an internal ribosome entry site (IRES) sequence, in order to track the expression of HaloTag in live cells. For soma targeting, the sequence of C-terminal tail of $K_v2.1$ K^+ channel was fused with pDisplay. The cloned constructs were verified by sequencing. All the constructs were prepared using Qiagen Maxiprep kit, except those with CMV promoter. The following sequences were used (5' to 3'):

IgK

ATGGAGACAGACACACTCCTGCTATGGGTACTGCTGCTCTGGGTTCCAGGTTC
CACTGGTGAC

HaloTag

GCAGAAATCGGTACTGGCTTTCCATTCGACCCCCATTATGTGGAAGTCCTGGG
CGAGCGCATGCACTACGTCGATGTTGGTCCGCGCGATGGCACCCCTGTGCTG
TTCCTGCACGGTAACCCGACCTCCTCCTACGTGTGGCGCAACATCATCCCGCA
TGTTGCACCGACCCATCGCTGCATTGCTCCAGACCTGATCGGTATGGGCAAAT
CCGACAAACCAGACCTGGGTTATTTCTTCGACGACCACGTCCGCTTCATGGAT
GCCTTCATCGAAGCCCTGGGTCTGGAAGAGGTCGTCCTGGTCATTCACGACTG
GGGCTCCGCTCTGGGTTTCCACTGGGCCAAGCGCAATCCAGAGCGCGTCAAA
GGTATTGCATTTATGGAGTTCATCCGCCCTATCCCGACCTGGGACGAATGGCC
AGAATTTGCCCGCGAGACCTTCCAGGCCTTCCGCACCACCGACGTCGGCCGC
AAGCTGATCATCGATCAGAACGTTTTTATCGAGGGTACGCTGCCGATGGGTG
TCGTCCGCCCGCTGACTGAAGTCGAGATGGACCATTACCGCGAGCCGTTCCT
GAATCCTGTTGACCGCGAGCCACTGTGGCGCTTCCCAAACGAGCTGCCAATC
GCCGGTGAGCCAGCGAACATCGTCGCGCTGGTCGAAGAATACATGGACTGGC
TGCACCAGTCCCCTGTCCCGAAGCTGCTGTTCTGGGGCACCCCAGGCGTTCTG

ATCCCACCGGCCGAAGCCGCTCGCCTGGCCAAAAGCCTGCCTAACTGCAAGG
CTGTGGACATCGGCCCGGGTCTGAATCTGCTGCAAGAAGACAACCCGGACCT
GATCGGCAGCGAGATCGCGCGCTGGCTGTCGACGCTCGAGATTTCCGGC

HA
TATCCATATGATGTTCCAGATTATGCT

pDisplay
GCTGTGGGCCAGGACACGCAGGAGGTCATCGTGGTGCCACACTCCTTGCCCT
TTAAGGTGGTGGTGATCTCAGCCATCCTGGCCCTGGTGGTGCTCACCATCATC
TCCCTTATCATCCTCATCATGCTTTGGCAGAAGAAGCCACGT

Soma Targeting (ST)
CAGTCCCAGCCCATCCTCAACACCAAGGAGATGGCCCCGCAGAGCAAGCCTC
CAGAGGAGCTGGAGATGAGCAGCATGCCCAGCCCCGTGGCCCCTCTGCCCGC
ACGCACGGAGGGCGTCATCGACATGCGGAGCATGTCCAGCATTGACAGCTTC
ATCAGCTGTGCCACGGACTTCCCTGAAGCCACCAGATTC

IRES
GCCCCTCTCCCTCCCCCCCCCCTAACGTTACTGGCCGAAGCCGCTTGGAATAA
GGCCGGTGTGCGTTTGTCTATATGTTATTTTCCACCATATTGCCGTCTTTTGGC
AATGTGAGGGCCCGGAAACCTGGCCCTGTCTTCTTGACGAGCATTCCTAGGG
GTCTTTCCCCTCTCGCCAAAGGAATGCAAGGTCTGTTGAATGTCGTGAAGGA
AGCAGTTCCTCTGGAAGCTTCTTGAAGACAAACAACGTCTGTAGCGACCCTTT
GCAGGCAGCGGAACCCCCCACCTGGCGACAGGTGCCTCTGCGGCCAAAAGCC
ACGTGTATAAGATACACCTGCAAAGGCGGCACAACCCCAGTGCCACGTTGTG
AGTTGGATAGTTGTGGAAAGAGTCAAATGGCTCTCCTCAAGCGTATTCAACA
AGGGGCTGAAGGATGCCCAGAAGGCACCCCATTGTATGGGATCTGATCTGGG
GCCTCGGTGCACATGCTTTACATGTGTTTAGTCGAGGTTAAAAAAACGTCTAG
GCCCCCCGAACCACGGGGACGTGGTTTTCCTTTGAAAAACACGATGATAATA
TGGCCACA

Nuclear Localization Sequencing
ATGGTGCCCAAGAAGAAGAGGAAAGTCGTGAGCAAGGGCGAGGAGGACAAC
ATGGCCATCATCAAGGAGTTCATGCGCTTCAAGGTGCAC

mCherry
ATGGAGGGCTCCGTGAACGGCCACGAGTTCGAGATCGAGGGCGAGGGCGAG
GGCCGCCCCTACGAGGGCACCCAGACCGCCAAGCTGAAGGTGACCAAGGGC
GGCCCCCTGCCCTTCGCCTGGGACATCCTGTCCCCTCAGTTCATGTACGGCTC
CAAGGCCTACGTGAAGCACCCCGCCGACATCCCCGACTACTTGAAGCTGTCC
TTCCCCGAGGGCTTCAAGTGGGAGCGCGTGATGAACTTCGAGGACGGCGGCG
TGGTGACCGTGACCCAGGACTCCTCCCTGCAGGACGGCGAGTTCATCTACAA
GGTGAAGCTGCGCGGCACCAACTTCCCCTCCGACGGCCCCGTAATGCAGAAG
AAGACCATGGGCTGGGAGGCCTCCTCCGAGCGGATGTACCCCGAGGACGGC
GCCCTGAAGGGCGAGATCAAGCAGAGGCTGAAGCTGAAGGACGGCGGCCAC

TACGACGCCGAGGTCAAGACCACCTACAAGGCCAAGAAGCCCGTGCAGCTG
CCCGGCGCCTACAACGTCAACATCAAGCTGGACATCACCTCCCACAACGAGG
ACTACACCATCGTGGAACAGTACGAGCGCGCCGAGGGCCGCCACTCCACCGG
CGGCATGGACGAGCTGTACAAG

EGFP
AGCAAGGGCGAGGAGCTGTTCACCGGGGTGGTGCCCATCCTGGTCGAGCTGG
ACGGCGACGTAAACGGCCACAAGTTCAGCGTGTCCGGCGAGGGCGAGGGCG
ATGCCACCTACGGCAAGCTGACCCTGAAGTTCATCTGCACCACCGGCAAGCT
GCCCGTGCCCTGGCCCACCCTCGTGACCACCCTGACCTACGGCGTGCAGTGCT
TCAGCCGCTACCCCGACCACATGAAGCAGCACGACTTCTTCAAGTCCGCCAT
GCCCGAAGGCTACGTCCAGGAGCGCACCATCTTCTTCAAGGACGACGGCAAC
TACAAGACCCGCGCCGAGGTGAAGTTCGAGGGCGACACCCTGGTGAACCGC
ATCGAGCTGAAGGGCATCGACTTCAAGGAGGACGGCAACATCCTGGGGCAC
AAGCTGGAGTACAACTACAACAGCCACAACGTCTATATCATGGCCGACAAGC
AGAAGAACGGCATCAAGGTGAACTTCAAGATCCGCCACAACATCGAGGACG
GCAGCGTGCAGCTCGCCGACCACTACCAGCAGAACACCCCCATCGGCGACGG
CCCCGTGCTGCTGCCCGACAACCACTACCTGAGCACCCAGTCCGCCCTGAGC
AAAGACCCCAACGAGAAGCGCGATCACATGGTCCTGCTGGAGTTCGTGACCG
CCGCCGGGATCACTCTCGGCATGGACGAGCTGTACAAGTAA

WPRE
GCTTATCGATAATCAACCTCTGGATTACAAAATTTGTGAAAGATTGACTGGTA
TTCTTAACTATGTTGCTCCTTTTACGCTATGTGGATACGCTGCTTTAATGCCTT
TGTATCATGCTATTGCTTCCCGTATGGCTTTCATTTTCTCCTCCTTGTATAAAT
CCTGGTTGCTGTCTCTTTATGAGGAGTTGTGGCCCGTTGTCAGGCAACGTGGC
GTGGTGTGCACTGTGTTTGCTGACGCAACCCCCACTGGTTGGGGCATTGCCAC
CACCTGTCAGCTCCTTTCCGGGACTTTCGCTTTCCCCCTCCCTATTGCCACGGC
GGAACTCATCGCCGCCTGCCTTGCCCGCTGCTGGACAGGGGCTCGGCTGTTG
GGCACTGACAATTCCGTGGTGTTGTCGGGGAAATCATCGTCCTTTCCTTGGCT
GCTCGCCTGTGTTGCCACCTGGATTCTGCGCGGGACGTCCTTCTGCTACGTCC
CTTCGGCCCTCAATCCAGCGGACCTTCCTTCCCGCGGCCTGCTGCCGGCTCTG
CGGCCTCTTCCGCGTCTTCGCCTTCGCCCTCAGACGAGTCGGATCTCCCTTTG
GGCCGCCTCCCCGCATCGATACCG

CMV promoter
GACATTGATTATTGACTAGTTATTAATAGTAATCAATTACGGGGTCATTAGTT
CATAGCCCATATATGGAGTTCCGCGTTACATAACTTACGGTAAATGGCCCGCC
TGGCTGACCGCCCAACGACCCCCGCCCATTGACGTCAATAATGACGTATGTT
CCCATAGTAACGCCAATAGGGACTTTCCATTGACGTCAATGGGTGGACTATTT
ACGGTAAACTGCCCACTTGGCAGTACATCAAGTGTATCATATGCCAAGTACG
CCCCCTATTGACGTCAATGACGGTAAATGGCCCGCCTGGCATTATGCCCAGT
ACATGACCTTATGGGACTTTCCTACTTGGCAGTACATCTACGTATTAGTCATC
GCTATTACCATGGTGATGCGGTTTTGGCAGTACATCAATGGGCGTGGATAGC
GGTTTGACTCACGGGGATTTCCAAGTCTCCACCCCATTGACGTCAATGGGAGT
TTGTTTTGGCACCAAAATCAACGGGACTTTCCAAAATGTCGTAACAACTCCGC

CCCATTGACGCAAATGGGCGGTAGGCGTGTACGGTGGGAGGTCTATATAAGC
AGAGCT

Synapsin Promoter
GTGTCTAGACTGCAGAGGGCCCTGCGTATGAGTGCAAGTGGGTTTTAGGACC
AGGATGAGGCGGGGTGGGGGTGCCTACCTGACGACCGACCCCGACCCACTG
GACAAGCACCCAACCCCCATTCCCCAAATTGCGCATCCCCTATCAGAGAGGG
GGAGGGGAAACAGGATGCGGCGAGGCGCGTGCGCACTGCCAGCTTCAGCAC
CGCGGACAGTGCCTTCGCCCCCGCCTGGCGGCGCGCGCCACCGCCGCCTCAG
CACTGAAGGCGCGCTGACGTCACTCGCCGGTCCCCCGCAAACTCCCCTTCCC
GGCCACCTTGGTCGCGTCCGCGCCGCCGCCGGCCCAGCCGGACCGCACCACG
CGAGGCGCGAGATAGGGGGGCACGGGCGCGACCATCTGCGCTGCGGCGCCG
GCGACTCAGCGCTGCCTCAGTCTGCGGTGGGCAGCGGAGGAGTCGTGTCGTG
CCTGAGAGCGCAGTCGAGA

Benchling links for constructs

CMV-IgK-HaloTag-HA-pDisplay-IRES-mCherry
https://benchling.com/s/seq-3iB3t8JmLupY99jEd7ui

Synapsin-IgK-HaloTag-HA-pDisplay-IRES-mCherry-WPRE
https://benchling.com/s/seq-DkNtujCDk5FLpTwp0B3V

Synapsin-IgK-HaloTag-HA-pDisplay-ST-WPRE
https://benchling.com/s/seq-g55yVpVAS4MIThH0gpcM

Figures and Schemes

Scheme 5-1-1. *Design of covalent labeling of VF2.1.Cl in specific cells of interest.*

a)

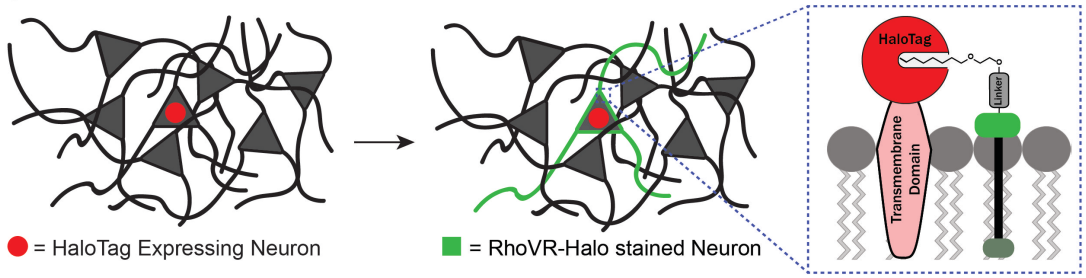

b)

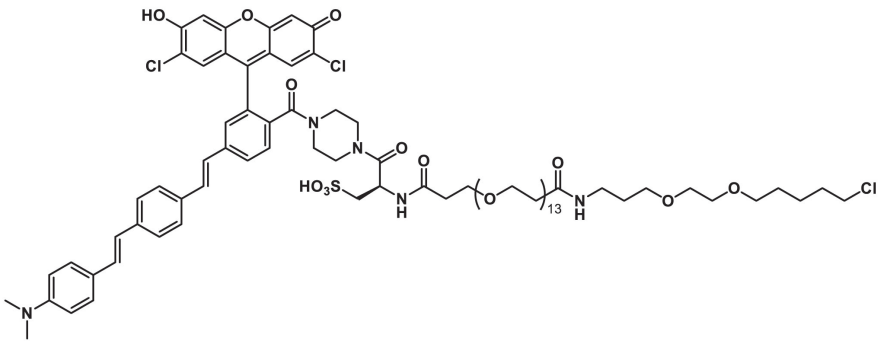

Scheme 5-1-1. (a) Scheme of neuron-specific targeting with cell-surface HaloTag and VF-HaloTag (components are not to scale). (b) Structure of VF-PEG$_{13}$-HaloTag used in this study.

Figure 5-1-1. *HaloTag constructs used in this study.*

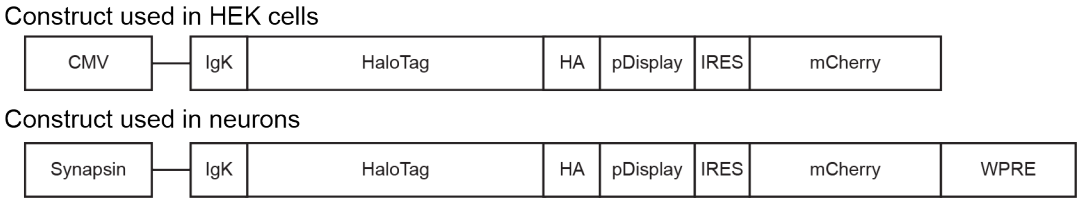

Figure 5-1-1. HaloTag constructs used in this study.

Figure 5-1-2. *Characterization of VF-HaloTag in HEK cells.*

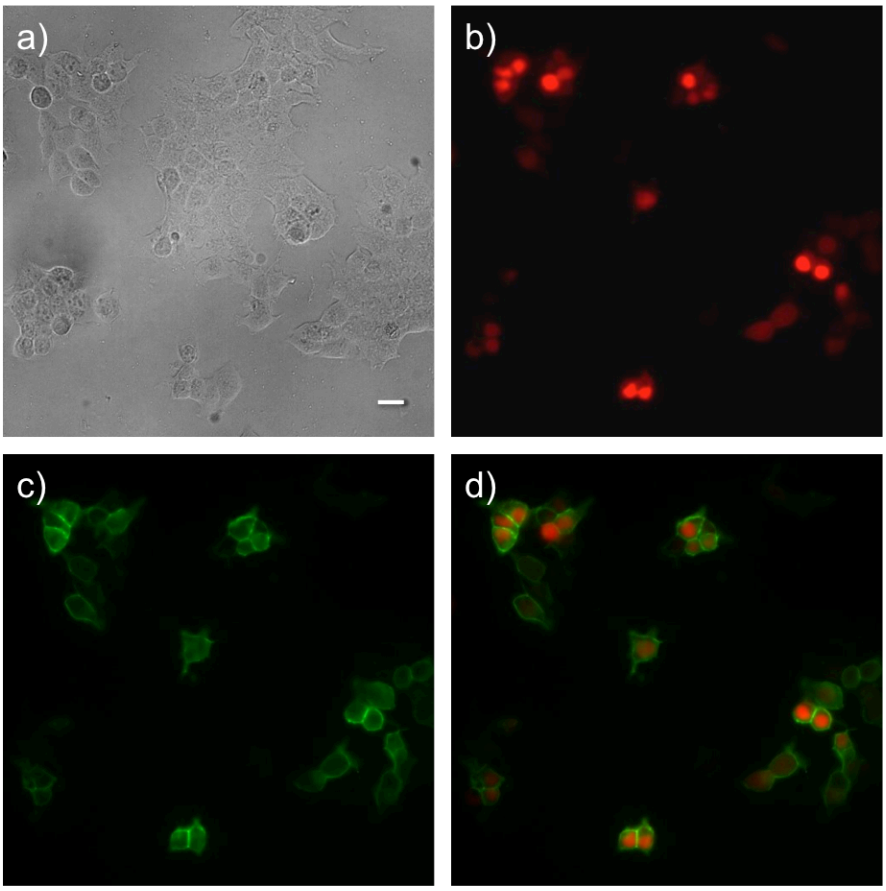

Figure 5-1-2. Wide-field fluorescence microscopy of HEK cells stained with VF-HaloTag (50 nM, 30 min). (a) Differential interference contrast (DIC) image of HEK cells. (b) Nulcear mCherry fluorescence indicates HaloTag expression. (c) Membrane-associated VF fluorescence. (d) Merge image of VF and mCherry fluorescence. Scale bar is 20 μm.

Figure 5-1-3. *Characterization of VF-HaloTag in cultured hippocampal neurons.*

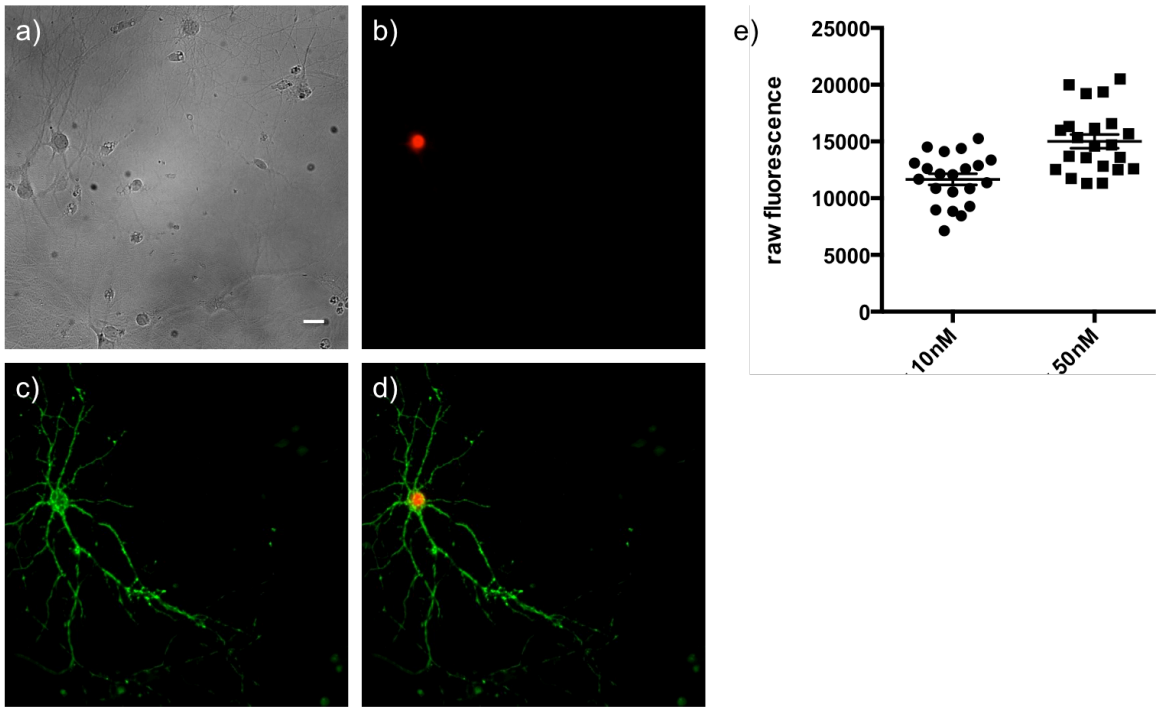

Figure 5-1-3. Cellular characterization of VF-HaloTag in cultured hippocampal neurons. (a-d) Wide-field fluorescence microscopy of HEK cells stained with VF-HaloTag (10 nM, 30 min). (a) DIC image of cultured neurons. (b) Nulcear mCherry fluorescence indicates HaloTag expression. (c) Membrane-associated VF fluorescence showing clear staining in both cell body and neuronal processes. (d) Merge image of VF and mCherry fluorescence. Scale bar is 20 μm. (e) Quantification of VF-HaloTag staining at different dye concentrations.

Figure 5-1-4. *Characterization of VF-HaloTag in cultured hippocampal neurons.*

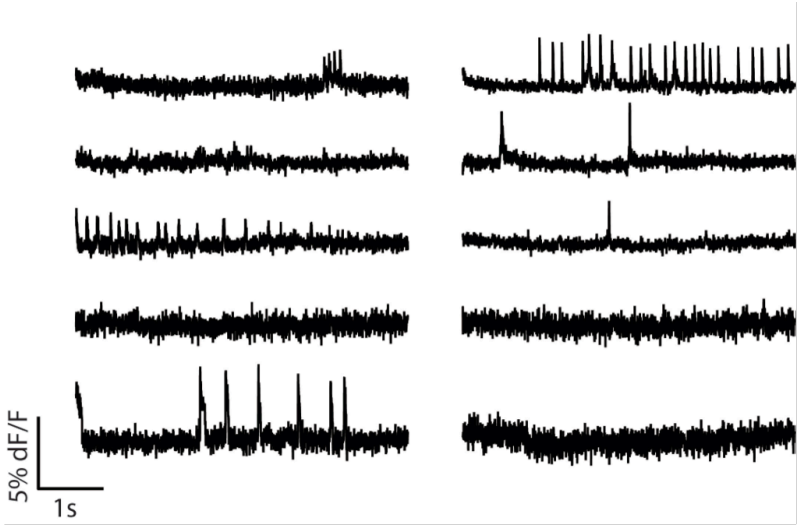

Figure 5-1-4. Cellular characterization of VF-HaloTag in cultured neurons. Representative ΔF/F traces for spontaneous activity of neurons transfected with Syn-HaloTag-mCherry and stained with VF-HaloTag (50 nM, 30 min). Images were acquired at 500 Hz and represent single-trial acquisitions.

***Figure 5-2-1**. Structure of mBeRST-PEG$_{25}$-HaloTag used in this study.*

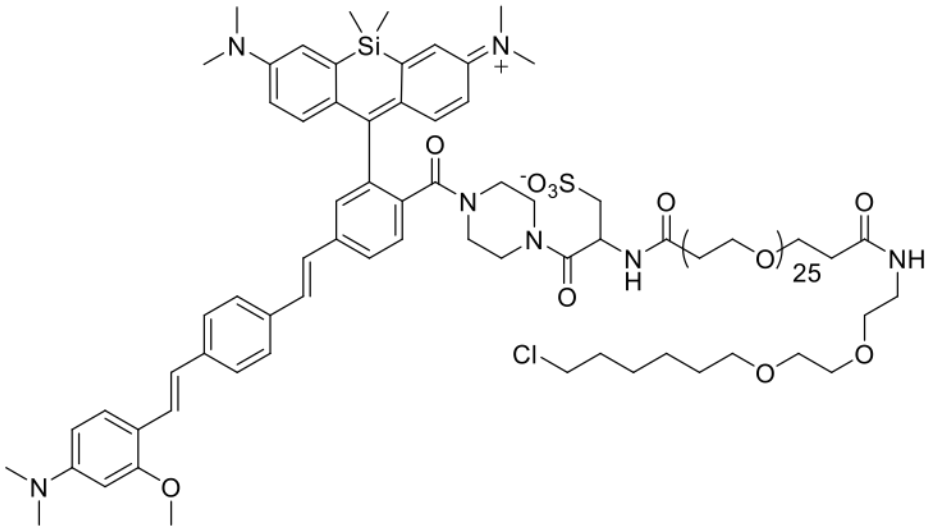

Figure 5-2-1. Structure of mBeRST-PEG$_{25}$-HaloTag used in this study.

Figure 5-2-2. *Characterization of mBeRST-PEG$_{25}$-HaloTag in HEK cells.*

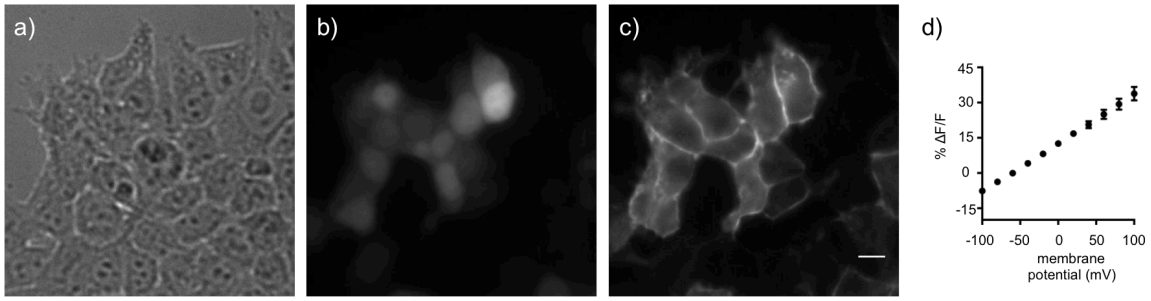

Figure 5-2-2. Wide-field fluorescence microscopy of HEK cells transfected with CMV-HaloTag-pDisplay and stained with mBeRST-PEG$_{25}$-HaloTag (50 nM, 30 min). (a) DIC image of HEK cells. (b) Nulcear EGFP fluorescence indicates HaloTag expression. (c) Membrane-associated BeRST fluorescence. Scale bar is 10 μm. (d) Plot of ΔF/F vs membrane potential (in mV) for mBeRST-PEG$_{25}$-HaloTag. Data are mean ± S.D. for 7 cells.

Figure 5-2-3. *Characterization of mBeRST-PEG$_{25}$-HaloTag in cultured neurons.*

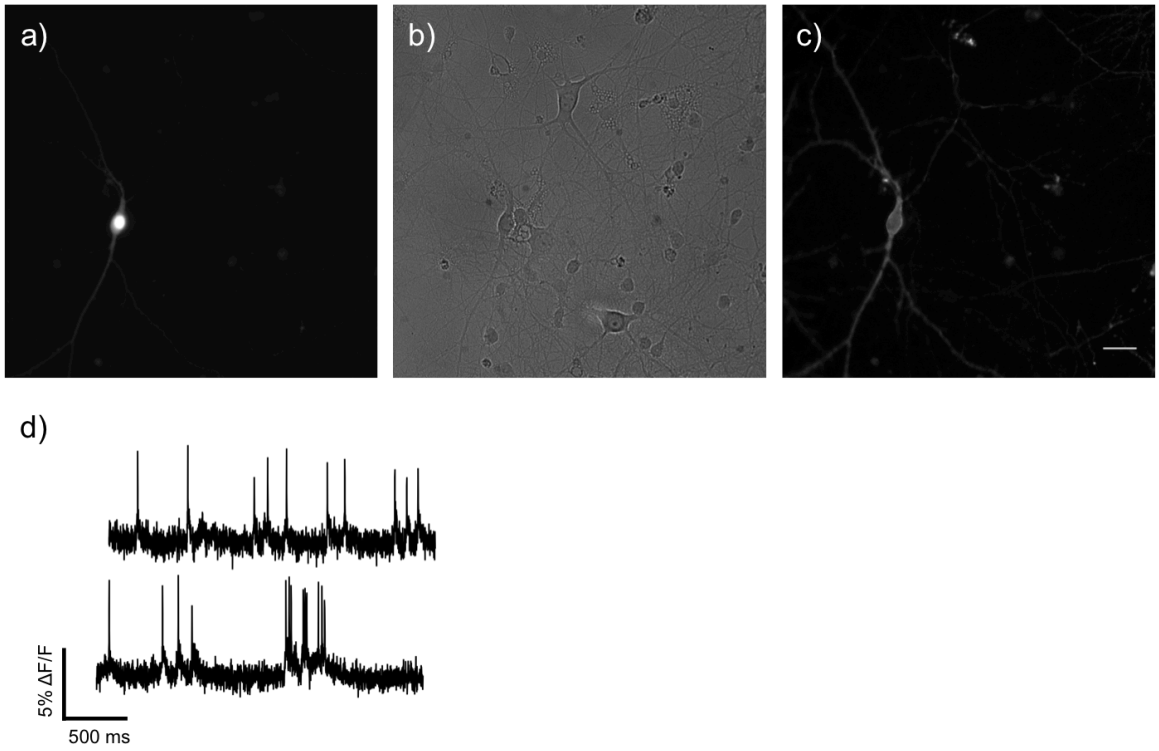

Figure 5-2-3. Cellular characterization of mBeRST-PEG$_{25}$-HaloTag in cultured hippocampal neurons transfected with Syn-HaloTag-pDisplay. (a-c) Wide-field fluorescence microscopy of neurons stained with mBeRST-PEG$_{25}$-HaloTag (50 nM, 30 min). (a) Nulcear EGFP fluorescence indicates HaloTag expression. (b) DIC image of cultured neurons. (c) Membrane-associated BeRST fluorescence showing clear staining in both cell body and neuronal processes. Scale bar is 30 μm. (d) Representative ΔF/F traces for spontaneous activity recorded by mBeRST-PEG$_{25}$-HaloTag. Images are acquired at 500 Hz and represent single-trial acquisitions.

***Figure 5-2-4**. Characterization of mBeRST-PEG$_{25}$-HaloTag in mouse brain slice.*

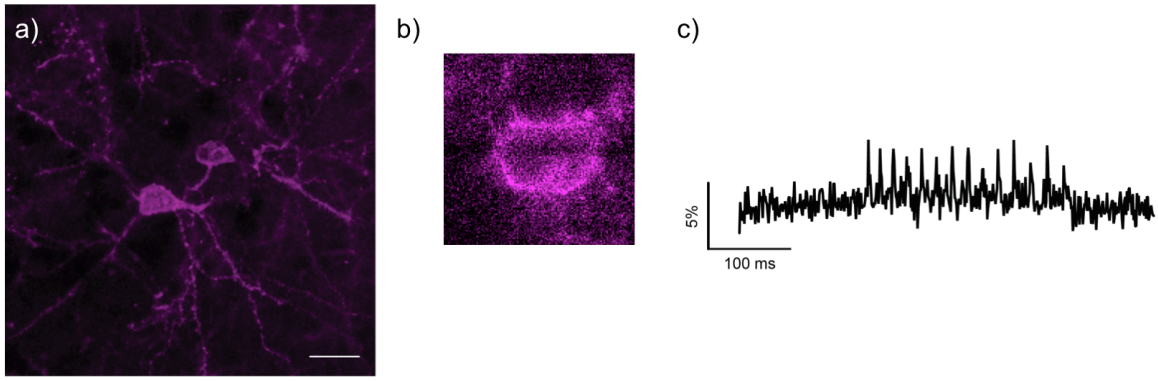

Figure 5-2-4. Imaging mBeRST-PEG$_{25}$-HaloTag in mouse brain slice expressing HaloTag-pDisplay and pCAG-EGFP following *in utero* electroporation. (a) Representative image of a slice stained with mBeRST-PEG$_{25}$-HaloTag (250nM, 15 min at RT). Sample was excited and visualized with a 633 nm laser on confocal microscope. (b) Wide-field image of the stained slice acquired during patch-clamp electrophysiology. (c) Example ΔF/F trace of evoked voltage activity recorded by mBeRST-PEG$_{25}$-HaloTag in a neuron patch-clamped for current injection. Images are acquired at 1 kHz and represent single-trial acquisitions. Scale bar is 20 μm.

Figure 5-3-1. *Soma-targeting HaloTag construct used in this study.*

Figure 5-3-1. Soma-targeting HaloTag construct used in this study.

Figure 5-3-2. *Characterization of soma-targeting HaloTag construct in cultured neurons.*

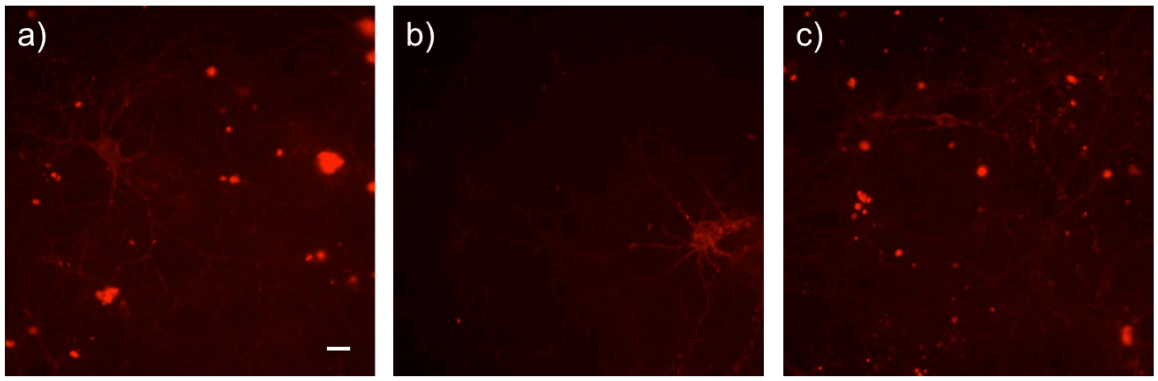

Figure 5-3-2. Representative wide-field images of cultured hippocampal neurons transfected with Syn-HaloTag-pDisplay-ST and stained with RhoVR1-PEG_{25}-HaloTag (50 nM, 30min). Brighter fluorescence signal was observed from the cell body compared to the processes. Scale bar is 20 μm.

Figure 5-3-3. *Characterization of soma-targeting HaloTag construct in mouse brain slice with RhoVR1-PEG$_{25}$-HaoTag.*

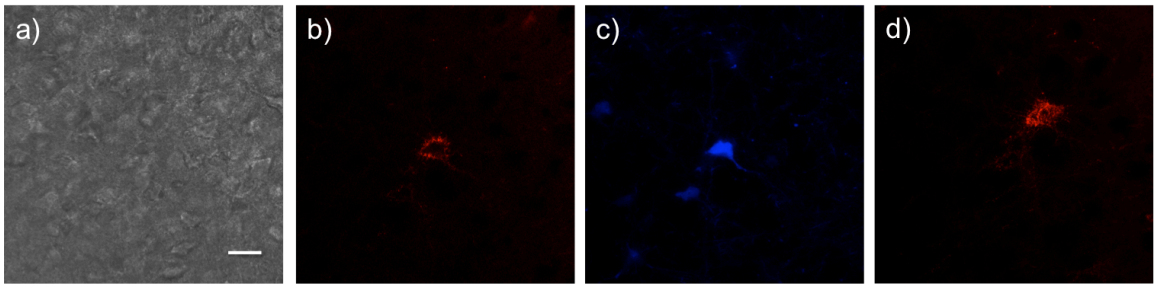

Figure 5-3-3. Imaging RhoVR1-PEG$_{25}$-HaloTag in mouse brain slice expressing HaloTag-pDisplay-ST and pCAG-mTagBFP2 following in utero electroporation. (a-d) Representative image of a slice stained with RhoVR1-PEG$_{25}$-HaloTag (250nM, 15 min at RT). Sample was excited and visualized with a 561 nm laser on a confocal microscope. (a) Bright-field image of the slice. (b) Membrane-associated fluorescence stains only cell body. (c) Cytosolic BFP fluorescence indicates HaloTag expression. (d) Max intensity projection of Z-stack images over 22 μm depth in another region of interest. Scale bar is 20 μm.

Figure 5-3-4. *Characterization of soma-targeting HaloTag construct in mouse brain slice* with mBeRST-PEG$_{25}$-HaoTag.

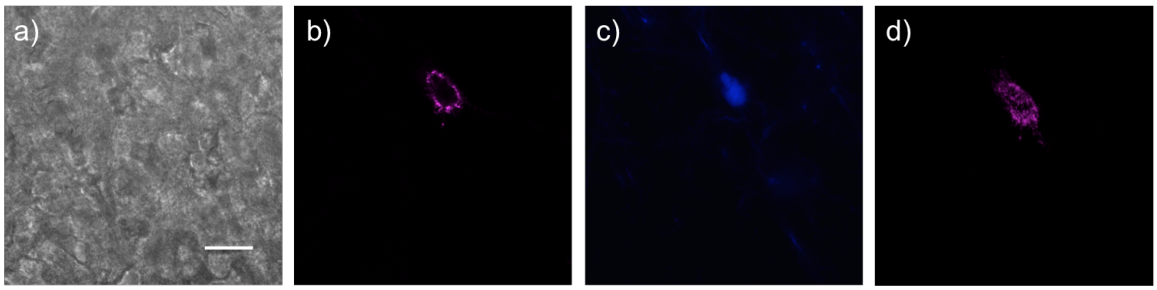

Figure 5-3-4. Imaging mBeRST-PEG$_{25}$-HaloTag in mouse brain slice expressing HaloTag-pDisplay and pCAG-mTagBFP2 following in utero electroporation. (a-d) Representative image of a slice stained with mBeRST-PEG$_{25}$-HaloTag (250nM, 15 min at RT). Sample was excited and visualized with a 633 nm laser on a confocal microscope. (a) Bright-field image of the slice. (b) Membrane-associated fluorescence stains only cell body. (c) Cytosolic BFP fluorescence indicates HaloTag expression. (d) Max intensity projection of Z-stack images over 17 μm depth in the same region of interest. Scale bar is 20 μm.

Reference

1. Miller, E. W.; Lin, J. Y.; Frady, E. P.; Steinbach, P. A.; Kristan, W. B., Jr.; Tsien, R. Y., *Proc Natl Acad Sci U S A* **2012,** *109* (6), 2114-9.
2. Grenier, V.; Walker, A. S.; Miller, E. W., *J. Am. Chem. Soc.* **2015,** *137* (34), 10894-10897.
3. Liu, P.; Grenier, V.; Hong, W.; Muller, V. R.; Miller, E. W., *J. Am. Chem. Soc.* **2017**, *139*, 17334-17340.
4. Huang, Y. L.; Walker, A. S.; Miller, E. W., *J. Am. Chem. Soc.* **2015**, *137* (33), 10767-10776.
5. Kulkarni, R. U.; Vandenberghe, M.; Thunemann, M.; James, F.; Andreassen, O. A.; Djurovic, S.; Devor, A.; Miller, E. W., *ACS Cent. Sci*. **2018**, *4* (10), 1371-1378.
6. Deal, P. E.; Kulkarni, R. U.; Al-Abdullatif, S. H.; Miller, E. W., *J. Am. Chem. Soc.* **2016**, *138* (29), 9085-9088.
7. Ortiz, G., PhD Dissertation, **2019**.
8. Lim, S. T.; Antonucci, D. E.; Scannevin, R. H.; Trimmer, J. S., *Neuron*. **2000**, *25* (2), 385-397.

Chapter 6:

Design and application of *meso*-Methylhydroxy BOIDPY

as a scaffold for photo-labile protecting groups

Part of this work has published in the following scientific journal:
N. Rubinstein, P. Liu, E.W. Miller and R. Weinstain. *meso*-Methylhydroxy BOIDPY: a Scaffold for Photo-labile Protecting Groups, *Chem. Commun.,* 2015, 51(29), 6369-72.

Portions of this work were performed in collaboration with the following persons:
Synthesis was assisted by Naama Rubinstein and Dnyaneshwar Kand

Abstract

The use of light to control the bioactivity of small molecule has attracted increasing attention in the past years due to its high spatial and temporal resolution. A photo-labile group can be used to quench the function of the bioactive molecule until photolysis reaction occurs. Here, we show that by installing a meso-methylhydroxy moiety, the boron dipyrromethene (BODIPY) scaffold can be converted into an efficient caging group, removable by green light. Water solubility of the scaffold can be further enhanced by installing sulfonic acid groups on the 3, 5 positions while retaining the photolysis kinetics. We describe caging and uncaging of important chemical functionalities and demonstrate green light mediated control over biological processes in cultured cell lines and neurons.

Introduction

The molecular mechanisms that govern biological functions are highly sophisticated and complex. Elucidation and manipulation of such processes on a molecular level requires precise external spatiotemporal control over their function. Light is an attractive way to achieve this goal, as it is non-invasive and readily delivered with high spatial and temporal precision. Thus, light has been harnessed to control biological processes through a method termed "caging"[1], in which the biological activity of a target small- or macro-molecule is abrogated by covalent ligation to a photolabile protecting group (PPG or caging groups). Exposure to light at a specific wavelength releases the molecule in its active form (Scheme 6-1a). This useful method has been applied to investigate and manipulate the activity of a wide range of biological processes by controlling the activity of small-molecules, proteins, RNA and gene expression.[2]

Over the years, dozens of caging groups have been developed, yet most operate in the UV range[3] (250-400 nm), which is problematic due to low tissue penetration and high tissue damage caused by the high energy UV irradiation. In addition, the narrow window limits the ability to control multiple cues through differentially caged compounds. While some of these concerns have been ameliorated through the use of two-photon excitation[4], the technique's applicability to several important fields (synthetic chemistry, material sciences, therapeutics delivery) is inherently limited by its small focal-point and low conversion throughput. Thus, there still exists a strong need for PPGs that operate by one-photon outside of the 250-400 nm window, to enable multiplex imaging and optical control of biological systems. Recently, several efforts have been made to identify novel scaffolds that would address this need.

Specific modifications in the structure of the known caging group 4-methylhydroxycoumarin enabled pushing their absorbance to the blue-cyan range.[5-6] Very recently, 4-arylalkoxy-boron dipyrromethene were demonstrated to release phenols when photolized with green light.[7] The light-induced cleavage of the boron-arylalkoxy bond was elegantly utilized to uncage a biogenic amine through a self-immolating linker, yet caging with these molecules requires a multi-step synthesis (up to 5 synthetic steps) and the stability of the boron-arylalkoxy bond under physiological conditions is a concern. Cyanine dyes were also converted into near-IR caging groups though uncaging in biological settings required prolonged irradiation times[8] (30 minutes). Metal complexes have likewise been explored as potential scaffolds for photocaging. Photolysis of amines from ruthenium complexes by blue-green light has been demonstrated and was

applied in cellular environment.[9-11] Nevertheless, their broad absorption spectrum impedes multiplex fluorescence imaging and their photosensitizer-based design leads to sensitizer-dependent phototoxicity. Another interesting approach is the contact-quenching induced scission of a Co–C bond that enables tuning of the light absorbance wavelength, up to the near-IR range, by selecting an appropriate fluorophore serving as an antenna.[12-13]

Here, we demonstrate that a specific derivatization of the boron dipyrromethene (BODIPY) core (Scheme 6-1b) enables its translation into an efficient green light excitable caging group. The excellent spectroscopic properties of BODIPYs render them potentially attractive caging groups. This family of chromophores is characterized by sharp and tunable light absorption (490-650 nm), high molar absorption coefficient (30,000-80,000 $L \cdot mol^{-1} \cdot cm^{-1}$) and chemical flexibility and stability, making them ideally suited for biological applications.[14] Taking a cue from the structures of coumarin-based PPGs, the recent efforts to convert xanthenes into PPGs[15-16], and the ease with which multiple functional groups are incorporated into the meso position of BODIPY[14,17-23], we hypothesized that equipping the BODIPY scaffold with a methylhydroxy moiety on at this position (Scheme 6-1c) will similarly enable caging and uncaging of molecules of interest.

Results & Discussion

6-1: Synthesis and application of first generation m&m-BODIPY compounds

To test our hypothesis, we synthesized 2,6-diethyl-1,3,5,7-tetramethyl-BODIPY bearing a methylhydroxy group on the meso position (m&m-BODIPY, Scheme 6-1-1). The molecule features strong absorbance centered at 537 nm, high molar absorption coefficient (ε_{537} = 53,300 $L \cdot mol^{-1} \cdot cm^{-1}$) and is highly fluorescent (Φ_{fl} = 0.90). The hydroxyl group of m&m-BODIPY can be straightforwardly conjugated to various chemical functionalities. Thus, conjugation of several model leaving groups to m&m-BODIPY through distinct chemical bonds was efficiently accomplished in one or two synthetic steps (Scheme 6-1-1). Upon green light illumination, the photolysis product was verified by spectroscopy and HPLC, proving that the novel scaffold can be applied to cage diverse chemical functionalities

To establish the utility of m&m-BODIPY as a platform for photocaging and activation of biomolecules in living cells, we synthesized the histamine-conjugated form of m&m-BODIPY (Scheme 6-1-1). Histamine is an important physiological effector molecule, with diverse consequences for human health and disease. Binding of histamine to the histamine H1 receptor initiates a cascade of intracellular events, including Ca^{2+} release.[24] We hypothesized that capping of the primary amine of histamine with a carbamate-linked m&m-BODIPY would mask the functionality of histamine and enable light-induced photoactivation and delivery of histamine.

To test this, we loaded HeLa cells with the Ca^{2+}-selective fluorescent indicator, fura-2. Treatment with histamine (5 μM, Figure 6-1-1a,b,f) resulted in 89% of the cells (in the field of view) responding by prompt oscillations in intracellular $[Ca^{2+}]_i$, as measured by changes in fura-2 fluorescence. Upon incubation with m&m-BODIPY-caged histamine (5 μM), no oscillations were observed prior to uncaging with 540 nm light. Uncaging light, in the presence of m&m-BODIPY-histamine, recapitulated the

oscillations seen with treatment by free histamine in 27% of the cells (Figure 6-1-5c,f). Pre-incubation of cells with the H1 receptor antagonist pyrilamine completely blocked this response (Figure 6-1-1c), demonstrating that the Ca^{2+} response is evoked by histamine photochemically liberated from the m&m-BODIPY cage. Importantly, no oscillations were observed in the presence of m&m-BODIPY-histamine but in the absence of light (Figure 6-1-1e). Additional control experiments further establish that Ca^{2+} flux depends on caged m&m-BODIPY-histamine and light, as light alone (no m&m-BODIPY-histamine, Figure 6-1-1g) and m&m-BODIPY-OH combined with irradiation (as a non-histamine releasing control, Figure 6-1-1h) do not promote correspondingly similar $[Ca^{2+}]_i$ changes. Taken together, these data establish m&m-BODIPY cages as an effective platform for photocaging biologically active molecules.

To further explore the versatility of m&m-BODIPY-type PPGs, we sought to apply this strategy to caging the catecholamine neurotransmitter dopamine (Scheme 6-1-1). This important neurotransmitter is vital for movement, motivation and cognition, and its misregulation is implicated in a number of human pathologies.[25] Methods to photocage dopamine exist, but rely on photocages with UV uncaging profiles[26] or use of transition metals.[27] A visible-light uncaging strategy with dopamine would be of utility for interrogating the role of dopamine in neuronal signalling. In a manner similar to the caging of histamine, the amino group of dopamine was modified with a carbamate-linked m&m-BODIPY.

In vitro characterization establish that the photocage shows good stability in the absence of light, but prompt release of dopamine following irradiation. (Figure 6-1-6). To examine the efficiency of m&m-BODIPY-dopamine, we again used fura-2 to monitor changes in $[Ca^{2+}]_i$ upon photo-induced release of dopamine. Mixed hippocampal/cortical rat neurons loaded with fura-2, sensitized with KCl, and treated with dopamine (10 μM) substantial fluxes in $[Ca^{2+}]_i$ in 88% of the cells, similar to those observed with histamine (Figure 6-1-2a,b,f). Incubation with m&m-BODIPY-dopamine (10 μM) followed by uncaging with 540 nm light resulted in similar oscillations of Ca^{2+} (51% of cells respond, Figure 6-1-2c,f), consistent with dopamine receptor agonism.[28] Importantly, control experiments established that hippocampal/cortical neuron activation by m&m-BODIPY-dopamine and light is abolished by the dopamine receptor antagonist (+)-butaclamol (100 μM Figure 6-1-2d), and that m&m-BODIPY-dopamine with no light (Figure 6-1-2e), light only (Figure 6-1-2g) or non-photolyzable m&m-BODIPY with light (Figure 6-1-2h), all result in baseline neuronal activity.

6-2: Synthesis and application of second generation m&m-BODIPY compounds

Following the success of m&m-BODIPY as a photo-labile group to mask the bioactivity of small molecules until the action of light, a second generation scaffold that aims to address the issue of hydrophobicity of the m&m-BODIPY scaffold is synthesized and tested. The inherently high hydrophobicity complicates the calculation of the effective compound concentration in aqueous buffer and the cage-compound complex is more likely to enter the cellular membrane, which is advantageous if intracellular events are targeted but poses potential challenges for studying processes occurring extracellularly such as ligand-receptor interaction on the cell surface. Efforts have been made to improve the water-solubility of the m&m-BODIPY scaffold by incorporating

anionic moieties on the structure while maintaining its favorable spectroscopic and photoreaction properties.

Previous studies focused on increasing solubility of BODIPY involve introducing long polyethylene glycol (PEG) chains or charged moieties such as carboxylates, sulfonates, phosphonates and quaternary ammonium.[29] Using sulfonates as the target moiety, we first incorporated the sulfonates on the 2, 6 positions and *p*-nitroaniline (PNA) as a model leaving group. However, mono- and di-sulfonated BODIPYs did not respond to green light (545/30 nm, 40 mW/cm^2) to release PNA (data not shown). It is possible that the electron withdrawing effect of sulfonate diminishes the rate if photolysis significantly. Alternatively, we modified the 3, 5 positions with sulfonic acid groups using 2-mercaptoethanesulfonic acid sodium salt (mesna) as a preferred nucleophile to prepare mono- and di-mesnaBODIPY. Both underwent efficient photolysis to yield free PNA in vitro (data not shown).

We next tested this scaffold in a biological context by conjugating to a bioactive molecule, histamine. Intracellular calcium increase induced by histamine is well-studied in various cell types including neurons. Thus, we used cultured rat hippocampal neurons to study the effect of light-controlled release of histamine on neuronal calcium fluctuations. Neurons were loaded with a Ca^{2+} fluorescent sensor, fura-2 and fluorescence intensity change was measured to reflect Ca^{2+} concentration changes. When treated with 5 μM (Figure 6-2-1a), calcium fluctuations were detected in cells. A similar and strong response was observed in di-mesnaBODIPY-histamine with 540 nm uncaging light (Figure 6-2-1b) while a reduced response was seen with compound alone (Figure 6-2-1c), suggesting that light is required for the release of the caged compound. In the presence of histamine receptor H1 antagonist pyrilamine (1 μM, Figure 6-2-1e), calcium response was completely quenched despite the release of histamine after photolysis, indicating that the calcium fluctuation was mediated through the H1 receptor pathway. We also recorded the cellular response with green light only (Figure 6-2-1d) and did not observe any effect, which again establishes the fact that the effect is histamine-related.

Sulfonated BODIPY compounds also exhibited increased water-solubility in cultured cells, compared to previously synthesized scaffold, m&m-BODIPY. Using caged dopamine as an example, we examined the localization of these compounds in cultured neurons under 540 nm light excitation. While m&m-BODIPY-dopamine shows significant cytosolic accumulation, sulfonated BODIPYs mostly remain in the extracellular buffer (Figure 6-2-2). To probe the effect of caged-dopamine on cultured neurons, we monitored $[Ca^{2+}]_i$ change using fura-2 and green light activation, similar to the histamine studies. Dopamine is also an essential neurotransmitter that regulates many neuronal signaling pathways and involved in several neurological disorders such as Parkinson's disease.[25] Thus, strategies for controlled delivery of dopamine would be beneficial to investigate its specific impact at different stages of biological pathways or even diseases. These data have also highlighted the generalizability of this novel di-mesnaBODIPY scaffold to cage a variety of biomolecules and their application in biological studies.

Neuronal response to dopamine was primed by KCl before treatment of the caged compound. Neurons incubated with di-mesnaBODIDY-dopamine (5 μM) following 540 nm light activation (Figure 6-2-3b) showed a robust calcium response, similar to the control dopamine treatment (5 μM, Figure 6-2-3a). When a dopamine receptor

antagonist, (+)-butaclamol (100 μM) was added (Figure 6-2-3c) or light alone (Figure 6-2-3e), we noted a considerable decrease in calcium fluctuations, suggesting a dopamine-dependent effect. Additional control experiment with di-mesnaBOIDPY-dopamine alone further confirms the light-dependent release of the bioactive molecule as no cellular activity was observed in the absence of light (Figure 6-2-3d).

6-3: Voltage imaging in cultured neurons treated with mono-mesnaBODIPY-serotonin.

Besides Ca^{2+} imaging, we also attempted voltage imaging with a far-red voltage sensitive dye (BeRST 1)[30] to study the effect of caged serotonin and effect of photolysis. Spontaneous activity of mature neurons (13 to 15 DIV) was recorded and firing frequency was calculated from a 10 s activity trace of spiking events. The neurotransmitter serotonin (5-HT) is known to exert an inhibitory effect on neuronal activity with a decrease in the firing frequency through the 5-HT1A receptor.[31] We first established a baseline firing frequency in imaging buffer HBSS and noticed no change in firing frequency when 2 μM of mono-mesnaBODIPY-serotonin was added, suggesting that the caging is effective to quench the bioactivity of serotonin. When green light was shone, a strong inhibitory effect was seen, with all the neurons remaining quiescent and displaying an average frequency close to zero. The effect is reversible since washing out the compound and replenishing with fresh HBSS restored the neuronal activity (Figure 6-3-1a). Nonetheless, when we repeated the experiment with a 5-HT1A-selective antagonist, WAY 100635 (10 nM; 1.4 nM IC50)[32], a similar and still robust inhibitory effect was observed, indicating that the reduction in firing frequency was not through 5-HT mediated pathway or the released 5-HT from mono-mesnaBODIPY was not responsible for the effect (Figure 6-3-1b). Green light or acetic acid, another by-product in the BODIPY photolysis reaction, did not seem to affect neuronal activity (data not shown), suggesting that other factors such as some sort of interactions involving the dye, green light, BODIPY or released serotonin might play a role.

Conclusions

The incorporation of a methylhydroxy moiety at the meso position of BODIPY core transforms this commonly used fluorophore into an effective, green-light excitable photo-labile protecting group. The introduced hydroxyl group can be straightforwardly conjugated to diverse chemical functionalities, enabling simple caging of molecules of interest through a variety of chemical bonds. Caging of 6 separate substrates, including phenol, aniline, a primary amine and acetic acid was readily accomplished within one or two synthetic steps and similar chemistry should be applicable for caging additional functional groups, including alcohols and thiols. These cageable functional groups are frequently represented in many biogenic and bioactive molecules. Uncaging from m&m-BODIPY was effectively facilitated by green light for all caged functionalities, with small variations in release rate and yield, which seems to depend on the nature of the leaving group, as well as on the chemical bond connecting it to the BODIPY cage. Additional modifications of introducing sulfonic acid groups enhance water solubility of the scaffold, which effectively inhibits cellular entrance of the compound and ensures that the caged molecule remains in the aqueous buffer for reaction with cell surface receptors after photolysis.

Using both types of scaffold, the bioactivity of two biogenic amines, histamine and dopamine, was successfully controlled in cell cultures and in neurons by biologically benign green light, demonstrating the biological relevance and practical application of this novel caging group. Finally, m&m-BODIPY's structure readily enables tuning of color to encompass the whole cyan-red range, as well as to determine cellular permeability or impermeability. Thus, we expect that the general strategy presented herein will enable expansion of the BODIPY cage to include these properties.

Experimental section

General Cell Culture Methods

All animal procedures were approved by the UC Berkeley Animal Care and Use Committees and conformed to the NIH Guide for the Care and Use and Laboratory Animals and the Public Health Policy.

HeLa cells were cultured in DMEM with 10% FBS and plated on 12 mm round poly-D-lysine coated coverslips in 24 well trays at a density of 1.6×10^5 cells/well 12-18 hours prior to imaging experiments. Prior to imaging, cells were incubated with 2 μM fura2-AM (LifeTech) in HBSS at room temperature (25 °C) for 1 hour, washed once, and transferred to a 35 mm imaging dish containing 2 mL HBSS. Compounds (m&m-BODIPY photocages) were diluted from stocks in DMSO (1000x) to 3x concentration in 1 mL HBSS. This was added to the imaging dish and then the experiment began. Pyrilamine maleate (1 μM, Sigma) was added prior to addition of the BODIPY compounds.

Neurons were harvested from rat embryonic hippocampus and cortex. After culturing for 14 days in vitro (DIV) in neurobasal media supplemented with B27, cells were loaded in a fashion identical to the HeLa cells described above. (+)-butaclamol (100 μM, Sigma) was added prior to treatment with dopamine (10 μM) or BODIPY compounds (10 μM). Neurons were treated with a 3x stock of KCl (150 mM stock, 50 mM final) to prime the response to dopamine. After initial Ca^{2+} transients, as measured by fura-2 reached baseline levels, dopamine or BODIPY was added and the photolysis began.

Imaging Instrumentation and Experimental

All imaging was performed on an AxioExaminer Z-1 (Zeiss) equipped with a Spectra-X Light engine LED light (Lumencor). Light was delivered through a W-Plan-Apo 20x/1.0 objective and focused onto an OracFlash4.0 sCMOS camera (Hamamatsu). Excitation for fura-2 imaging was provided at 390/22, passed through a quadruple dichroic mirror (432/38, 509/22, 586/40, 654LP), and a quadruple emission filter (430/32, 508/14, 586/30, 708/98). In this configuration, increases in $[Ca^{2+}]_i$ result in decreases in fura-2 fluorescence. Samples were uncaged with 542 nm light for 15 seconds at maximum power, followed by fura-2 imaging, 25 ms exposures every second for ~5 minutes after uncaging. For BeRST 1 voltage imaging, the excitation light was delivered from a LED at 631/28 (bandpass) nm and emission was collected with a quadruple emission filter (430/32, 508/14, 586/30, 708/98 nm) after passing through a quadruple dichroic mirror (432/38, 509/22, 586/40, 654 nm LP). Images were binned 4x4 to allow sampling rates of 0.5 kHz and 5000 frames (10 s) were acquired for each recording.

Data Analysis

Plots of ΔF/F were constructed by creating regions of interest (ROI) around cells, subtracting background (ROI of non-cell region), and dividing by the mean fluorescence for the first 10 frames of the acquisition. These values were plotted as ΔF/F vs. time.

HeLa cells: Images opened in FIJI (v1.49b, FIJI is just ImageJ, NIH). Corrected drift, with Plugins>Registration>StackReg>Rigid Body Transformation. Bleaching was corrected, if necessary, with Image>Adjust>Bleach Correction>Exponential Fit. Then an average intensity Z-project was calculated for the first 10 frames (to set F_0). The Registered, Bleach-corrected stack was then divided by F_0 to give the F/F_0 movie, which was scaled from 0.75 to 1.25 in all cases, except for m&m-BODIPY540 control.

Neurons: Images opened in FIJI (v1.49b, FIJI is just ImageJ, NIH). Corrected drift, with Plugins>Registration>StackReg>Rigid Body Transformation. Bleaching was corrected, if necessary, with Image>Adjust>Bleach Correction>Exponential Fit. Then an average intensity Z-project was calculated for the 10 frames near the beginning of the acquisition (to set F_0). The Registered, Bleach-corrected stack was then divided by F_0 to give the F/F_0 movie, which was scaled from 0.75 to 1.25 in all cases.

Figures and Schemes

Scheme 6-1. *Design and structure of meso-methylhydryoxy BODIPY as a photo-labile group to cage biomolecules.*

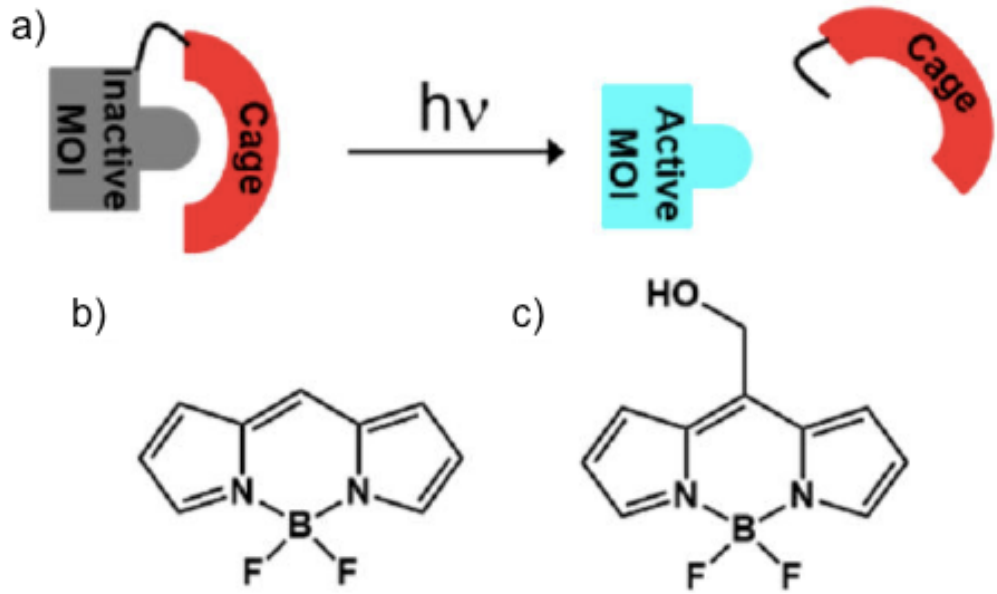

Scheme 6-1. (a) Schematic representation of light-mediated control over a small- or macro-molecule of interest (MOI) activity. (b,c) General structure of BODIPY core (b) and meso-methylhydroxy BODIPY (m&m-BODIPY) applied for photocaging (c).

Scheme 6-1-1. *Synthesis of m&m-BODIPY and its conjugates.*

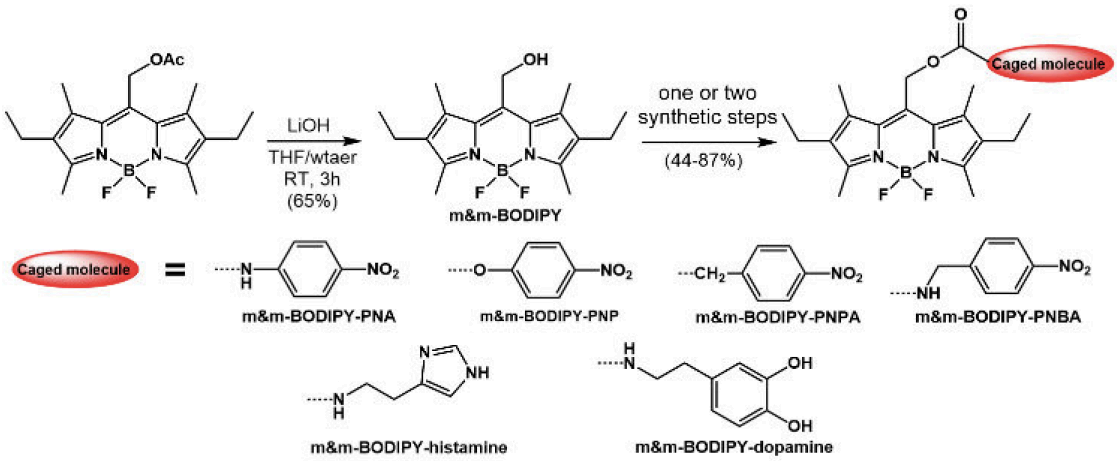

Scheme 6-1-1. Synthesis and chemical structures of m&m-BODIPY and its conjugates. In parentheses: chemical yields.

***Figure 6-1-1**. Characterization of m&m-BODIPY-histamine in HeLa cells.*

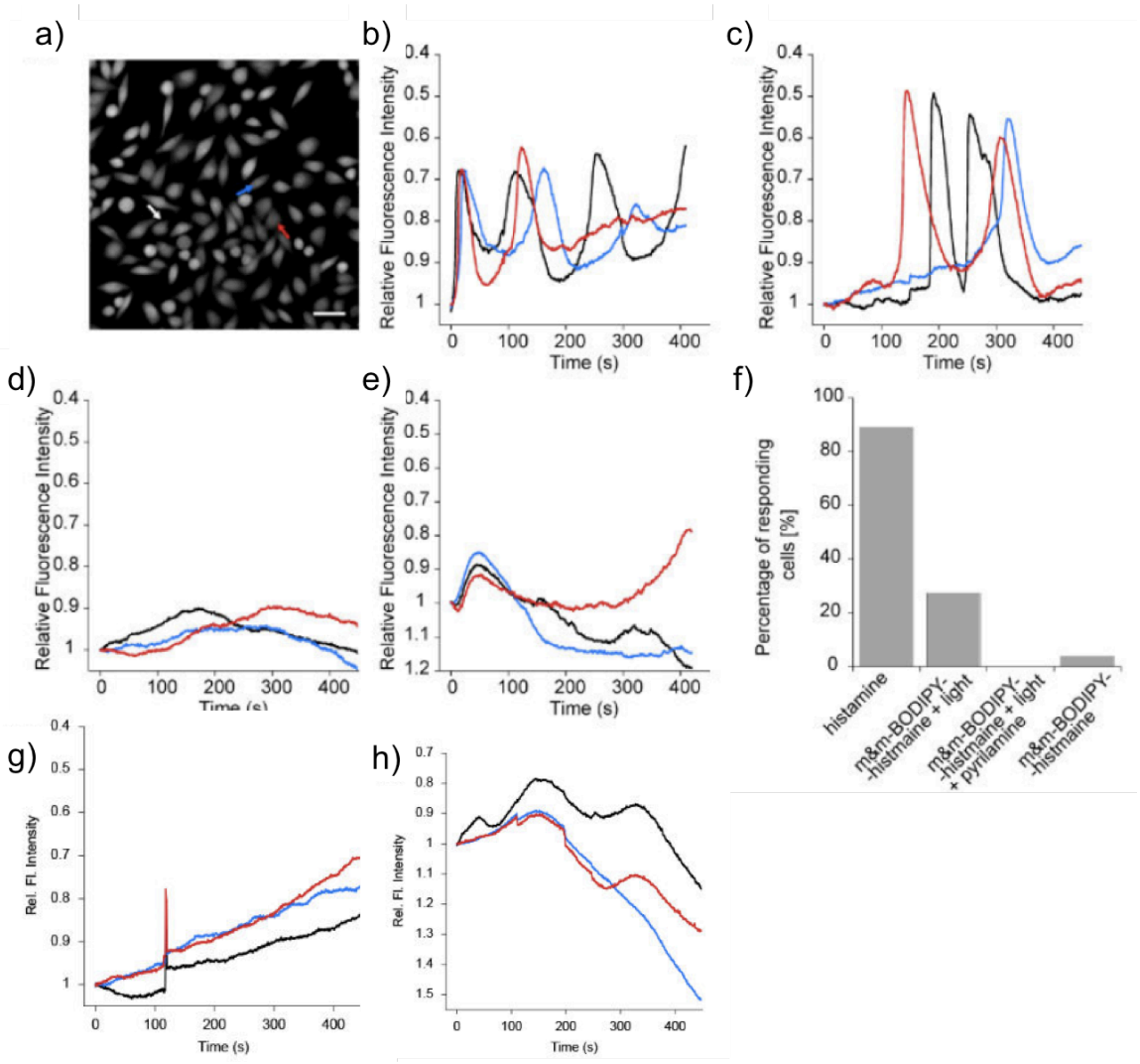

Figure 6-1-1. Live cell epifluorscence imaging of Ca^{2+} release triggered by m&m-BODIPY-histamine in HeLa cells. All cells were loaded with fura-2 AM and then treated with either 5 μM histamine (a, b), 5 μM BODIPY-histamine and green light (c), 5 μM BODIPY-histamine, light, and the H1 receptor antagonist, pyrilamine (d), or 5 μM BODIPY-histamine without light (e), or green light alone (g) or 5 μM BODIPY-OH. Shown are changes in Fura-2 fluorescence as quantified from representative cells. Scale bar is 20 μm. (f) Percentage of responding cells in each treatment, as quantified for the whole field of view (n > 65 cells in each treatment).

Figure 6-1-2. *Characterization of m&m-BODIPY-dopamine in cultured neurons.*

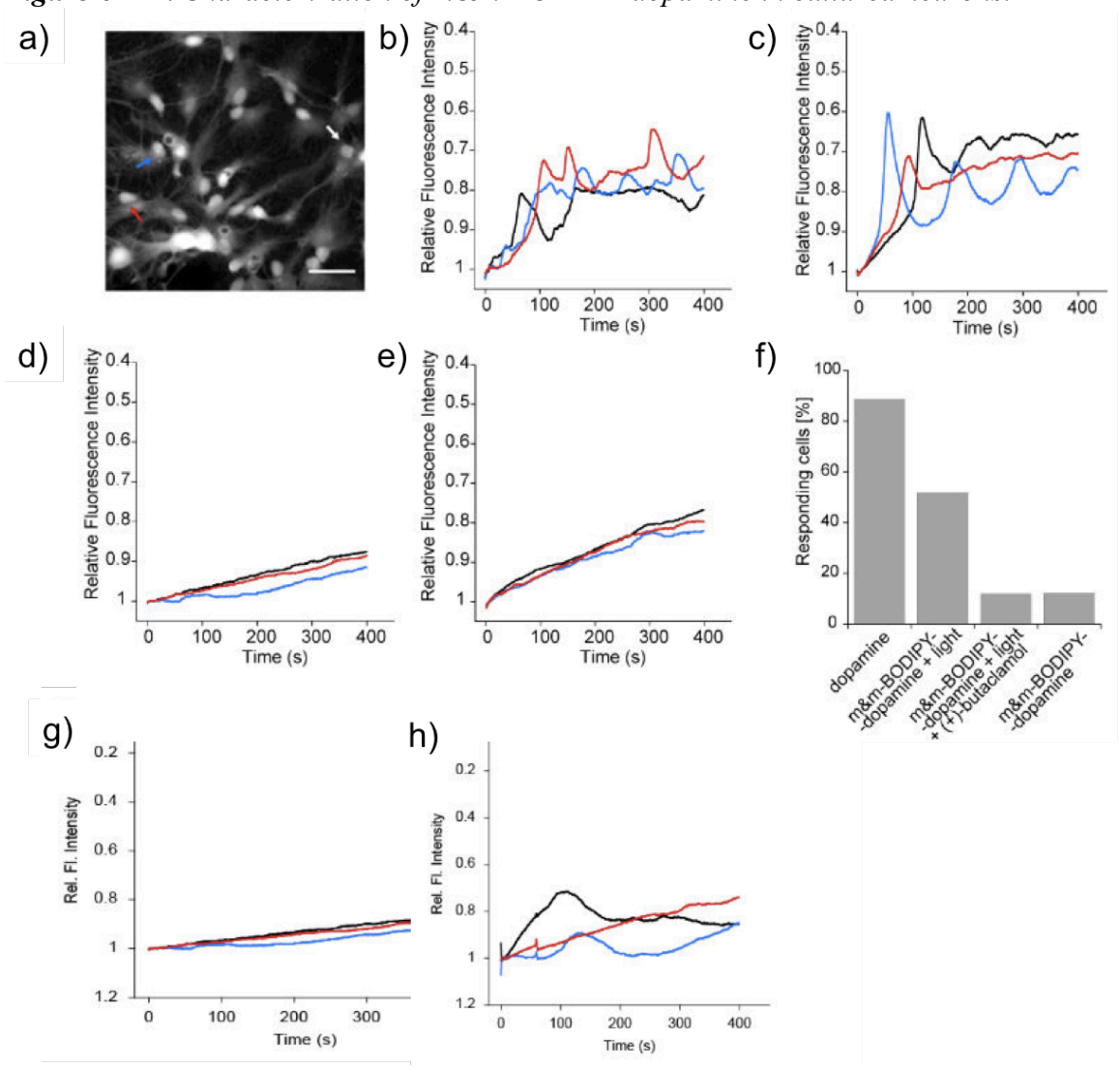

Figure 6-1-2. Live cell epifluorscence imaging of Ca^{2+} release triggered by BODIPY-dopamine in KCl-primed rat cortical/hippocampal neurons. All cells were loaded with fura-2 AM and then treated with either dopamine (10 μM) (a,b), BODIPY-dopamine (10 μM) and green light (c), BODIPY dopamine, light, and the dopamine receptor antagonist, (+)-butaclamol (100 μM) (d), or BODIPY-dopamine without light (e), or green light only (g), or BODIPY-OH (h). Shown are changes in Fura-2 fluorescence as quantified from representative cells. Scale bar is 20 μm. (f) Percentage of responding cells in each treatment, as quantified for the whole field of view (n > 17 cells in each treatment).

Figure 6-2-1. *Characterization of di-mesnaBODIPY-histamine in cultured neurons.*

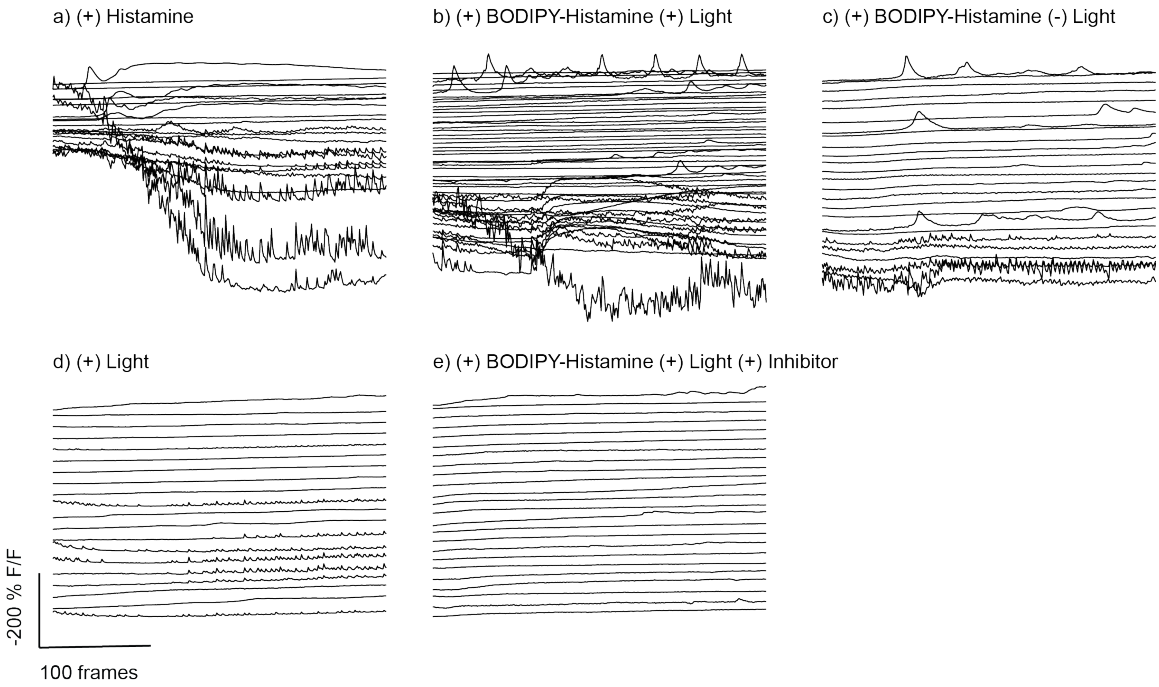

Figure 6-2-1. Uncaging of dopamine with di-mesna BODIPY histamine causes robust Ca^{2+} oscillations in cultured rat hippocampal neurons. Ca^{2+} imaging in neurons treated with (a) histamine (5 μM), or (b) di-mesna BODIPY histamine (5 μM) and uncaging light, or (c) di-mesna BODIPY dopamine (5 μM) *without* uncaging light, or (d) only with uncaging light, or (e) di-mesna BODIPY histamine (5 μM) and uncaging light in the presence of the dopamine receptor antagonist pyrilamine (1 μM). Plots represent F/F_{max} for representative cells vs. time and are inverted. An increase in cellular Ca^{2+} concentration results in a decrease in fura-2 fluorescence, under the illumination conditions used in this study.

Figure 6-2-2. *Compare localization of various BODIPY scaffold.*

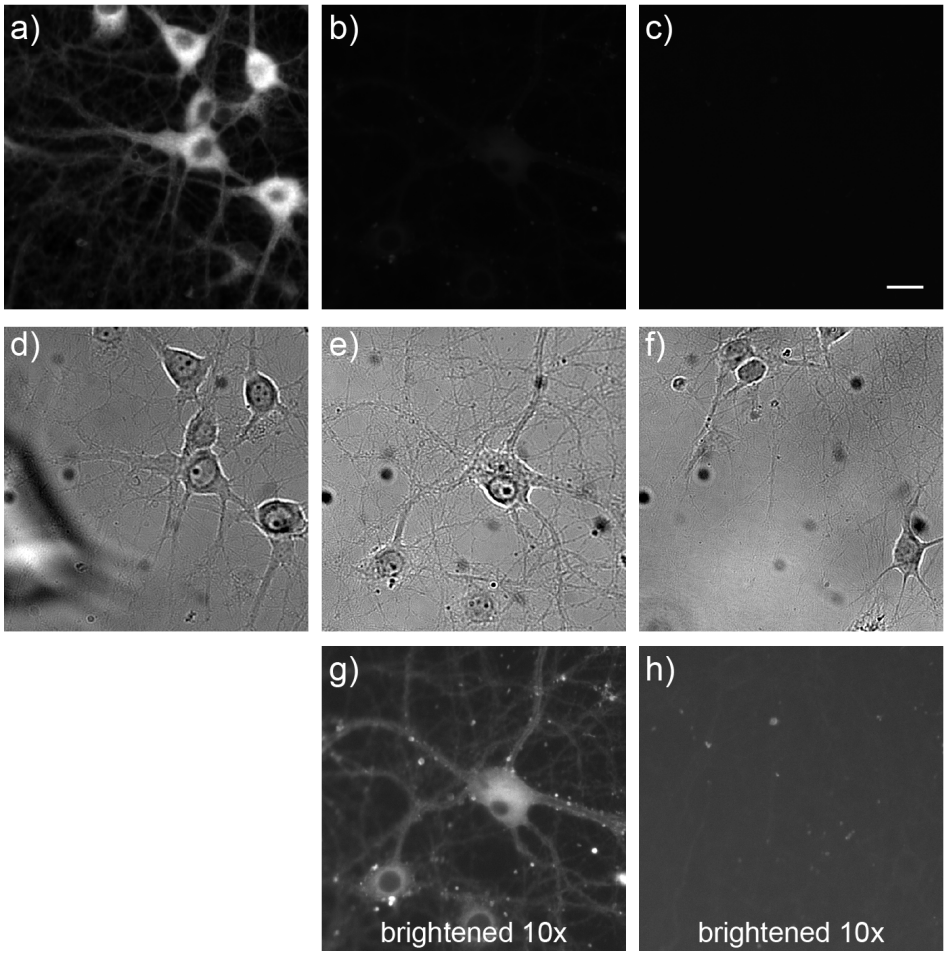

Figure 6-2-2. Sulfonated BODIPY caged compounds show differential accumulation in neurons. Wide-field epifluorescence microscopy of cultured rat hippocampal neurons stained with (a) EthylBODIPY-dopamine, (b) mono-mesnaBODIPY-dopamine, or (c) di-mesnaBODIPY-dopamine. DIC images of neurons stained with (d) EthylBODIPY-dopamine, (e) mono-mesnaBODIPY-dopamine, or (f) di-mesnaBODIPY-dopamine. Because of the low membrane-associated fluorescence of mono- and di-mesna BODIPY compounds, the images were brightened by 10x for (g) mono-mesnaBODIPY and (h) di-mesnaBODIPY-dopamine. Scale bar is 20 μm.

Figure 6-2-3. *Characterization of di-mesnaBODIPY-dopamine in cultured neurons.*

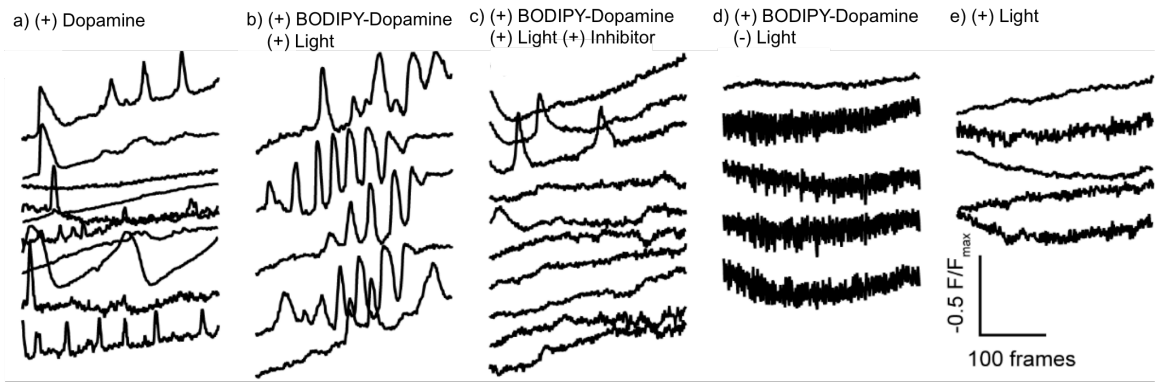

Figure 6-2-3. Uncaging of dopamine with di-mesna BODIPY dopamine causes robust Ca^{2+} oscillations in cultured rat hippocampal neurons. Ca^{2+} imaging in neurons treated with (a) dopamine (5 μM), or (b) di-mesna BODIPY dopamine (5 μM) and uncaging light, or (c) di-mesna BODIPY dopamine (5 μM) and uncaging light in the presence of the dopamine receptor antagonist butaclamol (100 μM), or (d) di-mesna BODIPY dopamine (5 μM) *without* uncaging light, and (e) only with uncaging light. Plots represent F/F_{max} for representative cells vs. time and are inverted. An increase in cellular Ca^{2+} concentration results in a decrease in fura-2 fluorescence, under the illumination conditions used in this study.

Figure 6-3-1. *Voltage imaging of spontaneous activity in cultured neurons treated with mono-mesnaBODIPY-serotonin.*

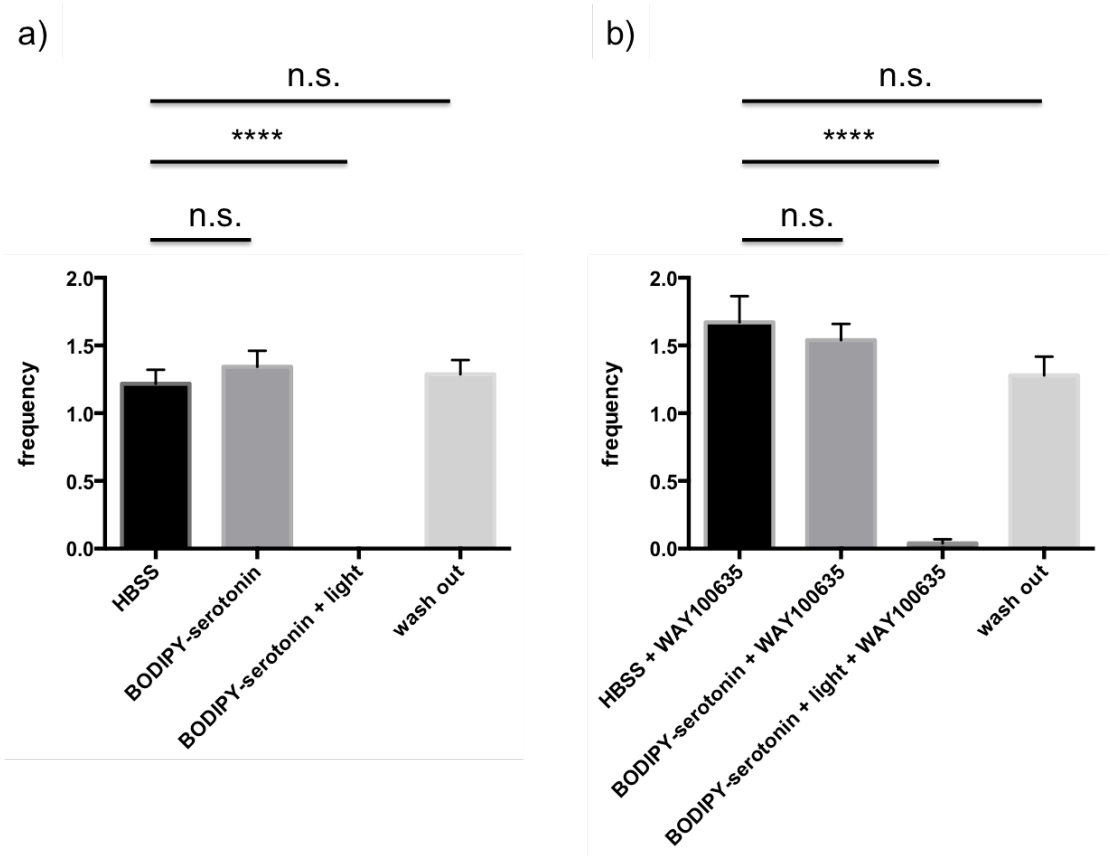

Figure 6-3-1. Optical recording of neuronal activity using BeRST1 in cultured hippocampal neurons upon various compound treatment. (a) Hippocampal neurons were treated with mono-mesnaBODIPY-serotonin (2 μM) alone and (b) in the presence of WAY 100635 (10 nM). The firing rate of neurons was measured before (first bars), during without light (second bars), during with light (third bards) and after (fourth bars) washout of mono-mesnaBODIPY-serotonin. Data are mean ± S.E.M. for the average firing rate of 2 different coverslips of neurons. Each coverslip's average firing frequency was measured from between 50-60 individual neurons, for a total of about 120 neurons for each condition. Two-tailed Mann-Whitney tests were used to determine statistical significance.
**** indicates $p < 0.001$.

Reference

1. Kaplan, J. H.; Forbush, B.; Hoffman, J. F., *Biochemistry* **1978**, *17* (10), 1929-1935.
2. Shao, Q.; Xing, B., *Chem. Soc. Rev.* **2010**, *39* (8), 2835-2846.
3. Klan, P.; Solomek, T.; Bochet, C. G.; Blanc, A.; Givens, R.; Rubina, M.; Popik, V.; Kostikov, A.; Wirz, J., *Chem. Rev.* **2013**, *113* (1), 119-191.
4. Bort, G.; Gallavardin, T.; Ogden, D.; Dalko, P. I., *Angew. Chem. Int. Ed. Engl.* **2013**, *52* (17), 4526-4537.
5. Fournier, L.; Gauron, C.; Xu, L.; Aujard, I.; Le Saux, T.; Gagey-Eilstein, N.; Maurin, S.; Dubruille, S.; Baudin, J. B.; Bensimon, D.; Volovitch, M.; Vriz, S.; Jullien, L.,. **2013**, *8* (7), 1528-1536.
6. Olson, J. P.; Banghart, M. R.; Sabatini, B. L.; Ellis-Davies, G. C., *J. Am. Chem. Soc.* **2013**, *135* (42), 15948-15954.
7. Umeda, N.; Takahashi, H.; Kamiya, M.; Ueno, T.; Komatsu, T.; Terai, T.; Hanaoka, K.; Nagano, T.; Urano, Y., *ACS Chem. Biol* **2014**, *9* (10), 2242-2246.
8. Gorka, A. P.; Nani, R. R.; Zhu, J.; Mackem, S.; Schnermann, M. J., *J. Am. Chem. Soc.* **2014**, *136* (40), 14153-14159.
9. Zayat, L.; Noval, M. G.; Campi, J.; Calero, C. I.; Calvo, D. J.; Etchenique, R., *Chembiochem : a European Journal of Chemical Biology* **2007**, *8* (17), 2035-2038.
10. Rial Verde, E. M.; Zayat, L.; Etchenique, R.; Yuste, R., *Front. Neural Circuits* **2008**, *2* (2).
11. Filevich, O.; Etchenique, R., *Photochemical & Photobiological Sciences* **2013**, *12* (9), 1565-1570.
12. Shell, T. A.; Shell, J. R.; Rodgers, Z. L.; Lawrence, D. S., *Angew. Chem. Int. Ed. Engl.* **2014**, *53* (8), 875-878.
13. Smith, W. J.; Oien, N. P.; Hughes, R. M.; Marvin, C. M.; Rodgers, Z. L.; Lee, J.; Lawrence, D. S., *Angew. Chem. Int. Ed. Engl.* **2014**, *53* (41), 10945-10948.
14. Ulrich, G.; Ziessel, R.; Harriman, A., *Angew. Chem. Int. Ed. Engl.* **2008**, *47* (7), 1184-1201.
15. Antony, L. A.; Slanina, T.; Sebej, P.; Solomek, T.; Klan, P., *Org. Lett.* **2013**, *15* (17), 4552-4555.
16. Sebej, P.; Wintner, J.; Muller, P.; Slanina, T.; Al Anshori, J.; Antony, L. A.; Klan, P.; Wirz, J., *J. Org. Chem.* **2013**, *78* (5), 1833-1843.
17. Palao, E.; de la Moya, S.; Agarrabeitia, A. R.; Esnal, I.; Banuelos, J.; Lopez-Arbeloa, I.; Ortiz, M. J., *Org. Lett.* **2014**, *16* (17), 4364-4367.
18. Krumova, K.; Cosa, G., *J. Am. Chem. Soc.* **2010**, *132* (49), 17560-17569.
19. Dhokale, B.; Jadhav, T.; Mobin, S. M.; Misra, R., *Chem. Commun*. **2014**, *50* (65), 9119-9121.
20. Zeng, L.; Miller, E. W.; Pralle, A.; Isacoff, E. Y.; Chang, C. J., *J. Am. Chem. Soc.* **2006**, *128* (1), 10-11.
21. Qi, H.; Teesdale, J. J.; Pupillo, R. C.; Rosenthal, J.; Bard, A. J., *J. Am. Chem. Soc.* **2013**, *135* (36), 13558-13566.
22. Ni, Y.; Zeng, L.; Kang, N. Y.; Huang, K. W.; Wang, L.; Zeng, Z.; Chang, Y. T.; Wu, J., *Chemistry* **2014**, *20* (8), 2301-2310.
23. Zhu, H.; Fan, J.; Li, M.; Cao, J.; Wang, J.; Peng, X., *Chemistry* **2014**, *20* (16), 4691-4696.

24. Smit, M. J.; Bloemers, S. M.; Leurs, R.; Tertoolen, L. G.; Bast, A.; de Laat. S. W.; Timmerman, H., *Br. J. Pharmacol.* **1992**, *107* (2), 448-455.
25. Rice, M. E.; Patel, J. C.; Cragg, S. J., *Neuroscience* **2011**, *198*, 112-137.
26. Lee, T. H.; Gee, K. R.; Ellinwood, E. H.; Seidler, F. J., *J. Neurosci. Methods* **1996**, *67* (2), 221-231.
27. Araya, R.; Andino-Pavlovsky, V.; Yuste, R.; Etchenique, R., ACS Chem. Neurosci. **2013**, *4* (8), 1163-1167.
28. Lezcano, N.; Bergson, C., *J Neurophysiol*. **2002**, *87* (4), 2167-2175.
29. Fan, G.; Yang, L.; *Front Chem Sci Eng* **2014,** *8* (4), 405-417.
30. Huang, Y. L.; Walker, A. S.; Miller, E. W., *J. Am. Chem. Soc.* **2015**, *137* (33), 10767-10776.
31. Mahgoub, M. A.; Sara, Y.; Kavalali, E. T.; Monteggia, L. M., *J Pharmacol Exp Ther* **2006**, *317* (1), 88-96.
32. Fletcher, A.; Forster, E. A.; Bill, D. J.; Brown, G.; Cliffe, I. A.; Hartley, J. E.; Jones, D. E.; McLenachan, A.; Stanhope, K. J.; Critchley, D. J.; Childs, K. J.; Middlefell, V. C.; Lanfumey, L.; Corradetti, R.; Laporte, A. M.; Gozlan, H.; Hamon, M.; Dourish, C. T., *Behav Brain Res* **1996**, *73* (1-2), 337-53.

Appendix 1:

Fluorogenic Activation by a Cell-Surface β-galactosidase

Portions of this work were performed in collaboration with the following persons:
AO-β-gal cloning and immunostaining were assisted by Hannah Thorner

Introduction

Fluorescein-based VoltageFluor dyes such as VF2.1.Cl contain phenolic oxygens, which are ideal targets for masking by a small molecule moiety. The presence of these protection groups efficiently reduce the fluorescence and voltage sensitivity while a turn-on response can be accomplished in cells of interest expressing a specific enzyme that removes the protection group. One example is the cyclopropyl ester and PLE pair that has been demonstrated in Chapter 2 (VF-EX)[1] and Chapter 3-1 (carboVF-EX)[2] in which targeted staining and voltage imaging are observed in defined cells, including cultured neurons. Nonetheless, preliminary efforts that translate this strategy to mouse brain slice failed to produce sufficient contrast between PLE-expressing and non-expressing cells. In addition, due to the bulky and relative hydrophobic ester group, a solubilizing reagent is required for dye loading, which may become a potential problem as detergent-based delivery reagents are usually not favored in biology. As a result, we decided to explore other enzyme-substrate pairs that can circumvent these problems and become applicable to a more complex biological sample.

We have chosen β-galactosidase, which cleaves a glycosidic bond in β-galactoside.[3] One common chromogenic assay that involves β-galactosidase is the blue-white colony screening in molecular cloning. Bacterial lacZ gene encodes a β-galactosidase that reacts with a synthetic substrate X-Gal to form a blue precipitate, allowing for screening when bacteria were plated on X-Gal-containing agar plates.[4-6] One of the appealing features of the β-galactosidase approach to our fluorogenic activation is its galactose sugar substrate that can be adapted as a protecting group. The hydroxyl groups would substantially enhance the water solubility of our relatively hydrophobic VF dye containing the greasy molecular wire. Also, galactose has already been used as caging moiety for fluorescein including FDG (Fluorescein di-β-D-galactopyranoside), a fluorogenic substrate to assess β-galactosidase activity.[7-10] These prior examples have motivated us to use galactose to quench the fluorescence of VF2.1.Cl and to engineer a cell-surface β-galactosidase for fluorogenic activation.

Results & Discussions

We designed and prepared four constructs for expressing bacterial β-galactosidase (lacZ) in HEK cells (Scheme A1-1). We used either the GPI-anchor (DAF) or transmembrane domain (pDisplay) and the IgK secretion signal peptide for cell-surface targeting. Besides CMV promoter, a CAG promoter was also utilized to enhance the protein expression.[11-12] When immunostaining was performed under non-permeabilizing condition in which the antibody was only allowed to bind extracellular epitopes, we observed negligible anti-HA staining (Figure A1-2a-f), suggesting that none of the constructs expressed lacZ on the cell surface. Some lacZ expression was observed in the cytosol when cells were permeabilized (Figure A1-2g-l). In particular, protein expression was greatly boosted when driven by a CAG protmoer (Figure A1-2e,k) while the DAF construct seems to express better than the pDisplay version (Figure A1-2k,l). Since lacZ is a tetramer of four identical subunits of 116 kD each, we hypothesize that the large size hinders its trafficking to the cell surface.

To verity if lacZ is actually produced by the mammalian cell machinery and remains functional, we performed a X-Gal assay, where a blue precipitate forms after the indole released in the β-galactosidase reaction undergoes dimerization and oxidation

spontaneously (Figure A1-3a).[5-6] We plated and transfected HEK cells according to standard protocols, added the X-Gal to the cells about 24 h after transfection and monitored the formation of blue precipitate by checking the solution color (Figure A1-3b). Only a faint blue was noticed in the cells expressing CAG-lacZ-DAF after 4 hours. After 24 hours, we started to see color changes in cells transfected with all four constructs. Cells expressing CAG-lacZ-DAF exhibited the most intense blue and those expressing CMV-lacZ-pDislay showed the faintest while the solution for non-transfected control remained colorless. These observations indicate that DAF construct expresses better that the pDisplay construct while CAG increases protein production in general. As X-Gal is cell permeable and anti-HA staining detects no cell-surface expression, we believe that a portion of lacZ is generated inside the cell and is reactive to cleave β-galactose under physiological conditions although the kinetics seem rather slow with a conversion rate on the scale of hours. Therefore, other targeting moieties should be explored to improve extracellular export and localization.

On the other hand, we diverted our attention to other types of β-galactosidase, in search for a smaller monomeric enzyme that hopefully encounters fewer challenges for expression and trafficking. We chose the β-galactosidase from a fungus *Aspergillus oryzae*, which is known to hydrolyze lactose in an extracellular environment.[13] It functions at an optimal pH of 5.0 and temperature at 50 °C; at physiological conditions (pH 7.0 and 37 °C), it retains approximately 50% of its maximal activity.[13-14] In addition, AO-β-gal has been extensively used in industrial processing of dairy products and is commercially available for our in vitro characterization purposes.[15] Inspired by these findings, we cloned the AO-β-gal gene[15] into our pcDNA3 vector with a GPI-anchor for extracellular targeting. To our delight, immunostaining reveals very robust cell surface expression using the CMV-DAF construct (Figure A1-4). When we carried out the cellular assay using X-Gal, no color change was observed (data no shown). A variety of acidic pHs (pH = 2, 5 or 7) were experimented but cells didn't survive well. Nonetheless, X-Gal may not be the perfect substrate since it is cell permeable and the AO-β-gal is present on the cell surface. β-gal-VF2.1.Cl dye synthesis is undergoing and can be tested with our construct to further validate the enzyme activity.

Conclusion

We have attempted to express both a bacterial and fungal β-galactosidase to cell-surface in order to achieve fluorogenic activation of our voltage sensitive dye. LacZ from *E. coli* is indeed expressed in HEK cells, with the ability to convert X-Gal to products with a relatively slow kinetics, but fails to express extracellularly due to its large tetrameric size. On the contrary, the monomeric β-galactosidase from *A. oryzae* displays efficient localization on the cell-surface but favors a highly acidic environment for optimal enzymatic activity. Extensive literature research is required to pinpoint a most suitable β-galactosidase, with a relatively small size and good compatibility with physiological conditions to suit our purpose.

Experimental Sections

Cell Culture

Human embryonic kidney 293T (HEK) cells were maintained and plated in Dulbecco's modified eagle medium (DMEM) supplemented with 4.5 g/L D-glucose, 10% fetal bovine serum (FBS; Thermo Scientific) and 1% GlutaMax (Invitrogen) at 37 °C in a humidified incubator with 5 % CO_2. Cells were passaged and plated in DMEM (as above) at a density of 75,000 cells onto 12 mm glass coverslips pre-coated with Poly-D-Lysine (PDL; 1 mg/ml; Sigma-Aldrich) per well in a 24-well plate. Transfection of plasmids was carried out using Lipofectamine 3000 (Invitrogen) ~18-24 h after plating. Imaging was performed 12-18 h after transfection.

β-galactosidase activity assay using X-Gal

X-Gal (5-bromo-4-chloro-3-indolyl β-D-galactopyranoside) was purchased from Thermo Fischer (Cat. B1690) and stored at -20 °C as a solid and stock solution was prepared in DMSO. For activity assay of β-gal in HEK cells, cells were transfected with the constructs as stated above and the assay was conducted about 24 h after transfection. Media was aspirated and replaced with 0.5 mL of X-Gal in HBSS (final concentration 1 mg/mL). Reaction was done at 37 °C for 4 h or 24 h before taking images. For AO-β-gal, HBSS solutions of various acidic pHs were used.

Imaging Parameters

Epifluorescence imaging was performed on an AxioExaminer Z-1 (Zeiss) equipped with a Spectra-X Light engine LED light (Lumencor), controlled with Slidebook (v6, Intelligent Imaging Innovations). Images were acquired with a W-Plan-Apo 20x/1.0 water objective (20x; Zeiss). Images were focused onto an OrcaFlash4.0 sCMOS camera (sCMOS; Hamamatsu).

Immunocytochemistry

To detect expression and localization of β-galactosidase, HEK cells were fixed with 4% paraformaldehyde in PBS for 10 min. Permeabilization was performed with 0.3% Triton-X in PBS for 2 min at room temperature (RT). Blocking was done in 5% w/v bovine serum albumin (BSA; Sigma Aldrich) in PBS for 1 h. Primary anti-HA antibody (rabbit IgG, Cell Signaling Technologies Cat. 3724S) was incubated at 4 °C overnight, followed by anti-rabbit AlexaFluor 647 secondary antibody (goat IgG, Life Technologies A21244) at RT for 2 h. Hoechst 33342 was added for 15 min at RT to visualize the nucleus. All antibodies and counterstain were used at 1:1000 dilution.

DNA constructs

To express the β-galactosidase protein on the cell surface, an IgK leader sequence was fused to the N-terminal and either a signal peptide for GPI addition (DAF) or a transmembrane domain (pDisplay) was added to the C-terminal. For the purpose of immunostaining, an HA tag was inserted. Mammalian expression vector pcDNA3 with either a cytomegalovirus (CMV) promoter or chick beta-actin (CAG) promoter was used for protein expression in HEK cells. In all constructs, nuclear-targeted mCherry (NLS-mCherry) was inserted down stream of β-galactosidase, separated by an internal ribosome

entry site (IRES) sequence, in order to track the expression of β-galactosidase in live cells. All constructs were confirmed by sequencing. The following sequences were used (5' to 3'):

IgK
ATGGAGACAGACACACTCCTGCTATGGGTACTGCTGCTCTGGGTTCCAGGTTC
CACTGGTGAC

Bacterial β-galactosidase (lacZ) from *E. coli*
GTCGTTTTACAACGTCGTGACTGGGAAAACCCTGGCGTTACCCAACTTAATCG
CCTTGCAGCACATCCCCCTTTCGCCAGCTGGCGTAATAGCGAAGAGGCCCGC
ACCGATCGCCCTTCCCAACAGTTGCGCAGCCTGAATGGCGAATGGCGCTTTG
CCTGGTTTCCGGCACCAGAAGCGGTGCCGGAAAGCTGGCTGGAGTGCGATCT
TCCTGAGGCCGATACTGTCGTCGTCCCCTCAAACTGGCAGATGCACGGTTACG
ATGCGCCCATCTACACCAACGTAACCTATCCCATTACGGTCAATCCGCCGTTT
GTTCCCACGGAGAATCCGACGGGTTGTTACTCGCTCACATTTAATGTTGATGA
AAGCTGGCTACAGGAAGGCCAGACGCGAATTATTTTTGATGGCGTTAACTCG
GCGTTTCATCTGTGGTGCAACGGGCGCTGGGTCGGTTACGGCCAGGACAGTC
GTTTGCCGTCTGAATTTGACCTGAGCGCATTTTTACGCGCCGGAGAAAACCGC
CTCGCGGTGATGGTGCTGCGTTGGAGTGACGGCAGTTATCTGGAAGATCAGG
ATATGTGGCGGATGAGCGGCATTTTCCGTGACGTCTCGTTGCTGCATAAACCG
ACTACACAAATCAGCGATTTCCATGTTGCCACTCGCTTTAATGATGATTTCAG
CCGCGCTGTACTGGAGGCTGAAGTTCAGATGTGCGGCGAGTTGCGTGACTAC
CTACGGGTAACAGTTTCTTTATGGCAGGGTGAAACGCAGGTCGCCAGCGGCA
CCGCGCCTTTCGGCGGTGAAATTATCGATGAGCGTGGTGGTTATGCCGATCGC
GTCACACTACGTCTGAACGTCGAAAACCCGAAACTGTGGAGCGCCGAAATCC
CGAATCTCTATCGTGCGGTGGTTGAACTGCACACCGCCGACGGCACGCTGAT
TGAAGCAGAAGCCTGCGATGTCGGTTTCCGCGAGGTGCGGATTGAAAATGGT
CTGCTGCTGCTGAACGGCAAGCCGTTGCTGATTCGAGGCGTTAACCGTCACG
AGCATCATCCTCTGCATGGTCAGGTCATGGATGAGCAGACGATGGTGCAGGA
TATCCTGCTGATGAAGCAGAACAACTTTAACGCCGTGCGCTGTTCGCATTATC
CGAACCATCCGCTGTGGTACACGCTGTGCGACCGCTACGGCCTGTATGTGGT
GGATGAAGCCAATATTGAAACCCACGGCATGGTGCCAATGAATCGTCTGACC
GATGATCCGCGCTGGCTACCGGCGATGAGCGAACGCGTAACGCGAATGGTGC
AGCGCGATCGTAATCACCCGAGTGTGATCATCTGGTCGCTGGGGAATGAATC
AGGCCACGGCGCTAATCACGACGCGCTGTATCGCTGGATCAAATCTGTCGAT
CCTTCCCGCCCGGTGCAGTATGAAGGCGGCGGAGCCGACACCACGGCCACCG
ATATTATTTGCCCGATGTACGCGCGCGTGGATGAAGACCAGCCCTTCCCGGCT
GTGCCGAAATGGTCCATCAAAAAATGGCTTTCGCTACCTGGAGAGACGCGCC
CGCTGATCCTTTGCGAATACGCCCACGCGATGGGTAACAGTCTTGGCGGTTTC
GCTAAATACTGGCAGGCGTTTCGTCAGTATCCCCGTTTACAGGGCGGCTTCGT
CTGGGACTGGGTGGATCAGTCGCTGATTAAATATGATGAAAACGGCAACCCG
TGGTCGGCTTACGGCGGTGATTTTGGCGATACGCCGAACGATCGCCAGTTCTG
TATGAACGGTCTGGTCTTTGCCGACCGCACGCCGCATCCAGCGCTGACGGAA
GCAAAACACCAGCAGCAGTTTTTCCAGTTCCGTTTATCCGGGCAAACCATCG
AAGTGACCAGCGAATACCTGTTCCGTCATAGCGATAACGAGCTCCTGCACTG

GATGGTGGCGCTGGATGGTAAGCCGCTGGCAAGCGGTGAAGTGCCTCTGGAT
GTCGCTCCACAAGGTAAACAGTTGATTGAACTGCCTGAACTACCGCAGCCGG
AGAGCGCCGGGCAACTCTGGCTCACAGTACGCGTAGTGCAACCGAACGCGAC
CGCATGGTCAGAAGCCGGGCACATCAGCGCCTGGCAGCAGTGGCGTCTGGCG
GAAAACCTCAGTGTGACGCTCCCCGCCGCGTCCCACGCCATCCCGCATCTGA
CCACCAGCGAAATGGATTTTTGCATCGAGCTGGGTAATAAGCGTTGGCAATT
TAACCGCCAGTCAGGCTTTCTTTCACAGATGTGGATTGGCGATAAAAAACAA
CTGCTGACGCCGCTGCGCGATCAGTTCACCCGTGCACCGCTGGATAACGACA
TTGGCGTAAGTGAAGCGACCCGCATTGACCCTAACGCCTGGGTCGAACGCTG
GAAGGCGGCGGGCCATTACCAGGCCGAAGCAGCGTTGTTGCAGTGCACGGCA
GATACACTTGCTGATGCGGTGCTGATTACGACCGCTCACGCGTGGCAGCATC
AGGGGAAAACCTTATTTATCAGCCGGAAAACCTACCGGATTGATGGTAGTGG
TCAAATGGCGATTACCGTTGATGTTGAAGTGGCGAGCGATACACCGCATCCG
GCGCGGATTGGCCTGAACTGCCAGCTGGCGCAGGTAGCAGAGCGGGTAAACT
GGCTCGGATTAGGGCCGCAAGAAAACTATCCCGACCGCCTTACTGCCGCCTG
TTTTGACCGCTGGGATCTGCCATTGTCAGACATGTATACCCCGTACGTCTTCC
CGAGCGAAAACGGTCTGCGCTGCGGGACGCGCGAATTGAATTATGGCCCACA
CCAGTGGCGCGGCGACTTCCAGTTCAACATCAGCCGCTACAGTCAACAGCAA
CTGATGGAAACCAGCCATCGCCATCTGCTGCACGCGGAAGAAGGCACATGGC
TGAATATCGACGGTTTCCATATGGGGATTGGTGGCGACGACTCCTGGAGCCC
GTCAGTATCGGCGGAATTCCAGCTGAGCGCCGGTCGCTACCATTACCAGTTG
GTCTGGTGTCAAAAA

Fungal β-galactosidase from *A. oryzae*

ATGAAGCTCCTTTCAGTTGCAGCCGTCGCTTTGCTTGCAGCACAAGCAGCAGG
CGCCTCAATCAAACATCGCTTGAACGGTTTCACAATTTTGGAGCATCCAGATC
CAGCCAAACGCGACTTGCTCCAAGATATCGTGACCTGGGACGACAAGAGTCT
TTTCATAAATGGTGAGAGGATAATGCTTTTTAGCGGTGAGGTCCATCCTTTTC
GCCTGCCCGTGCCTAGTCTTTGGTTGGATATATTCCATAAGATCCGAGCTCTG
GGCTTTAACTGTGTCAGTTTCTATATAGATTGGGCATTGCTGGAAGGGAAACC
AGGCGATTACAGAGCAGAGGGTATATTCGCTCTTGAGCCATTTTTTGACGCA
GCCAAGGAGGCAGGGATATATCTTATAGCACGACCAGGGAGTTACATTAACG
CAGAAGTATCAGGCGGCGGTTTTCCCGGTTGGTTGCAGCGAGTAAACGGCAC
ACTGCGGAGCTCTGATGAACCTTTTCTGAAAGCAACAGATAATTATATTGCCA
ACGCTGCAGCCGCTGTCGCCAAGGCACAAATCACTAATGGCGGACCCGTCAT
CCTGTACCAGCCAGAGAATGAGTATTCAGGTGGCTGCTGCGGTGTTAAATAC
CCTGACGCTGATTACATGCAGTATGTTATGGACCAGGCACGGAAGGCCGATA
TAGTGGTGCCCTTCATCTCAAACGACGCTTCACCCTCAGGACACAACGCACCT
GGCAGCGGAACTTCTGCAGTAGATATATATGGACACGACAGCTACCCCCTGG
GGTTTGATTGCGCCAATCCCTCAGTCTGGCCCGAAGGTAAGCTCCCTGACAAT
TTCAGGACTTTGCACTTGGAGCAGTCACCATCCACCCCATACTCCCTGCTCGA
ATTTCAGGCAGGGGCCTTTGACCCTTGGGGTGGTCCAGGCTTCGAGAAGTGC
TACGCCCTGGTGAACCATGAATTTTCCCGGGTCTTTTACCGGAATGATCTTTC
CTTTGGTGTTAGCACTTTTAACCTGTATATGACCTTTGGCGGTACAAACTGGG
GTAACCTCGGACATCCTGGCGGGTACACTTCCTACGACTACGGTTCTCCAATC
ACAGAAACCAGGAATGTAACCAGAGAGAAGTATTCCGACATTAAATTGCTTG

CTAACTTTGTCAAAGCTTCTCCCTCATACCTTACAGCCACACCTCGGAATCTG
ACTACTGGAGTATACACCGATACCAGTGATCTGGCCGTTACACCCCTCATTGG
CGATAGTCCAGGCTCTTTTTTTGTTGTGCGGCATACTGACTATTCTTCTCAAGA
ATCTACAAGCTATAAATTGAAATTGCCCACATCCGCCGGTAATCTGACCATTC
CTCAGTTGGAGGGGACCTTGAGCCTTAACGGGCGCGACAGTAAGATTCACGT
TGTTGATTACAATGTCAGCGGTACCAACATTATATATTCAACTGCCGAGGTCT
TCACCTGGAAAAAGTTCGATGGTAACAAGGTACTCGTACTGTATGGGGGACC
TAAGGAACACCATGAACTCGCTATCGCCAGCAAGAGCAATGTTACTATTATC
GAGGGTTCAGACAGTGGGATAGTAAGCACTCGCAAGGGATCCAGCGTTATTA
TAGGGTGGGACGTTAGTAGCACCCGACGGATAGTGCAGGTCGGGGACCTTAG
GGTATTCCTTTTGGACCGGAACTCTGCTTATAATTACTGGGTGCCCGAGTTGC
CTACTGAAGGGACCAGTCCTGGGTTTAGCACTAGTAAAACCACCGCTAGCAG
CATTATAGTGAAAGCTGGCTACCTCCTGCGGGGTGCACATTTGGACGGTGCC
GATCTGCATCTTACAGCAGATTTCAACGCTACTACTCCAATAGAAGTAATAG
GCGCTCCCACAGGAGCAAAAAATTTGTTTGTTAACGGGGAGAAGGCATCACA
CACCGTCGACAAAAATGGAATTTGGAGTTCCGAGGTTAAATACGCAGCACCC
GAAATTAAACTGCCTGGTCTTAAGGACCTGGATTGGAAGTACCTGGATACCC
TCCCTGAGATTAAAAGCTCATACGACGACTCTGCCTGGGTCTCCGCAGATTTG
CCCAAGACCAAGAACACACATCGGCCTCTTGACACACCAACCAGTCTCTATA
GTTCCGACTACGGCTTTCATACCGGGTACCTGATTTATCGGGGCCATTTTGTA
GCTAACGGCAAAGAGTCTGAGTTCTTCATCCGCACACAGGGAGGGTCTGCTT
TCGGATCTAGCGTCTGGCTGAATGAAACTTACCTCGGCAGCTGGACTGGAGC
CGACTATGCAATGGATGGTAACTCTACTTACAAGCTGAGTCAACTGGAAAGT
GGAAAGAATTACGTAATCACTGTGGTAATCGATAATCTTGGCTTGGACGAGA
ACTGGACTGTAGGTGAGGAAACTATGAAAAATCCAAGAGGCATCCTCTCCTA
CAAATTGTCAGGGCAGGATGCCAGTGCAATTACATGGAAGCTCACTGGGAAC
CTCGGCGGTGAAGATTATCAGGACAAAGTGAGAGGTCCATTGAATGAAGGCG
GCCTCTACGCAGAGCGACAAGGTTTTCACCAGCCCCAGCCCCCATCTGAAAG
TTGGGAATCTGGGAGCCCCCTGGAAGGTCTGTCAAAACCAGGTATTGGCTTC
TATACCGCACAATTCGACTTGGACCTGCCTAAAGGCTGGGACGTCCCTCTTTA
TTTTAATTTTGGAAATAATACACAGGCTGCCCGCGCTCAGCTTTACGTCAACG
GCTACCAATATGGGAAATTCACTGGGAACGTTGGCCCTCAAACTTCCTTCCCC
GTTCCAGAGGGGATCCTCAACTATCGCGGAACTAATTATGTGGCTTTGAGCCT
GTGGGCTCTCGAAAGCGACGGTGCTAAACTTGGATCCTTTGAGCTTTCTTATA
CAACCCCCGTGCTCACTGGTTATGGTAACGTAGAGAGTCCAGAGCAACCAAA
GTATGAGCAACGCAAAGGTGCTTAT

HA
TATCCATATGATGTTCCAGATTATGCT

DAF
CCAAATAAAGGAAGTGGAACCACTTCAGGTACTACCCGTCTTCTATCTGGGC
ACACGTGTTTCACGTTGACAGGTTTGCTTGGGACGCTAGTAACCATGGGCTTG
CTGACTTAG

pDisplay

GCTGTGGGCCAGGACACGCAGGAGGTCATCGTGGTGCCACACTCCTTGCCCT
TTAAGGTGGTGGTGATCTCAGCCATCCTGGCCCTGGTGGTGCTCACCATCATC
TCCCTTATCATCCTCATCATGCTTTGGCAGAAGAAGCCACGT

IRES
GCCCCTCTCCCTCCCCCCCCCCTAACGTTACTGGCCGAAGCCGCTTGGAATAA
GGCCGGTGTGCGTTTGTCTATATGTTATTTTCCACCATATTGCCGTCTTTTGGC
AATGTGAGGGCCCGGAAACCTGGCCCTGTCTTCTTGACGAGCATTCCTAGGG
GTCTTTCCCCTCTCGCCAAAGGAATGCAAGGTCTGTTGAATGTCGTGAAGGA
AGCAGTTCCTCTGGAAGCTTCTTGAAGACAAACAACGTCTGTAGCGACCCTTT
GCAGGCAGCGGAACCCCCCACCTGGCGACAGGTGCCTCTGCGGCCAAAAGCC
ACGTGTATAAGATACACCTGCAAAGGCGGCACAACCCCAGTGCCACGTTGTG
AGTTGGATAGTTGTGGAAAGAGTCAAATGGCTCTCCTCAAGCGTATTCAACA
AGGGGCTGAAGGATGCCCAGAAGGCACCCCATTGTATGGGATCTGATCTGGG
GCCTCGGTGCACATGCTTTACATGTGTTTAGTCGAGGTTAAAAAAACGTCTAG
GCCCCCCGAACCACGGGGACGTGGTTTTCCTTTGAAAAACACGATGATAATA
TGGCCACA

Nuclear localization sequence (NLS)
ATGGTGCCCAAGAAGAAGAGGAAAGTC

mCherry
GTGAGCAAGGGCGAGGAGGACAACATGGCCATCATCAAGGAGTTCATGCGC
TTCAAGGTGCACATGGAGGGCTCCGTGAACGGCCACGAGTTCGAGATCGAGG
GCGAGGGCGAGGGCCGCCCCTACGAGGGCACCCAGACCGCCAAGCTGAAGG
TGACCAAGGGCGGCCCCCTGCCCTTCGCCTGGGACATCCTGTCCCCTCAGTTC
ATGTACGGCTCCAAGGCCTACGTGAAGCACCCCGCCGACATCCCCGACTACT
TGAAGCTGTCCTTCCCCGAGGGCTTCAAGTGGGAGCGCGTGATGAACTTCGA
GGACGGCGGCGTGGTGACCGTGACCCAGGACTCCTCCCTGCAGGACGGCGAG
TTCATCTACAAGGTGAAGCTGCGCGGCACCAACTTCCCCTCCGACGGCCCCGT
AATGCAGAAGAAGACCATGGGCTGGGAGGCCTCCTCCGAGCGGATGTACCCC
GAGGACGGCGCCCTGAAGGGCGAGATCAAGCAGAGGCTGAAGCTGAAGGAC
GGCGGCCACTACGACGCCGAGGTCAAGACCACCTACAAGGCCAAGAAGCCC
GTGCAGCTGCCCGGCGCCTACAACGTCAACATCAAGCTGGACATCACCTCCC
ACAACGAGGACTACACCATCGTGGAACAGTACGAGCGCGCCGAGGGCCGCC
ACTCCACCGGCGGCATGGACGAGCTGTACAAG

CMV promoter
GACATTGATTATTGACTAGTTATTAATAGTAATCAATTACGGGGTCATTAGTT
CATAGCCCATATATGGAGTTCCGCGTTACATAACTTACGGTAAATGGCCCGCC
TGGCTGACCGCCCAACGACCCCCGCCCATTGACGTCAATAATGACGTATGTTC
CCATAGTAACGCCAATAGGGACTTTCCATTGACGTCAATGGGTGGACTATTTA
CGGTAAACTGCCCACTTGGCAGTACATCAAGTGTATCATATGCCAAGTACGC
CCCCTATTGACGTCAATGACGGTAAATGGCCCGCCTGGCATTATGCCCAGTAC
ATGACCTTATGGGACTTTCCTACTTGGCAGTACATCTACGTATTAGTCATCGC
TATTACCATGGTGATGCGGTTTTGGCAGTACATCAATGGGCGTGGATAGCGG

TTTGACTCACGGGGATTTCCAAGTCTCCACCCCATTGACGTCAATGGGAGTTT
GTTTTGGCACCAAAATCAACGGGACTTTCCAAAATGTCGTAACAACTCCGCC
CCATTGACGCAAATGGGCGGTAGGCGTGTACGGTGGGAGGTCTATATAAGCA
GAGCT

CAG Promoter
TCGAGGTGAGCCCCACGTTCTGCTTCACTCTCCCCATCTCCCCCCCCTCCCCA
CCCCCAATTTTGTATTTATTTATTTTTTAATTATTTTGTGCAGCGATGGGGGCG
GGGGGGGGGGGGGGGCGCGCGCCAGGCGGGGCGGGGCGGGGCGAGGGGCG
GGGCGGGGCGAGGCGGAGAGGTGCGGCGGCAGCCAATCAGAGCGGCGCGCT
CCGAAAGTTTCCTTTTATGGCGAGGCGGCGGCGGCGGCGGCCCTATAAAAAG
CGAAGCGCGCGGCGGGCG

Benchling links for constructs

CMV-IgK-lacZ-HA-DAF-IRES-mCherry
https://benchling.com/s/a64YYj70

CAG-IgK-lacZ-HA-DAF-IRES-mCherry
https://benchling.com/s/22YaFaAm

CMV-IgK-lacZ-HA-pDisplay-IRES-mCherry
https://benchling.com/s/seq-nR4dGXprwx9GFqtbyb0W

CAG-IgK-lacZ-HA-pDisplay-IRES-mCherry
https://benchling.com/s/08GCP2uT

CMV-IgK-AO-β-gal-DAF-IRES-mCherry
https://benchling.com/s/seq-ZAPDqNkXC2fm1EZBnwgR

Figures and Schemes

Scheme A1-1. *Design of β-galactosidase-based fluorogenic activation.*

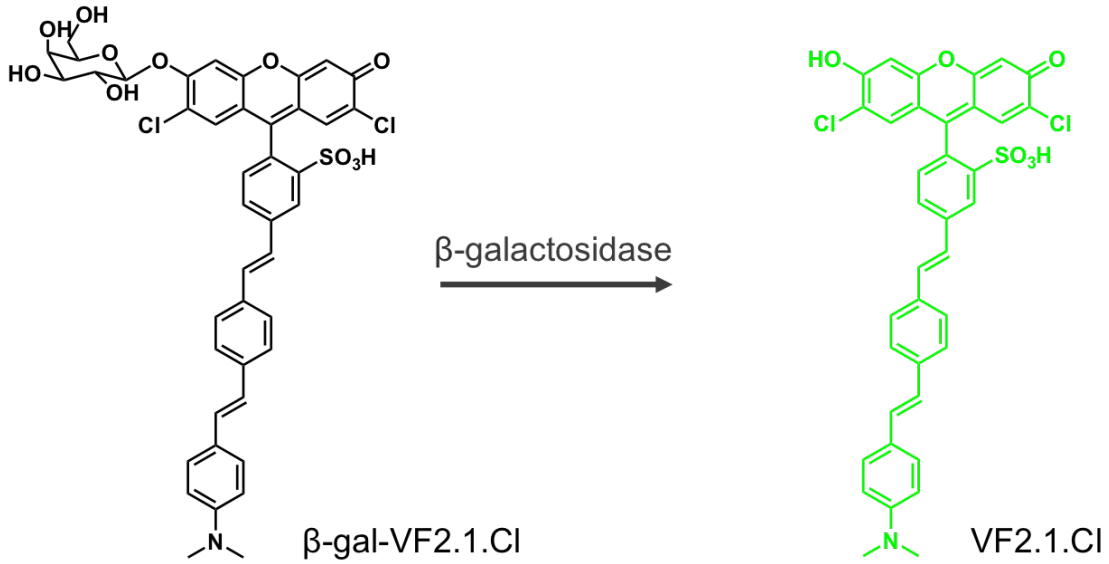

Scheme A1-1. Structure of galactose-masked dye β-gal-VF2.1.Cl and its fluorescence turn-on following β-galactosidase reaction.

***Figure A1-1**. β-galactosidase constructs used in this study.*

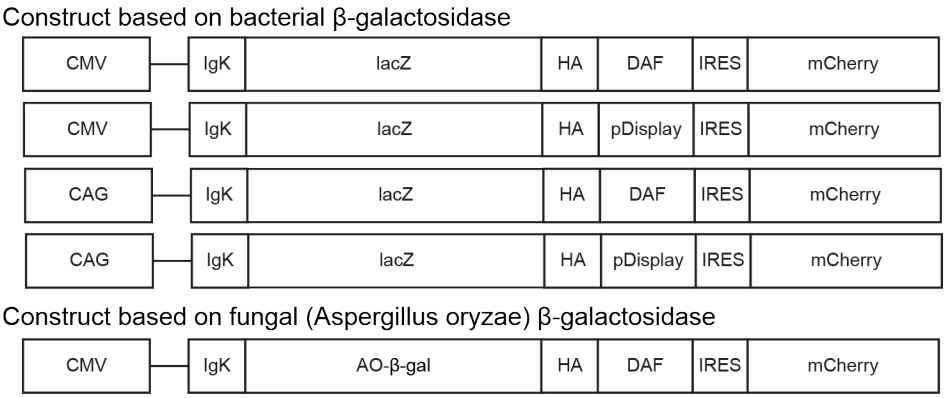

Figure A1-1. Constructs designed and tested for expressing β-galactosidase on the cell surface.

***Figure A1-2**. Characterization of bacterial β-galactosidase (lacZ) expression in HEK cells using immunohistochemistry.*

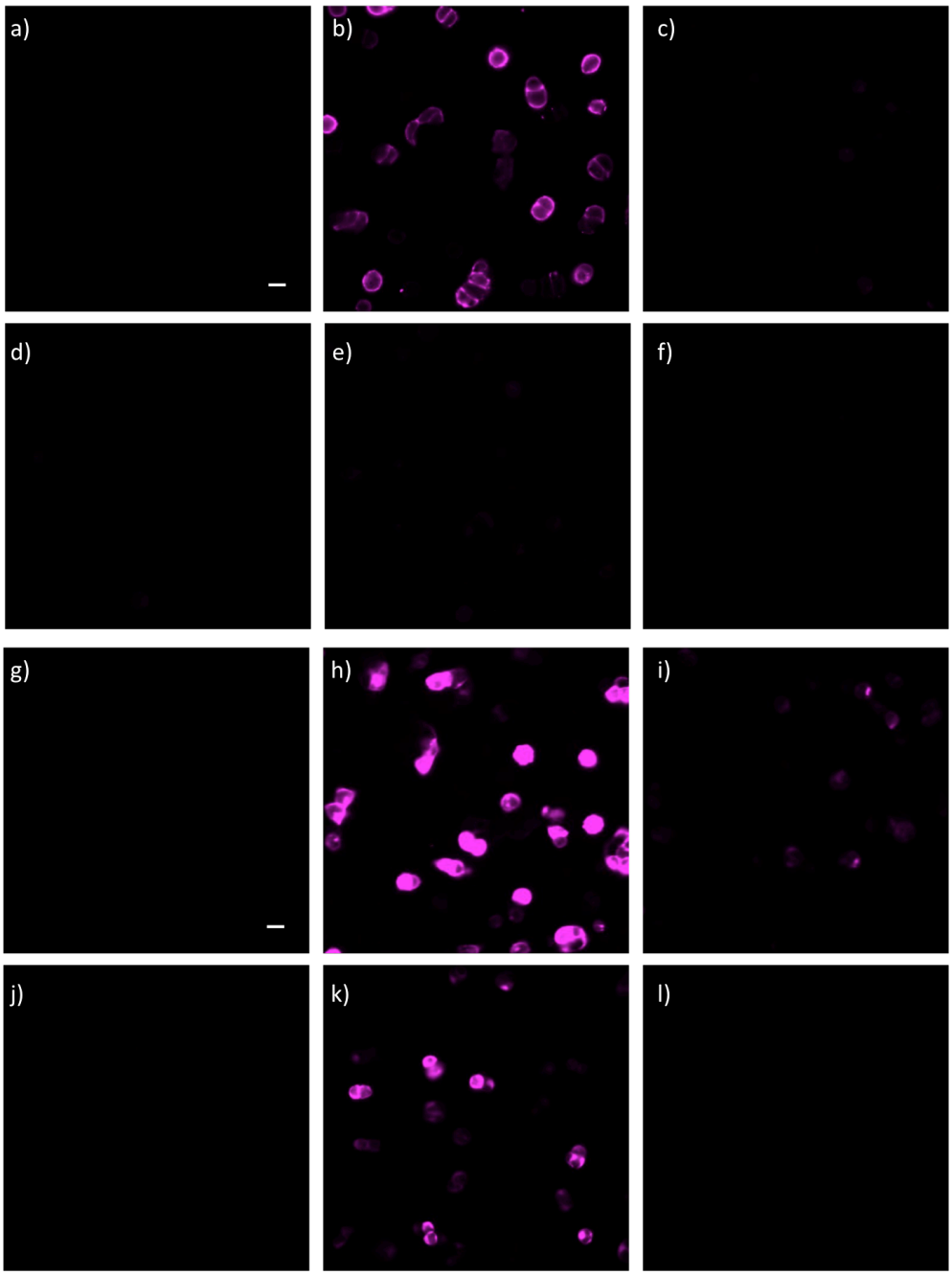

Figure A1-2. Wide-field images of anti-HA staining for fixed HEK cells (a,g) without any plasmid transfection or expressing (b,h) CMV-PLE-DAF positive control or (c,i) CMV-lacZ-DAF or (d,j) CMV-lacZ-pDisplay or (e,k) CAG-lacZ-DAF or (f,l) CAG-lacZ-pDisplay. Images a-f are acquired in non-permeable conditions and images g-l in permeable condition. Scale bar is 20 μm.

***Figure A1-3**. Functional assay of cell-surface lacZ in HEK cells.*

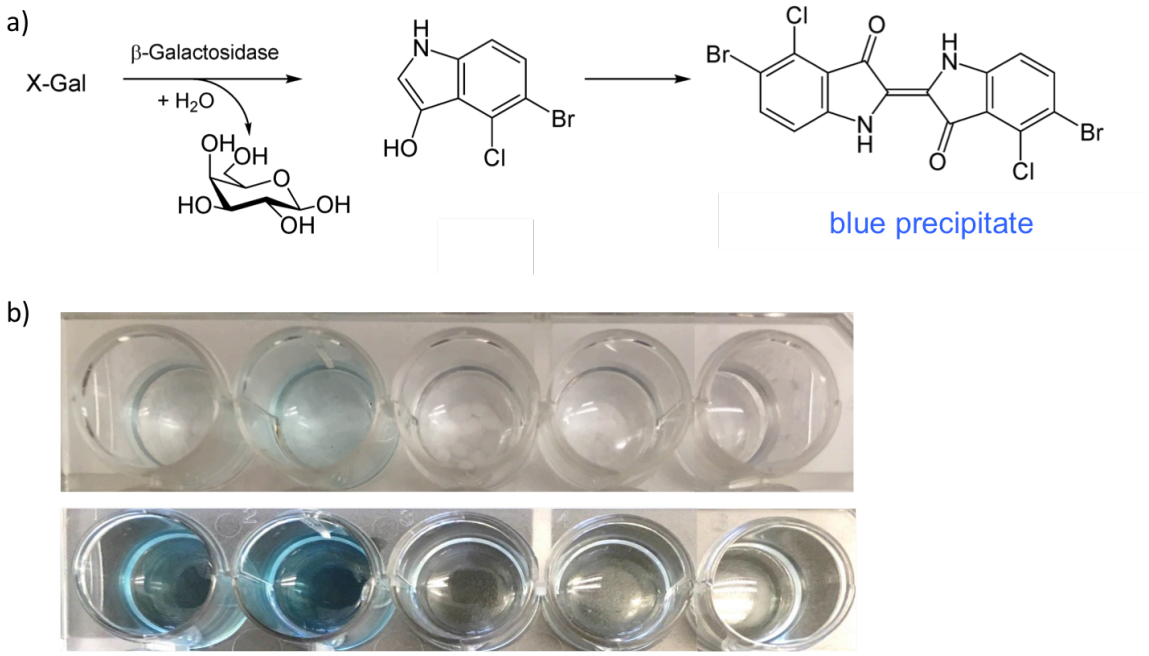

Figure A1-3. Activity assay of cell-surface lacZ in HEK cells using a cell permeable substrate X-Gal. (a) Indole released after galactosidase reaction dimerizes and is oxidized to form a blue precipitate. (b) Images of HEK cells in 24-well plate transfected with CMV-lacZ-DAF, CAG-lacZ-DAF, CMV-lacZ-pDisplay, CAG-lacZ-pDisplay or non-transfected (from left to right) after treatment with 1 mg/mL X-Gal for 4 h (top panel) or 24 h (bottom panel) in HBSS at 37 °C.

***Figure A1-4**. Characterization of fungal (Aspergillus oryzae) β-galactosidase (AO-β-gal) expression in HEK cells using immunohistochemistry.*

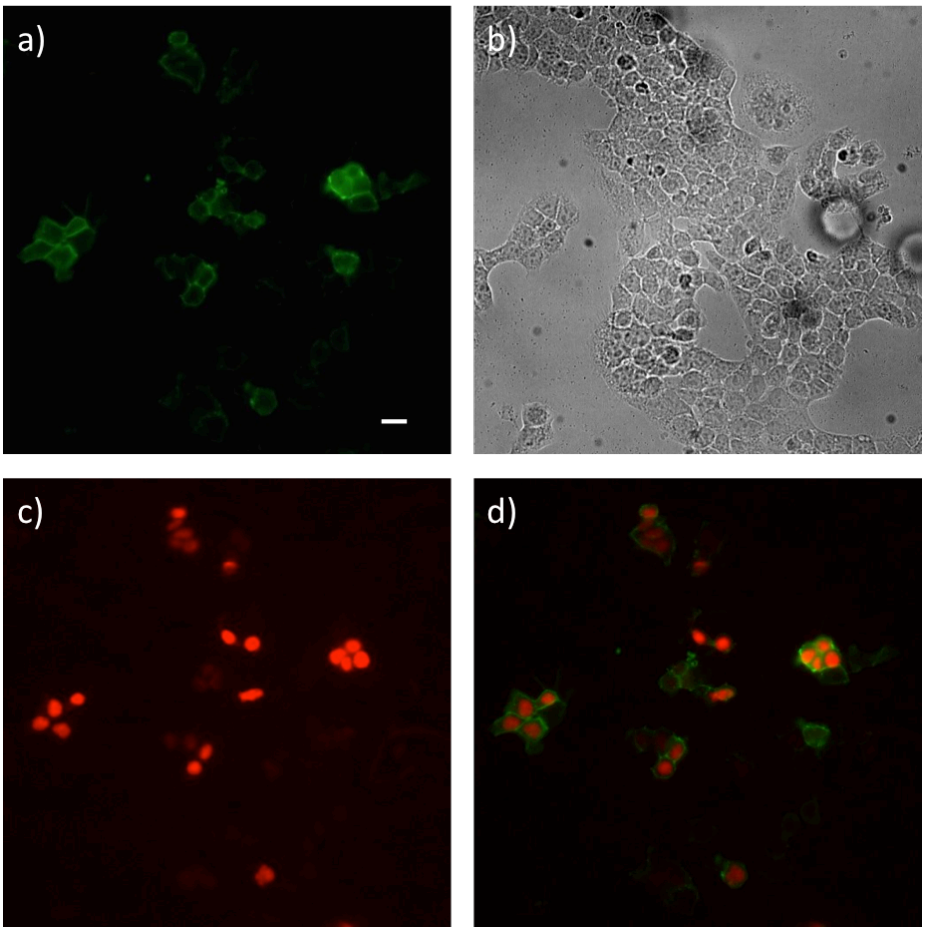

Figure A1-4. Wide-field images of fixed HEK cells expressing CMV-AO-β-gal-DAF under permeablizing condition. (a) Membrane-associated fluorescence of anti-HA staining indicates cell-surface expression for AO-β-gal. (b) Differential interference contrast (DIC) images of HEK cells. (c) Nulcear mCherry indicates AO-β-gal expression. (d) Merge image of anti-HA staining (AO-β-gal) and nuclear mCherry confirms co-expression. Scale bar is 20 μm.

Reference

1. Liu, P.; Grenier, V.; Hong, W.; Muller, V. R.; Miller, E. W., *J. Am. Chem. Soc.* **2017**, *139*, 17334-17340.
2. Ortiz, G.; Liu, P.; Naing, S. H. H.; Muller, V. R.; Miller, E. W., *J. Am. Chem. Soc.* **2019**, *141* (16), 6621-6638.
3. Husain, Q., *Crit. Rev. Biotechnol.* **2010**, *30* (1), 41-62.
4. Juers, D. H.; Matthews, B. W.; Huber, R. E., *Protein Sci.* **2012**, *21* (12), 1792–1807.
5. Horwitz, J. P.; Chua, J.; Curby, R. J.; Tomson, A. J.; Da Rooge, M. A.; Fisher, B. E.; Mauricio, J.; Klundt, I., *J. Med. Chem.* **1964**, *7* (4), 574-57.
6. Ullmann, A.; Jacob, F.; Monod, J., *Journal of Molecular Biology* **1967**, *24* (2), 339-343.
7. Nolan, G. P.; Fiering, S.; Nicolas, J. F.; Herzenberg, L. A., *Proc. Natl. Acad. Sci. U. S. A*. **1988**, *85* (8), 2603–2607.
8. Chilvers, K. F.; Perry, J. D.; James, A. L.; Reed, R. H., *J. Appl. Microbiol.* **2001**, *91* (6),1118-1130.
9. Tung, C. H.; Zeng, Q.; Shah, K.; Kim, D. E.; Schellingerhout, D.; Weissleder, R., *Cancer Res.* **2004**, *64* (5),1579-1583.
10. Perry, J. D.; James, A. L.; Morris, K. A.; Oliver, M.; Chilvers, K. F.; Reed, R. H.; Gould, F. K., *J. Appl. Microbiol*. **2006**, *101* (5), 977-985.
11. Miyazaki, J.; Takaki, S.; Araki, K.; Tashiro, F.; Tominaga, A.; Takatsu, K; Yamamura, K., *Gene* **1989**, *79* (2), 269–77
12. Niwa, H.; Yamamura, K.; Miyazaki, J., *Gene* **1991**, *108* (2), 193-199.
13. Tanaka, Y.; Kagamiishi, A.; Kiuchi, A.; Horiuchi, T., *J. Biochem.* **1975**, *77* (1), 241-247.
14. Park, Y. K.; De Santi, M. S. S.; Pastore, G. M., *Journal of Food Science* **1979**, *44* (1), 100-103.
15. Ito, Y.; Sasaki, T.; Kitamoto, K.; Kumagai, C.; Takahashi, K.; Gomi, K.; Tamura, G., *Journal of General and Applied Microbiology* **2002**, *48*, 135–142.

Appendix 2:

Fluorogenic Activation by a Cell-Surface β-lactamase

Portions of this work were performed in collaboration with the following persons:
Synthesis was assisted by Vincent Grenier

Introduction

Masking the phenolic oxygen in the VoltageFluor dyes successfully quenches their fluorescence and voltage sensitivity. The use of a specific protecting group followed by its cognate enzyme-mediated activation enables targeted fluorogenic turn-on in defined cells of interest. We have previously demonstrated the efficiency of a selectively expressed pig liver esterase to cleave a cyclopropyl ester protecting group to achieve specific staining with desirable contrast using both VF2.1.Cl (Chapter 2)[1] and carboVF (Chapter 3-1)[2]. Limitations of this strategy includes a relatively slow kinetics, in particular at room temperature, and inadequate cell-surface expression, probably due to a membrane-trafficking problem caused by its large size of 168 kD monomer and formation of trimer. As a result, it is worthwhile to explore other enzyme-substrate pairs for alternative fluorogenic activation to carry forward the strategy to more complex biological settings such as ex vivo brain slices or in vivo live animals.

β-lactamase is a small bacterial enzyme, existing and functional as a 29 kD monomer.[3-5] It is produced by certain bacteria species for antibiotic resistance such as penicillin[4], whose core structure involves a four-membered nitrogen-containing ring, also known as β-lactam. The mechanism of action relies on the ring opening with a very rapid kinetics due to the strained and unstable nature of the lactam ring.[6] In addition, a series of novel fluorogenic substrates to assay β-lactamase activity have been designed.[7-9] The synthesis to append the lactam-based protecting group to the phenolic oxygen is well-characterized. Combining these favorable features, we have decided to engineer a cell-surface β-lactamase (BLA) and synthesize a lactam-masked VF dye.

Results & Discussions

To express BLA on the surface, we again started with DAF and pDisplay targeting sequences and used CMV promoter for HEK cell expression and Synapsin promoter for neuron-specific expression (Figure A2-1). We verified the cell-surface expression using a non-permeablizing immunostaining protocol (Figure A2-2) where the anti-HA antibody is unlikely to cross the membrane to target any intracellular protein. Membrane-associate anti-HA fluorescence was observed (Figure A2-2a), which matched the nuclear mCherry expression (Figure A2-2d), suggesting that BLA is indeed expressed on the extracellular surface of the HEK cells expressing our fluorescent protein marker. We compared the efficiency of the DAF and pDisplay construct using immunostaining and found out that DAF construct had a higher anti-HA signal, indicating better expression or trafficking to the membrane, which is consistent with studies done with CMV-PLE constructs. In neurons, BLA is expressed on the cell surface too as shown from the immunostaining results (Figure A2-4). However, compared to Syn-PLE-DAF, the Syn-BLA constructs exhibited much weaker signal and pDisplay construct expression was barely seen, in agreement with the data from CMV constructs (Figure A2-5).

We next moved on to evaluate the functional aspect of BLA in both HEK cells and neurons. A cell impermeant substrate, nitrocefin was used to examine the activity of the cell-surface enzyme.[10] Nitrocefin displays a shift in absorbance during the BLA-mediated lactam ring opening (Figure 2-6a). Both control nitrocefin solution or nitrocefin exposed to non-transfected cells showed a major absorbance peak at 390 nm and minimal absorbance at 490 nm, while nitrocefin treated with BLA-expressing cells had a decrease in the starting material absorption with a concomitant appearance of the 490 nm product

absorption peak (Figure A2-6b, Figure A2-7). The shift is more prominent in treatment with HEK cells than neurons as it's dependent on the amount of BLA expression which is more robust in HEK cells. This also matched our results from PLE experiments in which a much larger fluorescence turn-on was measured in HEK cells than in neurons (Table 2).

Encouraged by the data from immunostaining and functional assay of cell-surface BLA in both HEK cells and neurons, my colleague, Vincent Grenier, synthesized the masked dye BLA-VF2.1.Cl based on the literature.[7] During the synthesis, we encountered a couple of challenges with the complexity and instability of the lactam and spent copious time and effort to achieve the final compound. When we applied the dye to HEK cells expression CMV-BLA-DAF (500 nM at RT for 15 min), all the cells were uniformly stained with no selectivity in mCherry-positive cells (Figure A2-8). We hypothesize that the dye was not stable enough and hydrolyzed quickly to release the fluorescent, non-specific VF2.1.Cl.

Conclusion

We have successfully expressed a β-lactamase on the cell surface for both HEK cells and neurons, with the capability to act on a cell-impermeant substrate nitrocefin. Expression is limited in neurons as proven from a less efficient nitrocefin conversion, which can be potentially solved by changing into a stronger promoter such as CAG. Unfortunately, the lactam-masked VF2.1.Cl is unstable and undergoes hydrolysis rapidly when treated to live cells and no selective staining was observed. A second-generation dye with improved stability and more accessible synthetic route would be desired to achieve BLA-mediated fluorogenic activation.

Experimental Sections

Cell Culture

All animal procedures were approved by the UC Berkeley Animal Care and Use Committees and conformed to the NIH Guide for the Care and Use and Laboratory Animals and the Public Health Policy.

Human embryonic kidney 293T (HEK) cells were maintained and plated in Dulbecco's modified eagle medium (DMEM) supplemented with 4.5 g/L D-glucose, 10% fetal bovine serum (FBS; Thermo Scientific) and 1% GlutaMax (Invitrogen) at 37 °C in a humidified incubator with 5 % CO_2. Cells were passaged and plated in DMEM (as above) at a density of 75,000 cells onto 12 mm glass coverslips pre-coated with Poly-D-Lysine (PDL; 1 mg/ml; Sigma-Aldrich) per well in a 24-well plate. Transfection of plasmids was carried out using Lipofectamine 3000 (Invitrogen) ~18-24 h after plating. Imaging was performed 12-18 h after transfection.

Hippocampi were dissected from embryonic day 19 Sprague Dawley rats (Charles River Laboratory) in cold, sterile HBSS (zero Ca^{2+}, zero Mg^{2+}, phenol red). All dissection products were supplied by Invitrogen, unless otherwise stated. Hippocampal tissue was treated with trypsin (2.5%) for 15 min at 37 °C. The tissue was triturated using fire polished Pasteur pipettes, in minimum essential media (MEM) supplemented with 5% FBS, 2% B-27, 2% 1M dextrose (Fisher Scientific) and 1% GlutaMax. The dissociated cells were plated onto 12 mm diameter coverslips (Fisher Scientific) pre-treated with PDL (as above) at a density of 25-30,000 cells per coverslip in MEM supplemented

media (as above). Neurons were maintained at 37 °C in a humidified incubator with 5% CO_2. At 1 day in vitro (DIV) half of the MEM supplemented media was removed and replaced with Neurobasal media containing 2% B-27 supplement and 1% GlutaMax. Transfection of plasmids was carried out using Lipofectamine 3000 (without P3000 reagent) at 6-7 DIV. Imaging was performed on mature neurons 13-16 DIV.

BLA activity assay using nitrocefin

Nitrocefin solid was purchased from VWR (Cat. 80017-706) and concentrated stock solution was prepared in DMSO and stored at -20 °C, protected from light. For activity assay of BLA in HEK cells, HEK cells were transfected with CMV-BLA-DAF as stated above and the assay was conducted about 24 h after transfection. Media was aspirated and replaced with 1 mL of nitrocefin in HBSS (final concentration 5 μg/mL). Reaction was done at RT for 15 min, protected from light. For activity assay in neurons, neurons were transfected with Syn-BLA-DAF as stated above and the assay was conducted 7 days after transfection. Media was aspirated and replaced with 1 mL of nitrocefin in HBSS (final concentration 100 μg/mL). Reaction was done at 37 °C for 1 h. For UV/Vis absorption measurement, the solution (supernatant) was transferred to a cuvette after the reaction was finished. Negative controls included non-treated 1mL of nitrocefin in HBSS and solution treated to non-transfected cells.

Imaging Parameters

Epifluorescence imaging was performed on an AxioExaminer Z-1 (Zeiss) equipped with a Spectra-X Light engine LED light (Lumencor), controlled with Slidebook (v6, Intelligent Imaging Innovations). Images were acquired with a W-Plan-Apo 20x/1.0 water objective (20x; Zeiss) and focused onto an OrcaFlash4.0 sCMOS camera (sCMOS; Hamamatsu). For VF dye, excitation light was delivered at 475 nm (LED, 475 nm, 34 nm bandpass) and emission was collected with a 540/50 nm bandpass filter after passing through a 510 nm longpass dichroic.

Immunocytochemistry

To detect expression and localization of BLA, HEK cells or neurons were fixed with 4% paraformaldehyde in PBS for 10 min. Blocking was done in 5% w/v bovine serum albumin (BSA; Sigma Aldrich) in PBS for 1 h. Primary anti-HA antibody (rabbit IgG, Cell Signaling Technologies Cat. 3724S) was incubated at 4 °C overnight, followed by anti-rabbit AlexaFluor 647 secondary antibody (goat IgG, Life Technologies A21244) at room temperature (RT) for 2 h. Hoechst 33342 was added for 15 min at RT to visualize the nucleus. All antibodies and counterstain were used at 1:1000 dilution.

DNA constructs

To express the BLA protein on the cell surface, an IgK leader sequence was fused to the N-terminal and either a signal peptide for GPI addition (DAF) or a transmembrane domain (pDisplay) was added to the C-terminal. An HA tag was inserted for immunstaining. Mammalian expression vector pcDNA3 with either a CMV promoter or Synapsin promoter was used for protein expression in HEK cells and neurons, respectively. To increase expression in neurons, a regulatory element from the woodchuck hepatitis virus (WPRE) was used. In all constructs, nuclear-targeted mCherry

(NLS-mCherry) was inserted down stream of BLA, separated by an internal ribosome entry site (IRES) sequence, to track the expression of BLA in live cells. All constructs were confirmed by sequencing. The following sequences were used (5' to 3'):

IgK
ATGGAGACAGACACACTCCTGCTATGGGTACTGCTGCTCTGGGTTCCAGGTTC
CACTGGTGAC

β-lactamase
ATGAGTATTCAACATTTCCGTGTCGCCCTTATTCCCTTTTTTGCGGCATTTTGC
CTTCCTGTTTTTGCTCACCCAGAAACGCTGGTGAAAGTAAAAGATGCTGAAG
ATCAGTTGGGTGCACGAGTGGGTTACATCGAACTGGATCTCAACAGCGGTAA
GATCCTTGAGAGTTTTCGCCCCGAAGAACGTTTTCCAATGATGAGCACTTTTA
AAGTTCTGCTATGTGGCGCGGTATTATCCCGTATTGACGCCGGGCAAGAGCA
ACTCGGTCGCCGCATACACTATTCTCAGAATGACTTGGTTGAGTACTCACCAG
TCACAGAAAAGCATCTTACGGATGGCATGACAGTAAGAGAATTATGCAGTGC
TGCCATAACCATGAGTGATAACACTGCGGCCAACTTACTTCTGACAACGATC
GGAGGACCGAAGGAGCTAACCGCTTTTTTGCACAACATGGGGGATCATGTAA
CTCGCCTTGATCGTTGGGAACCGGAGCTGAATGAAGCCATACCAAACGACGA
GCGTGACACCACGATGCCTGCAGCAATGGCAACAACGTTGCGCAAACTATTA
ACTGGCGAACTACTTACTCTAGCTTCCCGGCAACAATTAATAGACTGGATGG
AGGCGGATAAAGTTGCAGGACCACTTCTGCGCTCGGCCCTTCCGGCTGGCTG
GTTTATTGCTGATAAATCTGGAGCCGGTGAGCGTGGGTCTCGCGGTATCATTG
CAGCACTGGGGCCAGATGGTAAGCCCTCCCGTATCGTAGTTATCTACACGAC
GGGGAGTCAGGCAACTATGGATGAACGAAATAGACAGATCGCTGAGATAGG
TGCCTCACTGATTAAGCATTGG

HA
TATCCATATGATGTTCCAGATTATGCT

DAF
CCAAATAAAGGAAGTGGAACCACTTCAGGTACTACCCGTCTTCTATCTGGGC
ACACGTGTTTCACGTTGACAGGTTTGCTTGGGACGCTAGTAACCATGGGCTTG
CTGACTTAG

pDisplay
GCTGTGGGCCAGGACACGCAGGAGGTCATCGTGGTGCCACACTCCTTGCCCT
TTAAGGTGGTGGTGATCTCAGCCATCCTGGCCCTGGTGGTGCTCACCATCATC
TCCCTTATCATCCTCATCATGCTTTGGCAGAAGAAGCCACGT

IRES
GCCCCTCTCCCTCCCCCCCCCCTAACGTTACTGGCCGAAGCCGCTTGGAATAA
GGCCGGTGTGCGTTTGTCTATATGTTATTTTCCACCATATTGCCGTCTTTTGGC
AATGTGAGGGCCCGGAAACCTGGCCCTGTCTTCTTGACGAGCATTCCTAGGG
GTCTTTCCCCTCTCGCCAAAGGAATGCAAGGTCTGTTGAATGTCGTGAAGGA
AGCAGTTCCTCTGGAAGCTTCTTGAAGACAAACAACGTCTGTAGCGACCCTTT

GCAGGCAGCGGAACCCCCCACCTGGCGACAGGTGCCTCTGCGGCCAAAAGCC
ACGTGTATAAGATACACCTGCAAAGGCGGCACAACCCCAGTGCCACGTTGTG
AGTTGGATAGTTGTGGAAAGAGTCAAATGGCTCTCCTCAAGCGTATTCAACA
AGGGGCTGAAGGATGCCCAGAAGGCACCCCATTGTATGGGATCTGATCTGGG
GCCTCGGTGCACATGCTTTACATGTGTTTAGTCGAGGTTAAAAAAACGTCTAG
GCCCCCCGAACCACGGGGACGTGGTTTTCCTTTGAAAAACACGATGATAATA
TGGCCACA

Nuclear localization sequence (NLS)
ATGGTGCCCAAGAAGAAGAGGAAAGTC

mCherry
GTGAGCAAGGGCGAGGAGGACAACATGGCCATCATCAAGGAGTTCATGCGC
TTCAAGGTGCACATGGAGGGCTCCGTGAACGGCCACGAGTTCGAGATCGAGG
GCGAGGGCGAGGGCCGCCCCTACGAGGGCACCCAGACCGCCAAGCTGAAGG
TGACCAAGGGCGGCCCCCTGCCCTTCGCCTGGGACATCCTGTCCCCTCAGTTC
ATGTACGGCTCCAAGGCCTACGTGAAGCACCCCGCCGACATCCCCGACTACT
TGAAGCTGTCCTTCCCCGAGGGCTTCAAGTGGGAGCGCGTGATGAACTTCGA
GGACGGCGGCGTGGTGACCGTGACCCAGGACTCCTCCCTGCAGGACGGCGAG
TTCATCTACAAGGTGAAGCTGCGCGGCACCAACTTCCCCTCCGACGGCCCCG
TAATGCAGAAGAAGACCATGGGCTGGGAGGCCTCCTCCGAGCGGATGTACCC
CGAGGACGGCGCCCTGAAGGGCGAGATCAAGCAGAGGCTGAAGCTGAAGGA
CGGCGGCCACTACGACGCCGAGGTCAAGACCACCTACAAGGCCAAGAAGCC
CGTGCAGCTGCCCGGCGCCTACAACGTCAACATCAAGCTGGACATCACCTCC
CACAACGAGGACTACACCATCGTGGAACAGTACGAGCGCGCCGAGGGCCGC
CACTCCACCGGCGGCATGGACGAGCTGTACAAG

WPRE
GCTTATCGATAATCAACCTCTGGATTACAAAATTTGTGAAAGATTGACTGGTA
TTCTTAACTATGTTGCTCCTTTTACGCTATGTGGATACGCTGCTTTAATGCCTT
TGTATCATGCTATTGCTTCCCGTATGGCTTTCATTTTCTCCTCCTTGTATAAAT
CCTGGTTGCTGTCTCTTTATGAGGAGTTGTGGCCCGTTGTCAGGCAACGTGGC
GTGGTGTGCACTGTGTTTGCTGACGCAACCCCCACTGGTTGGGGCATTGCCAC
CACCTGTCAGCTCCTTTCCGGGACTTTCGCTTTCCCCCTCCCTATTGCCACGGC
GGAACTCATCGCCGCCTGCCTTGCCCGCTGCTGGACAGGGGCTCGGCTGTTG
GGCACTGACAATTCCGTGGTGTTGTCGGGGAAATCATCGTCCTTTCCTTGGCT
GCTCGCCTGTGTTGCCACCTGGATTCTGCGCGGGACGTCCTTCTGCTACGTCC
CTTCGGCCCTCAATCCAGCGGACCTTCCTTCCCGCGGCCTGCTGCCGGCTCTG
CGGCCTCTTCCGCGTCTTCGCCTTCGCCCTCAGACGAGTCGGATCTCCCTTTG
GGCCGCCTCCCCGCATCGATACCG

CMV promoter
GACATTGATTATTGACTAGTTATTAATAGTAATCAATTACGGGGTCATTAGTT
CATAGCCCATATATGGAGTTCCGCGTTACATAACTTACGGTAAATGGCCCGCC
TGGCTGACCGCCCAACGACCCCCGCCCATTGACGTCAATAATGACGTATGTT
CCCATAGTAACGCCAATAGGGACTTTCCATTGACGTCAATGGGTGGACTATTT

ACGGTAAACTGCCCACTTGGCAGTACATCAAGTGTATCATATGCCAAGTACG
CCCCCTATTGACGTCAATGACGGTAAATGGCCCGCCTGGCATTATGCCCAGT
ACATGACCTTATGGGACTTTCCTACTTGGCAGTACATCTACGTATTAGTCATC
GCTATTACCATGGTGATGCGGTTTTGGCAGTACATCAATGGGCGTGGATAGC
GGTTTGACTCACGGGGATTTCCAAGTCTCCACCCCATTGACGTCAATGGGAGT
TTGTTTTGGCACCAAAATCAACGGGACTTTCCAAAATGTCGTAACAACTCCGC
CCCATTGACGCAAATGGGCGGTAGGCGTGTACGGTGGGAGGTCTATATAAGC
AGAGCT

Synapsin Promoter
GTGTCTAGACTGCAGAGGGCCCTGCGTATGAGTGCAAGTGGGTTTTAGGACC
AGGATGAGGCGGGGTGGGGGTGCCTACCTGACGACCGACCCCGACCCACTG
GACAAGCACCCAACCCCCATTCCCCAAATTGCGCATCCCCTATCAGAGAGGG
GGAGGGGAAACAGGATGCGGCGAGGCGCGTGCGCACTGCCAGCTTCAGCAC
CGCGGACAGTGCCTTCGCCCCCGCCTGGCGGCGCGCGCCACCGCCGCCTCAG
CACTGAAGGCGCGCTGACGTCACTCGCCGGTCCCCCGCAAACTCCCCTTCCC
GGCCACCTTGGTCGCGTCCGCGCCGCCGCCGGCCCAGCCGGACCGCACCACG
CGAGGCGCGAGATAGGGGGGCACGGGCGCGACCATCTGCGCTGCGGCGCCG
GCGACTCAGCGCTGCCTCAGTCTGCGGTGGGCAGCGGAGGAGTCGTGTCGTG
CCTGAGAGCGCAGTCGAGA

Benchling links for constructs

CMV-IgK-BLA-HA-DAF-IRES-mCherry
https://benchling.com/s/0wwx4e8t

CMV-IgK-BLA-HA-pDisplay-IRES-mCherry
https://benchling.com/s/G49opVl6

Synapsin-IgK-BLA-HA-DAF-IRES-mCherry-WPRE
https://benchling.com/s/iuGArWYF

Synapsin-IgK-BLA-HA-pDisplay-IRES-mCherry-WPRE
https://benchling.com/s/seq-Oh8DkivFBsIV6I9e4T73

Figures and Schemes

Scheme A2-1. *Design of β-lactamase-based fluorogenic activation.*

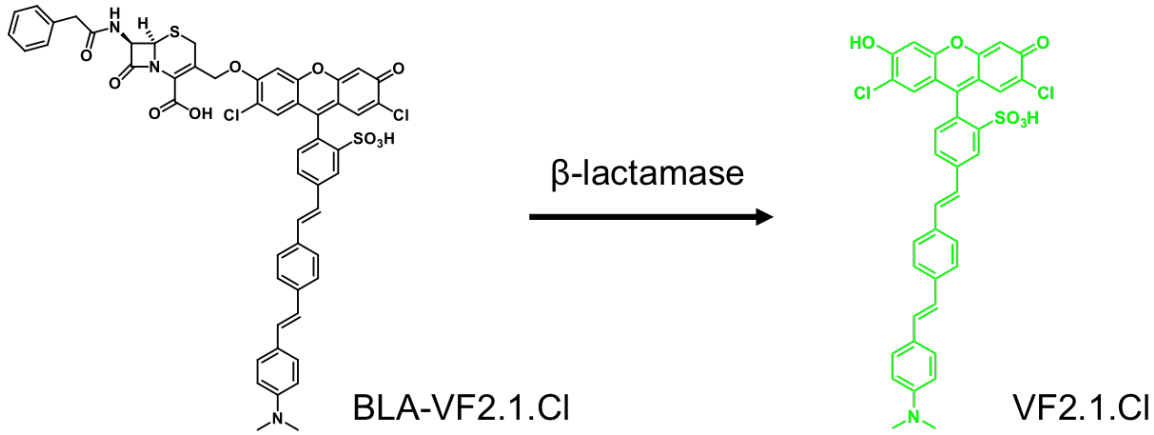

Scheme A2-1. Structure of lactam-masked dye BLA-VF2.1.Cl and its fluorescence turn-on following β-lactamase reaction.

***Figure A2-1**. β-lactamase constructs used in this study.*

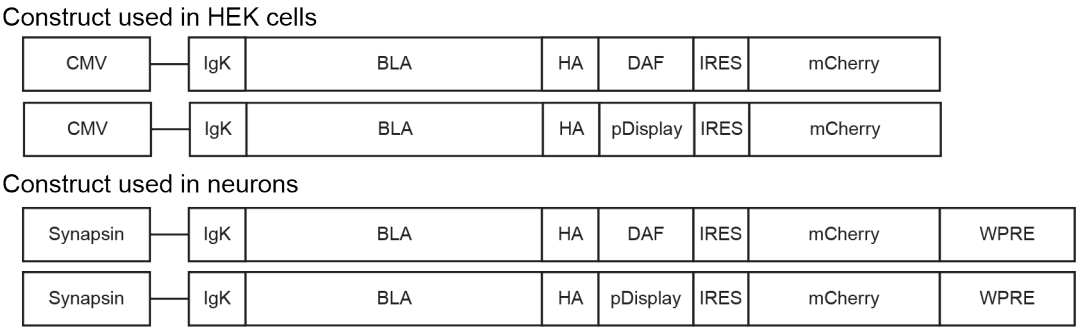

Figure A2-1. Constructs designed and tested for expressing β-lactamase on the cell surface.

Figure A2-2*. Characterization of BLA expression in HEK cells using immunohistochemistry.*

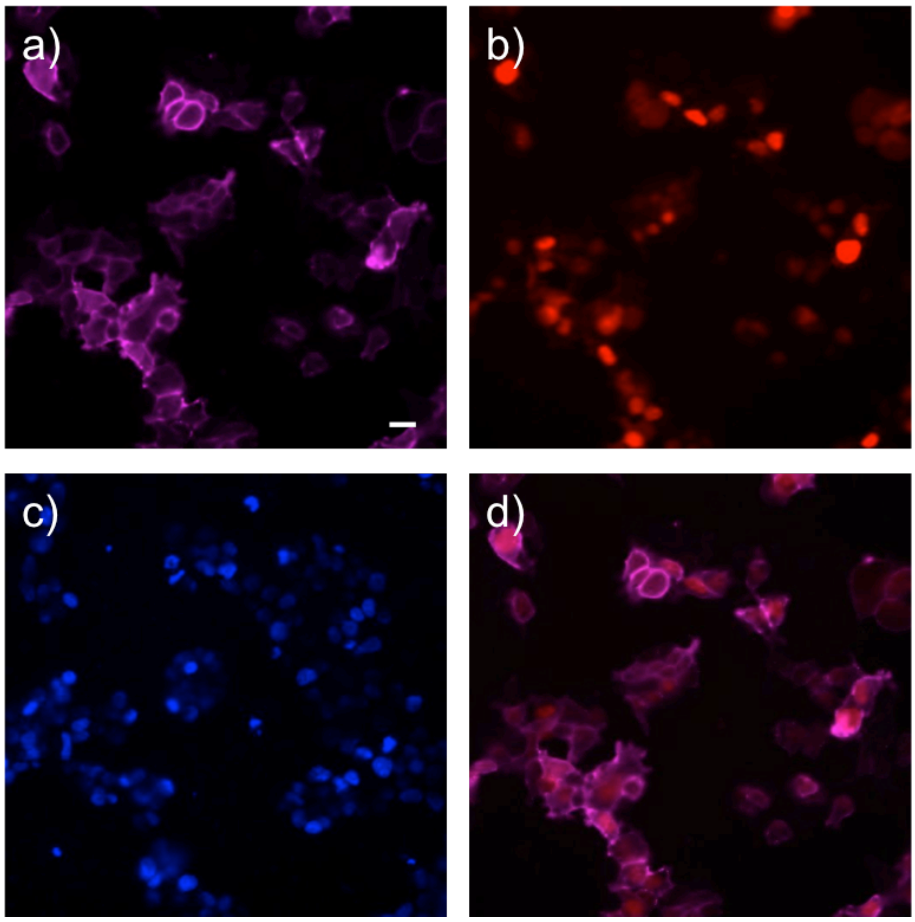

Figure A2-2. Wide-field images of fixed HEK cells expressing CMV-BLA-DAF under non-permeablizing condition. (a) Anti-HA staining shows membrane-associated fluorescence. (b) Nuclear mCherry indicates BLA expression. (c) Hoechst 33342 stains nucleus. (d) Merge image of anti-HA staining and mCherry. Scale bar is 20 μm.

***Figure A2-3**. Compare DAF and pDisplay construct by immunohistochemistry.*

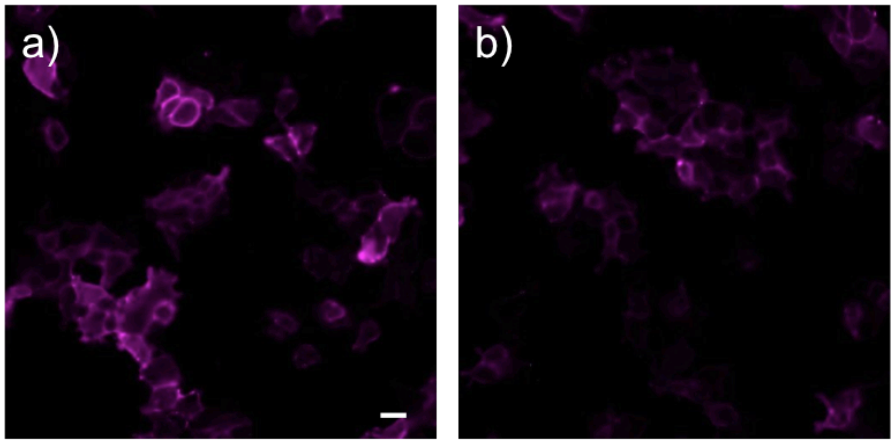

Figure A2-3. Wide-field images of anti-HA staining in fixed HEK cells expressing CMV-BLA-DAF (a) or CMV-BLA-pDisplay (b) under non-permeablizing condition. Scale bar is 20 μm.

***Figure A2-4**. Characterization of BLA expression in cultured hippocampal neurons using immunohistochemistry.*

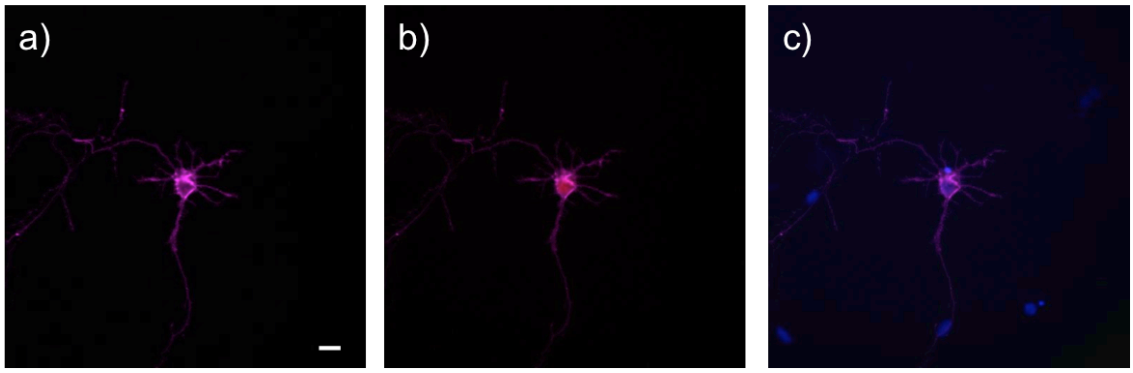

Figure A2-4. Fixed cell wide-field images of rat hippocampal neurons expressing Synapsin-BLA-DAF. (a) Anti-HA staining shows membrane-associated fluorescence. (b) Merge image of anti-HA staining and nuclear mCherry which indicates BLA expression. (c) Merge image of anti-HA staining and Hoechst 33342 which stains nucleus. Scale bar is 20 μm.

***Figure A2-5**. Characterization of BLA expression in cultured hippocampal neurons using immunohistochemistry.*

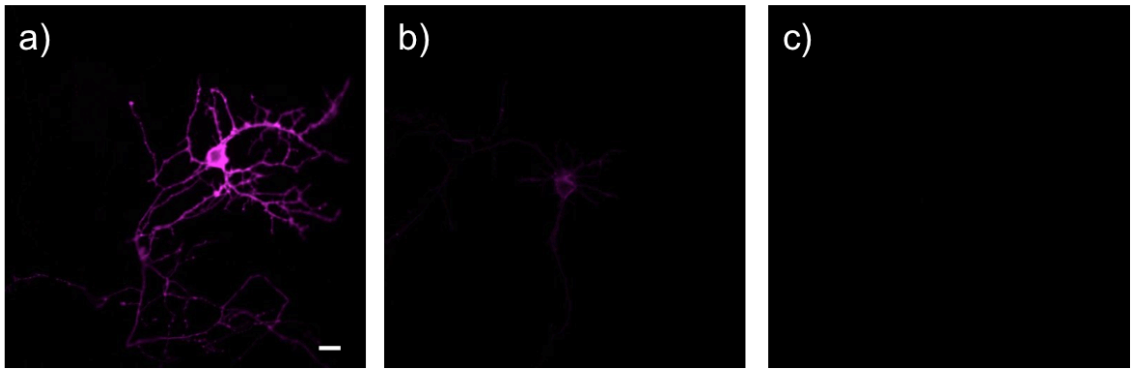

Figure A2-5. Wide-field images of anti-HA staining in fixed hippocampal neurons expressing (a) Synapsin-PLE-DAF or (b) Synapsin-BLA-DAF or (c) Synapsin-BLA-pDisplay. The settings (acquisition and display) for all images are the same. Scale bar is 20 μm.

***Figure A2-6**. Functional assay of cell-surface BLA in HEK cells.*

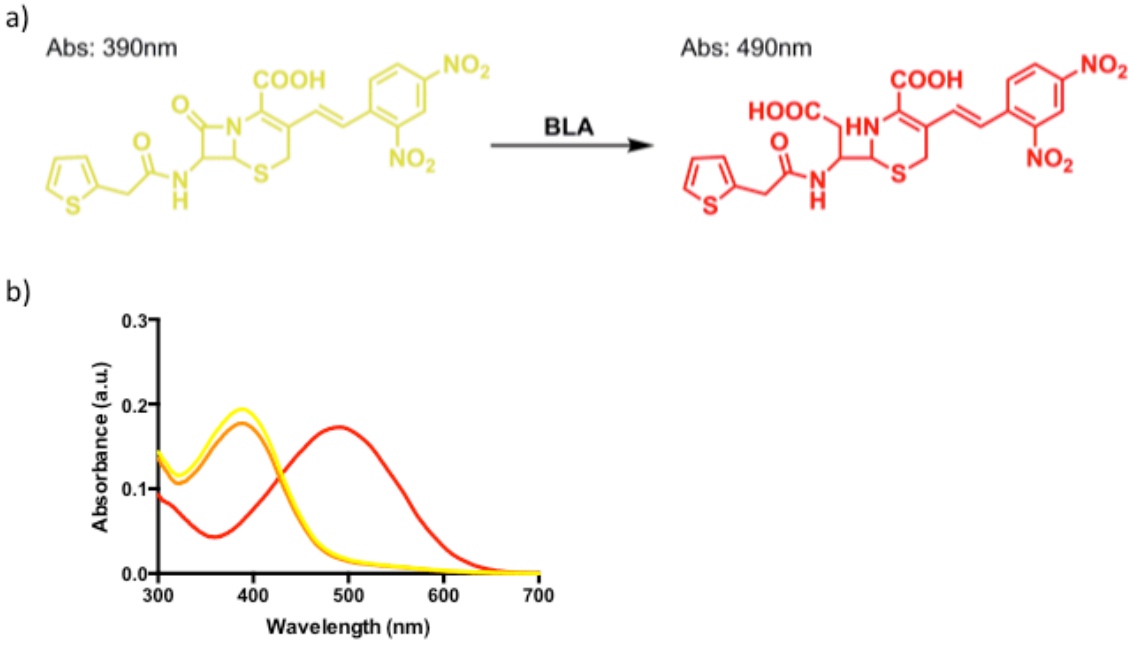

Figure A2-6. Activity assay of cell-surface BLA in HEK cells using a cell impermeable lactam substrate nitrocefin. (a) Absorbance change of nitrocefin from 390 nm to 490 nm upon reaction with BLA. (b) UV/Vis absorption spectra of control nitrocefin only (yellow), nitrocefin reacted with plated non-transfected HEK cells (orange) or nitrocefin reacted with plated CMV-BLA-DAF transfected HEK cells (red). Concentration of nitrocefin used is 5 μg/mL and reactions with HEK cells are done at room temperature for 15 min before measurement.

Figure A2-7*. Functional assay of cell-surface BLA in cultured hippocampal neurons.*

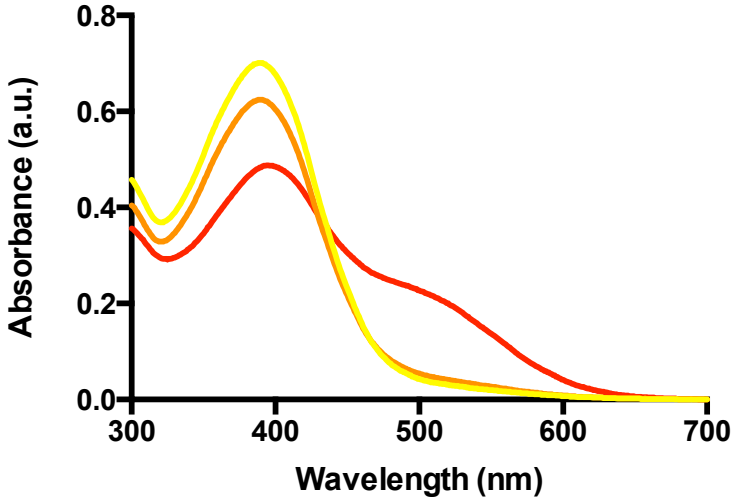

Figure A2-7. Activity assay of cell-surface BLA in neurons using a cell impermeable lactam substrate nitrocefin. (a) Absorbance change of nitrocefin from 390 nm to 490 nm upon reaction with BLA. (b) UV/Vis absorption spectra of control nitrocefin only (yellow), nitrocefin reacted with plated non-transfected neurons (orange) or nitrocefin reacted with plated Syn-BLA-DAF transfected neurons (red). Concentration of nitrocefin used is 100 μg/mL and reactions with neurons are done at 37 °C for 1 h before measurement.

***Figure A2-8**. Characterization of BLA-VF2.1.Cl in BLA-expressing HEK cells.*

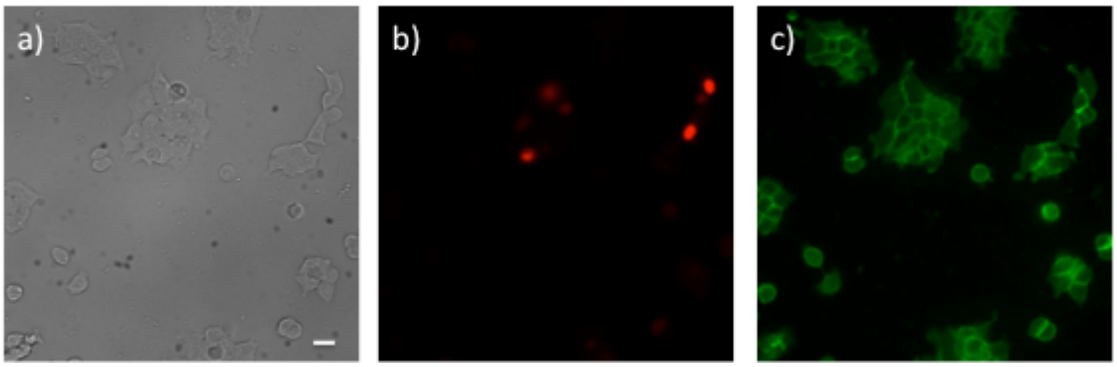

Figure A2-8. Wide-field fluorescence microscopy of HEK cells stained with BLA-VF2.1.Cl (500 nM, 15 min, RT) shows membrane labeling of the cell expressing cell surface BLA. (a) Differential interference contrast (DIC) images of HEK cells. (b) Nuclear mCherry indicates BLA expression. (c) VF staining stains all cells uniformly. Scale bar is 20 μm.

Reference

1. Liu, P.; Grenier, V.; Hong, W.; Muller, V. R.; Miller, E. W., *J. Am. Chem. Soc.* **2017**, *139*, 17334-17340.
2. Ortiz, G.; Liu, P.; Naing, S. H. H.; Muller, V. R.; Miller, E. W., *J. Am. Chem. Soc.* **2019**, *141* (16), 6621-6638.
3. Ambler, R. P., *Philos. Trans. R. Soc. Lond. B Biol. Sci.* **1980**, *289* (1036), 321-331.
4. Abraham, E. P.; Chain, E., *Nature* **1940**, *46* (3713), 837.
5. Bush, K., *Antimicrob Agents Chemother.* **1989**, *33* (3), 259-263.
6. Tipper, D. J.; Strominger, J. L., *Proc. Natl. Acad. Sci. U. S. A.* **1965**, *54* (4), 1133-1141.
7. Gao, W.; Xing, B.; Tsien, R. Y.; Rao, J., *J. Am. Chem. Soc.* **2003**, *125* (37), 11146-11147.
8. Xing, B.; Khanamiryan, A.; Rao, J., *J. Am. Chem. Soc.* **2005**, *127* (12), 4158-4159.
9. Xie, H.; Mire, J.; Kong, Y.; Chang, M.; Hassounah, H. A.; Thornton, C. N.; Sacchettini, J. C.; Cirillo, J. D.; Rao, J., *Nature Chemistry* **2012**, *4*, 802-809.
10. O'Callaghan, C. H.; Morris, A.; Kirby, S. M.; Shingler, A. H., *Antimicrob Agents Chemother.* 1972, *1* (4), 283-288.

Appendix 3:

Designing a HaloTag Virus for In Vivo Applications

Portions of this work were performed in collaboration with the following persons:
Adult mice viral injection and slice imaging were assisted by Daniel Kramer

Abstract

In chapter 4, we have demonstrated that covalent labeling of VoltageFluor dyes using cell-surface HaloTag allows for selective staining in HEK cells, cultured neurons and live mouse brain slice. The targeted dye is able to report membrane potential changes in the abovementioned samples in a fast and sensitive manner. However, due to the 1:1 stoichiometric nature of the labeling system, the amount of dye entering the membrane depends on the enzyme expression. In this chapter, we describe some of the efforts to modify the HaloTag expression using viral vector-based delivery system. We used adeno-associated viral vectors to generate the HaloTag plasmids which worked well in HEK cells. The plasmids were readily packaged into the viral genome with AAV2/9 serotype that is known to infect and express rigorously in the central nervous system. However, when we tested the virus in cultured cells and later in mouse brain slice through neonatal viral injection, the low efficiency of the virus resulted in not only a small percentage of cells being transduced but also a weak expression in those infected cells, which ultimately led to a dim RhoVR signal with significantly eroded contrast. Ongoing efforts aim at solving the viruses' efficiency issue or exploring alternative methods to increase HaloTag expression.

Introduction

Covalent labeling of VoltageFluor dyes to cells of interest has proven to generate high contrast between transfected and non-transfected cells.[1] Cell-surface HaloTag, a small bacterial enzyme that reacts with a haloalkane ligand conjugated to VF dyes, enables fast and highly specific staining of RhoVR1-PEG_{25}-HaloTag in both cultured cells and mouse brain slices with plasmid-based transfection techniques. While the contrast is remarkable in a complex tissue environment when nanomolar dye concentration was applied, the signal from the stained cells is so low that functional imaging to record voltage changes is only applicable to a small portion of HaloTag-expressing cells. We realized this problem when trying to conduct patch-clamp electrophysiology on the transfected cells after in utero electroporation. Only very few brightly stained cells would emit enough photons to record distinctly resolved spikes above noise level. We believe that the HaloTag binding site is probably saturated as an increased dye concentration only raised the background non-specific staining. Thus, to boost the dye signal, we have decided to use a virus to enhance HaloTag expression. Virus-mediated delivery has been commonly utilized to send genetic materials to host cells due to its superb infectivity and expression efficiency.[2-3]

Adeno-associated virus (AAV) has been chosen as an ideal delivery vehicle for several reasons. Besides its desirable infectivity and expression, one of the most favorable reasons is its safety as AAV generally elicits little immune response.[4] Also, the AAV system has been extensively used in targeting the central nervous system with well-studied distribution pattern and expression efficiency of various AAV serotypes.[5-6] Nonetheless, the drawback includes a relatively limited packaging size of 4.7 kb exogenous gene of interest.[7] This is not a concern in our case since the HaloTag enzyme is roughly 900 bp[8] while the transmembrane targeting domain, either pDisplay or DAF, is only approximately 150 bp[9] and the fluorescent protein marker, mTagBFP2 or EGFP is around 700 bp[10-11]. All the key fragments have compact sizes that would fit nicely into the cassette when designing the construct for virus packaging.

Besides, we also incorporated the specificity feature by inserting the Lox sequences. The Cre-Lox recombination system is one of the most frequently applied strategies to control gene expression in cells of interest.[12-13] Cre recombinase expressed in selected cell types recognizes a specific pair of Lox sequences flanking the target gene of reversed sequence and thus inverts the reversed gene to its normal orientation for expression.[14] There has been a diverse range of commercially available mouse lines expressing Cre recombinase in different cell types, such as CaMKIIα-Cre for excitatory cells[15] and VGAT-Cre for inhibitory cells expression[16]. As a result, we can simply inject a virus containing the HaloTag sequence flanked by Lox sites (floxed-HaloTag) to those mice of specific Cre genotype for targeted expression and dye labeling.

The workflow is as follows: we inserted the HaloTag components to a viral vector backbone to yield the plasmids. After characterization in cultured cells, we then sent the plasmids to Dr. Mei Li at School of Optometry, UC Berkeley to make viruses of AAV2/9 serotype. The whole process of cloning and virus prep took about five weeks. The virus was first tested in cultured cells before injection into Cre mouse lines and the slices were obtained for staining and imaging. In the meanwhile, another collaborator, the Heppenstall lab, has sent us a HaloTag AAV virus that allows us to do some initial test in cells and slices.

Results & Discussions

A3-1: Characterization of pAAV-hSyn-HaloTag-DAF virus.

The pAAV-hSyn-HaloTag-DAF virus with AAV1/2 serotype and titer of 3.1×10^{13} vg/mL is a gift from the Heppenstall lab (EMBL). Before using the virus in vivo, we tested it in cultured hippocampal neurons and stained the cells with RhoVR1-PEG_{25}-HaloTag. The virus infected cells with very high efficiency, evidenced by uniform and bright staining throughout the culture (Figure A3-1-1a,b) while the non-transduced control did not display any labeling (Figure A3-1-1 c,d). For virus injection to adult mice, we collaborated with the Bateup lab (UC Berkeley) to delivery the virus to cortex and striatum using four different concentrations (Figure A3-1-2a,b). We observed specific staining in areas of injection when stained with TMR-PEG_{13}-HaloTag (Figure A3-1-2a) and RhoVR1-PEG_{25}-HaloTag (Figure A3-1-2b). We also took a closer look and spotted cell body-like structures (Figure A3-1-2c), but due to a lack of marker for the HaloTag enzyme, it was challenging to accurately differentiate specific, expression-dependent staining from non-specific background or debris staining. On the other hand, a non-injected region of interest showed minimal dye signal (Figure A3-1-2d). As result, we found it necessary to include a fluorescent protein marker in the construct to pinpoint HaloTag expression in a complex environment.

A3-2: Design and characterization DIO-based viruses

We cloned a cell-surface HaloTag construct using the transmembrane domain pDisplay and a bright blue fluorescent protein mTagBFP2[10] as expression marker for spectral separation from the rhodamine-based dye (Figure A3-2-1). A self-cleaving peptide sequence, P2A[17], was selected to replace the long sequence of IRES, considering the limitation in viral genome packaging length. A strong promoter CAG was used to boost the enzyme expression. The cloning was carried out using the recombinase-free

Sure2 strain as the presence of inverted terminal repeats (ITRs) in the vector backbone is prone to recombination.[18] For virus preparation, endotoxin-free maxiprep DNA was obtained and confirmed by sequencing as well as SmaI restriction digestion to rule out recombination (Figure A3-2-2).[18] Additional characterization in HEK cells was conducted by co-transfecting the construct with a Cre recombinase plasmid. Only BFP-positive cells were stained with RhoVR1-PEG_{25}-HaloTag (Figure A3-2-2c,d,e) and all BFP-positive cells expressed Cre recombinase as indicated by the nuclear EGFP marker (Figure A3-2-2b,c,f). Selective staining was also observed in cultured neurons when Cre-EGFP plasmid was co-transfected (Figure A3-2-3). These results suggest that the DIO plasmid was Cre-dependent and had efficient expression in cultured cells.

The virus was prepared with a high titer of 5.14×10^{14} vg/mL. To determine its efficiency in cultured cells, we transduced HEK cells with the virus and transfected with a Cre recombinase plasmid containing an EGFP marker. We stained and imaged the cells 4 days after transduction and observed very little cytosolic BFP or membrane-associated RhoVR dye fluorescence, despite robust Cre recombinase expression (Figure A3-2-4a-d). Nonetheless, in the controls cells where only the virus was transduced, we saw completely no BFP or RhoVR signal (Figure A3-2-4e-h), suggesting that the recombinase is necessary for the expression of the floxed virus. We checked the expression again 4 days later (i.e. 8 days after transduction) where the cells were 100% confluent and fewer than 10 cells displayed bright dye labeling which matched the cytosolic BFP expression (Figure A3-2-5).

For in vivo characterization, the virus was injected to neonatal mice (P2-P5) expressing Cre recombinase in specific cell types. Parvalbumin (PV) neurons, a class of GABAergic interneurons, were chosen because of their sparse expression and fast-spiking activity profile.[19] We first crossed a PV-Cre (i.e. Cre recombinase is only expressed in PV cells) homozygous female with a floxed-GCaMP6f heterozygous male, producing offsprings, which all expressed PV-Cre and half of them expressed GCaMP6f in PV cells. When we collected and stained P28 (post-natal day 28) acute brain slices, there was no BFP or RhoVR fluorescence when imaged under confocal microscope (data not shown). In some animals, GCaMP6f signal was detected which was most abundant in the cerebellum, indicating that Cre-recombinase was indeed present in specific cells and expression pattern matched the expected distribution of PV cells in the brain.[20] We then repeated the neonatal viral injections twice more in PV-Cre heterozygous animals, but no BFP expression or RhoVR staining was seen (data now shown).

Besides the PV-Cre line, we also tested the virus in EMX-Cre mouse. The EMX1 gene encodes for a transcription factor that distributes ubiquitously in the cortex.[21] Abundance of EMX-positive neurons exceeds that of PV neurons and given the low expression efficiency in HEK cells, infecting a larger pool of Cre-positive cells might yield more HaloTag-positive cells. We acquired some P20 slices, stained with RhoVR1-PEG_{25}-HaloTag and saw that BFP expression was not only dim but also sparser than the expected EMX distribution. Nonetheless, the dye was selectively stained on the cell surface despite a low contrast against the background (Figure A3-2-6a-c). At P26, we imaged again and observed an increase in BFP expression and brighter dye staining with better contrast (Figure A3-2-6d-f), suggesting that HaloTag expression was enhanced relative to a week earlier. Compared to previous experiments with plasmid-based in utero electroporation, a much higher light power (almost twice high) was used to illuminate the

sample to visualize the dim staining. We attribute the compromised contrast to a weak HaloTag expression that led to fewer dye molecules bound. All the results in both PV-Cre and EMX-Cre slices corroborated the HEK cell data and emphasized the fact that the virus is ineffective that very few cells could successfully express HaloTag or get labeled with our dye. It is puzzling that the plasmid itself is very effective but the virus did not work as well as imagined. Nonetheless, other researchers have constantly used the same viral vector and virus serotype for gene delivery very efficiently.

Meanwhile, since the pAAV-hSyn-HaloTag-DAF virus was shown to work in slices, we decided to prepare two other constructs using the GPI-anchor targeting moiety DAF and using an EGFP marker (Figure A3-2-1) and these variations could hopefully offer some explanations to the low efficiency of the pDisplay-mTagBFP2 virus. Both constructs were successfully obtained and confirmed by sequencing and SmaI digestion (Figure A3-2-7). HEK cells transfected DAF-mTagBFP2 or DAF-EGFP plasmid alone did not show any BFP or RhoVR fluorescence (Figure A3-2-8e-h, Figure A3-2-9g-i). Co-transfection of DAF-mTagBFP2 and pCAG-Cre-H2B-EGFP expressed cytosolic BFP and effectively labeled TMR-PEG_{13}-HaloTag on the cell surface (Figure A3-2-8a-d). For the DAF-EGFP construct, we first co-transfected HEK cells with pCAG-Cre-H2B-mCherry and stained with dye. Cytosolic EGFP was clearly visualized, suggesting that the floxed HaloTag construct was expressed; on the other hand, the nuclear mCherry was so bright that it obscured the signal from the relatively dim membrane-bound TMR dye (Figure A3-2-9a-c). Alternatively, we used a pCAG-Cre-H2B-EGFP plasmid for transfection, in which dim cytosolic EGFP from DAF-EGFP could not be seen but membrane-bound TMR signal was detected (Figure A3-2-9d-f).

Having demonstrated that the plasmids function well in HEK cells, we sent them for virus packaging and got the DAF-mTagBFP2 and DAF-mTagBFP2 viruses with a titer of 1.10×10^{15} vg/ml and 2.61×10^{15} vg/ml, respectively. We transduced the DAF-mTagBFP2 to HEK cells followed by pCAG-Cre-H2B-EGFP plasmid transfection. The expression of Cre recombinase expression is very robust as indicated by the bright nuclear EGFP fluorescence (A3-2-10b). While cytosolic BFP fluorescence was seen in a few cells that also had TMR staining, the TMR signal was very low and complicated with bleed-through from the EGFP fluorescence (Figure A3-2-10c-f). We did a control experiment with the DAF-mTagBFP2 virus alone and saw no expression or staining (Figure A3-2-11), suggesting that HaloTag expression was dependent on Cre recombinase. We repeated the experiment with the DAF-EGFP virus and pCAG-Cre-H2B-EGFP plasmid transfection and observed fairly sparse and weak dye staining (Figure A3-2-12). Transduction of both viruses in cultured hippocampal neurons resulted in selective staining of low contrast above the background in expressing neurons (Figure 3-2-13). It may seem that DAF-mTagBFP2 and DAF-EGFP viruses performed better than the pDisplay-mTagBFP2 since stronger selective staining was detected in both HEK cells and neurons; however, a brighter TMR dye was used for characterization, rather than the dimmer RhoVR dye in the previous experiments. We are currently waiting for EMX-Cre mice for characterization in brain slices.

Conclusion

We have cloned and verified three new plasmids that worked well in cultured cells to express HaloTag and capture RhoVR1-PEG_{25}-HaloTag in a Cre-dependent and

cell-type specific manner. However, when the plasmids were packaged into the viral genome and used for viral infection, only a limited portion of cells expressed HaloTag with little dye labeled. We are still investigating the reasons underlying the ineffective viruses. Current work focuses on designing and testing a non-floxed virus to rule out the possibility of any problems with Cre recombinase.

Experimental Sections

Cell Culture

All animal procedures were approved by the UC Berkeley Animal Care and Use Committees and conformed to the NIH Guide for the Care and Use and Laboratory Animals and the Public Health Policy.

Human embryonic kidney 293T (HEK) cells were maintained and plated in Dulbecco's modified eagle medium (DMEM) supplemented with 4.5 g/L D-glucose, 10% fetal bovine serum (FBS; Thermo Scientific) and 1% GlutaMax (Invitrogen) at 37 °C in a humidified incubator with 5 % CO_2. Cells were passaged and plated in DMEM (as above) at a density of 75,000 cells onto 12 mm glass coverslips pre-coated with Poly-D-Lysine (PDL; 1 mg/ml; Sigma-Aldrich) per well in a 24-well plate. Transfection of plasmids was carried out using Lipofectamine 3000 (Invitrogen) ~18-24 h after plating. Viral transduction was conducted immediately after plating with a multiplicity of infection (MOI) of approximately 10^6. No media change was conducted for both plasmid transfection and viral transduction; reagents were added directly to cells in regular media.

Hippocampi were dissected from embryonic day 19 Sprague Dawley rats (Charles River Laboratory) in cold, sterile HBSS (zero Ca^{2+}, zero Mg^{2+}, phenol red). All dissection products were supplied by Invitrogen, unless otherwise stated. Hippocampal tissue was treated with trypsin (2.5%) for 15 min at 37 °C. The tissue was triturated using fire polished Pasteur pipettes, in minimum essential media (MEM) supplemented with 5% FBS, 2% B-27, 2% 1M dextrose (Fisher Scientific) and 1% GlutaMax. The dissociated cells were plated onto 12 mm diameter coverslips (Fisher Scientific) pre-treated with PDL (as above) at a density of 25-30,000 cells per coverslip in MEM supplemented media (as above). Neurons were maintained at 37 °C in a humidified incubator with 5% CO_2. At 1 day in vitro (DIV) half of the MEM supplemented media was removed and replaced with Neurobasal media containing 2% B-27 supplement and 1% GlutaMax. Transfection of plasmids was carried out using Lipofectamine 3000 (without P3000 reagent) at 6-7 DIV. Viral transduction was conducted 1 – 3 h after cells were plated in regular culture media and half media change at 1DIV was conducted as normal. Imaging was performed on mature neurons about 7 days after plasmid transfection.

Imaging Parameters

Epifluorescence imaging was performed on an AxioExaminer Z-1 (Zeiss) equipped with a Spectra-X Light engine LED light (Lumencor), controlled with Slidebook (v6, Intelligent Imaging Innovations). Images were acquired with a W-Plan-Apo 20x/1.0 water objective (20x; Zeiss). Images were focused onto an OrcaFlash4.0 sCMOS camera (sCMOS; Hamamatsu). Confocal imaging was performed with a Zeiss LSM 880 NLO AxioExaminer equipped with a Diode 405 nm laser line, Argon 458, 488, and 514 laser lines, and a DPSS 561 nm laser line and a BiG-2 detector with a 690+

dichroic. Images were acquired using a W-Plan-Apo 20x/1.0 water objective and a Zeiss Airyscan detector.

Acute brain slice preparation

Mice were deeply anesthetized with isoflurane and quickly decapitated. After removing the scalp and skull, ice cold sucrose cutting solution (in mM: NaCl, 83; KCl, 2.5; $MgSO_4$, 3.3; NaH_2PO_4, 1; $NaHCO_3$, 26.2; D-glucose, 22; sucrose, 72; and $CaCl_2$, 0.5) was applied to the brain. BFP fluorescence was checked with a hand held 405 nm laser before the brain was taken out. The brain was cut into 300 μm thick slices with a DTK-1000 slicer in ice cold sucrose cutting solution. The cut slices were incubated in sucrose cutting solution, bubbled with 95% O_2 and 5% CO_2, first at 31 °C for about 30 min and then at room temperature until further use. For bath application of the dye and cell staining, a slice was transferred to a 35 mm dish with sucrose cutting solution bubbled with 95% O_2 and 5% CO_2 to which dye stock solution was added (250 nM final concentration, 3 mL total volume). The slice was incubated with the dye at room temperature for 15 min before imaging.

Virus injection

For adult animal injection, 450 nl of virus was injected to 4 regions at 4 different concentrations. After around two weeks, the animals were sacrificed to acquire 150 μm thick slices. After recovery at 34 °C for 15 min, the slices were incubated with 125 nM dye for 30 min at RT. The slices were then fixed overnight in 4% PFA, washed with PBS and mounted for imaging.

For neonatal animal injection, P2-P5 animals were used. The viruses were not diluted and injected to 3 spots with 3 depths in each spot (roughly 350, 250 and 150 μm beneath surface) and 18.4 nl per injection. The visual cortex of the left hemisphere was targeted and the 3 spots are about 1 – 2 mm apart forming an equilateral triangle. Slices of 300 μm thickness were acquired around P12 – 25.

Cloning

It is recommended to contact Dr. Mei Li (mei.li@berkeley.edu), who can offer suggestions or specific requirements on viral vector cloning. The HaloTag inserts were cloned into a paavCAG vector with flanking loxP sites. The paavCAG vector plasmids were provided by Savitha (savi.sridharan@berkeley.edu) from the Adesnik lab. Due to the presence of inverted terminal repeats (ITRs) in the backbone, recombinase-free strains are used (for example Sure2 or Stbl3). DH5α strains can be used but often led to a low chance of getting the correct sequence. Sequencing and SmaI digestion were done on the Miniprep DNA before retransformation. Maxiprep DNA was prepared from the retransformed colonies and characterized by sequencing, SmaI digestion and transfection in cultured cells before sending it out for virus prep by Dr. Mei Li at School of Optometry, UC Berkeley. Dr. Li usually requires sequencing and digestion data before accepting the plasmids. Contact her early (maybe when the miniprep DNA is obtained) to inquire about her schedule and order the reagents she might need.

SmaI-digested products were analyzed by DNA gel electrophoresis. Briefly, 1 μg DNA was digested with 0.5 μL enzyme in cut-smart buffer in a total volume of 20 μL.

The reaction was done at 25 °C for 30 min and all the reaction mixture was loaded to an agarose gel for analysis. The following sequences were used (5' to 3'):

IgK
ATGGAGACAGACACACTCCTGCTATGGGTACTGCTGCTCTGGGTTCCAGGTTC
CACTGGTGAC

HaloTag
GCAGAAATCGGTACTGGCTTTCCATTCGACCCCCATTATGTGGAAGTCCTGGG
CGAGCGCATGCACTACGTCGATGTTGGTCCGCGCGATGGCACCCCTGTGCTG
TTCCTGCACGGTAACCCGACCTCCTCCTACGTGTGGCGCAACATCATCCCGCA
TGTTGCACCGACCCATCGCTGCATTGCTCCAGACCTGATCGGTATGGGCAAAT
CCGACAAACCAGACCTGGGTTATTTCTTCGACGACCACGTCCGCTTCATGGAT
GCCTTCATCGAAGCCCTGGGTCTGGAAGAGGTCGTCCTGGTCATTCACGACTG
GGGCTCCGCTCTGGGTTTCCACTGGGCCAAGCGCAATCCAGAGCGCGTCAAA
GGTATTGCATTTATGGAGTTCATCCGCCCTATCCCGACCTGGGACGAATGGCC
AGAATTTGCCCGCGAGACCTTCCAGGCCTTCCGCACCACCGACGTCGGCCGC
AAGCTGATCATCGATCAGAACGTTTTTATCGAGGGTACGCTGCCGATGGGTG
TCGTCCGCCCGCTGACTGAAGTCGAGATGGACCATTACCGCGAGCCGTTCCT
GAATCCTGTTGACCGCGAGCCACTGTGGCGCTTCCCAAACGAGCTGCCAATC
GCCGGTGAGCCAGCGAACATCGTCGCGCTGGTCGAAGAATACATGGACTGGC
TGCACCAGTCCCCTGTCCCGAAGCTGCTGTTCTGGGGCACCCCAGGCGTTCTG
ATCCCACCGGCCGAAGCCGCTCGCCTGGCCAAAAGCCTGCCTAACTGCAAGG
CTGTGGACATCGGCCCGGGTCTGAATCTGCTGCAAGAAGACAACCCGGACCT
GATCGGCAGCGAGATCGCGCGCTGGCTGTCGACGCTCGAGATTTCCGGC

HA
TATCCATATGATGTTCCAGATTATGCT

DAF
CCAAATAAAGGAAGTGGAACCACTTCAGGTACTACCCGTCTTCTATCTGGGC
ACACGTGTTTCACGTTGACAGGTTTGCTTGGGACGCTAGTAACCATGGGCTTG
CTGACTTAG

pDisplay
GCTGTGGGCCAGGACACGCAGGAGGTCATCGTGGTGCCACACTCCTTGCCCT
TTAAGGTGGTGGTGATCTCAGCCATCCTGGCCCTGGTGGTGCTCACCATCATC
TCCCTTATCATCCTCATCATGCTTTGGCAGAAGAAGCCACGT

P2A
GCTACTAACTTCAGCCTGCTGAAGCAGGCTGGAGACGTGGAGGAGAACCCTG
GACCT

mTagBFP2
ATGGTGTCTAAGGGCGAAGAGCTGATTAAGGAGAACATGCACATGAAGCTGT
ACATGGAGGGCACCGTGGACAACCATCACTTCAAGTGCACATCCGAGGGCGA

AGGCAAGCCCTACGAGGGCACCCAGACCATGAGAATCAAGGTGGTCGAGGG
CGGCCCTCTCCCCTTCGCCTTCGACATCCTGGCTACTAGCTTCCTCTACGGCA
GCAAGACCTTCATCAACCACACCCAGGGCATCCCCGACTTCTTCAAGCAGTC
CTTCCCTGAGGGCTTCACATGGGAGAGAGTCACCACATACGAAGACGGGGGC
GTGCTGACCGCTACCCAGGACACCAGCCTCCAGGACGGCTGCCTCATCTACA
ACGTCAAGATCAGAGGGGTGAACTTCACATCCAACGGCCCTGTGATGCAGAA
GAAAACACTCGGCTGGGAGGCCTTCACCGAGACGCTGTACCCCGCTGACGGC
GGCCTGGAAGGCAGAAACGACATGGCCCTGAAGCTCGTGGGCGGGAGCCAT
CTGATCGCAAACGCCAAGACCACATATAGATCCAAGAAACCCGCTAAGAACC
TCAAGATGCCTGGCGTCTACTATGTGGACTACAGACTGGAAAGAATCAAGGA
GGCCAACAACGAGACCTACGTCGAGCAGCACGAGGTGGCAGTGGCCAGATA
CTGCGACCTCCCTAGCAAACTGGGGCACAAGCTTAATTAA

EGFP
AGCAAGGGCGAGGAGCTGTTCACCGGGGTGGTGCCCATCCTGGTCGAGCTGG
ACGGCGACGTAAACGGCCACAAGTTCAGCGTGTCCGGCGAGGGCGAGGGCG
ATGCCACCTACGGCAAGCTGACCCTGAAGTTCATCTGCACCACCGGCAAGCT
GCCCGTGCCCTGGCCCACCCTCGTGACCACCCTGACCTACGGCGTGCAGTGCT
TCAGCCGCTACCCCGACCACATGAAGCAGCACGACTTCTTCAAGTCCGCCAT
GCCCGAAGGCTACGTCCAGGAGCGCACCATCTTCTTCAAGGACGACGGCAAC
TACAAGACCCGCGCCGAGGTGAAGTTCGAGGGCGACACCCTGGTGAACCGC
ATCGAGCTGAAGGGCATCGACTTCAAGGAGGACGGCAACATCCTGGGGCAC
AAGCTGGAGTACAACTACAACAGCCACAACGTCTATATCATGGCCGACAAGC
AGAAGAACGGCATCAAGGTGAACTTCAAGATCCGCCACAACATCGAGGACG
GCAGCGTGCAGCTCGCCGACCACTACCAGCAGAACACCCCCATCGGCGACGG
CCCCGTGCTGCTGCCCGACAACCACTACCTGAGCACCCAGTCCGCCCTGAGC
AAAGACCCCAACGAGAAGCGCGATCACATGGTCCTGCTGGAGTTCGTGACCG
CCGCCGGGATCACTCTCGGCATGGACGAGCTGTACAAGTAA

WPRE
GCTTATCGATAATCAACCTCTGGATTACAAAATTTGTGAAAGATTGACTGGTA
TTCTTAACTATGTTGCTCCTTTTACGCTATGTGGATACGCTGCTTTAATGCCTT
TGTATCATGCTATTGCTTCCCGTATGGCTTTCATTTTCTCCTCCTTGTATAAAT
CCTGGTTGCTGTCTCTTTATGAGGAGTTGTGGCCCGTTGTCAGGCAACGTGGC
GTGGTGTGCACTGTGTTTGCTGACGCAACCCCCACTGGTTGGGGCATTGCCAC
CACCTGTCAGCTCCTTTCCGGGACTTTCGCTTTCCCCCTCCCTATTGCCACGGC
GGAACTCATCGCCGCCTGCCTTGCCCGCTGCTGGACAGGGGCTCGGCTGTTG
GGCACTGACAATTCCGTGGTGTTGTCGGGGAAATCATCGTCCTTTCCTTGGCT
GCTCGCCTGTGTTGCCACCTGGATTCTGCGCGGGACGTCCTTCTGCTACGTCC
CTTCGGCCCTCAATCCAGCGGACCTTCCTTCCCGCGGCCTGCTGCCGGCTCTG
CGGCCTCTTCCGCGTCTTCGCCTTCGCCCTCAGACGAGTCGGATCTCCCTTTG
GGCCGCCTCCCCGCATCGATACCG

CAG promoter
TCGAGGTGAGCCCCACGTTCTGCTTCACTCTCCCCATCTCCCCCCCCCTCCCCA
CCCCCAATTTTGTATTTATTTATTTTTTAATTATTTTGTGCAGCGATGGGGGCG

GGGGGGGGGGGGGGGCGCGCGCCAGGCGGGGCGGGGCGGGGCGAGGGGCG
GGGCGGGGCGAGGCGGAGAGGTGCGGCGGCAGCCAATCAGAGCGGCGCGCT
CCGAAAGTTTCCTTTTATGGCGAGGCGGCGGCGGCGGCCCTATAAAAAG
CGAAGCGCGCGGCGGGCG

Benchling links for constructs

CAG-DIO-IgK-HaloTag-HA-pDisplay-P2A-mTagBFP2-WPRE
https://benchling.com/s/seq-DB4ss4O7HHm7xurB8HwB

CAG-DIO-IgK-HaloTag-HA-DAF-P2A-mTagBFP2-WPRE
https://benchling.com/s/seq-9wY0aaiw2sW4FDrHaj71

CAG-DIO-IgK-HaloTag-HA-DAF-P2A-EGFP-WPRE
https://benchling.com/s/seq-0Yr7AvAXd4vYcX5m7b7K

Figures and Schemes

Figure A3-1-1*. Characterization of pAAV-hSyn-HaloTag-DAF in cultured neurons*.

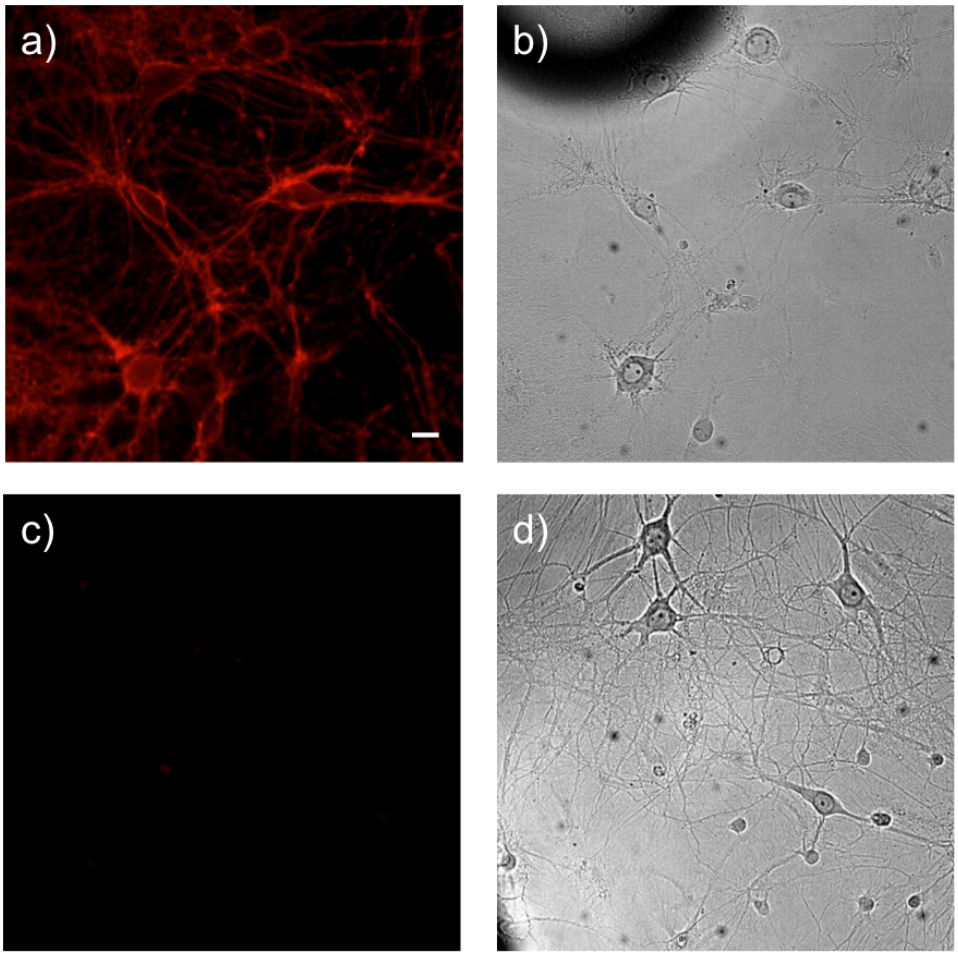

Figure A3-1-1. Wide-field fluorescence microscopy of cultured hippocampal neurons (a) transduced with pAAV-hSyn-HaloTag-DAF or (b) non-transduced, stained with RhoVR1-PEG_{25}-HaloTag (50 nM, 30 min). (a,c) RhoVR staining. (b,d) DIC image of HEK cells. Scale bar is 20 μm.

***Figure A3-1-2**. Characterization of pAAV-hSyn-HaloTag-DAF in mouse brain slice.*

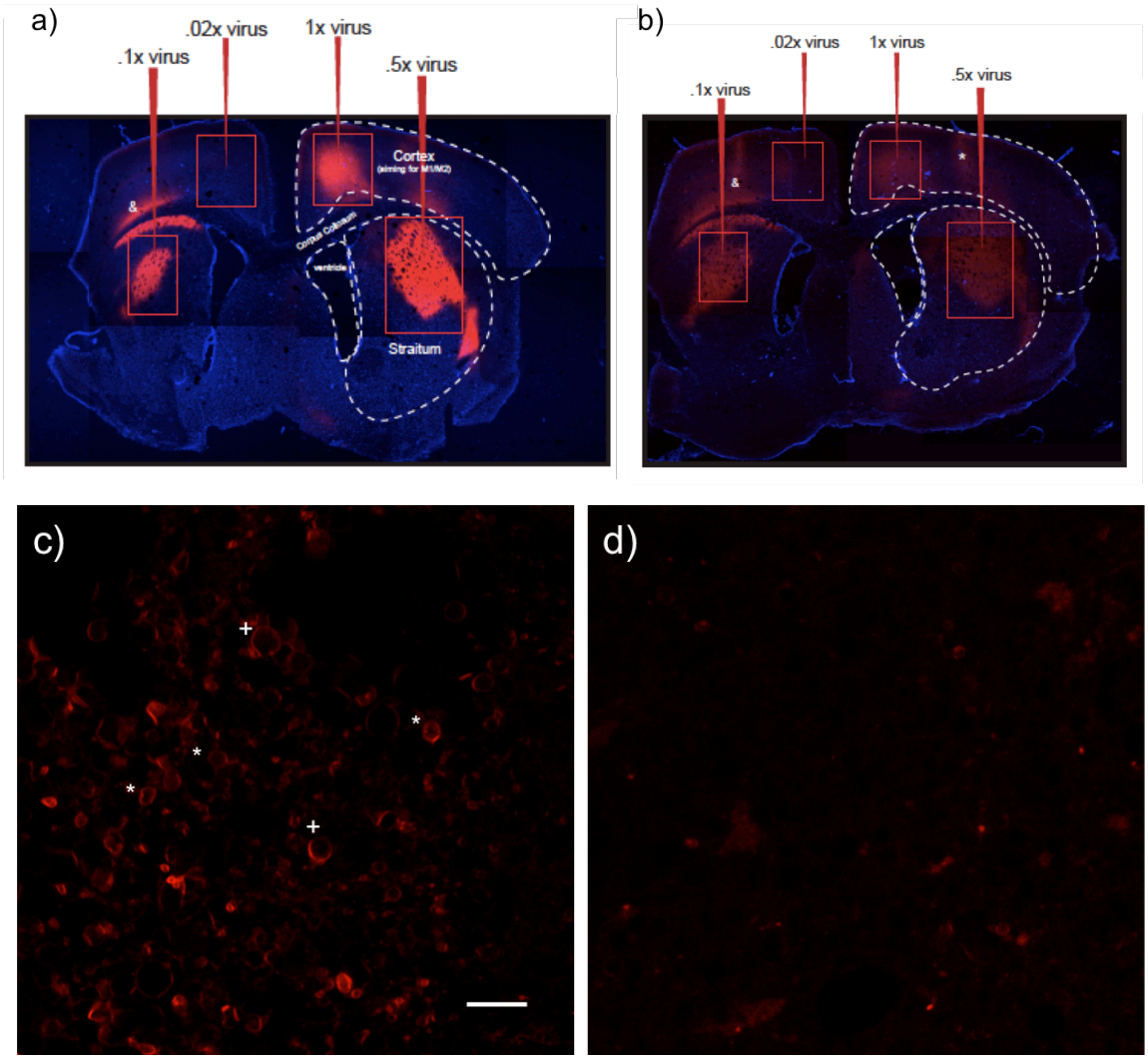

Figure A3-1-2. Mouse brain slices expressing pAAV-hSyn-HaloTag-DAF and stained with (a) TMR-PEG_{13}-HaloTag or (b-d) RhoVR1-PEG_{25}-HaloTag (125 nM, 30 min, RT). One-photon confocal microscopy imaging of stained slices in (a) area of injection or (b) non-injected area. Scale bar is 10 μm.

Figure A3-2-1. *Double-floxed inverted (DIO) constructs used in this study.*

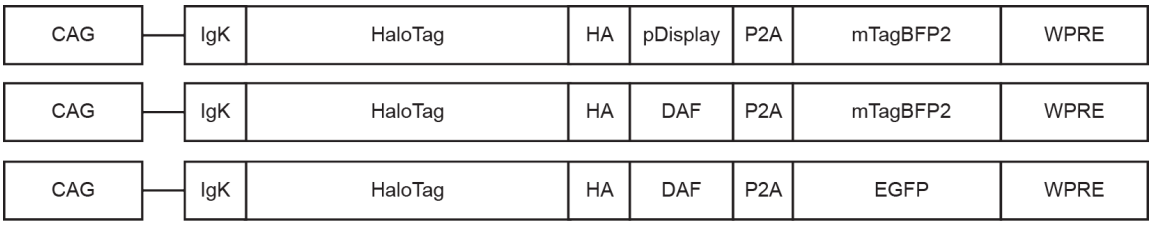

Figure A3-2-1. Double-floxed inverted (DIO) constructs used in this study.

Figure A3-2-2. *Characterization of paavCAG-DIO-IgK-HaloTag-HA-pDisplay-P2A-mTagBFP2 plasmid by SmaI digestion and gel electrophoresis.*

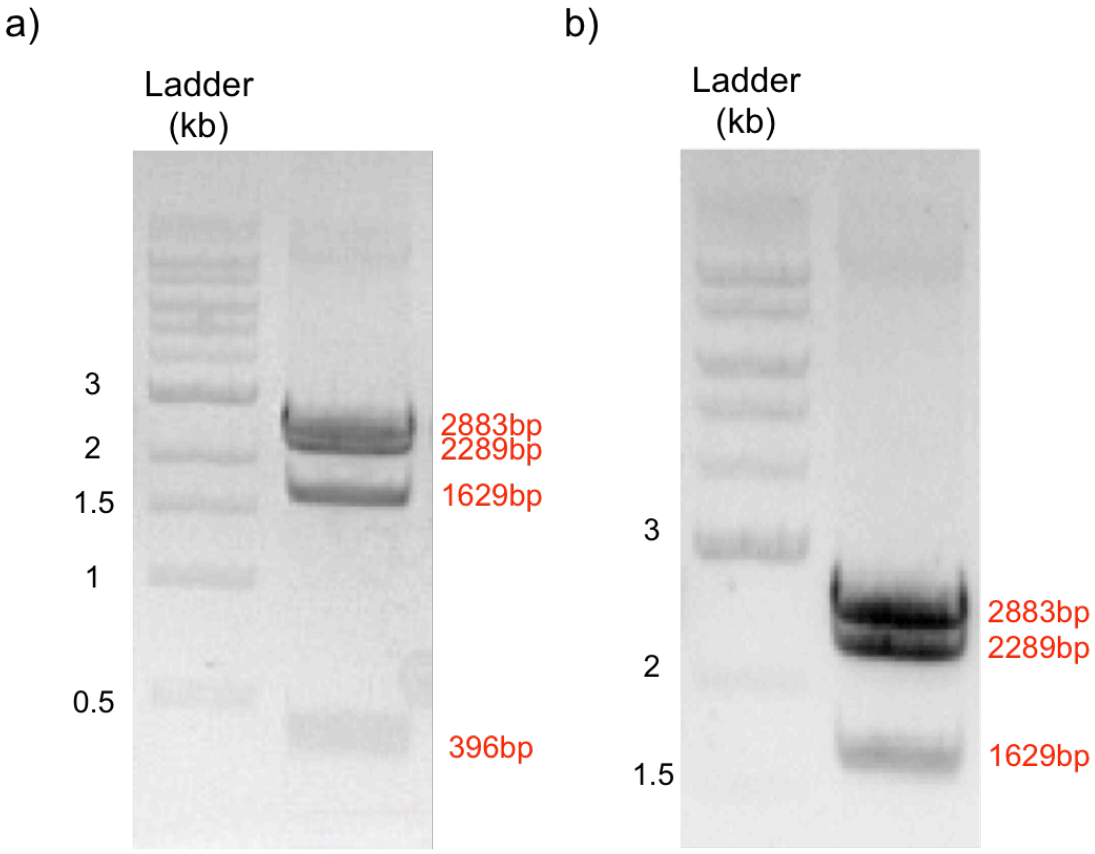

Figure A3-2-2. DNA gel images of SmaI-digested plasmid run at 100 V for (a) 20 min and (b) 50 min. The gels clearly showed the expected band sizes (2883bp, 2289bp, 1629bp and 396bp).

Figure A3-2-2. *Characterization of paavCAG-DIO-IgK-HaloTag-HA-pDisplay-P2A-mTagBFP2 plasmid in HEK cells.*

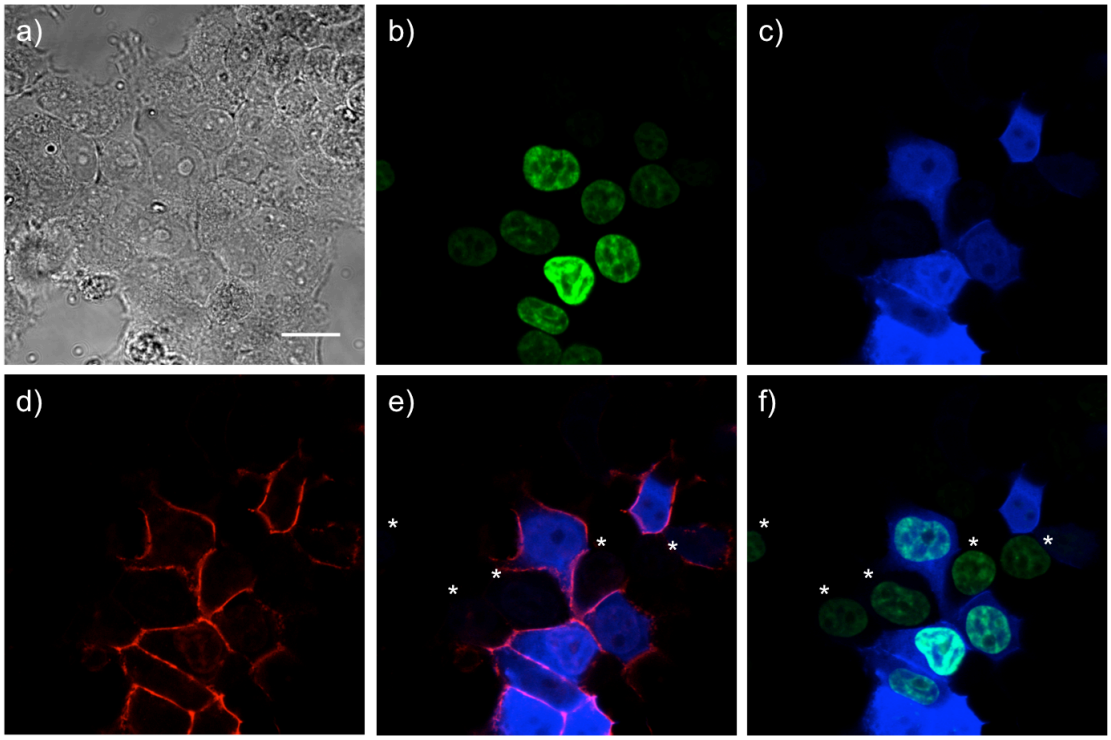

Figure A3-2-2. One-photon confocal microscopy of HEK cells transfected with paavCAG-DIO-IgK-HaloTag-HA-pDisplay-P2A-mTagBFP2 and pCAG-Cre-H2B-EGFP plasmids and stained with RhoVR1-PEG_{25}-HaloTag (50 nM, 30 min). (a) DIC image of HEK cells. (b) Nuclear EGFP fluorescence indicates Cre recombinase expression. (c) Cytosolic BFP fluorescence indicates HaloTag expression. (d) Membrane-associated RhoVR fluorescence. (e) Merge image of RhoVR and BFP. (f) Merge image of EGFP and BFP. Asterisks indicate cells that express Cre recombinase but have neither HaloTag expression nor RhoVR staining. Scale bar is 20 μm.

Figure A3-2-3. *Characterization of paavCAG-DIO-IgK-HaloTag-HA-pDisplay-P2A-mTagBFP2 plasmid in cultured neurons*.

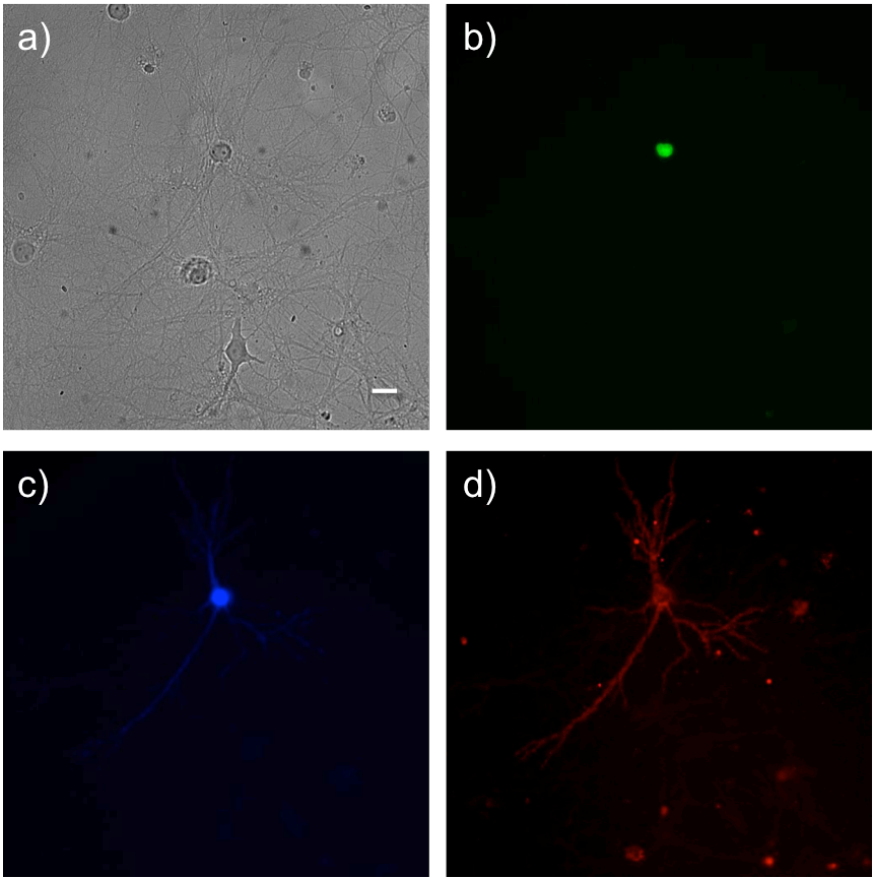

Figure A3-2-3. Wide-field fluorescence microscopy of cultured hippocampal neurons transfected with paavCAG-DIO-IgK-HaloTag-HA-pDisplay-P2A-mTagBFP2 and pCAG-Cre-H2B-EGFP plasmids and stained with RhoVR1-PEG_{25}-HaloTag (50 nM, 30 min). (a) DIC image of neurons. (b) Nuclear EGFP fluorescence indicates Cre recombinase expression. (c) Cytosolic BFP fluorescence indicates HaloTag expression. (d) Membrane-associated RhoVR fluorescence that is specific to BFP fluorescence or BFP expression. Scale bar is 20 μm.

Figure A3-2-4*. Characterization of paavCAG-DIO-IgK-HaloTag-HA-pDisplay-P2A-mTagBFP2 virus in HEK cells.*

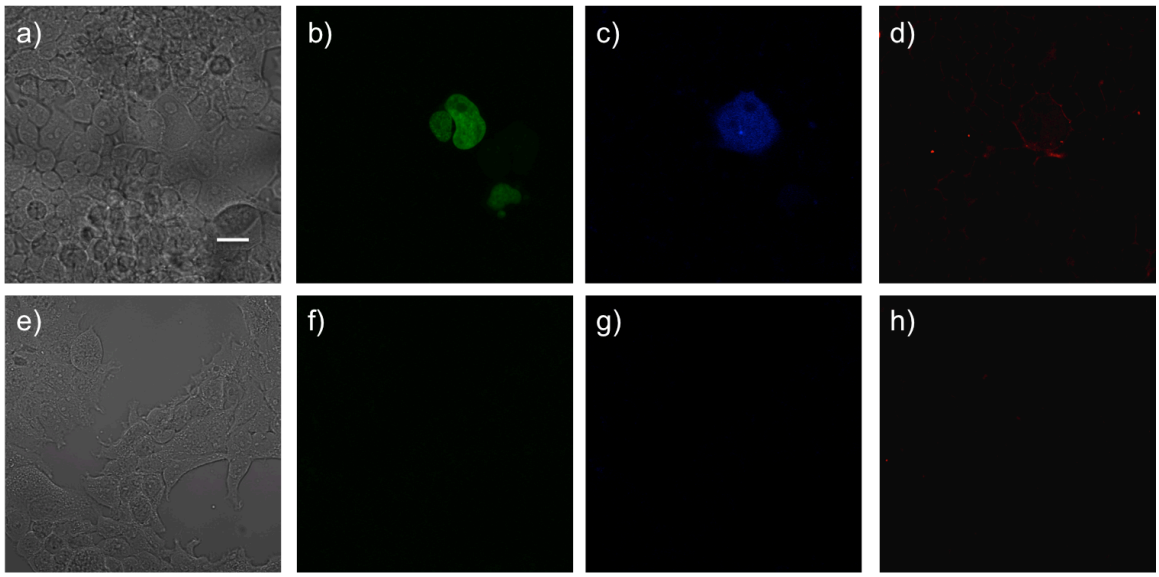

Figure A3-2-4. One-photon confocal microscopy of HEK cells (a-d) transfected with pCAG-Cre-H2B-EGFP plasmid and transduced with paavCAG-DIO-IgK-HaloTag-HA-pDisplay-P2A-mTagBFP2 virus or (e-h) transduced with virus alone. Cells are stained with RhoVR1-PEG_{25}-HaloTag (50 nM, 30 min) 4 days after viral transduction. (a,e) DIC image of HEK cells. (b,f) Nuclear EGFP fluorescence indicates Cre recombinase expression. (c,g) Cytosolic BFP fluorescence indicates HaloTag expression. (d,h) RhoVR fluorescence. Scale bar is 20 μm.

***Figure A3-2-5**. Characterization of paavCAG-DIO-IgK-HaloTag-HA-pDisplay-P2A-mTagBFP2 virus in HEK cells.*

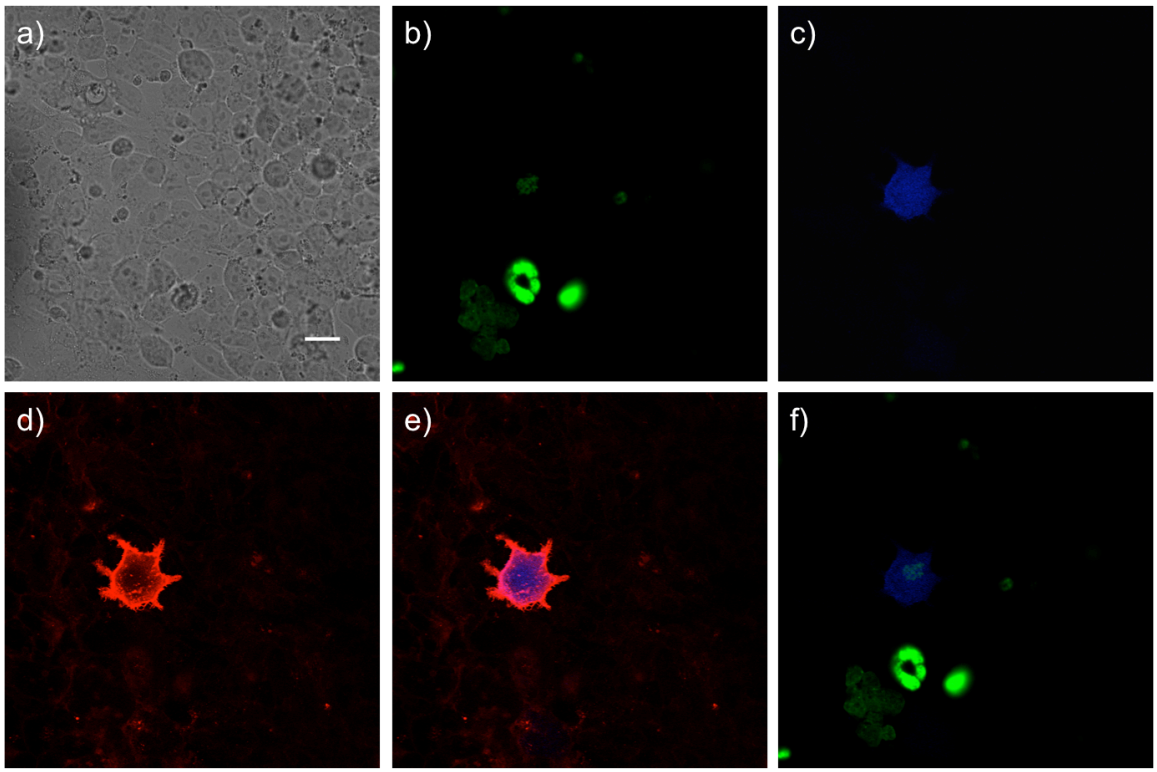

Figure A3-2-5. One-photon confocal microscopy of HEK cells transfected with pCAG-Cre-H2B-EGFP plasmid and transduced with paavCAG-DIO-IgK-HaloTag-HA-pDisplay-P2A-mTagBFP2 virus. Cells are stained with RhoVR1-PEG_{25}-HaloTag (50 nM, 30 min) 8 days after viral transduction. (a) DIC image of HEK cells. (b) Nuclear EGFP fluorescence indicates Cre recombinase expression. (c) Cytosolic BFP fluorescence indicates HaloTag expression. (d) Bright and membrane-associated RhoVR fluorescence. (e) Merge image of BFP and RhoVR. (f) Merge image of EGFP and BFP. Scale bar is 20 μm.

Figure A3-2-6. *Characterization of paavCAG-DIO-IgK-HaloTag-HA-pDisplay-P2A-mTagBFP2 virus in mouse brain slice.*

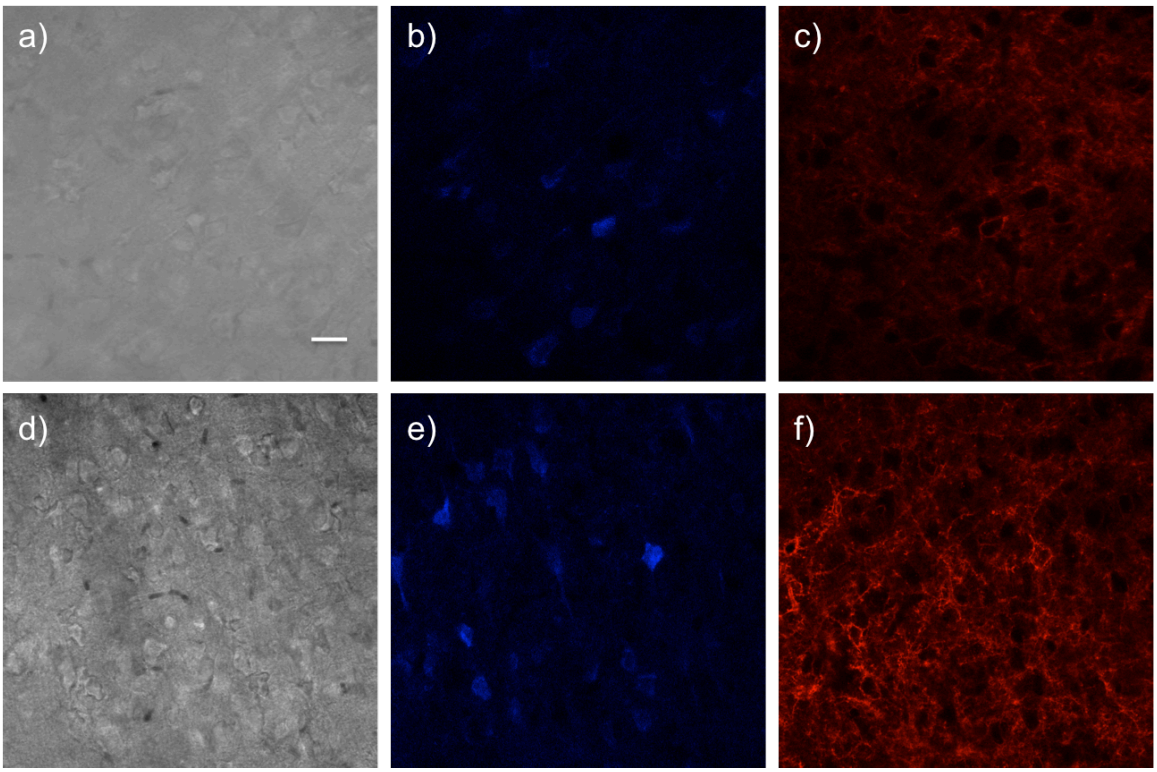

Figure A3-2-6. One-photon confocal microscopy of (a-c) P20 and (d-f) P26 EMX-Cre mouse brain slices infected with paavCAG-DIO-IgK-HaloTag-HA-pDisplay-P2A-mTagBFP2 virus at P2 and stained with 500 nM RhoVR1-PEG_{25}-HaloTag for 20 min at RT. (a,d) Bright field images of slices. (b,e) Cytosolic BFP fluorescence indicates HaloTag expression. (c,f) RhoVR staining. Scale bar is 20 μm.

Figure A3-2-7. *Characterization of paavCAG-DIO-IgK-HaloTag-HA-DAF-P2A-mTagBFP2 and paavCAG-DIO-IgK-HaloTag-HA-DAF-P2A-EGFP plasmids by SmaI digestion and gel electrophoresis.*

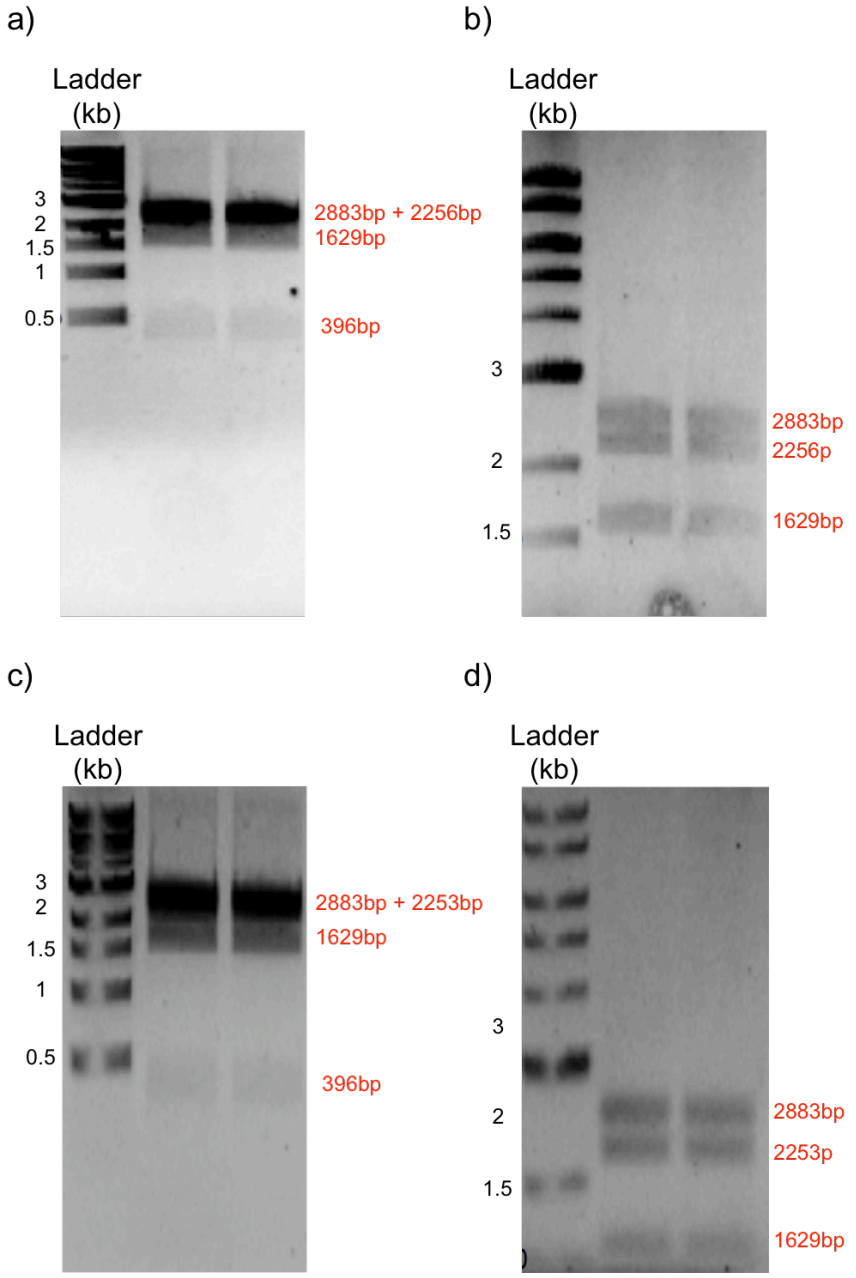

Figure A3-2-7. DNA gel images of SmaI-digested (a,b) paavCAG-DIO-IgK-HaloTag-HA-DAF-P2A-mTagBFP2 and (c,d) paavCAG-DIO-IgK-HaloTag-HA-DAF-P2A-EGFP plasmids. Gels were run at 100 V for (a,c) 20 min and (b,d) 50 min and each sample was duplicated (i.e. the two sample lanes were exactly the same). The gels clearly showed the expected band sizes (2883bp, 2256bp/2253bp, 1629bp and 396bp).

Figure A3-2-8. *Characterization of paavCAG-DIO-IgK-HaloTag-HA-DAF-P2A-mTagBFP2 plasmid in HEK cells.*

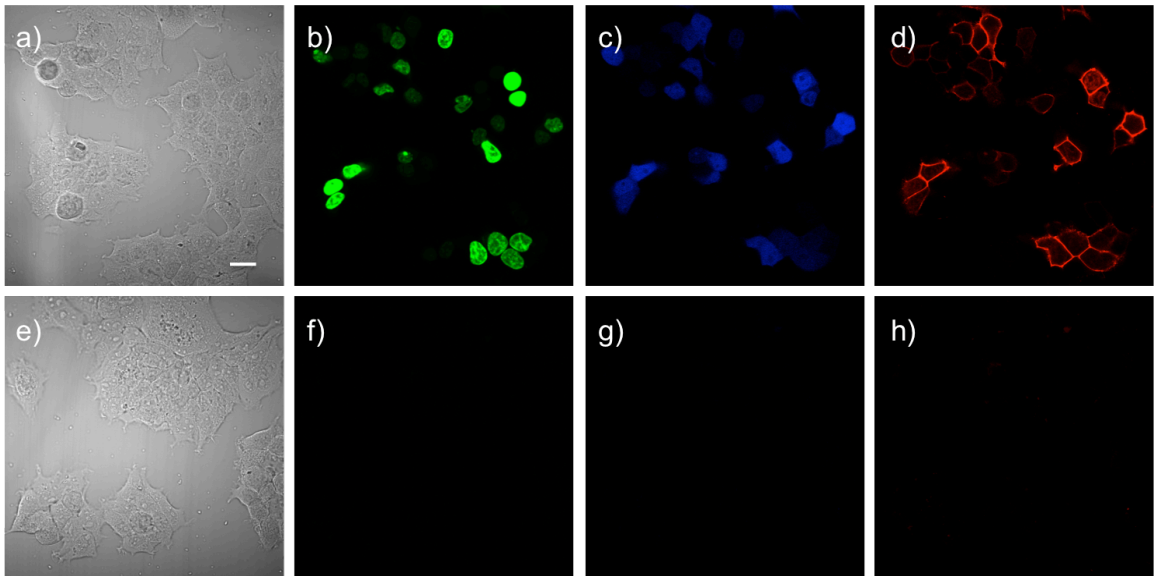

Figure A3-2-8. One-photon confocal microscopy of HEK cells transfected with (a-d) pCAG-Cre-H2B-EGFP and paavCAG-DIO-IgK-HaloTag-HA-DAF-P2A-mTagBFP2 plasmids, or (e-h) paavCAG-DIO-IgK-HaloTag-HA-DAF-P2A-mTagBFP2 plasmid alone. Cells are stained with TMR-PEG_{13}-HaloTag (50 nM, 15min, RT). (a,e) DIC image of HEK cells. (b,f) Nuclear EGFP fluorescence indicates Cre recombinase expression. (c,g) Cytosolic BFP fluorescence indicates HaloTag expression. (d,h) RhoVR fluorescence. Scale bar is 20 μm.

***Figure A3-2-9**. Characterization of paavCAG-DIO-IgK-HaloTag-HA-DAF-P2A-EGFP plasmid in HEK cells.*

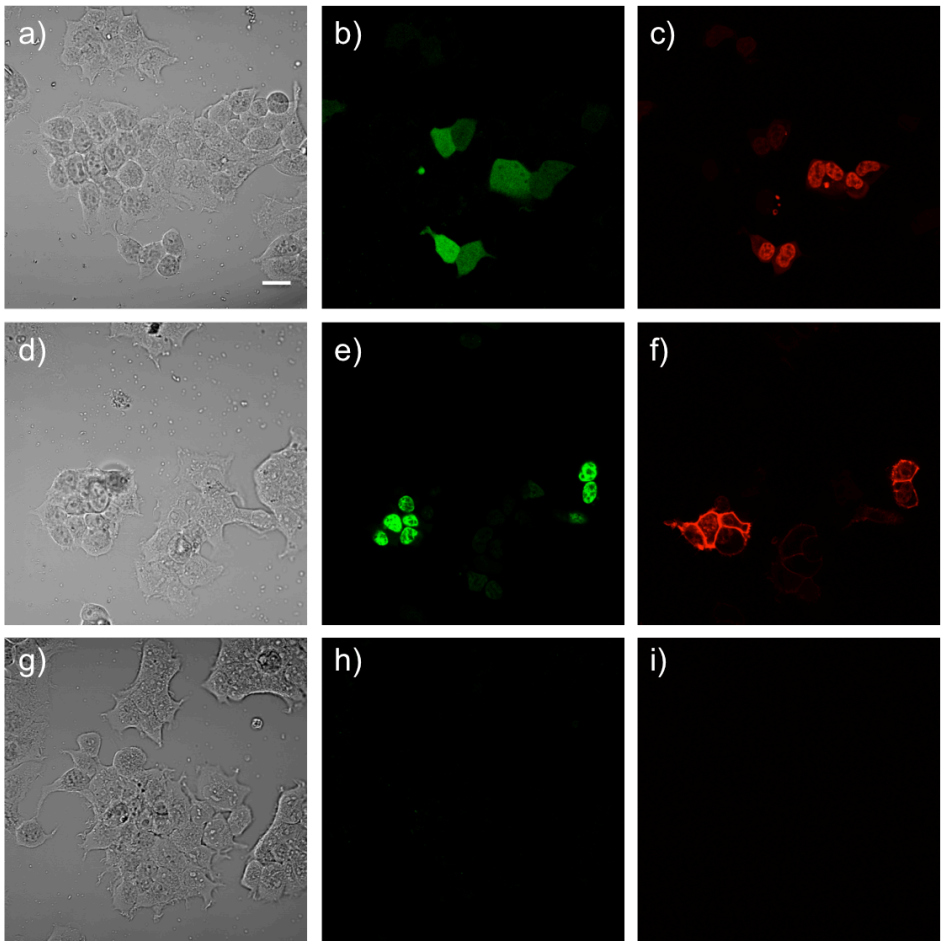

Figure A3-2-9. One-photon confocal microscopy of HEK cells transfected with (a-c) pCAG-Cre-H2B-mCherry and paavCAG-DIO-IgK-HaloTag-HA-DAF-P2A-EGFP plasmids, or (d-f) pCAG-Cre-H2B-EGFP and paavCAG-DIO-IgK-HaloTag-HA-DAF-P2A-EGFP plasmids, or (g-i) paavCAG-DIO-IgK-HaloTag-HA-DAF-P2A-EGFP plasmid alone. Cells are stained with TMR-PEG_{13}-HaloTag (50 nM, 15min, RT). (a,d,g) DIC image of HEK cells. (b) Cytosolic EGFP fluorescence indicates paavCAG-DIO-IgK-HaloTag-HA-DAF-P2A-EGFP expression. (e) Nuclear EGFP fluorescence indicates Cre recombinase expression. (h) No EGFP fluorescence was observed without the Cre plasmid. (c,f,i) RhoVR fluorescence. Scale bar is 20 μm.

Figure A3-2-10. *Characterization of paavCAG-DIO-IgK-HaloTag-HA-DAF-P2A-mTagBFP2 virus in HEK cells.*

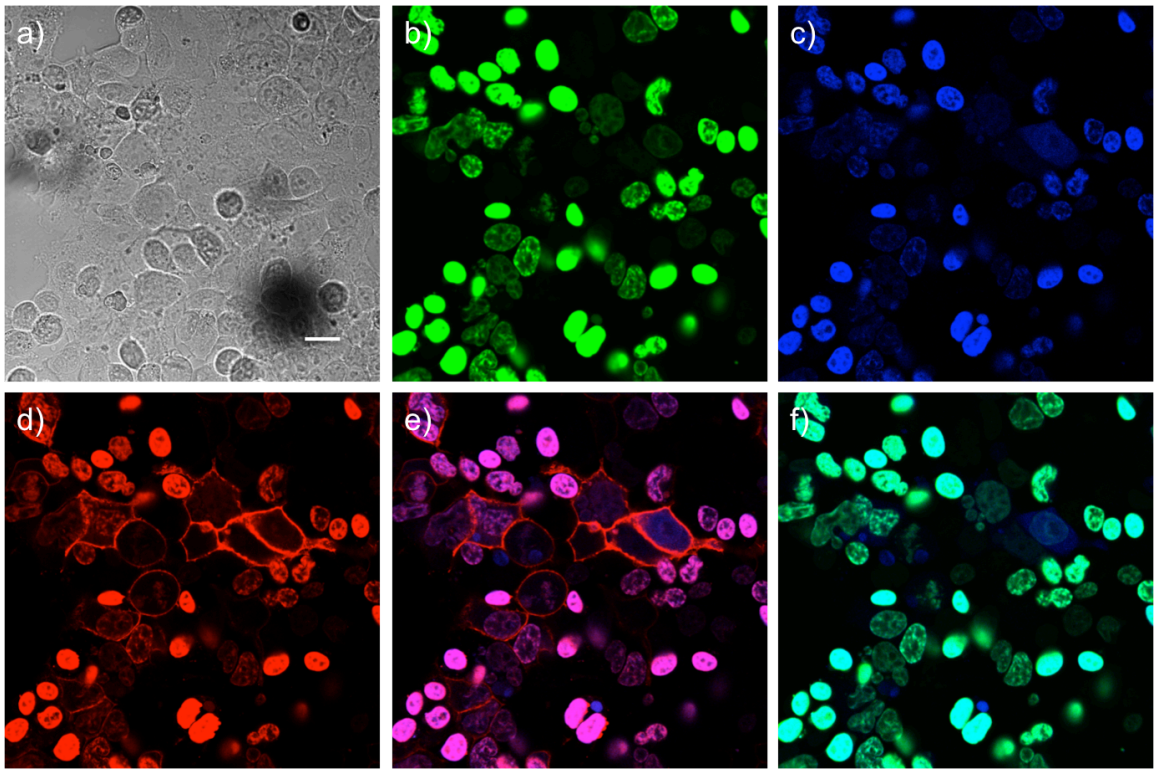

Figure A3-2-10. One-photon confocal microscopy of HEK cells transfected with pCAG-Cre-H2B-EGFP plasmid and transduced with paavCAG-DIO-IgK-HaloTag-HA-DAF-P2A-mTagBFP2 virus. Cells are stained with TMR-PEG_{13}-HaloTag (250 nM, 15min, 37 °C) 2 days after viral transduction. (a) DIC image of HEK cells. (b) Nuclear EGFP fluorescence indicates Cre recombinase expression. (c) Cytosolic BFP fluorescence indicates HaloTag expression but mostly shows bleed-through from the strong nuclear EGFP signal. (d) Membrane-associated RhoVR fluorescence indicates dye staining while nuclear fluorescence shows bleed-through from the EGFP signal. (e) Merge image of BFP and RhoVR. (f) Merge image of EGFP and BFP. Scale bar is 20 μm.

Figure A3-2-11. *Characterization of paavCAG-DIO-IgK-HaloTag-HA-DAF-P2A-mTagBFP2 virus without Cre expression in HEK cells.*

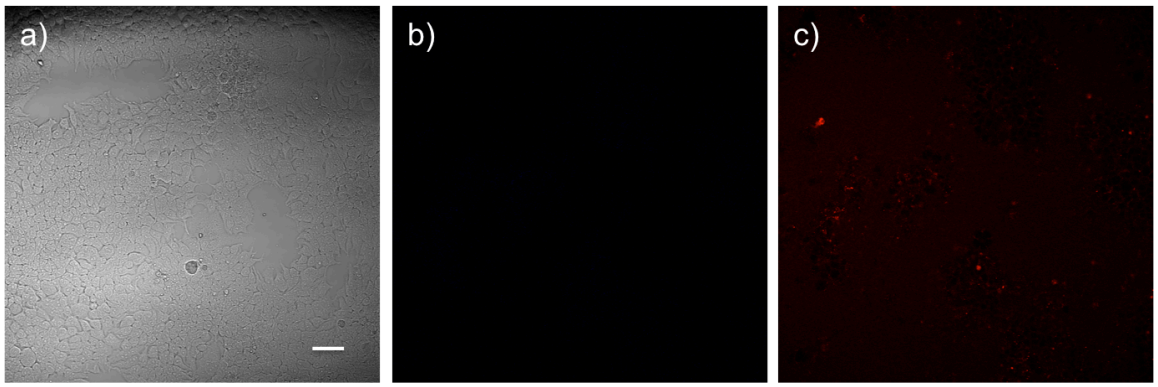

Figure A3-2-11. One-photon confocal microscopy of HEK cells transduced paavCAG-DIO-IgK-HaloTag-HA-DAF-P2A-mTagBFP2 virus. Cells are stained with TMR-PEG_{13}-HaloTag (250 nM, 15min, 37 °C) 2 days after viral transduction. (a) DIC image of HEK cells. (b) No BFP fluorescence or HaloTag expression was observed. (c) No RhoVR fluorescence was observed. Scale bar is 50 μm.

Figure A3-2-12. *Characterization of paavCAG-DIO-IgK-HaloTag-HA-DAF-P2A-EGFP virus in HEK cells.*

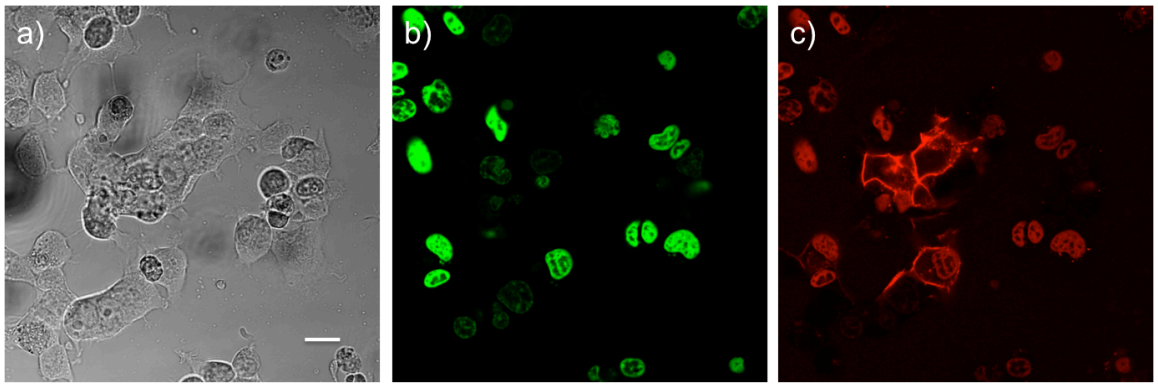

Figure A3-2-12. One-photon confocal microscopy of HEK cells transfected with pCAG-Cre-H2B-EGFP plasmid and transduced with paavCAG-DIO-IgK-HaloTag-HA-DAF-P2A-EGFP virus. Cells are stained with TMR-PEG_{13}-HaloTag (250 nM, 15min, 37 °C) 2 days after viral transduction. (a) DIC image of HEK cells. (b) Nuclear EGFP fluorescence indicates Cre recombinase expression. (c) Membrane-associated RhoVR fluorescence indicates dye staining while nuclear fluorescence shows bleed-through from the EGFP signal. Scale bar is 20 μm.

Figure A3-2-13. *Characterization of paavCAG-DIO-IgK-HaloTag-HA-DAF-P2A-mTagBFP2 and paavCAG-DIO-IgK-HaloTag-HA-DAF-P2A-EGFP viruses in cultured neurons.*

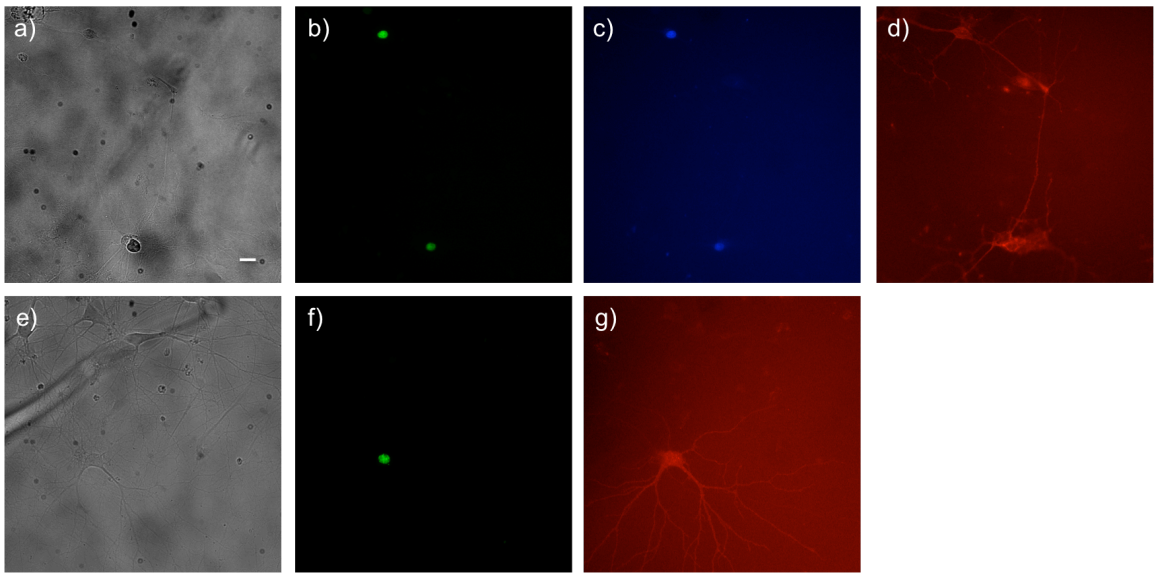

Figure A3-2-13. Wide-field fluorescence microscopy of cultured hippocampal neurons transfected pCAG-Cre-H2B-EGFP plasmid and transduced with (a-d) paavCAG-DIO-IgK-HaloTag-HA-DAF-P2A-mTagBFP2 or (e-g) paavCAG-DIO-IgK-HaloTag-HA-DAF-P2A-mTagBFP2 and stained with TMR-PEG_{13}-HaloTag (250 nM, 15 min, 37 °C) 14 days after viral transduction. (a,e) DIC image of neurons. (b,f) Nuclear EGFP fluorescence indicates Cre recombinase expression. (c) Cytosolic BFP fluorescence indicates HaloTag expression but signal is complicated with bleed-through from EGFP brightness. (d,g) Dim but membrane-associated RhoVR fluorescence. Scale bar is 20 μm.

Reference

1. Grenier, V.; Daws, B. R.; Liu, P.; Miller, E. W., *J. Am. Chem. Soc.* **2019**, *141* (3), 1349-1358.
2. Nayerossadat, N.; Maedeh, T.; Ali, P. A., *Adv. Biomed. Res.* **2012**, *1,* 27.
3. Lundstrom, K., *Diseases* **2018**, *6* (2), 42.
4. Teramato, S.; Ishii, T.; Matsuse, T., *Lancet* **2000**, *355* (9218), 1911-1912.
5. Hammond, S. L.; Leek, A. N.; Richman, E. H.; Tjalkens, R. B., *PLoS One* **2017**, *12* (12), e0188830.
6. Murlidharan, G.; Samulski, R. J.; Asokan, A., *Front Mol Neurosci.* **2014**, *7*, 76.
7. Wu, Z.; Yang, H.; Colosi, P., *Mol Ther.* **2010**, *18* (1), 80-86.
8. Los, G. V.; Encell, L. P.; McDougall, M. G.; Hartzell, D. D.; Karassina, N.; Zimprich, C.; Wood, M. G.; Learish, R.; Ohana, R. F.; Urh, M.; Simpson, D.; Mendez, J.; Zimmerman, K.; Otto, P.; Vidugiris, G.; Zhu, J.; Darzins, A.; Klaubert, D. H.; Bulleit, R. F.; Wood, K. V., *ACS Chem. Biol.* **2008**, *3* (6),373-382.
9. Liu, P.; Grenier, V.; Hong, W.; Muller, V. R.; Miller, E. W., *J. Am. Chem. Soc.* **2017**, *139*, 17334-17340.
10. Subach, O. M.; Cranfill, P. J.; Davidson, M. W.; Verkhusha, V. V., *PLoS One* **2011**, *6* (12):e28674.
11. Cormack, B. P.; Valdivia, R. H.; Falkow, S., *Gene* **1996**, *173* (1): 33-38.
12. Sauer, B., *Mol. Cell. Biol*. **1987**, *7* (6), 2087-2096.
13. Sauer, B.; Henderson, N., *Proc. Natl. Acad. Sci. U.S.A.* **1988**, *85* (14), 5166-5170.
14. Nagy, A., *Genesis* **2000**, *26* (2), 99-109.
15. Dragatsis, I.; Zeitlin, S., *Genesis* **2000**, *26* (2), 133-135.
16. Kaneko, R.; Takatsuru, Y.; Morita, A.; Amano, I.; Haijima, A.; Imayoshi, I.; Tamamaki, N.; Koibuchi, N.; Watanabe, M.; Yanagawa, Y., *J. Comp. Neurol.* **2018**, *526* (3), 373-396.
17. Liu, Z.; Chen, O.; Wall, J. B. J.; Zheng, M.; Zhou, Y.; Wang, L.; Ruth, V. H.; Qian, L.; Liu, J., *Sci Rep.* **2017**, *7* (1), 2193.
18. Gray, S. J.; Choi, V. W.; Asokan, A.; Haberman, R. A.; McCown, T. J.; Samulski, R. J., *Curr. Protoc. Neurosci.* **2011**, Chapter 4, Unit 4.17.
19. Hu, H.; Gan, J.; Jonas, P., *Science* **2014**, *345* (6196):1255263.
20. Schwaller, B.; Meyer, M.; Schiffmann, S., *Cerebellum* **2002**, *1* (4), 241-258.
21. Cecchi, C.; Boncinelli, E., *Trends Neurosci.* **2000**, *23* (8), 347-352.

Appendix 4:

In Utero Electroporation and Slice Preparation Protocols

Introduction

In utero electroporation is a commonly used technique to delivery genetic materials to animal. Briefly, plasmid DNA is injected to the ventricular space of embryonic rodent brains and enters surrounding cells via electroporation. Expression from IUE is transient and less efficient compared to virus-mediated genetic perturbation. Unlike viral transduction, IUE relies on plasmid, which is safer and easier to prepare. The procedure is relatively straightforward and can be done within an hour for a litter of embryos. Virus preparation takes about five weeks and is usually more expensive. As a result, we have chosen to use IUE to test and optimize plasmid expression and VoltageFluor dye labeling. This project is collaboration with Professor Hillel Adesnik's lab (UC Berkeley), who will perform IUE and maintain the animals in general.

IUE is done on E15 mice and a fluorescent marker is injected for screening at P0 or P1. Positive animals are kept while the others are sacrificed. Acute brain slices can be acquired from P12 to P35 animals. Animals younger than P12 have soft and fragile brain tissue that cannot withstand microtome cutting. Those older than P35 produce slices that are more challenging to survive ex vivo or conduct electrophysiology on. ACSF buffer with slightly different compositions may be required for older slices. Unused animals that are too old for slice preparation and experiments can be maintained for adult animal imaging.

General Experimental Considerations

Preparation of plasmid construct

The plasmid has to be prepared using an endotoxin-free maxiprep kit. The DNA can be eluted with sterile water or buffer TE. The concentration is preferably at least 1 μg/μL since 1 μL of DNA is usually used per injection and the amount of DNA affects expression level. It is recommended to sequence and characterize the DNA in cultured cells before sending it out for IUE.

Choice of co-injection plasmid

When the pups are born, it is possible to use a hand held laser or fluorescence macroscope to screen for expression at P0 or P1. Pups older than that are difficult to screen due to increased thickness of skull and skin auto-fluorescence. The construct containing IRES-FP (i.e. IRES-mCherry or IRES-BFP) does not express enough fluorescent protein for neonatal screening, which is often too dim to confirm or complicated with tissue auto-fluorescence. Injection with SpyCather-T2A-mCherry construct cannot be screened either, suggesting all the constructs have relatively low expression. As a result, for the HaloTag constructs used for IUE, the IRES-EGFP portion is removed completely as a smaller plasmid is expected to enter the cells more readily. However, it is necessary to include a FP as an expression marker, which helps to identify positive animals and slices. We have tried pCAG-mTagBFP2 and pCAG-EGFP with the HaloTag construct for co-injection. The ratio of HaloTag plasmid to FP plasmid is usually 5:1. We first attempted pCAG-EGFP and were able to screen for and keep positive pups. Unfortunately, there was significant bleed-through from the EGFP to the RhoVR channel during two-photon imaging. We then lowered the amount of EGFP plasmid used for co-injection (1:20) but the problem still persisted. Then we switched to

pCAG-mTagBFP2 but could not screen for positive pups due to its blue-shifted spectral profile and relatively low expression when the animals were young. However, during slice preparation at P12 or older, we were able to screen for BFP fluorescence after removing the skull or during slice cutting. There was no cross-talk between BFP and RhoVR in one-photon or two-photon imaging.

Buffer recipe and preparation

There are two different solutions used in slice preparation and imaging. The artificial cerebrospinal fluid with sucrose or ACSF-sucrose solution is used for cutting and storing the slices while ACSF recording solution is used for activity imaging. ACSF-sucrose solution has a lower sodium concentration to maintain slice health and increase chances of survival during cutting. Usually, 2L of 1x working solution is prepared and the compositions are as follows:

For 2 liters of ACSF-sucrose	**Grams**	**Concentration (mM)**	**MW**
NaCl	9.70	83	58.44
KCl	0.37	2.5	74.55
$MgSO_4$. $7H_2O$	1.63	3.3	246.47
Na_2HPO_4. $2H_2O$	0.36	1	177.99
$NaHCO_3$	4.37	26	84.01
Glucose	7.93	22	180.16
Sucrose	49.28	72	342.3
$CaCl_2$	0.4 mL of 2.5 mM	0.5	

For 2 liters of ACSF-recording	**Grams**	**Concentration (mM)**	**MW**
NaCl	13.91	119	58.44
KCl	0.37	2.5	74.55
$MgSO_4$. $7H_2O$	0.64	1.3	246.47
Na_2HPO_4. $2H_2O$	0.37	1.3	177.99
$NaHCO_3$	4.37	26	84.01
Glucose	7.21	22	180.16
$CaCl_2$	2 mL of 2.5 mM	2.5	

2.5 mM $CaCl_2$ stock solution is prepared in Milli-Q water. Other chemicals are weighed and transferred to a 2 L volumetric flask and Milli-Q is used. When all the solids are dissolved, transfer the solution to a 2 L glass bottle before $CaCl_2$ is added. For ACSF-sucrose solution, add $CaCl_2$ directly, mix well and the solution is ready to use. For ACSF recording solution, the solution will become cloudy with white precipitates immediately after $CaCl_2$ addition. Thus, the solution needed to be bubbled with carbogen (95% O_2 and 5% CO_2) for about 10 – 15 minutes or until the solution clears up. Osmolarity of the solutions should be around 300 – 320 mOsm/L. Solutions are stored at 4 °C.

Acute brain slice preparation

1. About 1 hour before slicing, take out ACSF-sucrose and ACSF-recording solutions from the cold room. The ACSF-sucrose solution for slice storage needs to be warmed to 31 °C while ACSF-recording solution should go to room temperature.

2. Pour some ACSF-sucrose solution to the incubation chamber with the 6-well insert (Figure A4-1), connect the chamber to tubing for carbogen perfusion and place the chamber in a water bath set at 31 °C.

3. Fill the glassware (one beaker and one crystallization dish) with about 60 mL ACSF-sucrose each (Figure A4-2), leave it on ice and start carbogen perfusion.

4. Tools for slicing include a pair ring-tip forceps, big spatula, small spatula, a pair of angled scissors, scalpel and a pair of big scissors (from left to right, Figure A4-3). All the tools except the big scissors are placed in the beaker (left, Figure A4-2) with perfused ice-cold ACSF-sucrose until usage. A 3mL plastic Pasteur pipette cut at the 1 mL mark will also be used for slice transfer.

5. The slicing chamber (top, Figure A4-3) should be cooled on ice and a piece of kimwipe can be placed inside the chamber to absorb condensation.

6. Install the blade and prepare a piece of absorbent unerpad, two pieces of filter paper , glue, a hand-held laser and goggles.

7. Allow the ACSF-sucrose in the incubation chamber to reach 31 °C, which takes roughly 45 minutes. Meanwhile, the cutting tools should be chilled as well.

8. Put a piece of paper towel in the anesthesia chamber (Figure A4-4), pour 1 – 2 mL of isoflurane and quickly put a mouse inside. Watch until the animal's breathing is about once per second and immediately take it out to decapitate using the big scissors.

9. Gently expose the brain by pushing the skin towards the rostral end and pipette ~1 mL ice-cold ACSF-sucrose to the brain. Use the angled scissors to remove the scalp if necessary.

10. Check the FP expression using the hand-held laser and note the hemisphere and rough region with expression. If the expression is weak, try another animal; it's not worth the effort to go through the whole slicing procedure since there are always extra animals.

11. Use the angled scissors to make a cut (perpendicular to the midline) at the rostral (behind the eye balls) and caudal (behind the cerebellum) side of the skull. From the opening on the caudal side, cut along the midline until the opening on the rostral side such that the skull is in two separate pieces. Carefully avoid stabbing into the brain tissue by pointing the tip upward and slightly toward the non-expressing hemisphere during cutting. Cutting in one fluid motion without withdrawing the scissors multiple times will help avoid stabbing of the brain.

12. Use the ring-tip forceps to peel off the skull gently to expose the brain tissue. Make sure that the skull does not scratch or damage the brain tissue. Pipette ~1 mL ice-cold ACSF-sucrose to the brain tissue.

13. Use the scalpel to make two cuts: one rostral to the expressing area and the other in the cerebellum to create a large base where it will be readily glued to the slicing chamber (Figure A4-5). Make sure that the cuts are perpendicular to the midline.

14. Use the small spatula to scoop out the brain from the caudal side and gently place it in the ice-cold ACSF-sucrose in the crystallization dish (right, Figure A4-2).

15. Take the slicing chamber off the ice, wipe away any condensation and put in a new piece of kimwipe. The chamber needs to be dry for the glue to stick well.

16. Use the big spatula (use the small spatula to assist if necessary) to take out the brain from ACSF-sucrose and let it 'stand' on the filter paper on the caudal side where a base is created from scalpel cut. Leave it there for a few seconds and move the brain to another dry area on the filter paper. It is necessary to absorb as much solution as possible; otherwise, the brain would not stick well on the glue.

17. Meanwhile, apply some glue in the center of the slicing chamber and immediately (before the glue dries) transfer the brain to glued area using the spatula and allow the base to stick to the glue. Briefly, I will use the big spatula to scoop up the brain with base (the caudal side) facing the tip and bring it close to the glued area. Then, use the small spatula to gently push down the brain while tilting the big spatula to let the brain slide down such that the base will fall to the glued area nicely. Try to make the brain perpendicular to the chamber as much as possible. In this manner, we are collecting coronal slices.

18. Gently press down on the caudal side using the small spatula to make sure the brain sticks well. Mount the slicing chamber to the microtome and gently pour the ice-cold ACSF-sucrose into the slicing chamber to immerse the brain completely.

19. Lower the blade such that it is parallel to the slicing chamber and in the cutting solution completely. Adjust the cutting frequency to 7 and cutting speed to in between 3 – 4 and start slicing. Cutting should be done within 15 minutes, which should be enough time to get at least 6 slices. I usually acquire 300 μm thick slices. Each time the blade moves forward and cuts through the brain, remember to raise the blade by 100 μm (one full turn on the dial knob) before backing the blade. Transfer the slice from slicing chamber to one of the wells in the incubation chamber. Then lower the blade by 400 μm such that the next slice is 300 μm thick. This is to ensure that the blade doesn't damage the tissue when going back.

20. During slicing, the brain and cutting solution needs to remain ice-cold and oxygenated for optimal slice health. Thus, for every 30 second or so, remove 1-2 mL of solution from the slicing chamber and replace with fresh solution from the crystallization

dish. Another purpose is to remove any debris and reduce the local heat generated from cutting.

21. Check the fluorescence constantly and only collect the slices with good expression.

22. About 30 minutes after the first slice is placed in the incubation chamber (i.e. recovery period), turn off the water bath heat and allow the slices to recover for another 30 minutes at room temperature before using. The slices should be healthy in the chamber with carbogen perfusion for 4 – 6 hours at room temperature.

23. Check the carbogen flow regularly to make sure it is bubbling.

Slice health evaluation

It is not possible to know if a slice is healthy or not by visual inspection. In general, be gentle when handling the tissue. For instance, during slice transfer using the plastic Pasteur pipette, be careful not to suction in or push out the slice too fast or too violently. Quality of the slice could be checked under a microscope with IR illumination. Cells closer to the surface are less healthier with lots of debris from the blade cutting. It seems that cells at a depth of 20 – 50 μm beneath the surface are healthy and easier to access for patching purpose. Morphologically, unhealthy neurons have a shriveled or irregular shape and there is no good contrast with the surrounding tissue. Alternatively, functional imaging such as patch-clamp electrophysiology is the confirmative assessment of slice health.

Slice dye loading

Dye loading is done in a 35 mm imaging dish. 2 mL of ACSF-sucrose is transferred to the dish first and bubbled with carbogen through a 27-gauge needle (Figure A4-6). Carbogen flow should be adjusted to the slowest possible (e.g. 1-2 bubbles per second and slice should remain steady in the solution) as too much bubbling causing excessive disturbance can compromise slice health. The dye of 3x concentration is then added to the dish and swirled to mix well. With the setup ready, check the fluorescence again with a hand-held laser and transfer the slice in 1 mL of ACSF-sucrose gently to the dish. Note that 3 mL total volume is used, so 3x dye is added to 2 mL of buffer initially. After incubation is done, the slice is transferred either to a new dish with fresh buffer for confocal imaging or to the perfusion chamber on patching rig in a plastic Pasteur pipette. No washing is required since a low concentration of dye is used.

Imaging

To visualize staining, Trinity at Molecular Imaging Center is used for confocal microscopy imaging. A harp or staple is used to press down the slice for even illumination. Perfusion setup and activity imaging on Trinity are not optimized yet, but the slice does not have to stay alive for taking snaps and without perfusion the signal of stained dye remains robust at least 1 h after dye loading. For activity imaging or patch-clamp electrophysiology, there is a rig set up for slice electrophysiology with fluorescence imaging in the Adesnik lab. The perfusion and electrophysiology are both in place, so no additional preparation is required.

Troubleshooting

Hydrocephalus

Sometimes, after cutting into the brain of a physically healthy mouse, a big hole in the injected hemisphere is seen. This is due to build-up of fluid in the ventricle or hydrocephalus, which happens with excess volume of DNA injected during IUE. There might still be expression but it is recommended to use a new animal since physiologically the brain slice is already compromised.

Animal issue

The IUE could fail because of the following problems with the animals: female not pregnant, pups aborted or female eats the pups (for nutrients). These do not occur very frequent but are definitely not rare. It is therefore important to plan the experiments and order back-up animals in advance.

No expression

The success rate or number of positive animals in a litter of injected animals depends highly on the proficiency of the person doing the IUE procedure. Quality of the DNA matters too, so try switching to a new maxiprep DNA if IUE keeps failing.

Figures & Schemes

Figure A4-1. *Incubation chamber.*

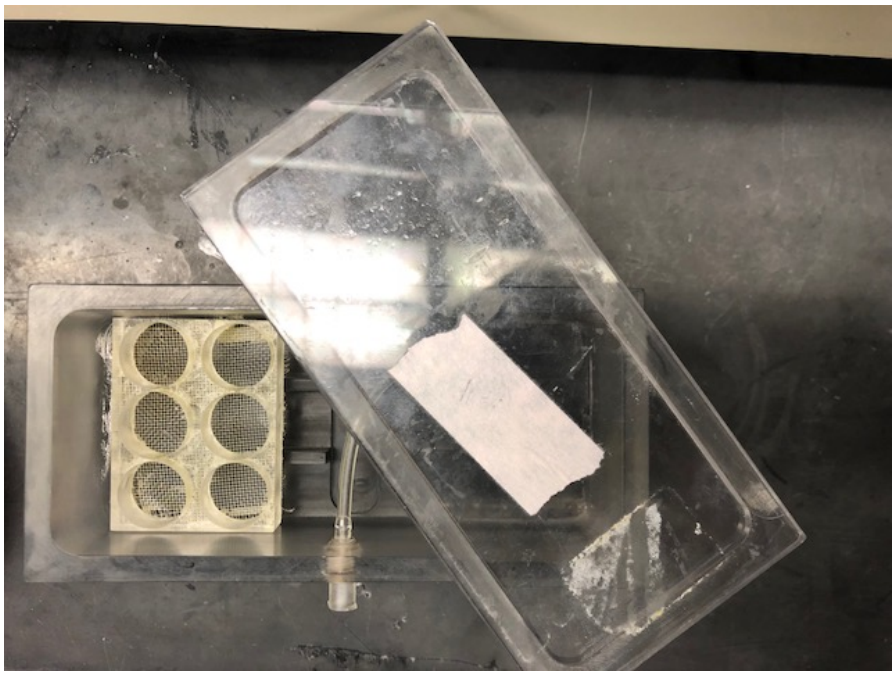

Figure A4-1. Incubation chamber with 6-well insert. ACSF-sucrose with carbogen perfusion is used to store the slices. It should be warmed up to 31 °C in a water bath before slicing starts. Put one slice per well.

Figure A4-2. *Glassware for storing ACSF-sucrose and tools.*

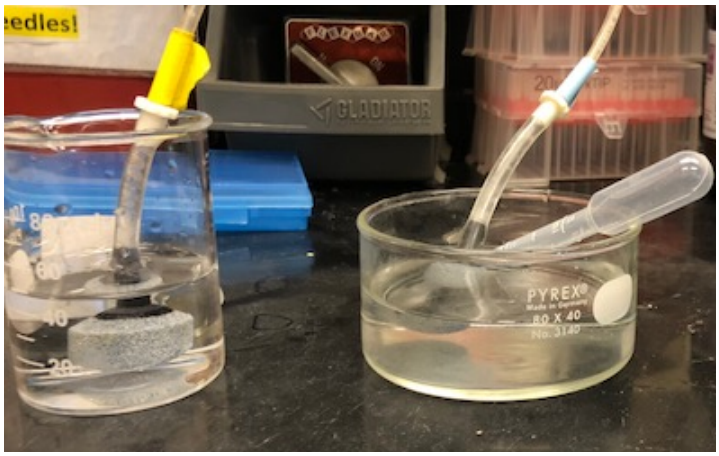

Figure A4-2. Both should have about 60 mL ACSF-sucrose solution and be kept on ice with carbogen perfusion. Tools are left in the beaker on the left while the extracted brain is placed in the crystallization dish on the right.

Figure A4-3. *Tools used in slicing.*

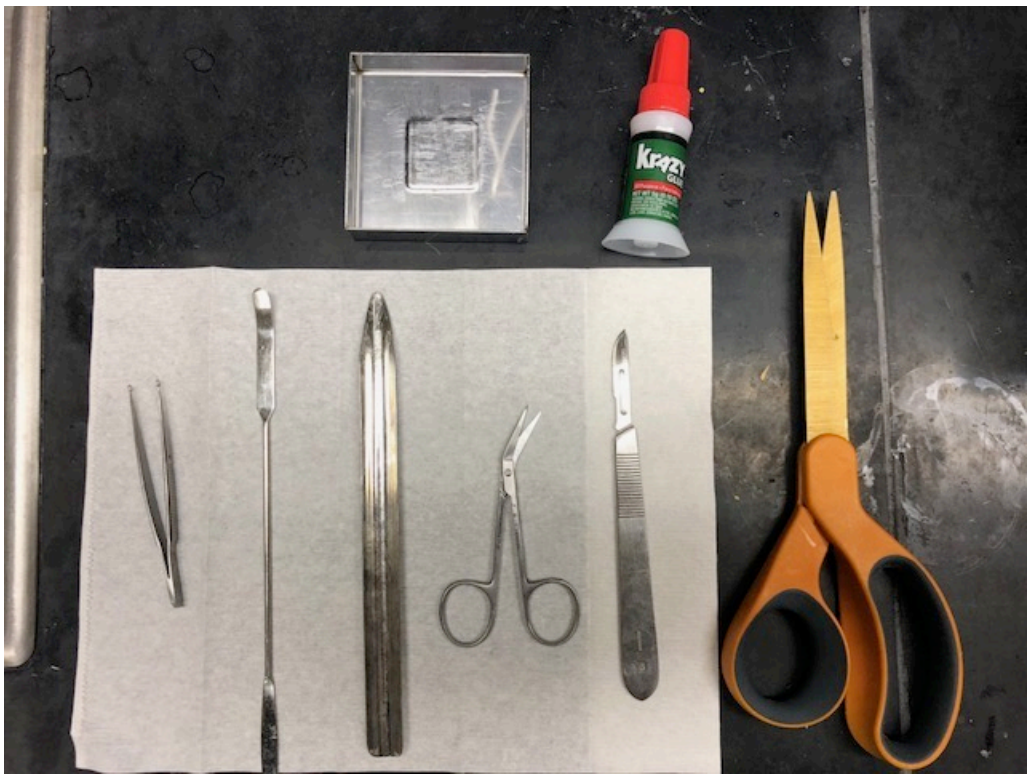

Figure A4-3. Tools used in slicing. Top: slicing chamber, glue. Bottom (from left to right): ring-tip forceps to peel off the skull, small spatula to transfer the brain, big spatula to transfer the brain, angled scissors to cut the scalp and skull, scalpel to cut the brain to create the base for glue, big scissors for animal decapitation.

Figure A4-4. *Anesthesia chamber.*

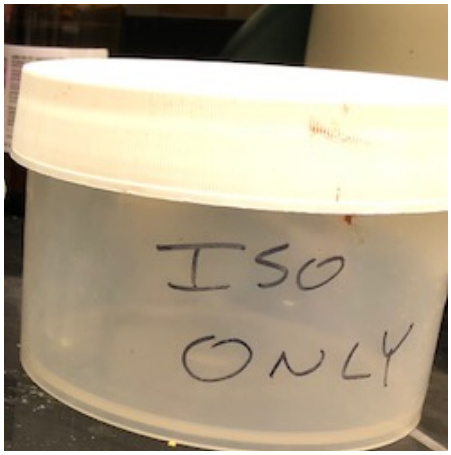

Figure A4-4. Use the chamber that says ‘iso only’. There are other chambers for survival procedures for pups.

Figure A4-5. *Scheme of mouse brain for scalpel cuts.*

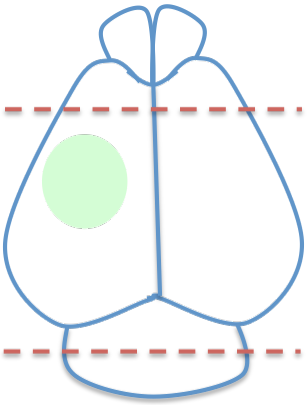

Figure A4-5. Scheme of where I use the scalpel to make cuts after exposing the brain (red dotted lines). Green area indicates FP expression

Figure A4-6. *Dye loading setup.*

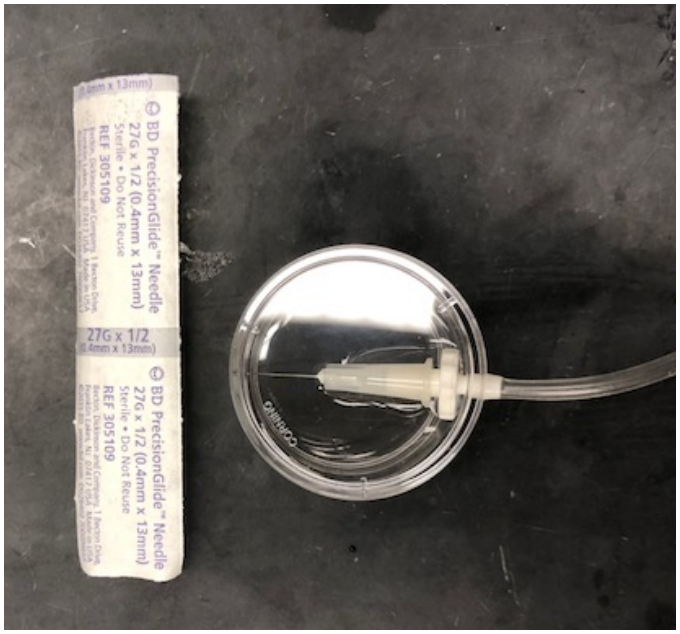

Figure A4-6. Needles and dish used for dye loading.